



The  
University  
Of  
Sheffield.

# **Investigation on Elastomer Compatibility with Alternative Aviation Fuels**

Yue Liu

Supervisor: Professor Chris W Wilson

Dr. Simon Blakey

Dissertation Submitted to the Department of Mechanical Engineering,  
University of Sheffield in Partial Fulfilment of the Requirements for the  
Degree of

Doctor of Philosophy

April 2013

## **Abstract**

The introduction of synthetic fuels produced from various alternative approaches has led to the concern over their compatibility with elastomeric seals used in current aircraft engines. The aim of this research is to investigate into this compatibility issue of alternative aviation fuels with typical elastomeric sealing materials. Experimental methodologies employed were the stress relaxation test (under both isothermal and temperature cycling conditions) and the Fourier Transform Infrared (FTIR) spectroscopy. A wide range of valuable data was collected and detailed analysis was carried out using statistical method and the Hansen Solubility Parameters (HSPs).

The outcome of this research establishes the fundamental stress relaxation characteristics of typical sealing materials in jet fuels produced via various sources. It demonstrates different impacts that individual fuel species may have on seals. A correlation has been found between the stress relaxation and the molecular structure changes of the O-rings. The HSP analysis suggests a good non-linear correlation between the equilibrium compression force and the RED number generated from the 'triangle' test data. It is proved that temperature is an influential factor in terms of the sealing performance of an O-ring. Generally, the stress relaxation process slows down (accelerates) as the temperature decreases (increases). At extremely low temperatures, seals become very inert and the relaxation process would stop. Temperature cycling tests show the relationship between seals' ability to recovery from thermal contraction and the aromatic content in the fuel. Based on the knowledge gained here, recommendations have been given on the potential future work related to this topic.

## **Acknowledgements**

I wish to express my sincere appreciation to my supervisors, Professor Chris Wilson and Dr. Simon Blakey for their patience, guidance, and support through my time at the University of Sheffield. I appreciate the opportunities they provided for me to be involved in a number of frontier research projects and international academic conferences. I have learned a lot from them both academically and personally.

I would like to thank Mr. Andrew Delorenzi for his help with the rig setup and modifications during my research. I would like to thank Dr. Spiros Siouris and Dr. Tim Dolmansley for teaching me the operation of the FTIR and Elastocon rig. Thanks to all staff in the Low Carbon Combustion Centre (LCCC) who made my time in Beighton very memorable.

I would like to thank the Qatar Science & Technology Park (QSTP) for sponsoring this research and my PhD study.

Finally, I extend my profound appreciation to my wife, Xiaoyu Sun. I would not be able complete my PhD study without her company and support all these years in Sheffield. I also would like to thank my parents, Xiaofeng Liu and Shukun Du, for their support as always.



## Table of Contents

Chapter 1 Introduction .....	13
1.1 Background and Motivation.....	13
1.2 Aims, Objectives and Methodologies .....	15
1.3 An Overview of the Research .....	16
Chapter 2 Literature Review .....	18
2.1 Development of Alternative Fuels in Aviation Industry .....	18
2.1.1 Current Jet Fuel.....	19
2.1.2 Alternative Fuels .....	20
2.1.2.1 <i>FAE</i> .....	20
2.1.2.2 <i>'XtL'</i> .....	21
2.1.2.3 <i>HRJ</i> .....	22
2.2 Elastomeric Seals .....	24
2.2.1 General properties of elastomers.....	24
2.2.2 How an elastomeric seal works.....	27
2.2.3 Swelling phenomena .....	28
2.2.3.1 <i>General thermodynamic principles</i> .....	28
2.2.3.2 <i>Relation between swelling and modulus</i> .....	29
2.2.3.3 <i>The dependence of swelling on strain</i> .....	29
2.2.4 The glass-rubber transition.....	30
2.3 Elastomer Compatibility Issue .....	32
2.3.1 Basic principles of fuel-polymer interaction.....	33
2.3.2 Molecular Transport of Solvent into Polymer .....	34
2.3.2.1 <i>Aromatic compounds</i> .....	35
2.3.2.2 <i>Paraffins</i> .....	35
2.3.3 Petroleum-Derived Fuel vs. Synthetic Fuel .....	36
2.3.4 Efforts to Promote the Seal-Swell ability of Synthetic Fuels.....	40

2.3.5	Summary of Previous Studies .....	49
2.4	Stress Relaxation.....	50
2.4.1	Theory of Stress Relaxation.....	50
2.4.2	Factors Influencing the Stress Relaxation of Elastomers.....	51
2.4.3	Testing Methods for Stress Relaxation in Compression .....	52
2.4.4	Applications of the Stress Relaxation Test .....	53
2.5	Fourier Transform Infrared Spectrometer (FTIR).....	53
2.5.1	Infrared Spectroscopy .....	53
2.5.2	FTIR.....	54
2.5.3	Attenuated Total Reflectance (ATR)-FTIR .....	55
2.5.4	Applications of FTIR and ATR-FTIR in Polymer Analysis.....	57
2.6	Hansen Solubility Parameters (HSP) .....	58
2.6.1	Theory of HSP .....	59
2.6.2	Applications of HSP in polymer-solvent interactions.....	61
2.7	Summary .....	62
Chapter 3	Experimental .....	64
3.1	Equipments .....	64
3.1.1	Elastocon EB 02 & EB 01 – For Isothermal Stress Relaxation Test .....	64
3.1.1.1	<i>Technical description</i> .....	64
3.1.1.2	<i>CombiLab software</i> .....	68
3.1.1.3	<i>Test procedure</i> .....	69
3.1.2	Elastocon EB 17 – For Temperature Cycling Test .....	70
3.1.2.1	<i>Technical description</i> .....	70
3.1.2.2	<i>Test procedure</i> .....	75
3.1.3	FTIR spectrometer – Perkin Elmer Spectrum One + ATR Accessory.....	75
3.1.3.1	<i>Technical description</i> .....	75
3.1.3.2	<i>Test procedure</i> .....	78
3.2	Candidate Fuels/Solvents.....	79
3.3	O-ring Materials.....	80
Chapter 4	Results – Stress Relaxation Tests .....	83

4.1	Nitrile O-Ring .....	83
4.1.1	Relaxation Characteristics in Jet A-1: Baseline .....	83
4.1.2	Relaxation Characteristics in Typical Alternative Fuels and Blends .....	85
4.1.2.1	<i>FSJF (CtL) vs. FT-SPK (GtL)</i> .....	86
4.1.2.2	<i>FT-SPK based blends</i> .....	87
4.1.2.3	<i>HVO and Bio-SPK blends</i> .....	92
4.1.2.4	<i>Comparison with Jet A-1</i> .....	94
4.1.3	Relaxation Characteristics in the ‘Triangle’ Blends .....	95
4.1.3.1	<i>Vertexes of the Triangle</i> .....	97
4.1.3.2	<i>Edges of the Triangle</i> .....	100
4.1.3.3	<i>Insides of the Triangle</i> .....	102
4.1.4	Summary .....	107
4.2	Fluorosilicone O-Ring .....	107
4.2.1	Relaxation Characteristics in Jet A-1: Baseline .....	108
4.2.2	Relaxation Characteristics in Typical Alternative Fuels and Blends .....	108
4.2.2.1	<i>FSJF (CtL) vs. FT-SPK (GtL)</i> .....	109
4.2.2.2	<i>FT-SPK based blends</i> .....	109
4.2.2.3	<i>HVO and Bio-SPK blends</i> .....	114
4.2.2.4	<i>Comparison with Jet A-1</i> .....	116
4.2.3	Relaxation Characteristics in the ‘Triangle’ Blends .....	117
4.2.3.1	<i>Vertexes of the Triangle</i> .....	117
4.2.3.2	<i>Edges of the Triangle</i> .....	118
4.2.3.3	<i>Insides of the Triangle</i> .....	119
4.2.4	Summary .....	120
4.3	Fluorocarbon O-Ring .....	121
4.3.1	Relaxation Characteristics in Jet A-1: Baseline .....	121
4.3.2	Relaxation Characteristics in Typical Alternative Fuels and Blends .....	122
4.3.2.1	<i>FSJF (CtL) vs. FT-SPK (GtL)</i> .....	122
4.3.2.2	<i>FT-SPK based blends</i> .....	122
4.3.2.3	<i>HVO and Bio-SPK blends</i> .....	127

4.3.2.4	<i>Comparison with Jet A-1</i> .....	128
4.3.3	Relaxation Characteristics in the “Triangle” Blends.....	129
4.3.3.1	<i>Vertexes of the Triangle</i> .....	129
4.3.3.2	<i>Edges of the Triangle</i> .....	131
4.3.3.3	<i>Insides of the Triangle</i> .....	131
4.3.4	Summary .....	132
Chapter 5	Results – FTIR.....	133
5.1	Nitrile O-ring .....	133
5.2	Fluorosilicone O-ring.....	134
5.3	Fluorocarbon O-ring .....	137
Chapter 6	Results – Temperature Impact on Stress Relaxation.....	140
6.1	Constant Temperature Testing .....	140
6.1.1	Nitrile O-rings .....	141
6.1.2	Fluorosilicone O-rings .....	143
6.1.3	Fluorocarbon O-rings.....	145
6.2	Temperature Switching Testing.....	147
6.3	24h-Cycle Testing.....	151
6.3.1	Nitrile O-rings .....	151
6.3.2	Fluorosilicone O-rings .....	153
6.3.3	Fluorocarbon O-rings.....	154
6.4	Stress Relaxation of Elastomeric Seals in O-ring Grooves.....	157
6.5	Summary .....	161
Chapter 7	Discussions.....	163
7.1	Hansen Solubility Parameters (HSPs) Analysis.....	163
7.2	Temperature Factor Analysis .....	166
7.2.1	Nitrile O-rings .....	166
7.2.1.1	<i>In O-ring grooves</i> .....	166
7.2.1.2	<i>Without O-ring grooves</i> .....	173
7.2.2	Fluorosilicone O-rings .....	176
7.2.2.1	<i>In O-ring grooves</i> .....	176

7.2.2.2	<i>Without O-ring grooves</i> .....	182
7.2.3	Fluorocarbon O-rings .....	185
7.2.3.1	<i>In O-ring grooves</i> .....	185
7.2.3.2	<i>Without grooves</i> .....	191
Chapter 8	Conclusions and Future Work.....	195
8.1	Conclusions.....	195
8.2	Future Work.....	198
References	.....	199
Appendix 1	List of Publications.....	207

## List of Figures

Figure 1 2D GC analysis results of a typical jet fuel composition. [27].....	19
Figure 2 The transesterification process of producing FAME [26]. .....	21
Figure 3 The Fischer-Tropsch process to produce synthetic fuel [29].....	21
Figure 4 Typical GC analysis results of a range of FT fuels. Sasol IPK is a CtL, S-8 syntrolyums GtL, Shell GtL and two Sasol GtL's from Sasol Oryx plant [1]. .....	22
Figure 5 Hydroprocessing of vegetable oil [31]. .....	23
Figure 6 Typical compositions of HRJs produced by the UOP process [32].....	23
Figure 7 Typical force-extension curve for natural rubber. ....	25
Figure 8 The structure of the molecule of isoprene (A-B=isoprene unit; C=methyl group).....	26
Figure 9 O-ring sealing in low pressure application.....	27
Figure 10 Relation between equilibrium swelling ( $1/v_2$ ) and modulus for butyl rubbers with various degrees of cross-linking. ....	29
Figure 11 Volume-temperature relationship for purified rubber, showing second-order transition at $-72^\circ\text{C}$ and crystal melting at $11^\circ\text{C}$ .....	31
Figure 12 Force at constant length as function of absolute temperature (extension 350 per cent) .....	32
Figure 13 Average volume change (%) of nitrile O-rings after 43 days [40]. .....	38
Figure 14 Comparison of volume change between nitrile coupon and O-ring in S-5/JP-5 fuel pair cycling [41].....	39
Figure 15 Semi-quantitative composition of the coal-based jet fuel [43].....	40
Figure 16 Volume swell for nitrile O-rings aged in selected fuels at room temperature [43].....	40
Figure 17 Left: schematic of the optical dilatometry system used to measure volume swell as a function of time; .....	42
Figure 18 Comparison of the emission propensity (normalized particle number) at engine idle and volume swell of nitrile O-rings as a function of aromatic solvent type and concentration [44]. .....	42
Figure 19 Partition coefficient between nitrile O-ring and selected compound classes in S-5 and JP-5 vs. chromatographic retention time after aging at room temperature for 7 days [45].....	44
Figure 20 Volume swell as a function of time for nitrile O-rings aged in S-5 + 10% v/v of each aromatic compound at room temperature [45].....	44
Figure 21 Relations among intermolecular distance, binding energy, and vibrational frequency shift of the $\text{C}\equiv\text{N}$ stretching mode [47]. .....	48
Figure 22 Swelling coefficient against the (a) intermolecular distance, (b) binding energy, and (c) vibrational frequency shift of the $\text{C}\equiv\text{N}$ stretching mode [47]. .....	49
Figure 23 A discontinuous stress relaxation test rig [53].....	52
Figure 24 Stretching and bending vibration modes of $\text{CH}_4$ group [65]. .....	54
Figure 25 Schematic diagram of the instrumental process of an FTIR spectrometer [67].....	55
Figure 26 Principle of attenuated total reflectance (ATR) spectroscopy [68]. .....	56

Figure 27 Solubility of carbon dioxide [86].....	61
Figure 28 Elastocon EB02 continuous stress relaxation (CSR) tester (a) and with ageing cell oven EB 01 (b).....	66
Figure 29 Schematic diagram for compensating the spring effect [92]. F: force applied; D: compression during test; d: compression caused by the load cell; H: original height of the sample.....	68
Figure 30 Overview of the programme modules of CombiLab 5 [94]. .....	69
Figure 31 Elastocon EB 17 cycling cell oven with liquid circulator.....	71
Figure 32 Schematic diagram of the temperature cycling cell oven setup. ....	72
Figure 33 Operating principle of the liquid circulator [96].....	73
Figure 34 Operating principle of the FTIR [97].....	76
Figure 35 Perkin-Elmer Spectrum One FTIR spectrometer with ATR accessory.....	79
Figure 36 Typical molecular structure of: (a) nitrile polymer; (b) fluorocarbon polymer; and (c) fluorosilicone polymer [103].....	81
Figure 37 The stress relaxation characteristic of nitrile O-ring in Jet A-1.....	84
Figure 38 The relaxation characteristics of nitrile O-rings in FSJF and FT-SPK. ....	86
Figure 39 Overall stress relaxation characteristics of nitrile O-rings in 5 FT-SPK based blends, with comparison to FT-SPK and Jet A-1. ....	88
Figure 40 Comparison between FT-SPK based blends with different proportions of naphthenes (nitrile).....	89
Figure 41 Comparison between FT-SPK based blends with 20% aromatics/hexanol (nitrile).....	90
Figure 42 Comparison between FT-SPK based blends with (naphthenes + aromatics) and naphthenes only (nitrile).....	91
Figure 43 Comparison between FT-SPK based blends with (naphthenes + aromatics) and aromatics only (nitrile). ....	91
Figure 44 Stress relaxation performance comparison of 5 FT-SPK blends (nitrile). ..	92
Figure 45 Comparison between HVO and Bio-SPK based blends (nitrile).....	93
Figure 46 Comparison between HVO and FT-SPK (nitrile).....	93
Figure 47 Normalized final compression forces of nitrile O-rings in all alternative fuels or blends relative to the value in Jet A-1, %.....	94
Figure 48 “Normal-iso-cycloparaffins” solvent triangle.....	96
Figure 49 Relaxation process of nitrile O-ring: (a) in three single solvents respectively; (b) normalized by Jet A-1 with comparison to GTL kerosene (FT-SPK). ....	98
Figure 50 Relaxation process of nitrile O-rings in the blends of decalin and n-decane solvents.....	100
Figure 51 Relaxation process of nitrile O-rings in the blends of decalin and isoparaffins. ....	101
Figure 52 Relaxation process of nitrile O-rings in the blends of iso-paraffins and n-decane solvents. ....	102
Figure 53 Relaxation process of nitrile O-rings in the blends of ‘decalin region’ (in red). ....	103
Figure 54 Relaxation process of nitrile O-rings in the blends of ‘iso-paraffin region’	

(in yellow).....	104
Figure 55 Relaxation process of nitrile O-rings in the blends of ‘n-decane region’ (in blue). .....	105
Figure 56 Summary of the relaxation characteristics of nitrile O-rings in the solvent triangle. ....	106
Figure 57 The stress relaxation characteristic of fluorosilicone O-ring in Jet A-1..	108
Figure 58 Relaxation characteristics of fluorosilicone O-rings in FSJF and FT-SPK. ....	109
Figure 59 Overall stress relaxation characteristics of fluorosilicone O-rings in 5 FT-SPK based blends, with comparison to FT-SPK and Jet A-1. ....	110
Figure 60 Comparison between FT-SPK based blends with different proportions of naphthenes (fluorosilicone).....	111
Figure 61 Comparison between FT-SPK based blends with 20% aromatics/hexanol (fluorosilicone).....	112
Figure 62 Comparison between FT-SPK based blends with (naphthenes + aromatics) and naphthenes only (fluorosilicone).....	113
Figure 63 Comparison between FT-SPK based blends with (naphthenes + aromatics) and aromatics only (fluorosilicone). ....	113
Figure 64 Stress relaxation performance comparison of 5 FT-SPK blends (fluorosilicone).....	114
Figure 65 Comparison between HVO and Bio-SPK based blends (fluorosilicone).115	
Figure 66 Comparison between HVO and FT-SPK (fluorosilicone). ....	115
Figure 67 Normalized final compression forces in all alternative fuels or blends relative to the value in Jet A-1, % (fluorosilicone). ....	116
Figure 68 Relaxation behaviour of fluorosilicone O-rings: (a) in three single solvents respectively; (b) normalized by Jet A-1, with comparison to GTL kerosene. ....	118
Figure 69 Relaxation characteristics of fluorosilicone O-rings in the blends on the edges of the triangle. ....	119
Figure 70 Relaxation characteristics of fluorosilicone O-rings in the blends inside the triangle. ....	120
Figure 71 The stress relaxation characteristic of fluorocarbon O-ring in Jet A-1....	121
Figure 72 Relaxation characteristics of fluorocarbon O-rings in FSJF and FT-SPK. ....	122
Figure 73 Overall stress relaxation characteristics of fluorocarbon O-rings in 5 FT-SPK based blends, with comparison to FT-SPK and Jet A-1. ....	123
Figure 74 Comparison between FT-SPK based blends with different proportions of naphthenes (fluorocarbon). ....	124
Figure 75 Comparison between FT-SPK based blends with 20% aromatics/hexanol (fluorocarbon). ....	125
Figure 76 Comparison between FT-SPK based blends with (naphthenes + aromatics) and naphthenes only (fluorocarbon). ....	126
Figure 77 Comparison between FT-SPK based blends with (naphthenes + aromatics) and aromatics only (fluorocarbon).....	126
Figure 78 Comparison between HVO and Bio-SPK based blends (fluorocarbon). 127	

Figure 79 Comparison between HVO and FT-SPK (fluorocarbon).....	128
Figure 80 Normalized final compression forces in all alternative fuels or blends relative to the value in Jet A-1, % (fluorocarbon).....	129
Figure 81 Relaxation characteristics of fluorocarbon O-rings: (a) in three single solvents respectively; (b) normalized by Jet A-1, with comparison to GTL kerosene. ....	130
Figure 82 Relaxation characteristics of fluorocarbon O-rings in the blends on the edges of the triangle. ....	131
Figure 83 Relaxation behaviour of fluorocarbon O-rings in the blends inside the triangle.....	132
Figure 84 Spectra examples of nitrile O-rings. ....	134
Figure 85 Spectra of fluorosilicone O-rings (part 1).....	135
Figure 86 Spectra of fluorosilicone O-rings (part 2).....	135
Figure 87 Spectra of fluorocarbon O-rings (part 1). ....	138
Figure 88 Spectra of fluorocarbon O-rings (part 2); .....	138
Figure 89 Stress relaxation characteristics of nitrile O-ring under various constant temperatures in (a) Jet A-1 and (b) GtL fuels; and (c) comparison between the two fuels. ....	142
Figure 90 Stress relaxation characteristics of fluorosilicone O-ring under various constant temperatures in (a) Jet A-1 and (b) GtL fuels; and (c) comparison between the two fuels. ....	145
Figure 91 Stress relaxation characteristics of fluorocarbon O-ring under various constant temperatures in (a) Jet A-1; (b) GtL fuels; and (c) comparison between the two fuels. ....	146
Figure 92 Relaxation process of (a) nitrile, (b) fluorosilicone and (c) fluorocarbon O-rings in GtL and Jet A-1 fuel respectively, with temperature switching between 30 to -40 °C. ....	149
Figure 93 Performance comparison of three O-ring materials in the temperature switching test.....	150
Figure 94 (a) Relaxation performance of nitrile O-ring in the 24h-cycle testing; (b) normalized by Jet A-1. ....	151
Figure 95 Results from 24h-cycle testing compared with constant temperature testing (nitrile).....	152
Figure 96 (a) Relaxation performance of fluorosilicone O-ring in the 24h-cycle testing; (b) normalized by Jet A-1.....	153
Figure 97 Results from 24h-cycle testing compared with constant temperature testing (fluorosilicone).....	154
Figure 98 (a) Relaxation performance of fluorocarbon O-ring in the 24h-cycle testing; (b) normalized by Jet A-1.....	155
Figure 99 Results from 24h-cycle testing compared with constant temperature testing (fluorocarbon). ....	156
Figure 100 Comparison of normalized relaxation performances of three O-ring materials in the 24h-cycle testing.....	156
Figure 101 24h-cycle test results of preconditioned nitrile O-rings in grooves in fuels	

with various aromatic contents. ....	158
Figure 102 Fresh nitrile O-ring relaxation rate comparison in Jet A-1 and SPK.....	159
Figure 103 24h-cycle test results of fluorosilicone O-rings in grooves in fuels with various aromatic contents. ....	160
Figure 104 24h-cycle test results of fluorocarbon O-rings in grooves in fuels with various aromatic contents. ....	161
Figure 105 Plot of F/F0 at equilibrium (experimental) versus RED number for nitrile O-ring (theoretical). ....	165
Figure 106 Data analysis for the 24h-cycling test in groove in Jet A-1 (aged nitrile O-ring).....	168
Figure 107 Data analysis for the 24h-cycling test in groove in 8% aromatic fuel blend (aged nitrile O-ring). ....	169
Figure 108 Data analysis for the 24h-cycling test in groove in 4% aromatic fuel blend (aged nitrile O-ring). ....	170
Figure 109 Data analysis for the 24h-cycling test in groove in SPK (aged nitrile O-ring).....	171
Figure 110 Overall recovery ability of aged nitrile O-rings in fuels with various aromatic contents during the 24h-cycle testing. ....	173
Figure 111 Data analysis for the 24h-cycling test with no groove in Jet A-1 (fresh nitrile O-ring). ....	174
Figure 112 Data analysis for the 24h-cycling test with no groove in SPK fuel (fresh nitrile O-ring). ....	175
Figure 113 Average recovery ability of fresh nitrile O-rings in Jet A-1 and SPK during the 24h-cycle testing without grooves. ....	176
Figure 114 Data analysis for the 24h-cycling test in groove in Jet A-1 (fluorosilicone O-ring).....	178
Figure 115 Data analysis for the 24h-cycling test in groove in 8% aromatic fuel blend (fluorosilicone O-ring). ....	179
Figure 116 Data analysis for the 24h-cycling test in groove in 4% aromatic fuel blend (fluorosilicone O-ring). ....	180
Figure 117 Data analysis for the 24h-cycling test in groove in SPK (fluorosilicone O-ring).....	181
Figure 118 Overall recovery ability of fluorosilicone O-rings in fuels with various aromatic contents during the 24h-cycle testing. ....	182
Figure 119 Data analysis for the 24h-cycling test without groove in Jet A-1 (fluorosilicone O-ring). ....	183
Figure 120 Data analysis for the 24h-cycling test without groove in GtL fuel (fluorosilicone O-ring). ....	184
Figure 121 Average recovery ability of fluorosilicone O-rings in Jet A-1 and SPK during the 24h-cycle testing without grooves. ....	185
Figure 122 Data analysis for the 24h-cycling test in groove in Jet A-1 (fluorocarbon O-ring).....	187
Figure 123 Data analysis for the 24h-cycling test in groove in Jet A-1 (fluorocarbon O-ring).....	188

Figure 124 Data analysis for the 24h-cycling test in groove in 4% aromatic fuel blend (fluorocarbon O-ring).....	189
Figure 125 Data analysis for the 24h-cycling test in groove in SPK (fluorocarbon O-ring).....	190
Figure 126 Overall recovery ability of fluorocarbon O-rings in fuels with various aromatic contents during the 24h-cycle testing.....	191
Figure 127 Data analysis for the 24h-cycling test with no groove in Jet A-1 (fluorocarbon O-ring).....	192
Figure 128 Data analysis for the 24h-cycling test with no groove in GtL fuel (fluorocarbon O-ring).....	193
Figure 129 Average recovery ability of fluorocarbon O-rings in Jet A-1 and SPK during the 24h-cycle testing without grooves. ....	194

## List of Tables

Table 1 Swelling of nitrile O-rings after soaking in synthetic fuel (S-5) blended with various species [46].....	46
Table 2 Summary of previous achievements and future work.....	49
Table 3 Physical properties of commonly used ATR crystals [69]. ....	57
Table 4 Technical specifications of the Relaxation Tester EB 02 [92]. ....	66
Table 5 Technical specifications of Cell Ageing Oven EB 01 [93]. ....	67
Table 6 Technical specifications of Cycling Cell Oven EB 17 [95]. ....	74
Table 7 Technical specifications of Liquid Circulator LH 85 [96]. ....	74
Table 8 Optical performance of the DTGS detector. ....	78
Table 9 Descriptions of candidate fuel or solvent samples.....	80
Table 10 Specifications and physical properties of the sample O-rings. ....	82
Table 11 Compositions of alternative fuel samples tested. ....	85
Table 12 Solvent matrix for testing.....	96
Table 13 O-ring swelling property (OSP)* of five solvents. ....	100
Table 14 Possible molecular structures corresponding to peaks in the spectra (fluorosilicone O-rings) [62] [106]. ....	136
Table 15 Possible molecular structures corresponding to peaks in the spectra (fluorocarbon O-rings) [62] [106].....	139
Table 16 SAE ARP-1234 face seal O-ring groove specifications.....	157
Table 17 Hansen Solubility Parameters of the normal, iso- and cycloparaffin in the ‘triangle’ test. ....	163
Table 18 Hansen Solubility Parameters and equilibrium values of the ‘triangle’ solvent blends.....	164

# 1 Introduction

## 1.1 Background and Motivation

In 2008, the U.S. Air Force Research Laboratory funded a project to evaluate the properties of semi-synthetic jet fuels (SSJF) (50% Synthetic Paraffinic Kerosene (SPK) blended with 50% conventional jet fuel), compared with conventional petroleum-derived fuel [1]. Most of the properties or characteristics of SSJF were concluded to be typical when compared to conventional jet fuel, such as improved thermal stability; but with only one exception, which was its compatibility with elastomeric sealing materials in the engine.

Similarly, in January-February 2009, the NASA Alternative Aviation Fuel Experiment (AAFEX) Project was conducted at NASA's Palmdale, CA aircraft facility. The aim of the project was to investigate the effects of synthetic fuels on engine performance and auxiliary power unit (APU) emissions and characteristics. Fuels tested were regular JP-8 (19% aromatic content), Fischer-Tropsch (FT) fuel made from natural gas (no aromatic content). However, an 'accident' happened during the test as *'fuel leaks occurred in the aircraft fuel system and tanker trucks when the pure FT fuels were used due to the absence of aromatic compounds, which have been shown to increase seal swell. No leaks were seen when the right engine was fuelled with the blended fuels'* [2].

Both tests mentioned above show the same concern if alternative fuels are adopted in current jet engines, which is their compatibility issue with elastomeric sealing materials in the fuel system. Traditionally, conventional petroleum-derived jet fuel does not have any compatibility issue with elastomeric materials, as it is believed the aromatic content in the fuels can swell the seals and promote its sealing performance. However, when alternative fuels are adopted, fuel leakage may occur such as the accident happened during the AAFEX project because they are known for their trace or no aromatic content. As such, seals may shrink or no longer swell to the desired

volume to provide effective sealing. Polymer material compatibility issue has become the bottleneck in the development of alternative fuels in aviation industry.

Due to the lack of historical data on the impact of fuels on sealing materials in the engines, knowledge on this topic is mainly based on previous experience in practice. Current jet fuel specification requires 8%-25% (v/v) aromatic content to guarantee a promising sealing performance of polymer materials which is also specified based on experience. As the usage of alternative fuels should not cause any change to current engine structure, research need to be done to understand their interaction and impact on the seals. Previous tests focused on comparing the differences of changes in physical properties of these sealing materials, such as mass, volume, and hardness, etc. Such tests are referred as 'static' tests, which mean polymer sheets, or O-ring samples, are immersed in certain amount of fuel samples and left for a period of time. Measurements are then carried out at certain time intervals to compare how these properties change during this process. The advantage of this method is the data of physical property changes of the seals, especially volume, can be obtained from various alternative fuels. Then by comparing these data with that from current jet fuel, e.g. Jet A/Jet A-1, different impacts of the fuels on those properties can be seen.

However, data from the 'static' tests can not represent the real scenario in which seals are working due to the lack of pressure. Generally, seals are compressed between two mating surfaces or in grooves to prevent fuel leakage. As such, consideration needs to be given to the influence of pressure and also temperature conditions that seals are experiencing. The compatibility issue of alternative fuels with elastomeric seals should be considered as the combined impact of pressure, temperature and the interaction between fuels and polymers. This requires a 'dynamic' test with the capability of taking the pressure and temperature parameters into consideration, which is the main motivation driving this work.

Furthermore, it is also essential to explore deeper into the molecular level to

understand how fuels interact with polymers. In this way, further knowledge can be learned about the roles of each component in the fuel compositions play in this interaction process. Then additional procedures may be carried out to guarantee the fuel adopted is fully compatible with the seals being used. To achieve this, techniques that are capable to investigate into molecular level of polymers are required.

## **1.2 Aims, Objectives and Methodologies**

The aim of this work is to investigate the impact of alternative aviation fuels produced via various pathways on elastomeric sealing materials being used in the fuel system of an aircraft engine. Several key objectives need to be achieved, which are:

- To define high-risk sealing conditions, such as new seals and aged seals (which have experienced switch loading);
- To design low cost representative matrix of tests;
- To carry out standard relaxation tests on candidate elastomer materials and fuels in order to generate typical relaxation characteristics of each material under given circumstances;
- To compare the relaxation characteristics of each material in various intermediate and low swell (low aromatic) fuels to that in the baseline fuel (Jet A-1);
- To carry out temperature cycling tests to monitor seal performance under extreme temperature conditions;
- To investigate the molecular structure change of seals after the relaxation tests and to further understand the role of each fuel components plays in the fuel-polymer interaction process;
- To give recommendations with regards to specification limits for all jet fuels & system design rules.

For the ‘dynamic’ test, two types of Elastocon stress relaxation rigs were employed for this project; one was used to carry out the stress relaxation test under an isothermal condition, the other was capable to do the test under temperature cycling condition. In these ways, both pressure and temperature factors are taken into consideration while the elastomeric materials are soaked in the fuel. Fourier Transform Infrared (FTIR) Spectroscopy and Hansen Solubility Parameter (HSP) theory were employed to understand the fuel-polymer interaction at the molecular level.

### **1.3 An Overview of the Research**

This dissertation begins with an in-depth literature review to provide sufficient background information to support the topic discussed throughout the research. A wide range of tests are conducted in the project to generate a comprehensive data set to characterise seal performance in various alternative fuels under operating conditions. Detailed discussion and analysis are presented based on the test results via various analytical methods. Finally, solid conclusions are drawn with regards to the future work. The whole dissertation is divided into the following chapters:

- *Chapter 1:* A brief introduction is given to a practical problem faced in the aviation industry, which also highlights the importance of this study. Detailed objectives and methods used, along with the structure of the dissertation are presented.
- *Chapter 2:* This chapter provides a comprehensive literature review with regards to the following key topics: development of alternative fuels in aviation industry and their compatibility issues with seals, theory and application of stress relaxation, FTIR spectroscopy, and Hansen Solubility Parameter (HSP) theory.
- *Chapter 3:* Details about the experimental setup are presented in this chapter. Principles, functions, working procedures, modification where it was necessary

of the two stress relaxation rigs and FTIR spectrometer are introduced respectively. An overview is given to the seal materials tested with respect to their molecular structure; and the compositions of various candidate fuels are listed.

- *Chapter 4:* In this chapter, results obtained from a series of stress relaxation tests are presented. Results are divided into three parts regarding three different O-ring materials tested. Relaxation characteristics of each material in various alternative fuels and the ‘triangle’ tests are compared and summarized.
- *Chapter 5:* Results from the FTIR analysis from each seal sample taken after the relaxation tests are shown to see the impact of different fuels on the polymer structure.
- *Chapter 6:* This chapter presents the results obtained from the various temperature conditions and the temperature cycling tests to evaluate the impact of temperature factor on the sealing performance of O-rings.
- *Chapter 7:* In-depth discussions on the relationships between the data of stress relaxation and FTIR, as well as the latter with HSP, are given in this part. Better understanding on the fuel-polymer interaction and the role of each fuel component is gained from these discussions. To analyse the temperature influence, relationship between compression force change ( $\Delta (F/F_0)$ ) and the temperature gradient ( $\Delta T$ ) are presented and compared.
- *Chapter 8:* Solid conclusions are drawn based on the results and discussions in previous chapters. This chapter also provides recommendations for the future work in this area.

## 2 Literature Review

### 2.1 Development of Alternative Fuels in Aviation Industry

On 28<sup>th</sup> October 2011, a Boeing 747-400 aircraft with one of its four engines fuelled with half conventional jet fuel and half Jatropa-derived biofuel conducted a one-hour flight above Beijing. The Jatropa oil feedstock was grown in South China by PetroChina and the demonstration flight was part of a Sino-US energy cooperation program. It was China's first flight using aviation biofuels and the success could '*possibly pave the way for future biofuel use on commercial flights in the country*' [3].

Under the global background of reducing CO<sub>2</sub> emissions and tackling the problem of depleting petroleum resources, the aviation industry is putting great effort into the development of alternative fuel sources. The trial flight mentioned above is only one of many successful examples demonstrating the possibility to adopt alternative fuels in current fleet. Airlines including Virgin Atlantic Airways [4], Air New Zealand [5], Continental Airlines [6], Japan Airlines [7] and Qatar Airways [8], have already carried out similar demonstration flights on alternative fuels since 2008; while other carriers such as KLM Royal Dutch Airlines [9], Lufthansa [10] and AeroMexico [11] have conducted commercial biofuel flights in 2011. Although all the demonstration and commercial flights were based on alternative fuel blends with conventional jet fuel, from a technical point of view, it is clearly seen that it is only a matter of time when alternative fuels could be fully adopted.

To be qualified as alternative fuels, the most important criterion to address is that a candidate fuel must be fully compatible with current systems, which is the existing commercial aviation infrastructure, including fuel delivery and storage, and most importantly, the existing fleet of aircraft. As a result, current research focuses on the development of kerosene like 'drop-in' fuels [12] - [19]. Other criteria, such as maturity of the fuel-production technology, production potential and costs,

environmental benefits, also need to be examined during the assessment process of alternative fuels [20]. All fuel properties of the alternative candidates have to be comparable to those of current jet fuel, whose compositions may vary due to the diversity of feedstock and refinery processes [21] - [24].

### 2.1.1 Current Jet Fuel

Current jet fuel is a mixture of hydrocarbons with carbon chain length of C8-C16, as well as additives [25]. The composition of a typical jet fuel is presented in Figure 1. 70-85% of the fuel consists of paraffins, including straight-chain normal paraffins, branched-chain iso-paraffins and cycloparaffins which are also known as naphthenes. The high hydrogen to carbon ratio for normal and iso-paraffins provides a high heat to weight ratio and a clean burn. By contrast, the cycloparaffins reduce the hydrogen to carbon ratio and the heat to weight ratio; however, they help to reduce the freeze point of the fuel [26].

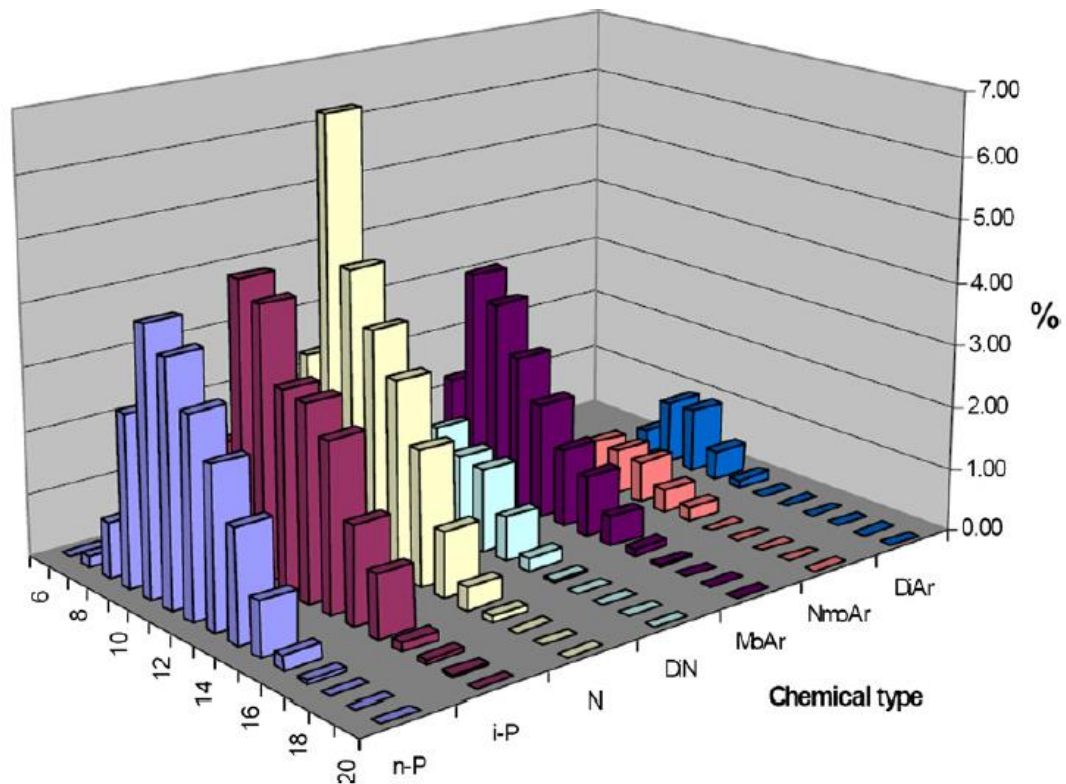


**Figure 1** 2D GC analysis results of a typical jet fuel composition. [27]

The content of aromatic compounds is less than 25% in the composition. Aromatics are unsaturated cyclic hydrocarbons containing one or more six carbon ring structures. Due to their relatively lower hydrogen to carbon ratio, an incomplete burn is likely to happen during combustion which results in the formation of soot. This is the reason for the upper limit of 25% (v) aromatics in current jet fuel. Aromatics are believed to be crucial for swelling the seals in the fuel system to provide satisfactory sealing performance. This has become one of the biggest concerns when alternative fuels are used as their low aromatic content may cause aged seals to shrink and eventually leak fuel. As a result, a minimum of 8% aromatic content is required for any synthetic fuel at the moment, though it is purely based on previous experience. Other components in the composition include sulphur, nitrogen and oxygen containing hydrocarbons, which are all in trace amount.

### **2.1.2 Alternative Fuels**

Currently, there are three possible production pathways to produce alternative fuels, which are Fatty Acid Ester (FAE) via transesterification process, 'XtL' via Fischer-Tropsch synthesis, and Hydroprocessed Renewable Jet fuel (HRJ) via hydroprocessing of vegetable oils. Restricted by the fuel specification in aviation industry, FAEs are not regarded as a suitable candidate alternative fuel due to the presence of metals in the final product [28].

#### **2.1.2.1 FAE**

FAEs are long chain fatty acid ester groups derived from the transesterification process. It is commonly known as biodiesel and when methanol is used in the transesterification process, FAME (fatty acid methyl ester) will be the final product (Fig. 2). As metal contamination may be introduced into FAME from the raw material, it can have an adverse effect on the hot end materials in the engine. So currently FAME is regarded as a type of contamination in aviation fuels.

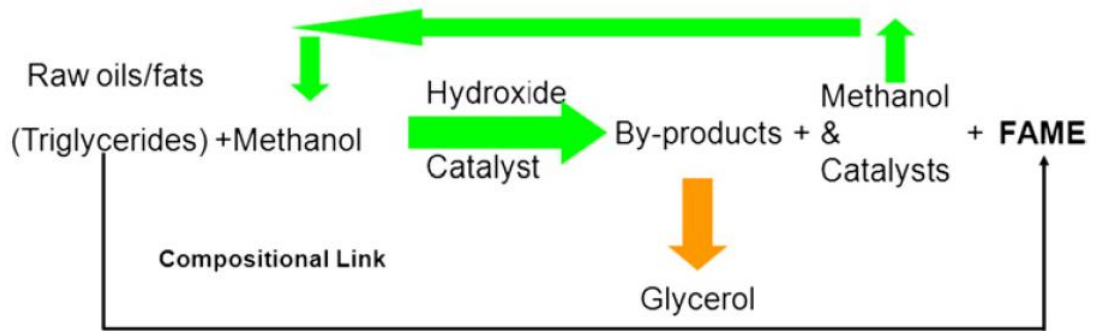
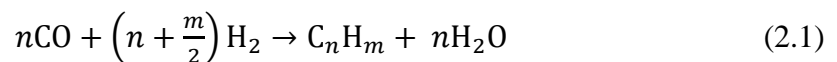


**Figure 2** The transesterification process of producing FAME [26].

#### 2.1.2.2 *'XtL'*

'XtL' means to convert 'anything to liquid' via the Fischer-Tropsch (FT) process. Depending on the feedstock used, the 'X' could be 'C' (coal), 'G' (gas) or 'B' (biomass). The FT process principally involves carbon chain building, requiring a synthesis gas (syngas) feedstock. Syngas is a gaseous mixture of hydrogen and carbon monoxide derived from coal, gas or biomass. The production process of long chain paraffins could be presented as the following equation:



Then, the crude yield goes through a hydrocracking process to produce the final product, synthetic paraffinic kerosene (SPK), the carbon numbers of which can be controlled depending on the operating temperature, pressure and syngas composition. The process is illustrated in Figure 3 and typical compositions of various FT fuels are shown in Figure 4.



**Figure 3** The Fischer-Tropsch process to produce synthetic fuel [29].

Comparing with current jet fuel, the compositions of synthetic fuels shown in Figure 4 are much ‘simpler’. Saturated hydrocarbons, i.e., normal, iso-, and cyclo-paraffins (up to 15% v), comprise the majority of the fuels, with near-zero sulphur, aromatics and metals. Due to the processing differences, significant difference exist amongst these fuels in the carbon number distribution as well as the ratio of normal to iso-paraffins and the presence of cycloparaffins. For instance, the Sasol IPK (Iso-Paraffinic Kerosene) and the Shell GtL are both confined to essentially 4-5 carbon numbers while S-8 and Sasol GtL-2 range over 9-10 carbon numbers. Sasol GtL-1 has the most normal paraffins that could be expected, while Sasol IPK is at the other extreme with almost no normal paraffins.

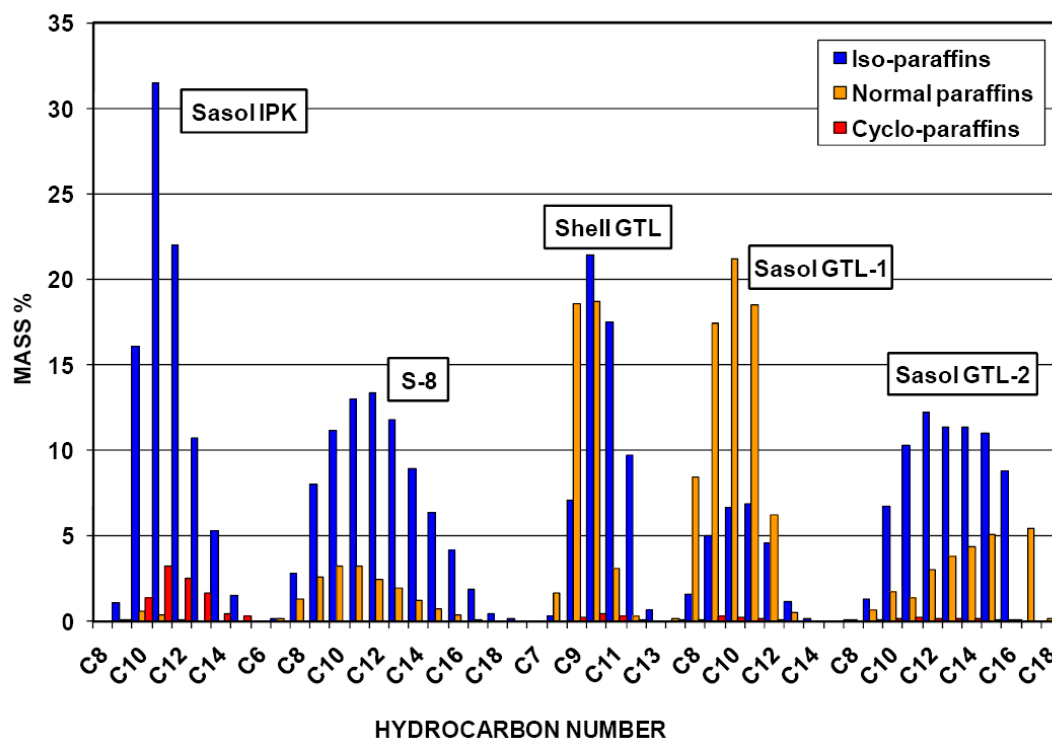


**Figure 4** Typical GC analysis results of a range of FT fuels. Sasol IPK is a CtL, S-8 syntrolyums GtL, Shell GtL and two Sasol GtL's from Sasol Oryx plant [1].

### 2.1.2.3 HRJ

An alternative fuel produced via the hydroprocessing of biomass oils is called ‘HRJ’ or ‘Hydroprocessed Renewable Jet’ Fuel [30]. These fuels are created using a

process that first uses hydrotreatment to deoxygenate the oil and then uses hydroisomerization to create normal and isoparaffinic hydrocarbons that fill the distillation range of current jet fuel (as shown in Fig. 5). A number of airline companies, as mentioned at the beginning of this chapter, have already carried out demonstration flights on HRJs. Typical compositions of HRJs used in tested flights are listed in Figure 6. The exact composition of HRJs vary, depending on the feedstock; however, their carbon numbers generally range from C9 to C16 (Fig. 2.6), and they mainly consist of iso-paraffins as well as a small proportion of normal paraffins.

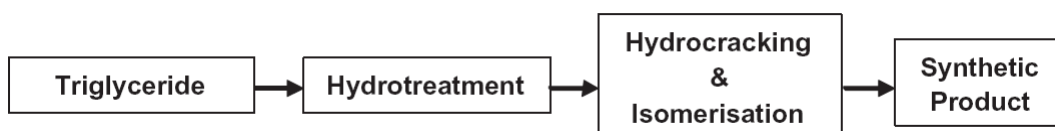


**Figure 5** Hydroprocessing of vegetable oil [31].

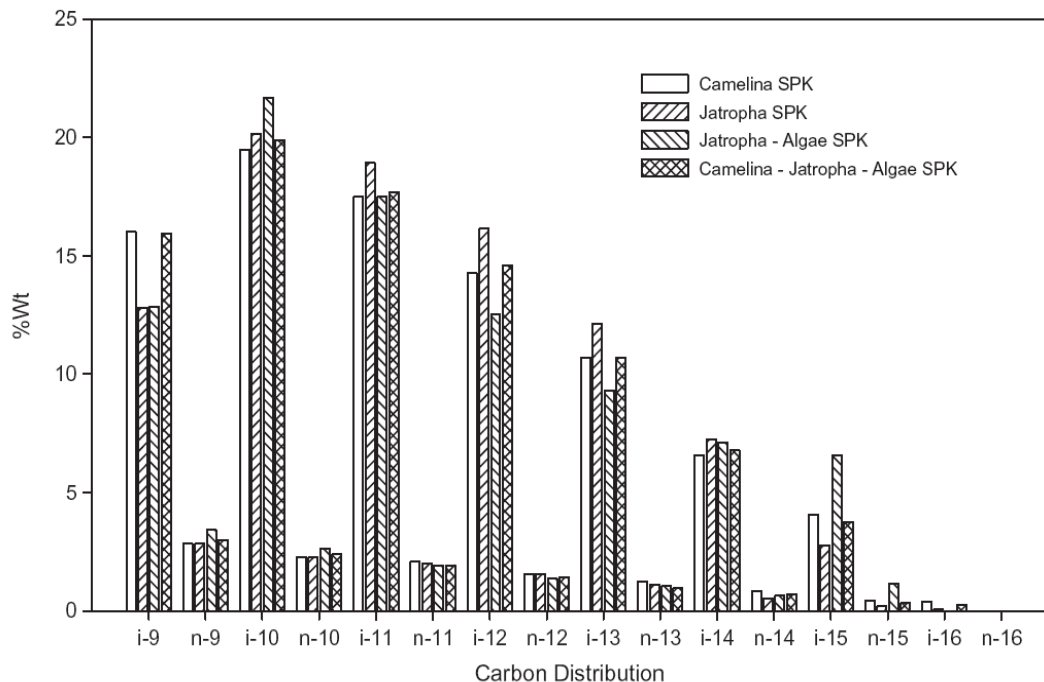


**Figure 6** Typical compositions of HRJs produced by the UOP process [32].

The composition of SPK derived from either FT or hydroprocessing process is quite different from conventional jet fuel. Generally, it is a combination of three paraffin species (normal, iso-and cyclo-) or two (normal and iso-) which makes up the main body of a fuel. No aromatic species becomes a significant difference. This change in composition has demonstrated some promising benefits in fuel properties. One of the main benefits gained is that alternative fuels provide significant environmental benefits due to reduced particulate emissions [26]. However, issues may arise as well, such as their compatibility with existing elastomeric sealing materials in the fuel system.

## **2.2 Elastomeric Seals**

An elastomer is a rubber-like polymer with the property of viscoelasticity, which means it exhibit both viscous and elastic characteristics when undergoing deformation. Its unique property is widely used in many industrial sealing applications.

### **2.2.1 General properties of elastomers**

The most important physical characteristic of elastomers is the high degree of deformability exhibited under the action of small stresses. Figure 7 shows a typical force-extension curve for natural rubber. The curve is non-linear, hence it is not possible to assign a definite value to Young's modulus except in the region of small strains. In this region its value is of the order of  $1.0\text{N mm}^{-2}$ . These properties-high extensibility and low modulus- are enormously different from a typical hard solid (e.g. steel), for which the value of Young's modulus is  $2.0 \times 10^5\text{N mm}^{-2}$  and the corresponding maximum elastic extensibility is about 1.0 per cent or less.

Elastomer also possesses a number of other properties such as the thermal or thermoelastic properties. Elastomer contracts (reversibly) on heating when held in the stretched state under a constant load; and gives out heat (reversibly) when stretched.

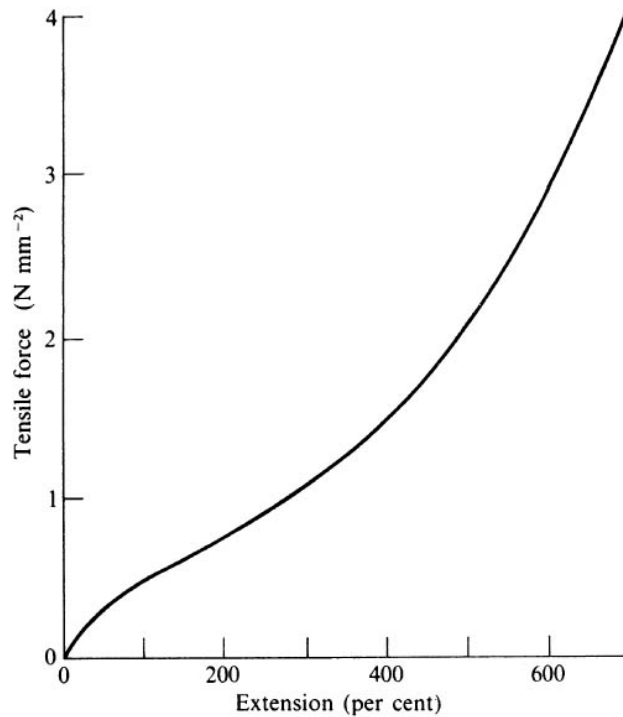


**Figure 7** Typical force-extension curve for natural rubber [113].

Chemically, a rubber is essentially a hydrocarbon. For example, a polymer of isoprene ( $C_5H_8$ ) built up in the form of a continuous chain having the structure shown in Fig. 8. The succession of isoprene units in the chain is perfectly regular, with every fourth carbon atom in the chain carrying the methyl ( $CH_3$ ) side-group. The presence of the double bond is very important, since it is this that largely determines the chemical reactivity of the molecule and its ability to react with sulphur or other reagents in the vulcanization process. The double bond is also responsible for the susceptibility of the molecule to oxidation or other degradative reactions leading to a deterioration of physical properties (aging).

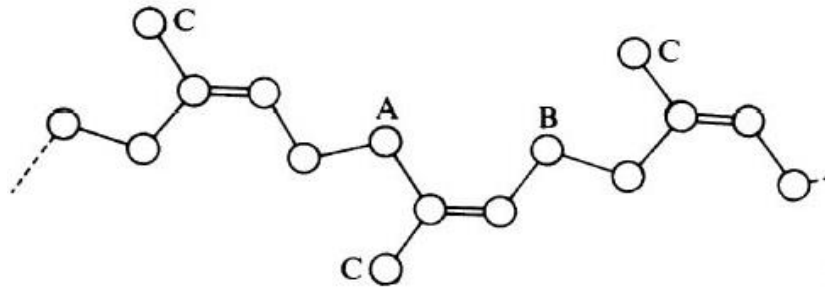


**Figure 8** The structure of the molecule of isoprene (A-B=isoprene unit; C=methyl group) [113].

The inherent elasticity of the long-chain molecule is sufficient in itself to confer highly elastic properties on a material in bulk. However, this is only one of the necessary conditions. In order for a material to exhibit rubber-like properties, the following three requirements must be satisfied:

1. the presence of long-chain molecules, with freely rotating links;
2. weak secondary forces between the molecules;
3. an interlocking of the molecules at a few places along their length to form a three-dimensional network.

The second arises from the consideration that, if the individual chain is to have the freedom to take up the variety of statistical conformations upon which the phenomenon of rubber-like elasticity ultimately depends, its motion must not be impeded by the surrounding molecules; this implies that the forces between the molecules shall be weak, as in a liquid. However, if this were the only requirement, the material would in fact behave as a liquid, and not as a solid. The third condition is introduced in order to overcome this difficulty. By the introduction of a certain number of cross-linkages or junction points between the chains at a very few points along their length it is possible to produce a coherent network in which all the molecules are linked together and hence can no longer move independently as in a liquid. The necessary cross-linkages between chains are normally introduced by the process of vulcanization, which is a chemical reaction with sulphur.

### 2.2.2 How an elastomeric seal works

An elastomeric seal (O-ring in this case) works by blocking any potential leak path of a fluid between two closely spaced surfaces. As the two surfaces are brought together, they squeeze the cross-section of the O-ring and this results in a deformation of the O-ring cross-section. The greater the squeeze, the larger the deformation. The unique characteristic of the elastomer, which has a capacity to remember its original shape for a long time, makes the O-ring such a good seal.

In low pressure applications (in which the confined fluid exerts little or no pressure on the O-ring), the tendency of the elastomer to maintain its original shape creates the seal (Fig. 9). As the O-ring is deformed when the mating surfaces are brought together, it exerts a force against the mating surfaces equal to the force necessary to squeeze it. The areas of contact between the O-ring and the mating surfaces (contact bands) act as a barrier that blocks the passage of the fluid. The sealing condition in this project applies the principle of this low pressure application.

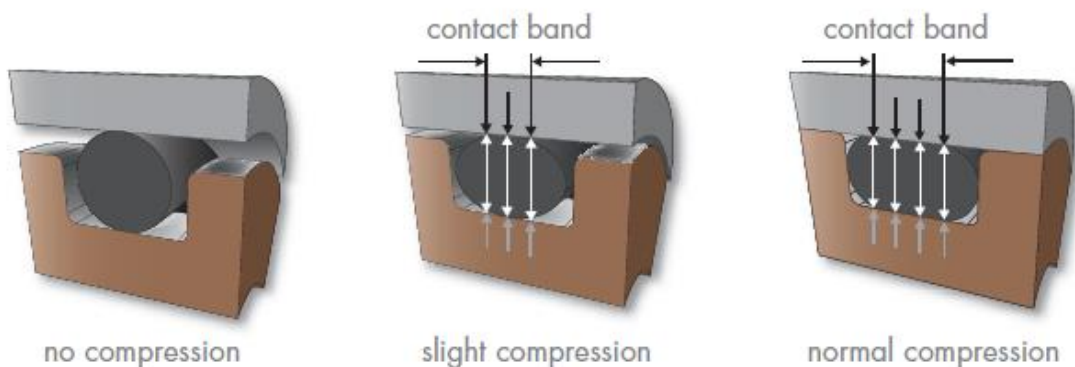


**Figure 9** O-ring sealing in low pressure application.

In applications in which higher pressure is exerted by the confined fluid (gas in most cases), the sealing action of the O-ring caused by the squeeze of its cross-section is augmented by fluid pressure, transmitted through the elastomer. The O-ring is forced to side of the groove and as a result, the O-ring cross-section is deformed into a ‘D’ configuration. The elastomer exerts equal force in all directions and is forced up to

the gap between the mating surfaces.

### 2.2.3 Swelling phenomena

The property of swelling in suitable low-molecular-weight liquids is one which is possessed by a wide range of polymers. It is markedly dependent on the nature of the swelling liquid. Both natural and synthetic rubbers are soluble in organic – hydrocarbon – solvents. It is important to understand the swelling behaviour of a rubber material in a solvent before any actual application.

#### 2.2.3.1 General thermodynamic principles

In swelling, the equilibrium between phases (mixed and pure phases) need to be considered. The mixed phase (contains two components) is the solid while the pure phase (contains one component) is the liquid. The equilibrium of this system is determined by the condition that its free energy shall be a minimum with respect to changes in the composition of the mixed phase. The *Gibbs free energy of dilution*  $\Delta G_1$  is introduced to represent this change quantitatively. It is defined as the transfer of unit quantity (1 mol) of liquid from the liquid phase to a very large quantity of the mixed phase. For a system at constant pressure the condition for equilibrium with respect to the transfer of liquid is

$$\Delta G_1 = 0 \quad (2.2)$$

The total free energy of dilution may be expressed as follows:

$$\Delta G_1 = \Delta H_1 - T\Delta S_1 \quad (2.3)$$

Where  $\Delta H_1$  is the heat of dilution and  $\Delta S_1$  is the entropy of dilution. When only one component has an appreciable vapour pressure, the molar free energy of dilution is given by

$$\Delta G_1 = RT \ln(p/p_0) \quad (2.4)$$

Where  $p$  is the vapour pressure of the liquid component in equilibrium (swollen rubber) at the temperature  $T$  and  $p_0$  is its saturation vapour pressure. Thus,

$$\Delta H_1 = \frac{\partial(\Delta G_1/T)}{\partial(1/T)} = -RT^2 \frac{\ln(p/p_0)}{\partial T} \quad (2.5)$$

### 2.2.3.2 Relation between swelling and modulus

For a given polymer, there is a unique relationship between the equilibrium degree of swelling and the modulus. Flory showed for high degrees of swelling, this relationship could be approximately presented as

$$(\rho V_1/M_c) \cong (\frac{1}{2} - \chi)v_2^{\frac{5}{3}} \quad (2.6)$$

Where  $M_c$  is the molecular weight, the elastic modulus  $G = \rho RT/M_c$ ;  $\chi$  is a parameter which includes a component due to the entropy in addition to the purely energetic contribution  $\Delta H_1$ , i.e.

$$\chi = \chi_0 + \alpha/RT \quad (2.7)$$

Using a series of differently cross-linked butyl rubbers, Flory presented his results in the form of a double logarithmic plot of the force per unit unstrained area at a given strain (which is proportional to  $\rho RT/M_c$ ) against the equilibrium degree of swelling ( $1/v_2$ ) in cyclohexane. The data (Fig. 10) fell on a straight line of slope  $-\frac{5}{3}$ , in agreement with Eq.2.6.

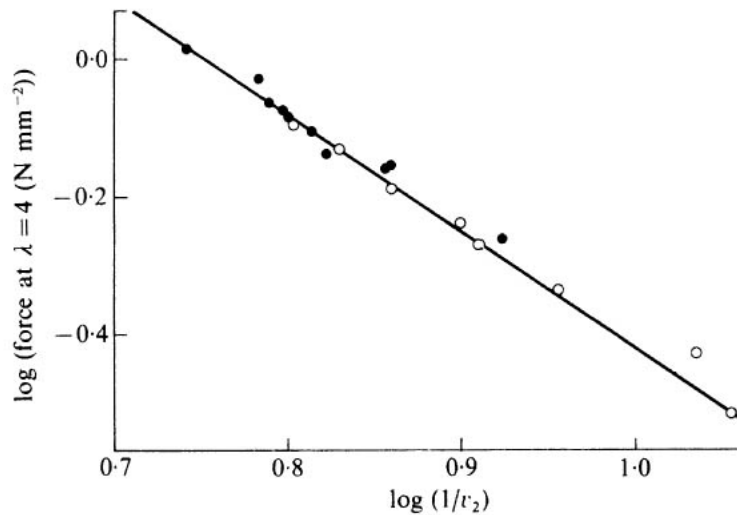


**Figure 10** Relation between equilibrium swelling ( $1/v_2$ ) and modulus for butyl rubbers with various degrees of cross-linking [113].

### 2.2.3.3 The dependence of swelling on strain

A series of experiments have confirmed the increase of swelling with extension. The quantity which determines the direction of the change of swelling is the hydrostatic

component of the applied stress. For a simple hydrostatic pressure this leads directly to a reduction of swelling with increasing pressure. A uniaxial compressive stress  $t$  is equivalent to a hydrostatic pressure of magnitude  $t/3$  together with two shear stresses of the same numerical value. It may be assumed that the shear stresses have no effect on the swelling. The total effect of the uniaxial compressive stress therefore arises from the hydrostatic pressure component, which produces a reduction in the swelling. Conversely, by the same argument, a tensile stress, for which the hydrostatic pressure component is negative, would be expected to lead to an increase in swelling.

#### **2.2.4 The glass-rubber transition**

The rubber-like state of an elastomer depends on the possibility of random thermal motion of chain elements by rotation about single bonds in the chain backbone. In reality, this rotation cannot be completely free due to the restrictions imposed by the presence of neighbouring groups of atoms either in the same molecule or in neighbouring molecules. The degree of freedom of rotation will be a function of the relative values of the thermal energy of the rotating group and the potential barrier that has to be overcome in order that rotation may occur. The probability that a given group will have sufficient energy to enable it to surmount a potential barrier  $\varepsilon$  will be governed by a Boltzmann factor of the type  $\exp(-\varepsilon/kT)$ , and will therefore increase rapidly with increase in temperature. Conversely, on lowering the temperature a point will be reached at which rotation will no longer take place at an appreciable rate. In this state, the material ceases to behave like a rubber and becomes hard and rigid like a glass.

The transition from the rubber-like to the glassy state is a phenomenon which is encountered in all rubbers, whether vulcanized or unvulcanized, though the temperature at which this transition occurs naturally depends on the chemical constitution of the molecule. The geometrical structure is not affected by the transformation, being still of the random or amorphous type. The transition to the

glassy state is accompanied by changes in certain other physical properties in addition to the changes in elastic properties. Of these the most important is the change in expansion coefficient. This is shown in the top curve in Figure 11, representing the volume-temperature relationship for raw rubber in the amorphous state. The change in slope at the transition temperature corresponds to a considerable increase in expansivity which is usually interpreted as a direct result of the increase in molecular mobility associated with the rubber-like structure. The glass-rubber transition is not a structural change there is no *first-order* change in specific volume (or density). For this reason the glass-rubber transition is sometimes referred to as a *second-order* transition.

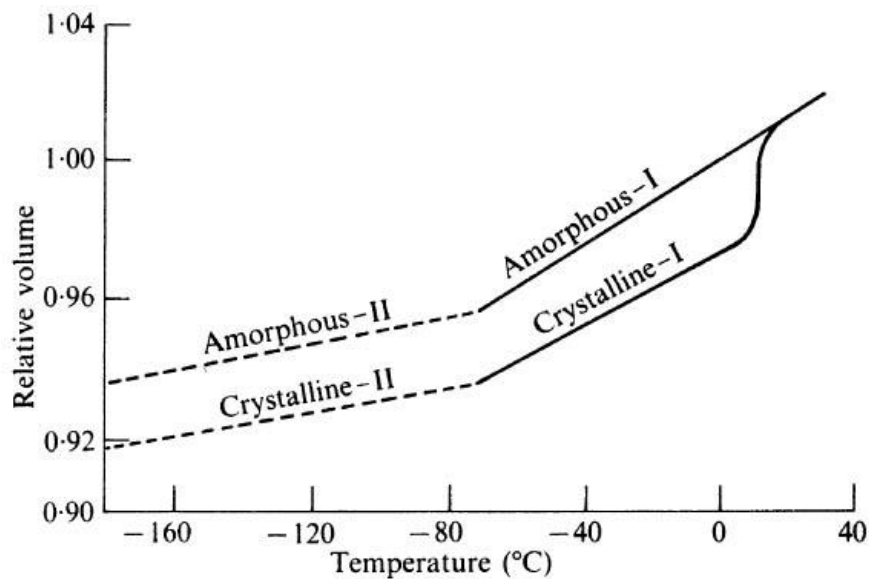


**Figure 11** Volume-temperature relationship for purified rubber, showing second-order transition at  $-72^{\circ}\text{C}$  and crystal melting at  $11^{\circ}\text{C}$  [113].

The temperature at which the rubber-glass transition occurs is an extremely important property of a polymer. For general-purpose rubbers, it is important that this temperature shall be sufficiently low to avoid undesirable energy losses over the range of temperature likely to be encountered in actual use. The factors which determine the transition temperature are primarily the strength of the intermolecular forces and the degree of flexibility of the chain. Bulky or highly polar side-groups

introduce steric hindrances to internal rotation about bonds as well as increasing the intermolecular forces; such groups therefore tend to raise the glass transition temperature.

The glass transition phenomenon also can be found in the stress-temperature relations (Fig.12). For a given state of strain, the stretching force should be proportional to the absolute temperature over a wide temperature range. In the region of lower strains, however, the behaviour appeared to be anomalous, the force increasing less rapidly than would be expected theoretically, or even actually decreasing as the temperature was raised. This reversal in slope of the stress-temperature plots occurs at an extension of about 10 per cent – the so-called *thermoelastic inversion point*.

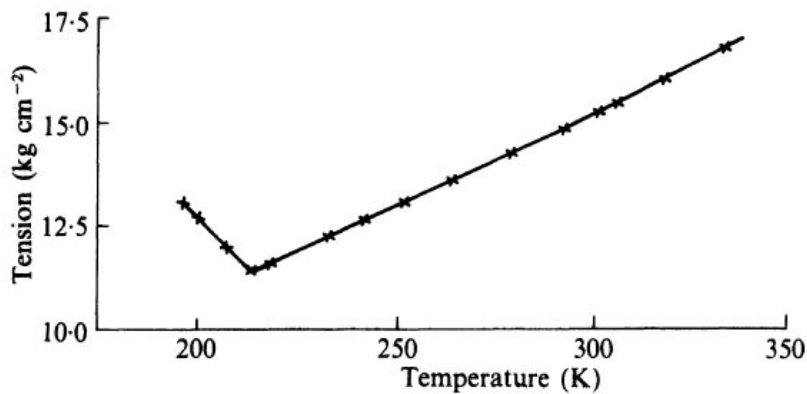


**Figure 12** Force at constant length as function of absolute temperature (extension 350 per cent) [113].

### 2.3 Elastomer Compatibility Issue

In an aircraft engines' fuel system, the most commonly used elastomeric material is O-rings. An O-ring is a doughnut-shaped ring moulded from elastomeric material which is squashed between two mating faces of a fuel system. It deforms into the gap between the faces, and thus provides a seal between them [33]. O-rings employed in the fuel system are typically comprised of nitrile, fluorosilicone and fluorocarbon polymers. In order to investigate the compatibility issue of elastomeric

material with alternative fuels, it is essential to understand generally what would happen when a polymer is in contact with fuels.

### **2.3.1 Basic principles of fuel-polymer interaction**

In the absence of chemical reactions, two processes can occur when a new polymeric material is exposed to fuel for the first time. First of all, the material may absorb components from the fuel (alkanes, aromatics, additives, etc.) which would usually cause the material to swell and soften. Secondly, the fuel may extract components from the material (plasticizers, processing aids, residual solvents, etc.) which would generally cause the material to shrink and harden. The overall effect of the fuel has on the material will be the balance of these two processes. Once the material has been in service for some time, the fuel-extractable components will have been removed and all subsequent changes in physical properties will result from a shifting equilibrium between the material and the fuel, which in turn will depend on the composition of the fuel [34].

Fundamentally, the process of an elastomeric material absorbing a fuel is governed by the chemical physics of polymer solutions, specifically when the fuel first wets and then penetrates into the polymer matrix. Thermodynamically, this process begins with the separation of fuel molecules from the bulk fluid through the breaking of fuel-fuel intermolecular bonds. Next, a cavity large enough to accept the fuel molecule must be opened in the polymer by breaking polymer-polymer intermolecular bonds on adjacent polymer strands, a process that imparts elastic strain on the polymer surrounding the penetration site. Finally, the fuel molecule is inserted into the polymer, creating polymer-fuel bonds. Energetically, this process can be expressed as the breaking of fuel-fuel intermolecular bonds (requiring energy), the separation of the polymer-polymer intermolecular bonds (requiring energy), and the making of polymer-fuel intermolecular bonds (releasing energy). Considering the overall energy balance of these processes, the strength of interaction between the fuel and polymer depends on the size and shape of the fuel molecules, the

intermolecular bonding of the polymer, the intermolecular bonding of the fuel, and the intermolecular bonds that form between the polymer and the fuel penetrants [34].

The more energetically favourable the overall diffusion and equilibrium processes become, the greater the corresponding volume swell of the polymer, especially for O-ring seals. The swelling behaviour is an important characteristic for an O-ring since it can have a significant impact on its sealing performance; appropriate degree of swelling can help seal the fuel to prevent leakage. Generally, the swelling ability of a species increases with increasing polarity and hydrogen bonding and decreasing molar volume [34]. The paraffinic species are relatively large and inert, having only dispersive intermolecular bonding. In contrast, aromatic compounds of similar molecular weight have a smaller molar volume and exhibit both polar and hydrogen bonding, typically resulting in enhanced volume swell characteristics.

### **2.3.2 Molecular Transport of Solvent into Polymer**

As mentioned above, when a polymer material is in contact with fuel or solvent, a transition of solvent molecules into the polymer occurs. Understanding this molecular transport process can help to comprehend the fuel-polymer interaction and furthermore, the impact of fuel on polymers. Soney and Sabu [35] summarized the factors that influence the molecular transport process through polymers in their work. From the polymer point of view, the nature of polymer, crosslinks, plasticisers and fillers are influential; while the characteristics of the penetrant and also temperature conditions have considerable impacts as well. Generally, the most influential factor determines the transport process is the nature of polymer itself; the free volume within the polymer and segmental mobility influence the transport process directly, while other factors such as the nature of crosslinking and substituents can indirectly influence the process by altering the polymer structure. The size and shape of penetrant molecule will influence the rate of transport within the polymer matrix; the diffusivity decreases with the increase in the size of penetrant. For instance, aromatic compounds are easier to penetrate into the polymers than paraffins due to their

smaller molecular size. Furthermore, the increase of temperature can also accelerate the transport process.

#### 2.3.2.1 Aromatic compounds

An early study investigating into the aromatic hydrocarbons (toluene, p-xylene and mesitylene) penetrating into and out of natural rubber (NR) was conducted by Sombatsompop and Christodoulou [36]. It was concluded with a few important indications which are helpful for further understanding the fuel-polymer interaction. Results indicated that a few factors determined the degree of swelling and deswelling of NR, which were the flexibility and mobility of polymer chains, size of the penetrants, temperature, and the desulphuration and decomposition reactions of the crosslinks. The overall degree of swelling, before and after reaching equilibrium, was affected by the characteristics of the penetrants; whereas during the equilibrium state, it was influenced by the types of crosslinks in the polymer. The reduction in mechanical properties, such as tensile strength during swelling was due to the conversion of mechanical energy into an activation energy, which was used to achieve the penetration of the solvents into the polymer matrix. After deswelling, the properties of NR were partial recovered which was related to the stress relaxation of the polymer molecules.

Saleem et al. investigated the effect of the size and shape of organic penetrant molecules on the rate of diffusion through low-density polyethylene (LDPE) [37]. The diffusivity was found to be higher for linear, flexible, or symmetrical molecules and generally decreases with increasing molar volume. An example presenting these two characteristics was they found the diffusivity of xylenes decreased as *p*-xylene (symmetrical molecule structure) > *m*-xylene > *o*-xylene, which is also the order of increasing molar volume.

#### 2.3.2.2 Paraffins

Results from another molecular transport experiment carried out by Aminabhavi and

Phayde [38] supported the conclusions that Sombatsompop and Christodoulou drew. Instead of aromatic compounds, aliphatic alkanes (normal paraffins such as n-decane and n-octane, iso-paraffins such as iso-octane, and cycloparaffins such as cyclohexane) were selected as the penetrants and the polymer used was Santoprene, a mixture of in-situ cross linking of EPDM rubber and polypropylene. The transport coefficients calculated in this study also showed a dependence on the penetrants size, temperature and the crosslink status of the Santoprene. An important observation was the diffusion ability of n-octane (straight-chain molecule) at all temperatures was better than that of its isomer, namely iso-octane (branched-chain molecule), which is due to the rigidity of iso-octane. This means iso-octane requires greater activation energy than n-octane to penetrate into the polymer network. Cyclic penetrants such as cyclohexane exhibited considerably higher sorption into the polymer than any of the normal or iso-paraffins tested. As the temperature increased, the diffusion and relaxation rates of the polymer increased as well as the free volume inside the polymer. This resulted in a higher volume of penetrants being absorbed into the polymer at the equilibrium status. None of the paraffins used has shown any degradative reactions towards Santoprene during the course of the study, indicating these solvents were chemically compatible with this polymer material.

### **2.3.3 Petroleum-Derived Fuel vs. Synthetic Fuel**

In early 2009, NASA conducted an Alternative Aviation Fuel Experiment (AAFEX) in California to investigate the effects of synthetic fuels on engine performance and emissions [2]. The results from the engine performance tests were satisfactory as the FT fuel tested presented similar combustion characteristics to the petroleum-derived fuel. However, an ‘accident’ occurred during the test as fuel leaked in the aircraft fuel system and tanker trucks when the pure FT fuels were used due to the absence of aromatic compounds. No leaks were seen with the engine fuelled with the blended fuels with conventional jet fuel. Based on this and other reasons, suggestions were given for the initial adoption of alternative fuels for aviation would be the synthetic/conventional blends.

The ‘accident’ happened in the AAFEX project demonstrated a significant impact of synthetic fuels on current aircraft fuel system. Historically, conventional jet fuel does not have any compatibility issue with O-ring seals due to the presence of aromatic compounds (up to 25% v) in its composition. However, if alternative fuels are used in current system, compatibility issues may arise due to the change of fuel composition, especially the absence of aromatic compounds. O-rings may harden and shrink, or no longer swell to the required volume, resulting in fuel leakage. A number of compatibility tests on alternative fuels with O-ring materials have already been conducted in recent years and research is going on to address and further understand this issue.

To investigate into the elastomer compatibility issue, the first step is to find out what impact synthetic fuels may have on seals compared with the conventional one. Measurements carried out by Gormley et al [39] showed that when nitrile O-rings were in contact with fuels, either JP-5 (petroleum-derived) or S-5 (a synthetic fuel derived from FT process), many of the plasticizer and stabilizer compounds were removed from the O-rings. The amount and type of plasticizers and stabilizers that were removed is roughly the same in both JP-5 and S-5 fuel. Molecules were observed to migrate into the O-rings for petroleum-derived fuel, but less for synthetic fuel. The important indication from this study is that the extent to which the components are removed from nitrile O-rings is similar for both petroleum-derived and synthetic fuels.

Muzzell et al [40] [41] compared the material compatibility of nitrile elastomer coupon and O-rings with a range of selected petroleum-derived fuels and FT synthetic fuels. These studies provided a baseline for predicting the effects of static elastomer swell to the potential degree of swell/shrink that can be expected when fuels are ‘switch-loaded’. The fuels tested had aromatic contents in increasing amounts as follows: S-5 (0% v), S-5+10% A150 (10% v), JP-5 (18% v), ECD-1 (19% v), and S-5+25% A150 (25% v). After a total static test period of 43 days,

changes of physical properties of the nitrile O-rings in various test fuels were measured according to ASTM D 471 [42] (Fig. 13). The non-linear responses of swell for nitrile coupons in JP-5, ECD-1 and S-5 + 25% A150 can be caused by the differences in fuel composition rather than only the concentration of aromatic compound. The differences in aromatic composition, such as the degree of alkylation on the aromatic ring and the molecular weight of the alkyl-substituted monoaromatic rings, could also explain the relative swelling effectiveness of these fuels [32]. For nitrile O-ring, it lost about 0.3% of its original mass and shrank by 3% of its original volume in S-5 due to the absence of aromatic compound. Both the mass and volume increased roughly proportional to the aromatic content in the fuels. When switch-loading between S-5 and JP-5 fuels, large swings in swell occur for both nitrile coupons and O-rings as shown in Figure 14. It was concluded that the impact on the nitrile elastomer when switch-loading synthetic and petroleum-derived fuel is highly dependent on aromatic hydrocarbon type and concentration.

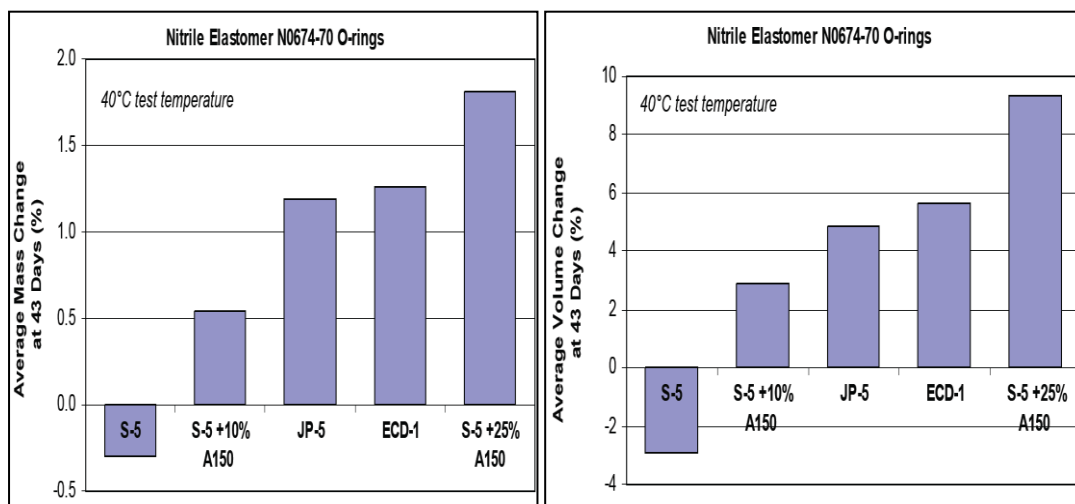


**Figure 13** Average volume change (%) of nitrile O-rings after 43 days [40].

S-5: a synthetic FT fuel; A150: a petroleum-based aromatic hydrocarbon fluid; JP-5: a petroleum fuel from Navy; ECD-1: petroleum-derived Emission Control Diesel.

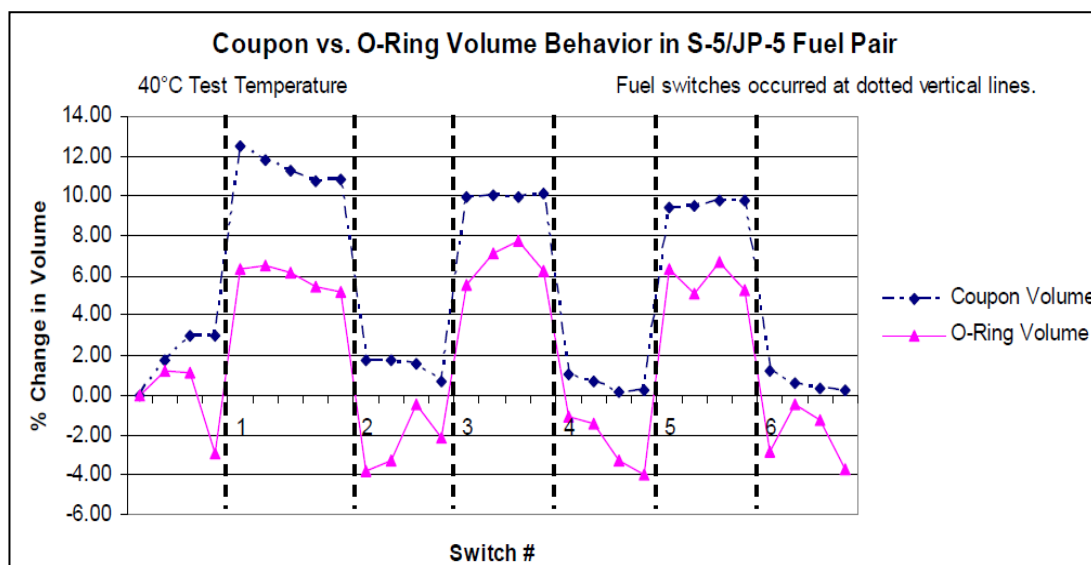


**Figure 14** Comparison of volume change between nitrile coupon and O-ring in S-5/JP-5 fuel pair cycling [41].

A different case was demonstrated in the study by Zabarnick et al, where they evaluated the properties of a coal-derived jet fuel [43]. Similar to other synthetic fuels, the coal-derived fuel also has only very low level of aromatic and polar species but has a very high level of cycloparaffins (as shown in Fig. 15). Cycloparaffins and dicycloparaffins comprise over 92% of its composition, while decalin, C<sub>2</sub>-decalin and C<sub>1</sub>-decalin consists nearly 50%. When comparing its volume swell with a typical petroleum-derived JP-8 fuel (containing 17% v aromatics) and an F-T fuel (S-8), interesting phenomena was observed as the coal-derived fuel presented the same swelling characteristics for nitrile O-ring as does JP-8, both of which swelled the O-ring by approximately 16% (Fig. 16). This observation suggested cycloparaffins, such as decalin and related compounds, may have excellent seal swell characteristics compared to paraffins. They recommended additional work to be done to confirm this observation and to identify if cycloparaffins can provide improved swell characteristics, not only as major fuel components, but also as additives at low level concentration to enhance the seal swell characteristics of FT fuels.

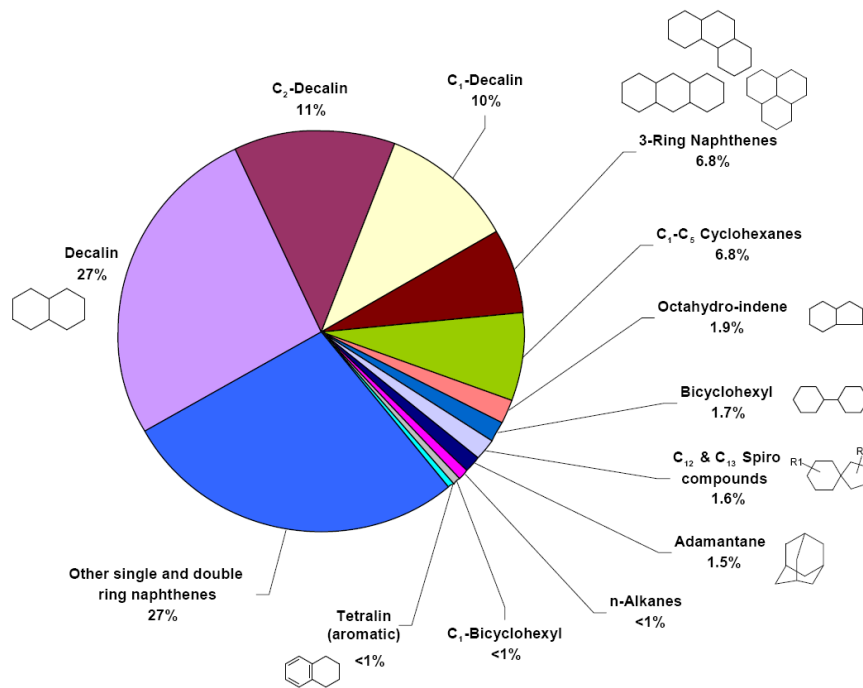


**Figure 15** Semi-quantitative composition of the coal-based jet fuel [43].

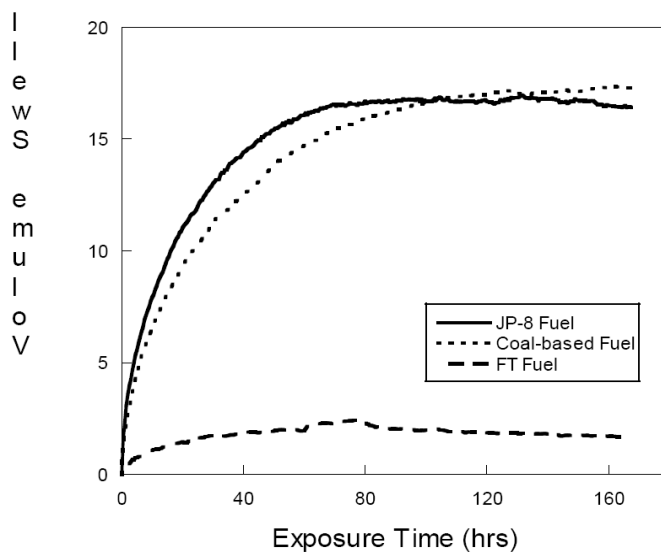


**Figure 16** Volume swell for nitrile O-rings aged in selected fuels at room temperature [43].

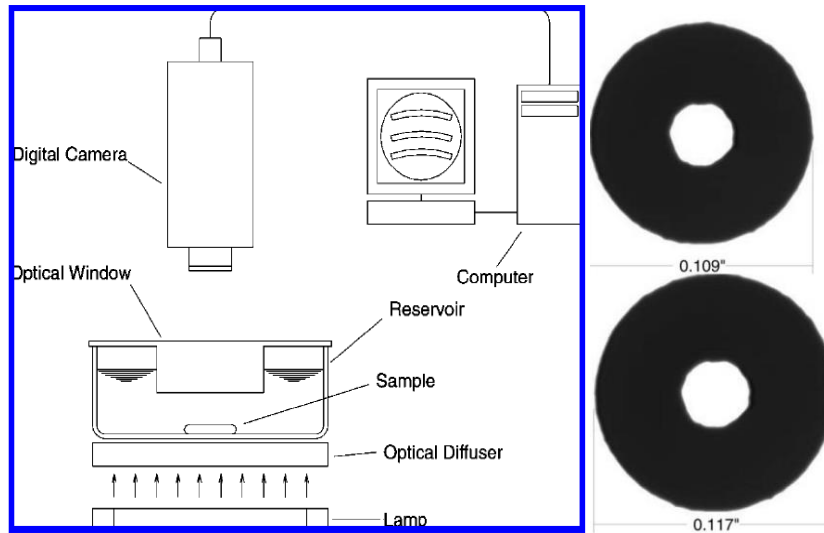
### 2.3.4 Efforts to Promote the Seal-Swell ability of Synthetic Fuels

A better understanding of the relationship between aromatic compounds and O-ring swell will help to find solutions for enhancing the compatibility of synthetic fuels with elastomeric seals. Due to their excellent ability to swell the O-rings, adding an

appropriate amount of aromatics into synthetic fuels is considered to be a potential solution to tackle the seal-swell problem. However, it needs to be bear in mind that the introduction of aromatics to synthetic fuels may significantly increase the cost of the fuel and cause changes to other fuel properties as well, such as to produce soot in emissions; as such, an overall evaluation of fuel properties is necessary.

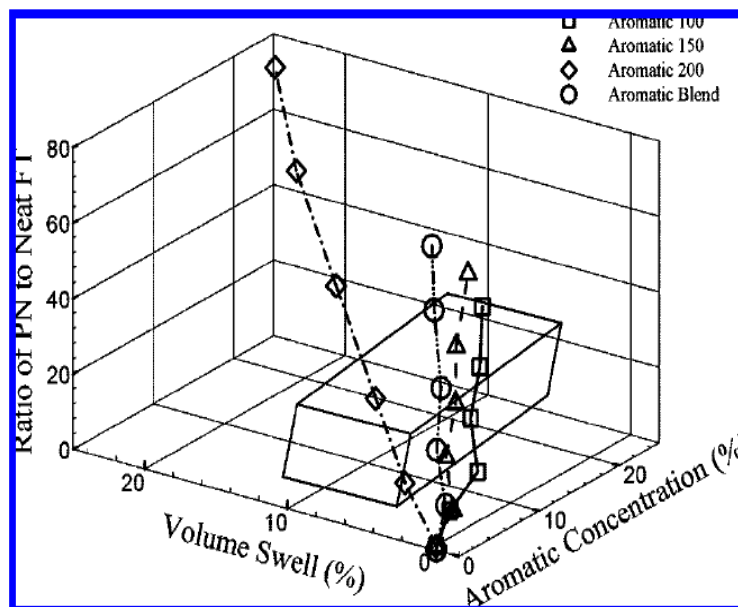
The ASTM D471 method to measure the volume change of O-rings is based on a water displacement technique which is not accurate enough. As the differences of O-ring volume changes in various fuels might be insignificant, more accurate measurement method is needed. DeWitt et al [44] developed a unique optical dilatometry system to measure the volume swell of O-rings in various fuels (Fig. 17). This system consists of a backlit fuel reservoir fitted with an optical window, the inner surface of which is immersed in the fuel to prevent condensation. A digital camera is mounted above the reservoir which periodically photographs the sample. The cross-sectional area of the O-ring sample is then extracted from the digital images. The test aimed to investigate the effect of aromatic solvent type and concentration on seal-swell characteristics as well as emissions. The aromatic solvents used were Aromatic 100, 150, and 200 produced by Exxon. Results obtained from this system further approved the volume swell characteristic of nitrile O-ring is linearly dependent on the total aromatic concentration and solvent type. It indicated that the overall swell is highly dependent on the naphthalene content within the fuel. The key factor influencing the volume swell of fluorosilicone O-ring was found to be the molar volume of fuel molecule; while fluorocarbon O-ring is relatively inert and as a result, presented very low percentage of volume swell. An interesting comparison made by DeWitt et al. was to relate particulate matter (PM) emissions to volume swell for various aromatic solvents as shown in Figure 18. It was noticed that the relation between PM emissions and volume swell appeared to be independent of aromatic type. This comparison showed that if either the PM emission production or volume swell was known, it might be possible to predict the other. However, this relationship might be limited to the types of aromatic solvents

used in this study.



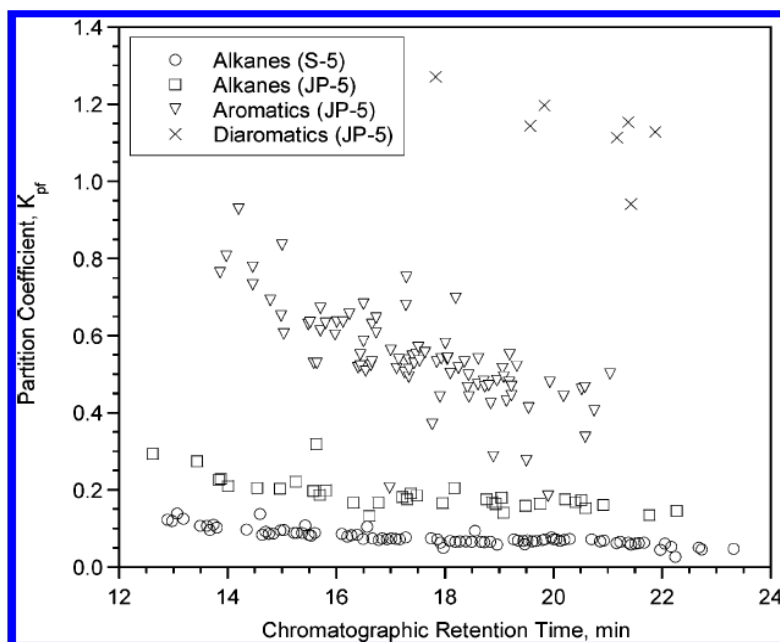
**Figure 17** Left: schematic of the optical dilatometry system used to measure volume swell as a function of time;

Right: representative optical dilatometry images of a nitrile O-ring before (up) and after (down) being immersed in fuel with aromatics for 16 hours [44].

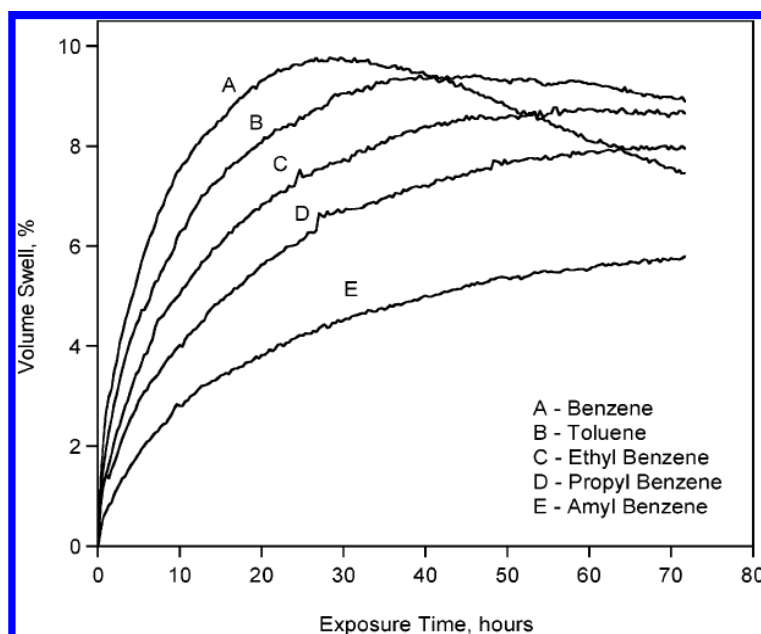


**Figure 18** Comparison of the emission propensity (normalized particle number) at engine idle and volume swell of nitrile O-rings as a function of aromatic solvent type and concentration [44].

Graham et al further examined the swelling of nitrile O-rings by selected aromatics blended in a synthetic jet fuel [45]. They employed a direct thermal desorption GC-MS system to calculate the partition coefficient between nitrile O-ring and selected compound classes in S-5 and JP-5. Results shown in Figure 19 indicated the partition coefficient increased as alkanes < aromatics < diaromatics, which was also the order of decreasing molar volume. Diaromatics, such as naphthalene, presented to be the most active species to swell the nitrile O-ring due to their relatively high hydrogen bonding as compared to that of the single-ring aromatics. The partition coefficient of alkanes in JP-5 was about twice as that for those of S-5. They explained the reason for this might be the higher degree of swelling of nitrile O-rings in JP-5 as compared to S-5. Volume swell data obtained from the optical dilatometry system (introduced above) showed the initial rate of swelling increases steadily with decreasing molecular weight (Fig. 20). However, in the case of benzene, the volume swell showed a maximum at about 27 h, after which the sample shrank. A much smaller effect was seen in the toluene data. They suggested that this observation indicates benzene is not only diffusing into the polymer but is also serving as a solvent to extract material from the O-ring, which results in a loss of volume swell following the initial stage of rapid swelling. This means it is possible to employ swelling promoters that can act too aggressively as solvents toward extractable components of the polymer. A contrast result obtained here compared with previous discoveries by Sombatsompop [36] and Saleem et al. [37], was the volume swell decreased as *o*-xylene > *m*-xylene > *p*-xylene, which is consistent with the order of decreasing rather than increasing polarity and molar volume. They argued the contrast in findings might reflect the importance of the strongly polar cyano group in nitrile rubber and how penetrant molecules interact with this group. And it might also indicate a difference in the behaviour of a neat polar penetrant against a penetrant diluted in a non-polar liquid phase. Details of discussion were included in their work. The overall conclusion they drew was the volume swell characteristic of nitrile O-ring in synthetic fuel can be promoted by small aromatic molecules with significant hydrogen-bonding or polar character.

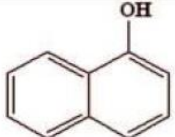
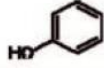
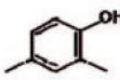
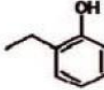
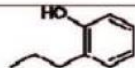
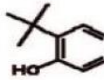
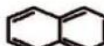
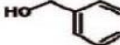
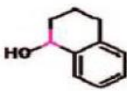
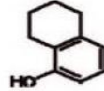


**Figure 19** Partition coefficient between nitrile O-ring and selected compound classes in S-5 and JP-5 vs. chromatographic retention time after aging at room temperature for 7 days [45].



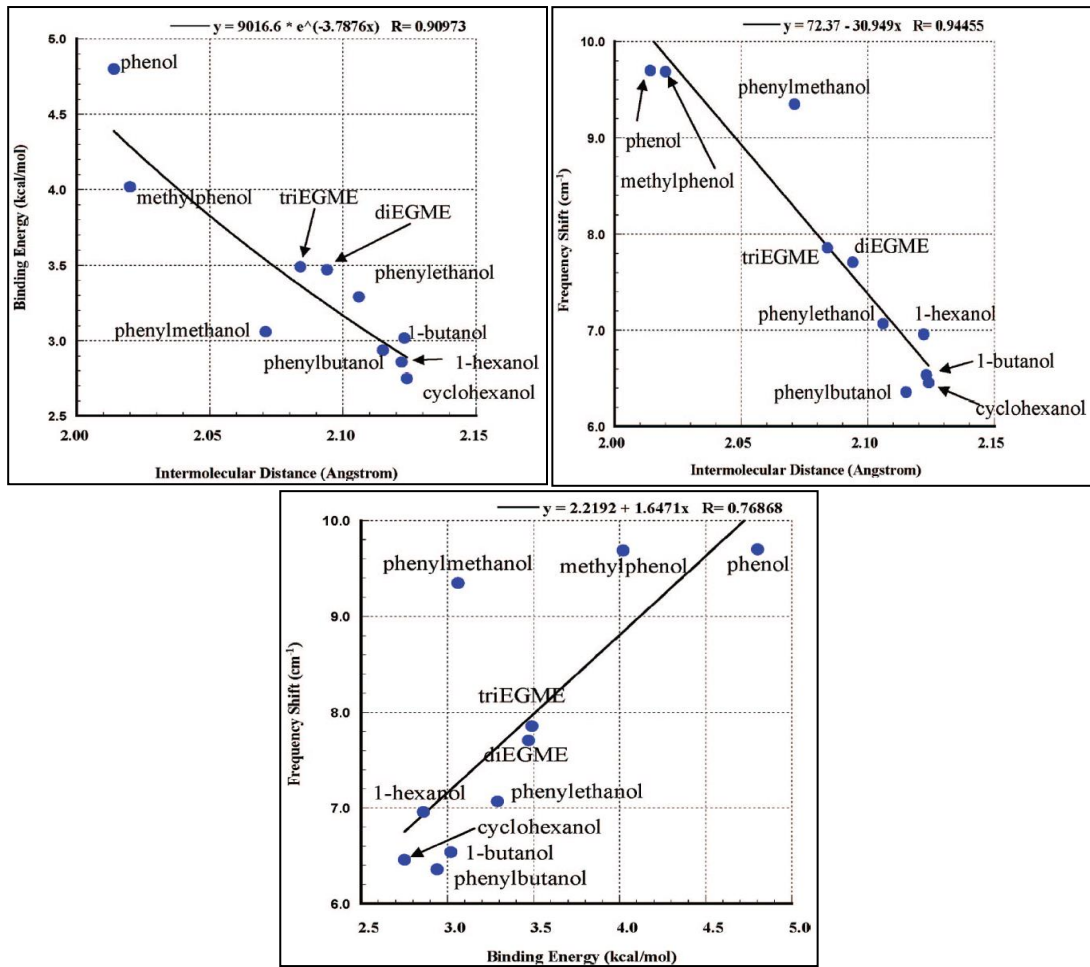
**Figure 20** Volume swell as a function of time for nitrile O-rings aged in S-5 + 10% v/v of each aromatic compound at room temperature [45].

Link et al compared the propensity of certain organic species to enhance the seal swell characteristics of synthetic fuels and identified promising additives [46]. A range of candidate species were blended with S-5 at 1% (wt.) for solids and 1% (v) for liquids and then measurement was carried out on the volume change of nitrile O-rings. Additionally, the performance of molecular structural analogues across phenol species was also studied to evaluate the role of molecular structure plays in the seal swelling process. Results suggested that the ability to swell the O-ring decreases as the level of substitution on the 5-membered ring increases, which was in agreement with the previous finding that smaller molar volume and symmetric species swell the polymer better. Phenolic structures showed the most promising volume swell ability; however, this class of species has moderate toxicity and oxidative instability mechanism. As a result, phenols are not an acceptable seal swell solution for synthetic fuels. Finally, they identified benzyl alcohol as the potential suitable additive as a concentration of 0.75% (v) induces similar swell as the petroleum-derived fuel. Furthermore, it was found that the addition of benzyl alcohol additive into S-5 did not degrade the high thermal oxidative stability of this synthetic fuel.

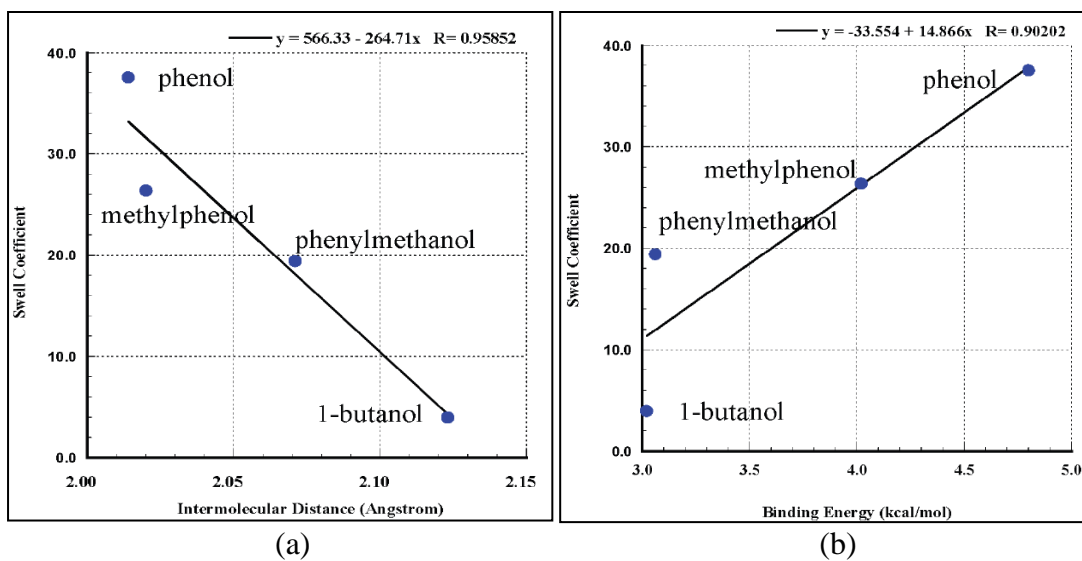
Spiked mixture (% v/v)	Structure of Additive	Volume change (%) <sup>a</sup>
S-5 + 1-naphthol (0.2%)		3.3 ± 0.1
S-5 + 1-octanol (1%)		2.5 ± 0.3
S-5 + 1-naphthol (0.5%) + 1-octanol (1%) <sup>b</sup>	See above	7.8 ± 0.1
S-5 + 1-naphthol (1%) + 1-octanol (1%) <sup>b</sup>	See above	13.3 ± 0.6
S-5 + phenol (1%)		15.4 ± 1.0
S-5 + 2,4-dimethylphenol (1%)		12.8 ± 0.4
S-5 + 2-ethylphenol (1%)		13.5 ± 0.5
S-5 + 2-propylphenol (1%)		12.0 ± 0.2
S-5 + 2- <i>t</i> -butylphenol (1%)		8.9 ± 0.1
S-5 + decalin (1%)		0.8 ± 0.1
S-5 + tetralin (1%)		0.9 ± 0.1
S-5 + naphthalene (1%)		1.2 ± 0.5
S-5 + benzyl alcohol (0.5%)		6.8 ± 0.1
S-5 + benzyl alcohol (0.75%)	See above	13.0 ± 0.0
S-5 + benzyl alcohol (1%)	See above	17.5 ± 0.4
S-5 + 1,2,3,4-tetrahydro-1-naphthol (1%)		4.6 ± 0.0
S-5 + 5,6,7,8-tetrahydro-1-naphthol (1%)		7.3 ± 0.4
S-5 + diEGME (1%)		1.7 ± 0.1

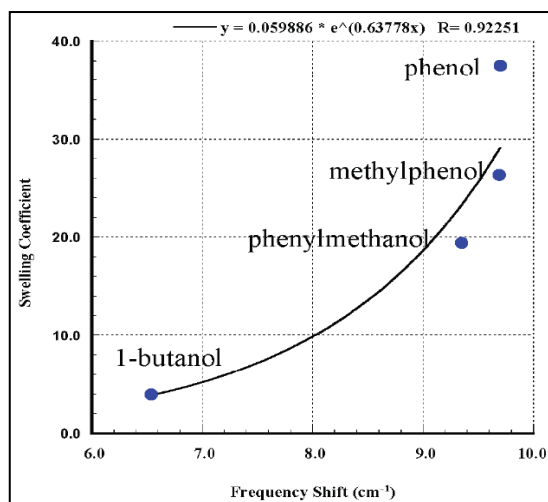
**Table 1** Swelling of nitrile O-rings after soaking in synthetic fuel (S-5) blended with various species [46].

Yamada et al investigated the interaction between nitrile O-ring and fuel species from a unique angle using the density functional theory (DFT) [47]. They developed a *cis*-butadiene-acrylonitrile-*trans*-butadiene model polymer to investigate three key parameters of 11 fuel species, namely the intermolecular distance, binding energy, and vibrational frequency shift associated with the cyano group (C≡N) stretching mode. Results presented a correlation among these three parameters as shown in Figure 21. Generally, the shorter the intermolecular distance between the fuel species and the model polymer becomes, the stronger the binding energy presents and the larger the C≡N peak shifts. These parameters also qualitatively correlated with the swelling coefficient calculated from experimentally observed swelling behaviour, as shown in Figure 22. This study suggested theoretical investigation can be used as a potential tool to predict polymer swelling efficiency.



**Figure 21** Relations among intermolecular distance, binding energy, and vibrational frequency shift of the  $C\equiv N$  stretching mode [47].





(c)

**Figure 22** Swelling coefficient against the (a) intermolecular distance, (b) binding energy, and (c) vibrational frequency shift of the C≡N stretching mode [47].

### 2.3.5 Summary of Previous Studies

Studies described above provide an essential fundamental understanding towards the elastomer compatibility issue with alternative aviation fuels. As aviation industry is keen to adopt alternative fuel sources for both commercial and military usage in the near future, more efforts need to be made to further understand and to eventually solve this problem. A summary of the understanding and achievements so far as well as the work needs to be done in this area are listed in Table 2.

**Table 2** Summary of previous achievements and future work.

Achievements so far	Remaining work
<ul style="list-style-type: none"> <li>• Understanding on the principle of fuel-polymer interaction;</li> <li>• Understanding on the factors that determine the transport process of fuel molecules into polymer;</li> <li>• Understanding the reason why aromatic compounds swell O-rings more effectively than other fuel species and theoretically what type of aromatic does better;</li> <li>• Knowledge about how O-ring</li> </ul>	<ul style="list-style-type: none"> <li>➤ To understand how O-rings would behave in real or simulated service scenario (undergo stress relaxation);</li> <li>➤ To further understand the effect of each fuel species has on the seal swell characteristics;</li> <li>➤ To further test and analyze the impact synthetic fuels produced from various pathways have on different sealing materials;</li> <li>➤ To further evaluate if cycloparaffins</li> </ul>

<p>would behave in a range of synthetic fuels have been tested;</p> <ul style="list-style-type: none"> <li>• Discovery of the relation between aromatic concentration and volume swell;</li> <li>• Preliminary selections on potential aromatic additives for synthetic fuels;</li> <li>• Theoretical, computational and experimental methodologies developed for the research on this topic.</li> </ul>	<p>or other non-aromatic compound have the potential to be a seal-swell promoter;</p> <ul style="list-style-type: none"> <li>➤ To look for suitable additive(s) which is (are) capable to promote the seal-swell property of synthetic fuels without scarifying other promising properties;</li> <li>➤ To develop new theoretical, computational or experimental methodologies;</li> <li>➤ To contribute to future synthetic fuel specification with regards to the material compatibility issue.</li> </ul>
--	--

## 2.4 Stress Relaxation

Under real service conditions, not only are the O-rings soaked in the fuel that is being sealed, but also are compressed by the two mating faces. While being compressed (a constant strain), the counterforce applied on the polymer undergoes a so called ‘stress relaxation’ process meaning the counterforce decays rather than is constant with time. Stress relaxation measured in compression is the most important testing method used for seals and gaskets [48]. To understand the stress relaxation characteristics of elastomer material will contribute to the better understanding of their compatibility with synthetic fuels in the sealing conditions.

### 2.4.1 Theory of Stress Relaxation

Generally, the stress relaxation process of an elastomer is caused by physical or chemical reason, or most commonly, a combination of both. Under normal conditions, both physical and chemical processes occur simultaneously. However, at lower temperatures and/or in short periods of time, the relaxation process is dominated by the physical processes, while at higher temperatures and/or long time periods the chemical processes dominate. Physical relaxation is associated with the reorientation of the network strands under strain, disengagement and rearrangement

of chain entanglements and movement of the chain ends. Furthermore, in filled elastomers, it is associated with the breaking and rearrangement of bonds due to secondary valence forces between filler network or in the polymer-filler interaction. Physical relaxation depends on the mobility of the polymer chains and temperature. Chemical relaxation is mainly caused by thermal or thermo-oxidative reactions and scission of the polymer chains or thermal breakage of crosslinks. Chain scission decreases the density of network strands producing new dangling ends with released stress. The release of stress is also caused by the breaking of crosslinks, resulting in longer strands and disentanglement [49].

#### **2.4.2 Factors Influencing the Stress Relaxation of Elastomers**

Several factors can influence the stress relaxation process of an elastomer, such as filler type and quantity, crosslink type and density, vulcanisation system, network structure, and thermal oxidation processes. The use of fillers can greatly enhance the viscoelastic response of elastomeric materials. Fillers, such as carbon black, which is most commonly used, can improve the hardness, abrasion resistance, tensile properties and tear strength of elastomers [50]. However, despite the many advantages, the presence of the filler normally can increase the relaxation rates during stress relaxation. This is probably caused by the strain in the filled polymer material being greater than the overall strain due to the inextensibility of the filler. As stress relaxation rates increase with increasing polymer extension, filled elastomers would show higher relaxation rates. Other reasons for higher relaxation rates in filled elastomers may be associated with filler-filler or filler-polymer breakdown [51]. Crosslinks between the polymer chains are formed through sulphur chemically reacts with the raw gum elastomer. Both the physical and chemical properties of an elastomer are affected by the number and type of crosslinks formed between network chains. Network structure degradation is a thermally driven process by which vulcanised rubber reverts back to raw gum. This degradation process might contribute to the deterioration of physical properties. Temperature is a significant factor influencing the relaxation process of polymers as higher temperatures may

cause the scission of crosslinks resulting in the structure breakdown and softening of the material. The presence of oxygen can induce the oxidation process resulting in crosslinking and chain scission as well. The oxidative degradation is the most important factor determining the durability of elastomers [50]. Besides these factors from the polymer material itself, the medium, most commonly solvents in which the material is immersed, also has an impact on the stress relaxation process as the interaction between solvent and polymer may result in a structure change of the elastomer.

### 2.4.3 Testing Methods for Stress Relaxation in Compression

There are two main types of instruments used for the testing of stress relaxation in compression; continuous and discontinuous apparatus [51]. A typical continuous relaxation test rig is the “Elastocon EB 02 Relaxation Tester”. Details of this rig will be given in section 3.1.1. For the discontinuous relaxation test, a representative rig is shown in Figure 23. This type of test is normally conducted over much longer period than a continuous test. The counter force is measured in a tensile tester or a special relaxometer before placing the rig at the test temperature. The rig is taken out of the test temperature at intervals and the counter force is measured [52].



**Figure 23** A discontinuous stress relaxation test rig [53]

#### **2.4.4 Applications of the Stress Relaxation Test**

The stress relaxation test has been used mainly for the life time prediction of elastomeric materials, as most rubber seals and gaskets require a very long period of service. Mitra et al [54] - [56] demonstrated that the stress relaxation of an accelerated sulphur cured ethylene propylene diene rubber (EPDM) was much faster in a harsh chemical solvent than in air. They argued the decrosslinking was the main reason for this as observed by a decrease in crosslink density. Comparison with similar specimens in the same exposure media under unstressed conditions showed that chemical degradation under stressed condition provided relatively quicker and also reliable results. The continuous compression stress relaxation (CSR) test was approved to be a precise and reliable method in predicting the life span of elastomers [57] - [60]. Ronan et al [61] also developed a forecasting procedure using the time-temperature superposition principle using Elastocon EB 02 Relaxation Tester. Another work conducted by Ronan et al. indicated that the primary relaxation process of a conventionally vulcanised natural rubber was mainly influenced by physical changes. The oxidation state of the elastomeric material could be observed by using Fourier Transform Infrared (FTIR) spectroscopy.

### **2.5 Fourier Transform Infrared Spectrometer (FTIR)**

#### **2.5.1 Infrared Spectroscopy**

Infrared spectroscopy, as one of the most important analytical techniques, deals with infrared region ( $4000\text{-}400\text{ cm}^{-1}$ ) of the electromagnetic spectrum. One of the great advantages of this technique is a wide range of samples such as liquids, fibres and surfaces can be studied [62] [63]. This technique is based on the vibrations of the atoms of a molecule which absorbs infrared radiation only at selected frequencies or energies. Radiation in this energy range corresponds to the range of the stretching or bending vibrational frequencies of the bonds in most covalent molecules [64]. The vibration modes of a  $\text{CH}_4$  group are shown in Figure 24 as an example. During the absorption process, the frequencies that match the natural vibrational frequencies of the molecules are absorbed and these absorbed energy increases the amplitude of the

vibrational motions of the bonds in the molecule. However, a ‘selection rule’ applies for infrared spectroscopy meaning only those bonds which have an electric dipole moment changing as a function of time during the vibration are capable to absorb infrared radiation. An infrared spectrum is commonly obtained by passing infrared radiation through a sample and determining what fraction of that radiation is absorbed at a particular energy. The energy at which any peak in an absorption spectrum appears corresponds to the frequency of a vibration of a part of a sample molecule [63]. Since every type of bond has a different natural frequency of vibration, no two molecules of different structure have exactly the same infrared spectrum. As a result, an infrared spectrum of the sample can be used as a fingerprint for molecules.

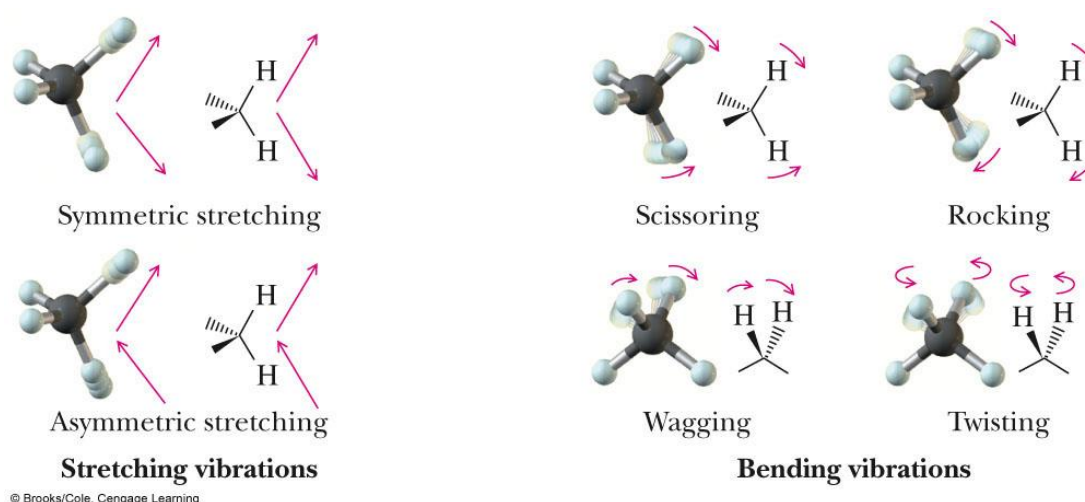


**Figure 24** Stretching and bending vibration modes of CH<sub>4</sub> group [65].

## 2.5.2 FTIR

Two types of infrared spectrometers are commonly used in laboratory: Dispersive Infrared Spectrometers and Fourier Transform Spectrometers (FTIR) [66]. FTIR is the most modern spectrometer and is preferred over dispersive instruments for the following reasons:

- Non-destructive technique;
- Higher precision, no need for external calibration;
- Much faster scanning speed, collecting one scan less than a second;

- Increased sensitivity resulting in better signal-to-noise ratio;
- Mechanically simple with only one moving part.

Figure 25 shows the typical sample analysis process of an FTIR spectrometer. Basically, the FTIR spectrometer employs an interferometer to process the energy sent to the sample. The infrared beam emitted from a ‘black-body’ source enters the interferometer where the ‘spectral encoding’ takes place. Then the resulting interferogram signal is transmitted through (for liquids) or reflected off the surface (for solids or powders) of the sample, where specific frequencies of energy are absorbed. Finally, the beam passes to the detector for final measurement and then is sent to the computer where the Fourier transformation takes place. The final infrared spectrum with the information on the sample compositions is presented to the user for further interpretation.

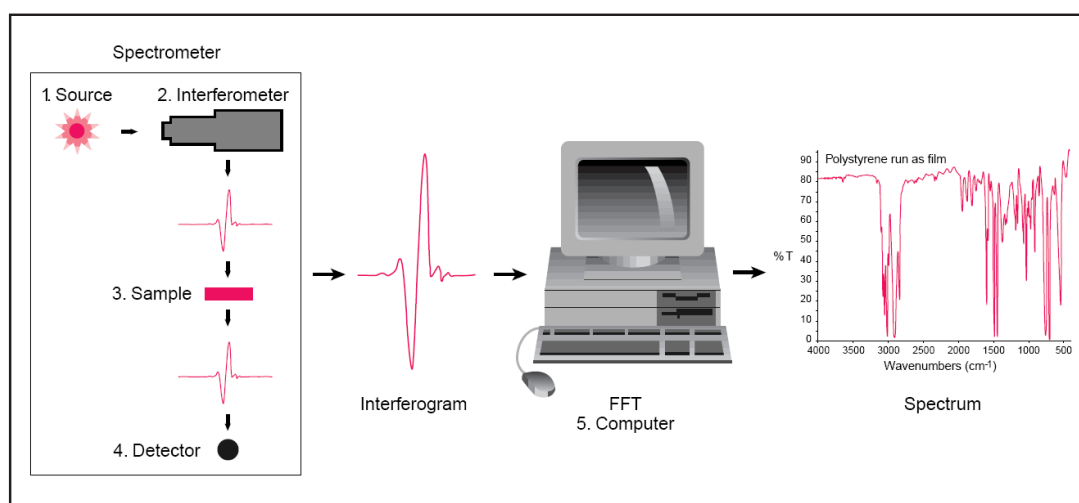


**Figure 25** Schematic diagram of the instrumental process of an FTIR spectrometer [67].

### 2.5.3 Attenuated Total Reflectance (ATR)-FTIR

For the analysis of thick or highly absorbing solid and liquid materials, it is difficult to use conventional transmittance method to pass the infrared radiation through the sample to obtain the spectrum. So an internal reflectance technique called attenuated

total reflectance (ATR) spectroscopy utilizing the phenomenon of total internal reflection is employed for this type of applications. Basic principle of ATR spectroscopy is presented in Figure 26. Generally, it utilizes a crystal to let the incident IR beam undergo total internal reflection as the angle of incidence at the interface between the sample (lower refractive index) and crystal (higher refractive index) is greater than the critical angle. The beam penetrates a very short distance into the sample surface and losses energy at the wavelength where the sample absorbs the radiation. The resulting attenuated radiation is plotted as a function of wavelength and provides the absorption characteristics of the sample in the final spectrum [62]. The depth of penetration ( $d_p$ ) of the evanescent wave is a function of the wavelength,  $\lambda$ , the refractive index of the crystal,  $n_2$ , and the angle of incident radiation,  $\theta$ , as shown is Eq. (2.8).  $n_1$  is the refractive index of the sample.

$$d_p = (\lambda/n_1)/\{2\pi[\sin \theta - (n_1/n_2)^2]^{1/2}\} \quad (2.8)$$

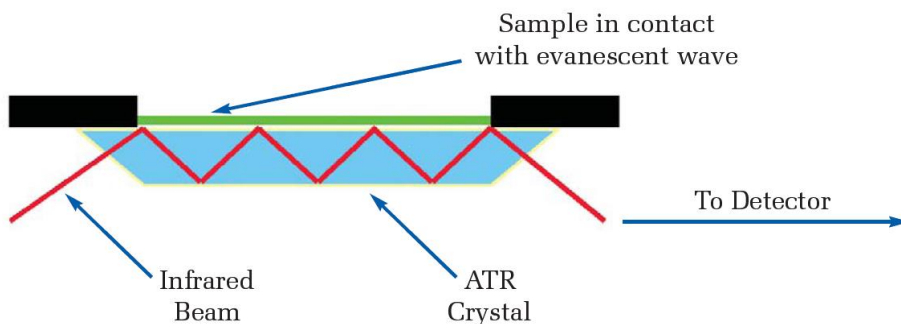


**Figure 26** Principle of attenuated total reflectance (ATR) spectroscopy [68].

The crystals used in ATR are made from materials that have low solubility in water and very high refractive index. Commonly used materials and their physical properties are summarized in Table 3. Diamond can withstand highly acidic samples and is normally used to analyse hard powders; but has relatively high absorbance in the region of  $2,500 \text{ cm}^{-1}$  to  $1,650 \text{ cm}^{-1}$ . Germanium (Ge) is excellent for highly absorbing samples e.g. rubber materials containing carbon black due to its high

refractive index. KRS-5, thallium-bromiodide, has a wide spectral range but relatively soft and unsuitable for aqueous samples. Silicone is ideal for the analysis of thin film samples but is easily affected by strong acids and has a limited spectral range. Zinc Selenide (ZnSe) is cost effective, easy to clean, and suitable for wet or aqueous samples [69].

**Table 3** Physical properties of commonly used ATR crystals [69].

<b>Materials</b>	<b>Spectral Range (cm<sup>-1</sup>)</b>	<b>Refractive Index</b>	<b>Depth of Penetration (µm)</b>
Diamond	45,000-10	2.4	1.66
Ge	5,000-600	4	0.65
KRS-5	20,000-400	2.37	1.73
Si	10,000-100	2.37	1.73
ZnSe	20,000-650	2.4	1.66

#### **2.5.4 Applications of FTIR and ATR-FTIR in Polymer Analysis**

FTIR technique has been widely used in the analysis of polymer properties and lifetime prediction in rubber industry [70] - [76]. Gunasekaran et al. reported the usage of FTIR for the evaluation of mechanical properties of selected rubber materials [71]. They analyzed these properties by calculating the internal standards among the methyl and methylene group vibrational frequencies obtained from the FTIR. Results obtained from FTIR technique were in good agreement with standard methods for quality control purpose. Another research group from India [72] proved that FTIR can be utilized to characterize nitrile rubber (NBR) by correlating the absorbance ratio of nitrile stretching (at 2238 cm<sup>-1</sup>) with the acrylonitrile content. Also to analyse nitrile rubber, Kawashiwa and Ogawa [73] focused on the thermal degradation process in order to predict the lifetime of this material. The absorbance of various functional groups measured by FTIR after thermal degradation at high temperatures indicated it was possible to quantitatively determine each of the functional groups. FTIR can be used in determining the thermal and chemical degradation of polymers were also proved by Jansson et al. [75] and Cervantes-Uc et al. [76].

A number of previous studies have been using ATR-FTIR spectroscopy to investigate the diffusion process of solvents into polymer structures [77] - [81]. An early study conducted by Farinas et al [79] indicated that ATR has the potential to evaluate changes in polymer swelling and polymer-solvent interactions because it provided an accurate measurement on the solvent diffusion process. Sammon et al. compared the diffusion processes of water and liquid methanol into poly (ethylene terephthalate) (PET) films using an in-situ ATR-FTIR, concluding the rate of diffusion of liquid methanol was faster than that of water due to the accompanying swelling of the polymer [81]. Torregrosa-Coque et al. demonstrated different crystals (Germanium and Zinc Selenide) were required depending on the different requirements on the penetration depths by monitoring the migration of paraffin wax additive through styrene-butadiene rubber (SBR)-polyurethane coating interface [77]. Do et al. showed ATR-FTIR method is simple and effective in the analysis of rubber materials due to the direct measurement on the surface of the rubber without sacrificing the sample [82].

## 2.6 Hansen Solubility Parameters (HSP)

Solubility parameters, first used by Hildebrand and Scott [83], are derived from the energy required to convert a liquid to a gas. During the vaporization process, the total energy required to break all types of bonds holding the liquid together can be measured by the Hildebrand solubility parameter,  $\delta$ , which was defined as the square root of the cohesive energy density:

$$\delta = (E/V)^{1/2} \quad (2.9)$$

$$E = \Delta H_v - RT \quad (2.10)$$

In Eq. (2.9), E is the measurable energy of vaporization of the pure solvent, and V is its molar volume. The unit for solubility parameter is  $\text{MPa}^{1/2}$ . Where  $\Delta H_v$  is the measured or predicted latent heat of vaporization, R is the universal gas constant, and T is the absolute temperature in Eq. (2.10).

Solubility parameters are widely used to predict compatibility of polymers, chemical resistance, and to select solvents in a variety of industries. The basic principle is ‘like dissolves like’, which means polymers will dissolve in solvents whose solubility parameters are similar to or not too different from their own. Hansen Solubility Parameters (HSP) developed by Charles Hansen since 1967 [84], is the most widely used approach to predict polymer solubility.

### 2.6.1 Theory of HSP

Based on previous theories on polymer solution thermodynamics and solubility parameters (e.g. Hildebrand solubility parameters), Charles Hansen developed his idea based on three sources of the total energy of vaporization of a liquid: dispersive forces, permanent dipole-permanent dipole forces, and hydrogen bonding (electron exchange). The cohesion energies corresponding to each of the three sources are named *dispersion cohesive energy* ( $E_D$ ), *polar cohesive energy* ( $E_P$ ), and *hydrogen bonding* ( $E_H$ ). The basic equation governing the assignment of HSP is that the total cohesion energy,  $E$ , must be the sum of the individual energies as shown in Eq. (2.11) [85].

$$E = E_D + E_P + E_H \quad (2.11)$$

The relationship between the total (or Hildebrand) solubility parameters and HSP is derived by dividing this equation by the molar volume.

$$E/V = E_D/V + E_P/V + E_H/V \quad (2.12)$$

$$\delta^2 = \delta_D^2 + \delta_P^2 + \delta_H^2 \quad (2.13)$$

These three parameters can be used as co-ordinates for a point in a three-dimensional space called *Hansen Space*. Generally, the nearer two materials (usually a solvent and a polymer) are in this space, the more likely they are to dissolve into each other. Based on experimental data, an equation for the solubility parameter ‘distance’,  $R_a$ , was developed to represent the distance between two materials based on their

respective partial HSPs [85]:

$$(R_a)^2 = 4(\delta_{D2} - \delta_{D1})^2 + (\delta_{P2} - \delta_{P1})^2 + (\delta_{H2} - \delta_{H1})^2 \quad (2.14)$$

The constant '4' can correctly represent the solubility data as a sphere which is convenient to present the HSP characteristics. To apply this equation in a more practical manner, an interaction radius (or the radius of the sphere),  $R_0$ , is defined to determine if the HSPs of two materials are within the range of being dissolved. The HSPs are in the centre of the sphere and a RED (relative energy difference) number is given as follows:

$$RED = R_a/R_0 \quad (2.15)$$

If  $RED < 1$ , the two materials will dissolve; if  $RED = 1$ , partially dissolve will happen; if  $RED > 1$ , no dissolution will take place. For instance, Figure 27 showed the solubility of carbon dioxide in various solvents in its Hansen Space. The HSP of carbon dioxide is  $15.7 \text{ MPa}^{1/2}$  ( $\delta_D$ ),  $6.3 \text{ MPa}^{1/2}$  ( $\delta_P$ ), and  $5.7 \text{ MPa}^{1/2}$  ( $\delta_H$ ), respectively, which determines the centre of the green sphere in the co-ordinate. The radius of the sphere,  $R_0$ , is calculated to be  $3.3 \text{ MPa}^{1/2}$ . It can be clearly seen that the blue dots, which are within the sphere ( $RED < 1$ ) represent the solvents which can dissolve  $\text{CO}_2$ . The red dots which are outside the sphere ( $RED > 1$ ), are the solvents that cannot dissolve it.

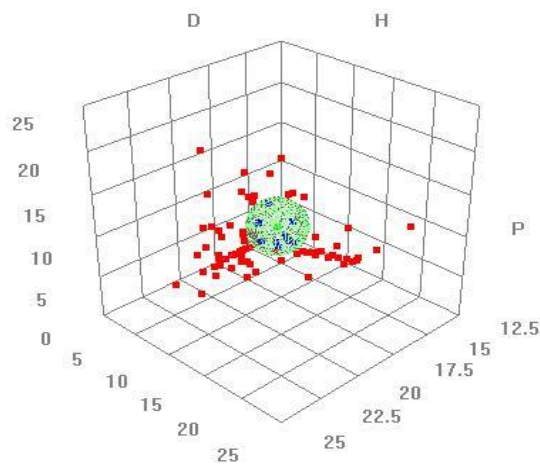


**Figure 27** Solubility of carbon dioxide [86].

### 2.6.2 Applications of HSP in polymer-solvent interactions

HSP has been widely used to correlate polymer solubility. Nielsen and Hansen [87] successfully correlated the HSP of two EPDM elastomers before vulcanisation to the degree of swelling of the same elastomers after vulcanisation. It was found that the degree of swelling of EPDM elastomers reduced as the RED number increased; in another words, larger differences in HSP between solvent and elastomer led to lesser degree of swelling. Results also showed the molecular weight and the degree of branching for the two EPDM elastomers did not have a significant effect on the HSP. As all the main components of EPDM such as ethylene, propylene, and a diene monomer have similar HSP, it led to better correlations with HSP. On the other hand, the three chemicals made up FKM has very different HSP, it was difficult to have a good correlation between HSP and swelling for this elastomeric material. The importance of this study is that it provides an approach to predict the swelling of elastomers in contact with a large number of untested solvents.

The latest application of HSP in the compatibility of polymers with alternative aviation fuels was conducted by Graham et al. [34]. With the aim to evaluate the activity of specific types of aromatics in the fuel-polymer interactions, a range of aromatics were selected to isolate the roles of molar volume, polarity, and hydrogen

bonding. These species were blended in a SPK fuel by 8% v/v with 3% for naphthalene due to the specification requirement of jet fuel. O-ring materials tested were nitrile, fluorosilicone, and fluorocarbon. They found that both the volume swell and the partition coefficient of all O-ring materials tend to increase as the molar volume of aromatics decreases, and as the polarity and hydrogen bonding increases. Amongst these three factors, molar volume had the least influence on the volume swell followed by polarity and hydrogen bonding, while the influence of hydrogen bonding is significantly higher than that of polarity. From the material point of view, nitrile O-ring was significantly influenced by these factors while relatively small changes were found for the other two materials.

HSP can also be employed to investigate the compatibility of additives with polymers [88] and the solubility of particular substances in polymers or solvents [86]. Efforts are being made to explore a better application of HSP with other theories and methodologies [89] [90].

## **2.7 Summary**

Elastomer compatibility issue induced by the introduction of alternative aviation fuels has been receiving more attention. The fundamental reason that causes this concern lies in the composition change of SPKs compared with conventional jet fuels (Jet A-1/Jet A). Research has shown that O-rings especially made of nitrile material experience low level of swell or even shrinkage when they are in contact with SPKs due to the absence of aromatic compound in these synthetic fuels. This phenomenon requires further understanding from both aspects of fuels and polymers in order to avoid any potential disastrous consequence.

Both theoretical and experimental efforts have been made to better understand the impact of fuel on polymer. Theoretically, the typical process of fuel-polymer interaction has been understood. Theories such as density functional theory (DFT) and Hansen Solubility Parameter (HSP) have been utilized to characterize what kind

of fuel species tend to be more effective in the seal-swelling process. Generally, smaller molar volume, relatively symmetric molecular structure, exhibiting polarity, and contributing in hydrogen bonding, are the characteristics desired for good seal-swell species, such as aromatics and diaromatics. Experimentally, efforts have been mainly focused on the volume swell of O-rings in various fuel species and blends. Results confirmed the high dependence of nitrile O-ring swelling on aromatic content and also proved the species having some or all the theoretical characteristics mentioned above swell O-rings better.

So far, research has been focused on the study of this fuel-polymer interaction from a scientific point of view. However, a better understanding of this elastomer compatibility issue in an engineering scenario is desired as the ultimate goal is to use alternative fuels in current aircraft engines as safely as conventional jet fuels. To understand the stress relaxation characteristics of elastomeric O-rings in various fuel scenarios would be a potential approach to investigate this problem as it provides a real service conditions for the seals. Furthermore, results from stress relaxation (dynamic) tests would be more representative than those obtained from static immersion tests that previously conducted. On the other hand, scientific methodologies are also critical in the analysis process; and this is where the FTIR technique and HSP theory are employed, as they have been successfully employed in the previous fuel-polymer studies.

### **3 Experimental**

Experiments conducted in this work consist of two main parts; the stress relaxation test and the FTIR analysis. The stress relaxation tests were carried out under two temperature conditions; isothermal and thermal cycling. The relaxation Tester EB 02 from Elastocon AB combining with cell ovens Elastocon EB 01 (for isothermal) and EB 17 (for thermal cycling) were employed to conduct the stress relaxation tests. The FTIR spectrometer ‘Spectrum One’ from Perkin Elmer was used for further structure change analysis. A wide range of fuels and solvents produced from conventional or synthetic ways were tested as well as three types of O-ring materials, namely nitrile, fluorosilicone and fluorocarbon. Details about the experimental setup, principles, compositions of fuels and O-rings and procedures are provided below.

#### **3.1 Equipments**

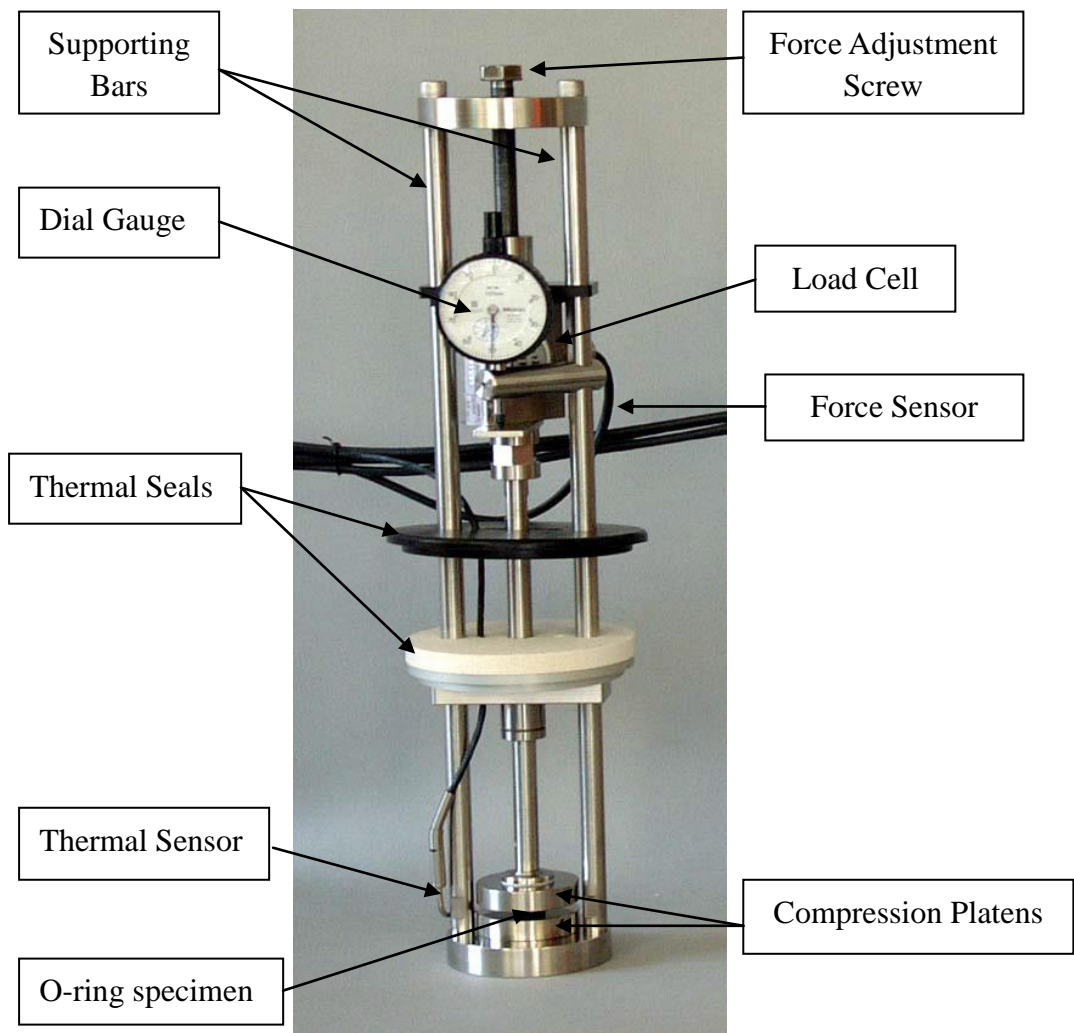
##### **3.1.1 Elastocon EB 02 & EB 01 – For Isothermal Stress Relaxation Test**

###### *3.1.1.1 Technical description*

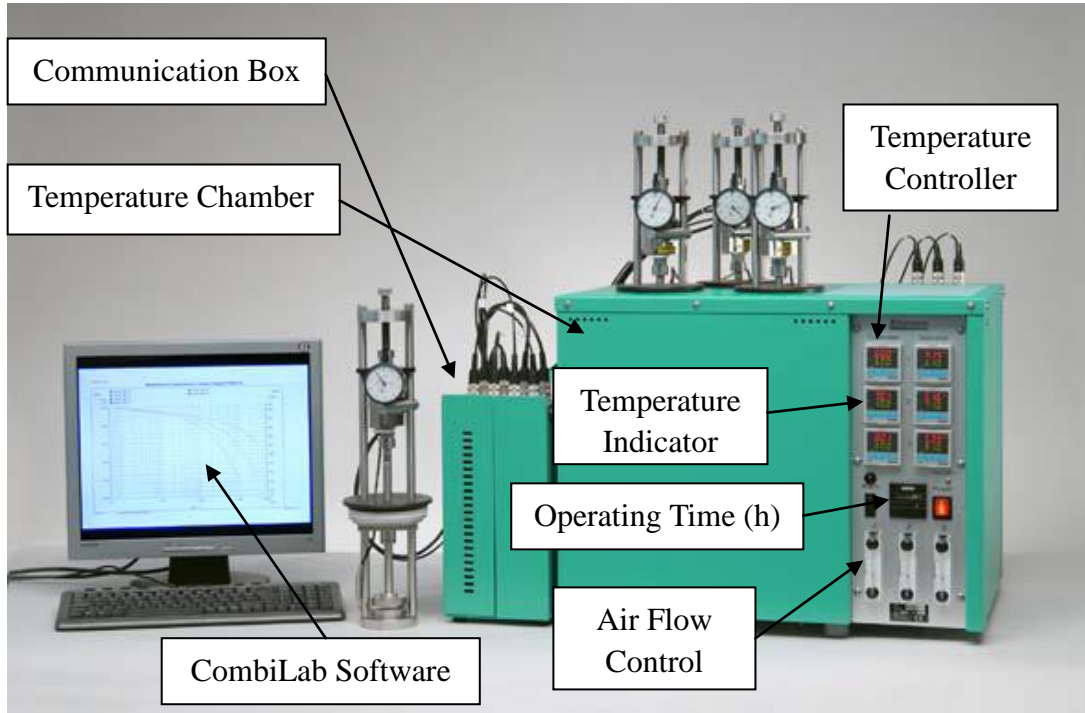
Elastocon EB02 is a relaxation tester or relaxometer used for the continuous compression stress relaxation (CSR) test. It complies with ‘ISO 3384’ [91], an international standard for determination of rubber stress relaxation in compression at constant temperatures. The structure of the relaxometer is shown in Figure 28 (a). Basically, it is an elongated rig being inserted inside the ageing cell oven. Two parallel stainless steel bars support the whole unit with two plates to secure their positions on top and bottom. Key components are arranged along the central axis of the unit, including a force adjustment screw, a load cell, a dial gauge, thermal seals, a thermal sensor and compression platens (from top to bottom).

When an O-ring sample is inserted between the two compression platens, compression is applied by screwing down the platen above. Counter force is sensed by the load cell and transmitted to the computer via the communication box. The dial gauge is used to indicate the degree of deformation of the sample. When the required

deformation is reached, the sample is immersed in the container filled with a certain amount (normally 150 mL) of candidate fuel or solvent, and then the whole unit is placed inside the oven (Fig. 28 (b)). The thermal sensor is inserted into the middle of the bottom platen, indicating the test temperature.



(a)



(b)

**Figure 28** Elastocon EB02 continuous stress relaxation (CSR) tester (a) and with ageing cell oven EB 01 (b).

The function of the ageing cell oven EB 01 is to create a constant temperature environment for the stress relaxation test (Fig. 28 (b)). The test temperature can be setup via the ‘Temperature Controller’ on the front panel. ‘Temperature Indicator’ indicates the real-time temperature condition inside the O-ring container, which is connected to the thermal sensor. Air flow running through the oven is controlled on the front panel as well to help maintain the inside temperature at a constant level. The relaxometers communicate with the computer via a communication box as all the force and thermal sensors are connected to it. Technical specifications of EB 02 and EB 01 are listed in Table 4 and Table 5.

**Table 4** Technical specifications of the Relaxation Tester EB 02 [92].

Attribute	Value
Manufacturer	Elastocon AB

Model	EB 02
Testing standard	ISO 3384
Force sensor	Youngzon YZ101B
Compression range, N	0 - 1000 N
Compression resolution, N	0.1
Accuracy, %	±0.1 of full range
Temperature sensors	PT100, 1/3 DIN
Material	Stainless steel

**Table 5** Technical specifications of Cell Ageing Oven EB 01 [93].

Attribute	Value
Manufacturer	Elastocon AB
Model	EB 01
Number of cells	4
Testing standard	ISO 188
Temperature sensors	PT100, 1/3 DIN
Temperature range, °C	20 - 200
Temperature control, °C	±0.5
Temperature variation, °C	±0.25
Air changes, changes/hour	3 – 20

If a very accurate measurement is required, it may be necessary to compensate for the spring effect in the load cell (Fig. 29). The spring effect is caused by the load cell slightly returning as the rubber sample relaxes, which as a result, increases the compression applied on the test specimen. All load cells are deformed when a force is applied and it is the deformation that is measured to read the force. To compensate for the spring effect, reading of the dial gauge needs to be recorded after the compression is applied. Then using the compression screw to return to the original

reading of the dial gauge at suitable intervals (e.g. 1, 2, 4 days/weeks, etc.). As comparative tests rather than accurate measurements are required in this work, compensation for the spring effect is not necessary.

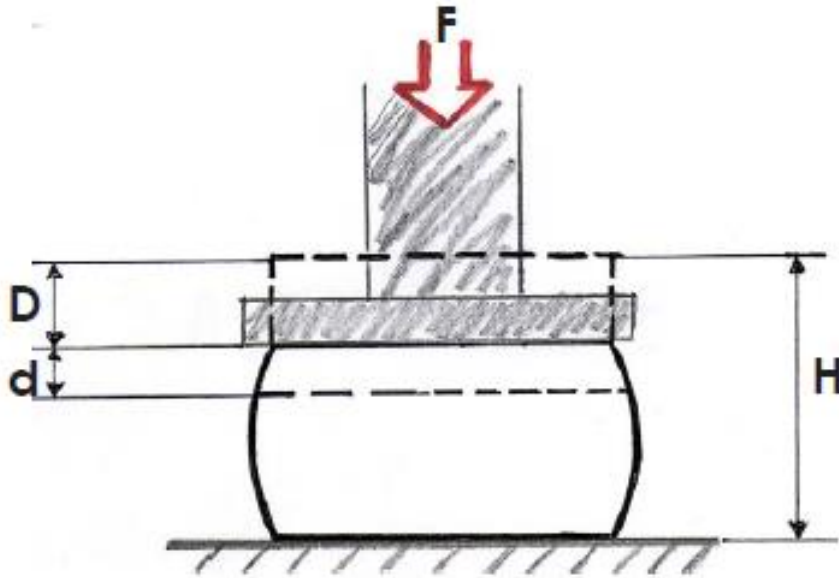


**Figure 29** Schematic diagram for compensating the spring effect [92]. F: force applied; D: compression during test; d: compression caused by the load cell; H: original height of the sample.

### 3.1.1.2 *CombiLab software*

The software used to control and communicate with the relaxometer is the CombiLab 5 developed by Eltex of Sweden AB [94]. It consists of three main program modules, which are the Scanner, the Log Manager and the Viewer, plus accessory modules as shown in Figure 30. The Scanner collects the measured values from the connected transducers from a DDE-server via the DDE Link. The real-time status of the forces and temperatures can be monitored in the Scanner throughout the whole test. The Log Manager continuously records the data in the measuring files like a ‘tape recorder’. The Viewer is a window where the relaxation curves and data points can be viewed, analysed and exported.

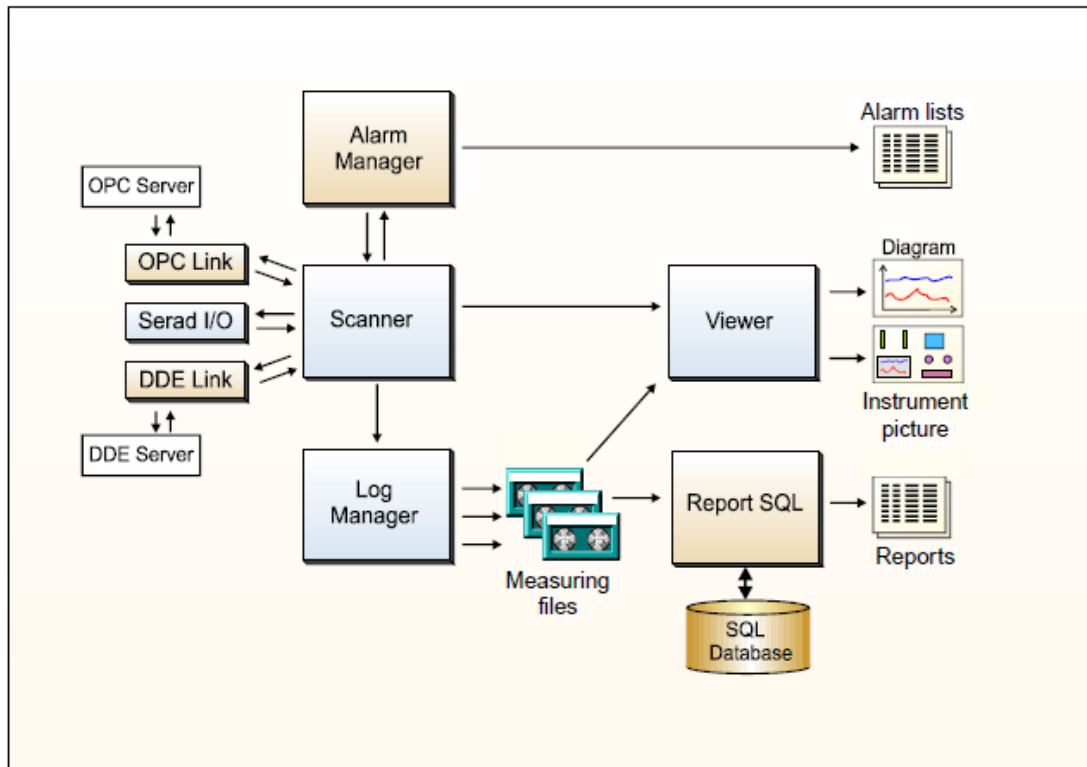


**Figure 30** Overview of the programme modules of CombiLab 5 [94].

### 3.1.1.3 Test procedure

The following test procedure is developed based on the standard procedure from the manuals and experimental experience gained during this work.

- 1) Switch on the ageing cell oven and set the test temperature on the front control panel, 30 °C for all the isothermal tests;
- 2) Inject the candidate fuel or solvent into the container, approximately 150 mL;
- 3) Place the relaxation rig into the temperature chamber of the oven and preheat it to the test temperature;
- 4) Measure the height/thickness of the O-ring specimen with a thickness gauge;
- 5) Calculate the compression in mm, normally 25%;
- 6) Lift the rig out of the oven and insert the O-ring specimen centred between the compression platens;
- 7) Apply a slight preload of about 10 N to prevent the O-ring from moving inside the container and place the compression platens in the container;
- 8) Replace the rig in the oven and compress the specimen to the calculated

- compression by screwing down the compression platens;
- 9) Start the logging with CombiLab Logger, setting the logging interval at 1min;
  - 10) The relaxation curves can be seen in the Viewer of CombiLab program, while the compression forces and temperatures can be monitored in the Scanner during the test;
  - 11) When the test is finished,  $F_0$  (force after 30 min from the start of the test) needs to be determined in the Viewer. Then the relaxation data can be exported for further analysis.

### **3.1.2 Elastocon EB 17 – For Temperature Cycling Test**

#### ***3.1.2.1 Technical description***

The Elastocon EB 17 cell oven is a recently developed ageing oven by Elastocon AB, with the capability of temperature cycling [95]. It can accommodate six relaxometers inside the oven with a draught hood on top to reduce the influence of ambient temperature on the relaxometers. All test conditions can be set on the PLC panel via a touch controlled screen. The major difference of this oven compared with EB 01 is the ramp function for temperature settings. The test temperatures can be set in cycles within a wide temperature range (-40 to 225 °C) and as such the performance of O-ring materials in a varying temperature condition can be evaluated. The temperature ramp is achieved by a liquid circulator connected to the oven (Fig. 31). The liquid circulator is a High Dynamic Temperature System, LH85, manufactured by Julabo. It is equipped with an integrated programmer to control the operation. Detailed experimental setup and the operating principle are described below.

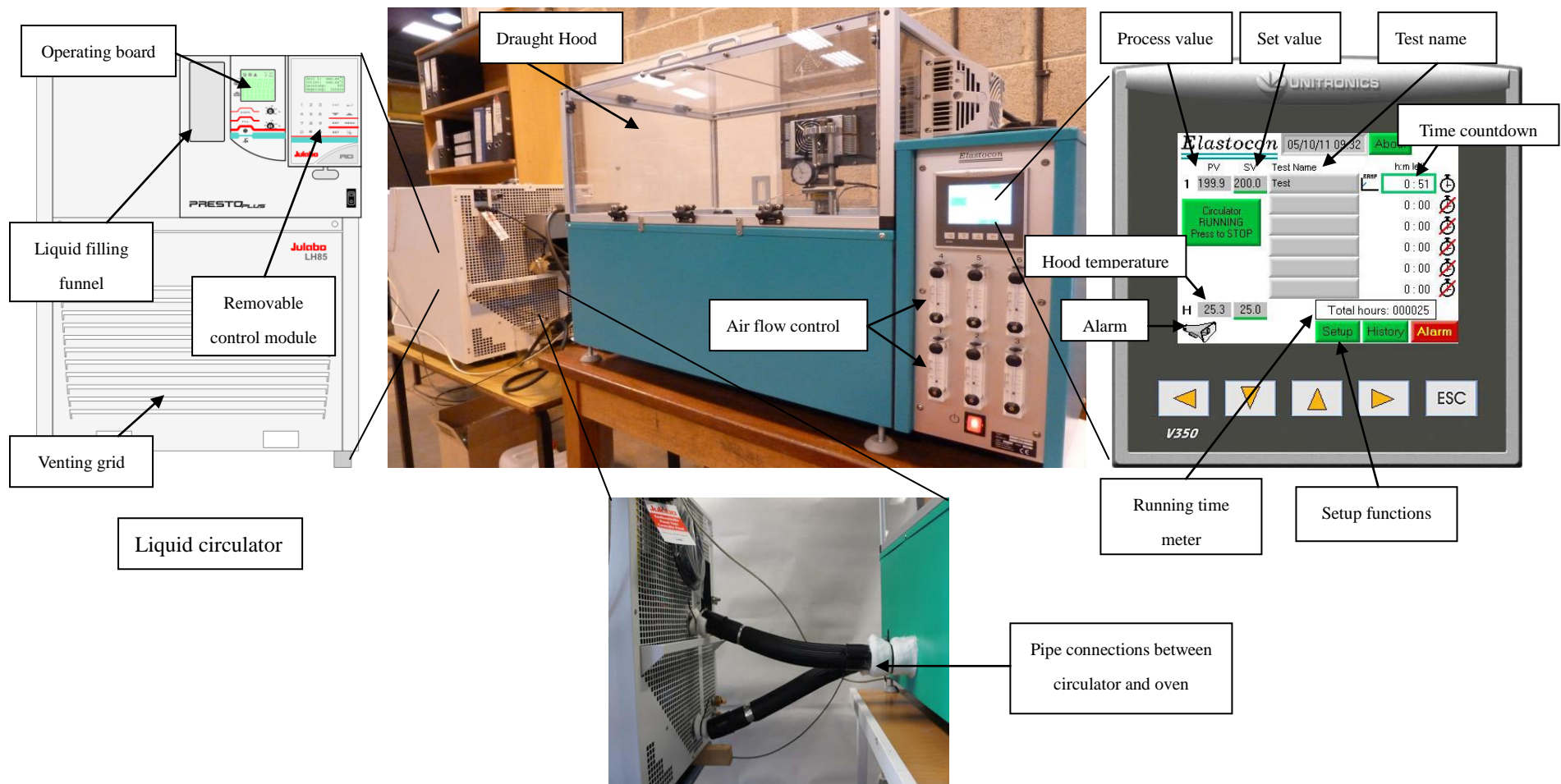


**Figure 31** Elastocon EB 17 cycling cell oven with liquid circulator.

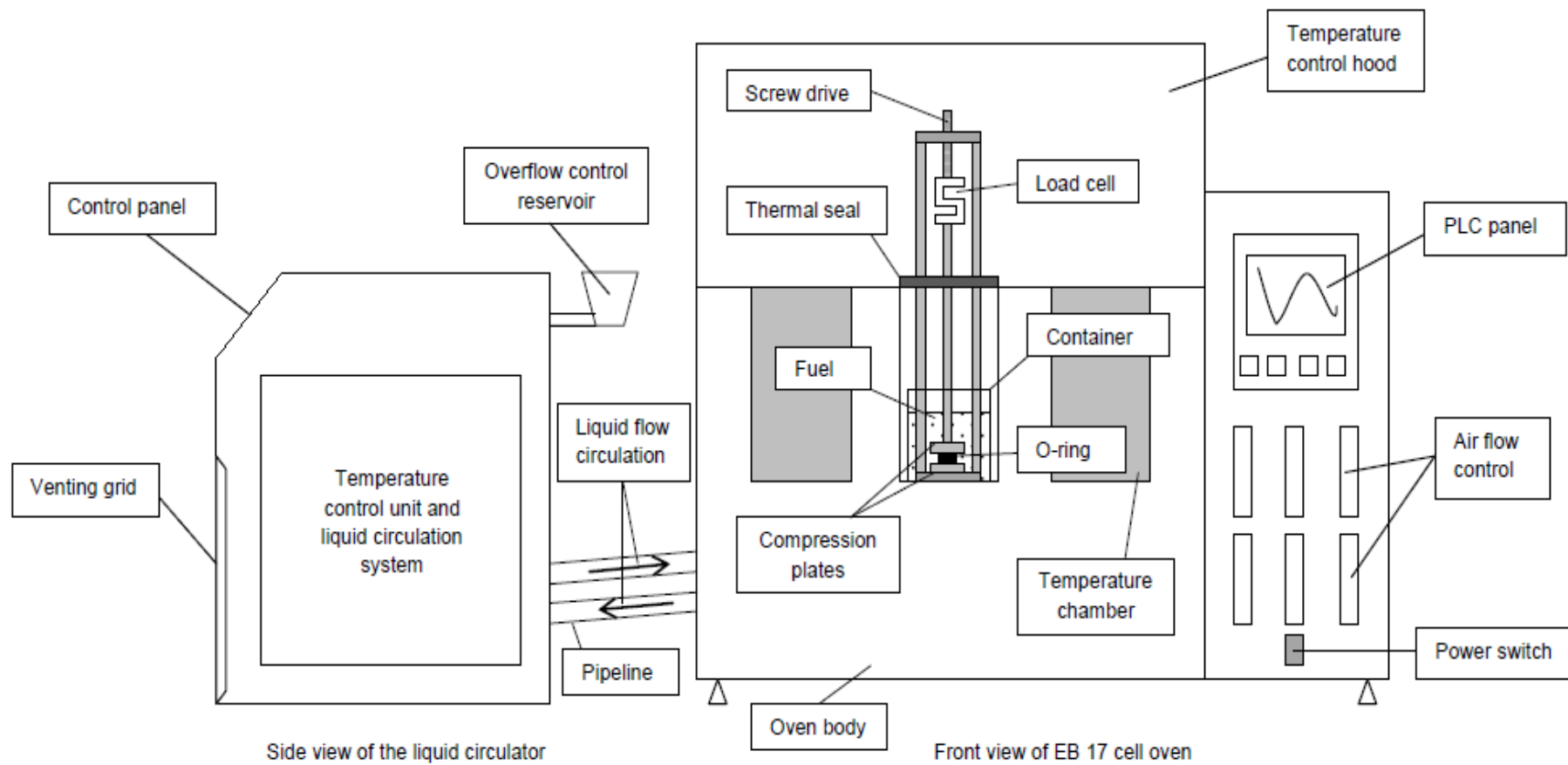


**Figure 32** Schematic diagram of the temperature cycling cell oven setup.

The operation of the temperature system is controlled via the local control panel (2) and the removable operating device RD (4). The bath liquid (thermal oil) is injected into the unit at the filling funnel (5) via the internal reservoir (5a). Then the bath liquid spreads into the external reservoir (16a) and the heat exchanger (20), where it is pumped into the external system (cell oven) (33) by the circulating pump (23) via connection hose (13) and led back via connection (14). When the system is started, the heating (21), cooling aggregate (22) and the circulating pump (23) start according to the desired adjustments made at the operating device RD (4). The pump pressure (29) and the actual temperature of the internal control sensor (28a) are measured. If the temperature control has to be effected externally, an external sensor (28b) needs to be connected.

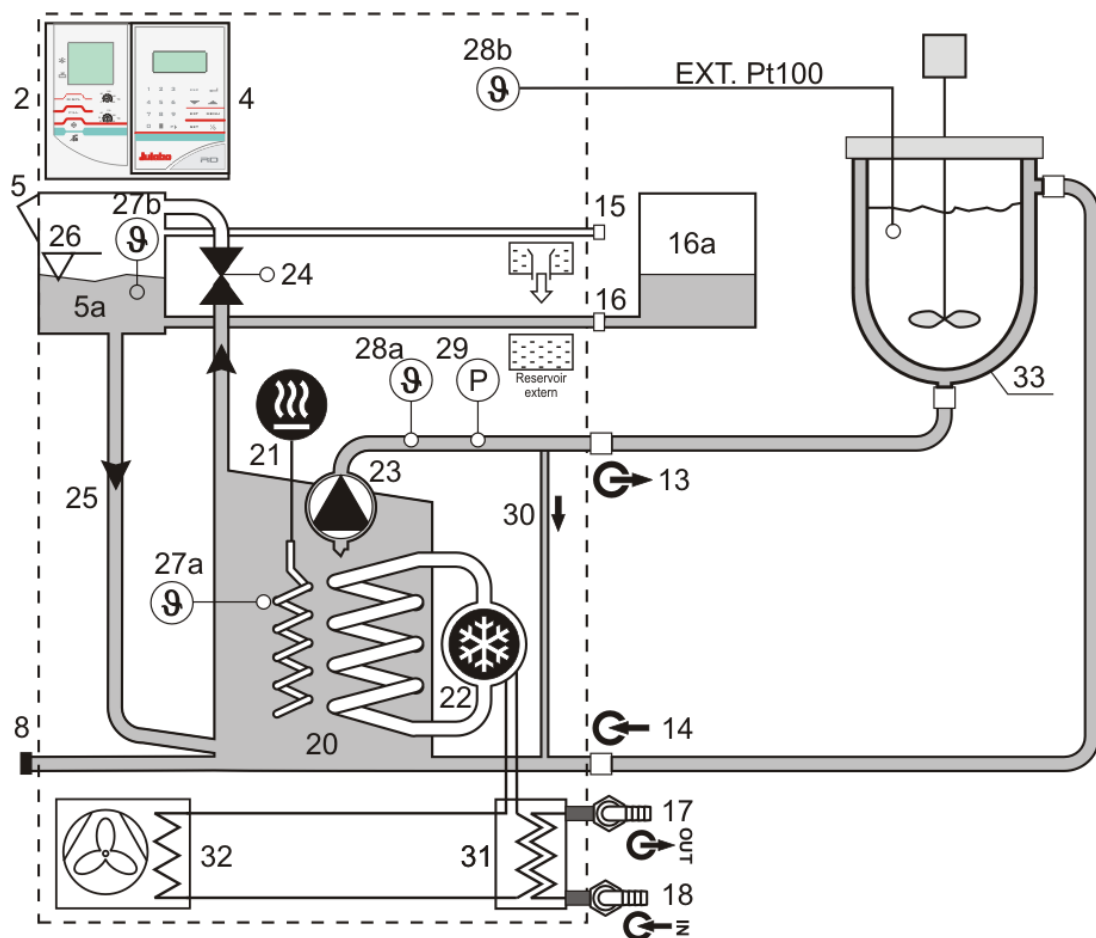


**Figure 33** Operating principle of the liquid circulator [96].

The technical specifications of EB 17 cycling cell oven and the liquid circulator Julabo LH85 are provided in Table 6 and Table 7.

**Table 6** Technical specifications of Cycling Cell Oven EB 17 [95].

Attribute	Value
Manufacturer	Elastocon AB
Model	EB 17
Number of cells	6
Testing standard	ISO 188
Temperature sensors	PT100, 1/3 DIN
Temperature range, °C	-40 - +225
Temperature control, -40 - 200 °C, °C	±0.5
> 201 °C, °C	±1.0
Temperature variation, °C	±0.25
Air changes, changes/hour	3 – 20

**Table 7** Technical specifications of Liquid Circulator LH 85 [96].

Attribute	Value
Manufacturer	Julabo
Model	LH 85
Heating power, W	1,800
Cooling power at +20 °C, W	900
Cooling power at -40 °C, W	700
Temperature range, °C	-80 - +250
Temperature stability, °C	±0.05
Pump flow rate, L/min	16 - 30
Cooling of compressor	air/water

### 3.1.2.2 Test procedure

The temperature cycling test is carried out as follows:

- 1) Prepare the O-ring specimen and fuel in the relaxation rigs, which follows the same procedure as that discussed for EB 02;
- 2) Place the relaxation rigs in the oven and close the lids of the draught hood;
- 3) Set the test temperature or temperature ramping on the cell oven via the PLC and switch on the circulator;
- 4) Set the controller of the hood at 50 °C;
- 5) Let the temperature stabilize in both the rigs and the hood;
- 6) Set the controller for the hood about 2 to 2.5 °C lower than the indicated maximum temperature without cooling;
- 7) Start the logging with CombiLab Logger, setting the logging interval at 1min;
- 8) The relaxation curves can be seen in the Viewer of CombiLab program, while the compression forces and temperatures can be monitored in the Scanner during the test;
- 9) When the test is finished,  $F_0$  (force after 30 min from the start of the test) needs to be determined in the Viewer. Then the relaxation data can be exported for further analysis.

### **3.1.3 FTIR spectrometer – Perkin Elmer Spectrum One + ATR Accessory**

#### 3.1.3.1 Technical description

The Perkin-Elmer Spectrum One FTIR Spectrometer is a bench-top instrument consists of a sample compartment (for liquid cell, which is changeable with an ATR accessory), an optical system, a mid-infrared detector and an electronics system. The internal layout of the spectrometer is shown in Figure 34.

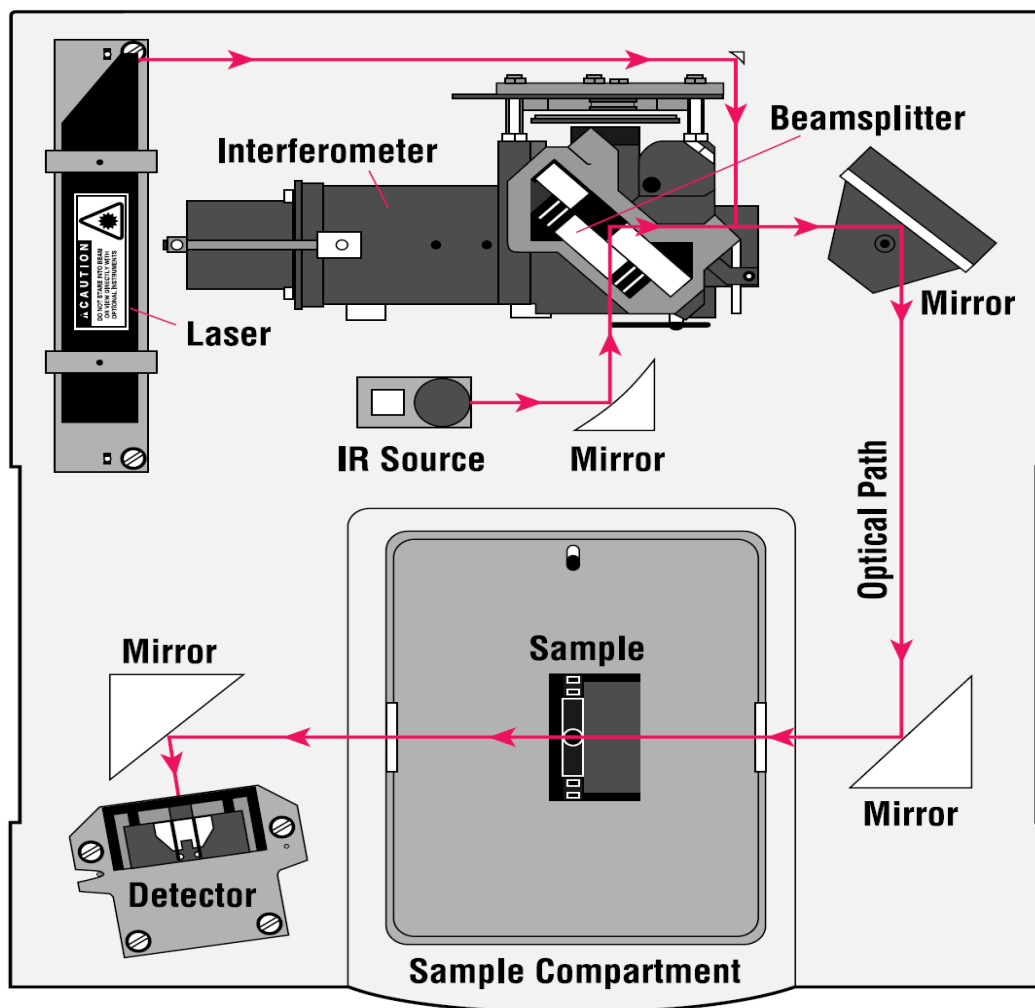


**Figure 34** Operating principle of the FTIR [97].

The Laser

The HeNe laser is employed as an internal wavelength calibration standard, which means the instrument is self-calibrating and does not need to be calibrated by the user.

The IR source

Infrared energy is emitted from a glowing black-body source, which is often ceramic. The beam passes through an aperture which controls the amount of energy that reaches the sample [67]. Due to the lack of photons, all IR spectrometers have limited energy, which means the hotter the source, the better. However, heating air to high temperatures could lead to the generation of (NO)<sub>x</sub>, which can cause unwanted

absorption and even corrosion of the metal and plastic components inside the sealed housing of an FTIR. As a result, the temperature should be controlled within a reasonable range [98].

### *The Michelson Interferometer*

As the heart of FTIR spectrometer, a Michelson interferometer analyses the infrared beam and generates the interferogram signal. The interferometer employs a beamsplitter which takes the incoming IR beam and divides it into two optical beams. One beam reflects off of a flat mirror which is fixed in place, and the other reflects off of a flat mirror which allows the mirror to move a few millimetres away from the beamsplitter. The two beams reflect off of their respective mirrors and are recombined when they meet back at the beamsplitter. Because of the optical path difference, the signal exits the interferometer is the result of these two beams interfering with each other. The resulting interferogram has the unique property that every data point (a function of the moving mirror position) which makes up the signal has information about every infrared frequency comes from the source [99] [100]. This means as the interferogram is measured, all frequencies are being measured simultaneously, rather than individually. It overcomes the main difficulty encountered with conventional dispersive instruments, which was the slow scanning process, making the whole operation easier and faster.

### *The Sample – ATR accessory*

In this work, the sample compartment is replaced by an ATR accessory for the O-ring analysis as shown in Figure 29. The IR beam enters the ATR crystal (ZnSe) where it is reflected off of the surface of the sample, as discussed in section 2.4.2. This is where the specific frequencies of energy, which are the unique characteristic of the sample, are absorbed.

### *The Detector*

The beam finally passes to the detector for final measurement. The detector used

here is a deuterated triglycine sulphate (DTGS) pyroelectric detector due to its higher sensitivity and shorter response time. The optical performance of the detector is listed in Table 8. The output from the detector then goes to a preamplifier where it is converted into a voltage signal varying with time. This signal has to be digitised and the job is usually done by a dedicated “analogue to digital” converter chip. The number of useful digits is governed by the quality (S/N ratio) of the signal [100].

**Table 8** Optical performance of the DTGS detector.

Attribute	Value
Wavelength range, $\text{cm}^{-1}$	7,800 – 350
Resolution, $\text{cm}^{-1}$	0.5 – 64
Wavelength accuracy	$0.1 \text{ cm}^{-1}$ at $1,600 \text{ cm}^{-1}$
Signal to noise (S/N) ratio	30,000/1 rms, 6,000/1 p-p for a 5 second measurement and 100,000/1 rms, 20,000/1 p-p for a 1 minute measurement
Available scanning velocities, cm/s	0.1, 0.2, 0.5, 1 and 2

### 3.1.3.2 *Test procedure*

- 1) With the aim to stabilise the optical system and to avoid moisture condensation, the FTIR spectrometer is left at ‘power on’ status constantly;
- 2) Start the ‘Spectrum’ software to communicate with the FTIR, and set the resolution at  $4 \text{ cm}^{-1}$ , spectrum range from  $4000$  to  $650 \text{ cm}^{-1}$ , and scanning speed at  $2 \text{ cm/s}$ ;
- 3) Take a background spectrum before the scanning of the sample, where normally 10 scans are applied and the result is the average of the 10 spectra obtained. The purpose of taking the background spectrum is to eliminate the interference by the instrument;
- 4) Take an O-ring sample tested from the stress relaxation test, absorb the solvent on its surface using a fuel absorbent material;

- 5) Place the O-ring sample on the top plate of the ATR accessory, adjust its position to ensure the surface of the sample is in contact with the crystal, and apply compression (being kept around 80N) to the sample by screw down the pressure arm;
- 6) Scan the sample at scan number of 20, after which the resulting spectrum is ready for further analysis.

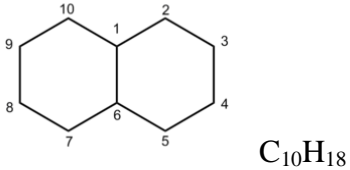


**Figure 35** Perkin-Elmer Spectrum One FTIR spectrometer with ATR accessory.

### **3.2 Candidate Fuels/Solvents**

Fuels or solvents tested in this work cover a wide range of chemical compounds and industrial interests which represent the potential fuel compositions of alternative aviation fuels in the future. Table 9 lists the descriptions of the candidate fuels or solvents.

**Table 9** Descriptions of candidate fuel or solvent samples.

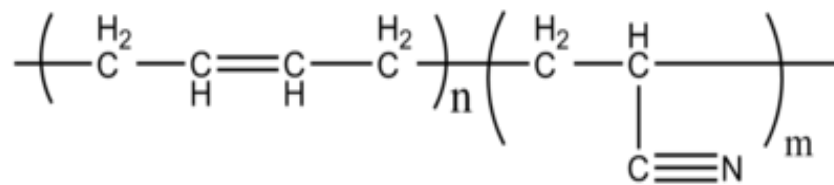
Name or Reference	Description
Jet A-1	A kerosene grade of aviation fuel; the most common jet fuel grade available worldwide (Jet A for USA); used as baseline fuel.
FSJF	Fully synthetic jet fuel (FSJF) derived from coal (Coal-to-Liquid; CtL) via Fischer-Tropsch (FT) process by Sasol; contains a significant amount of naphthenes; approved by DEF STAN 91-91 [101].
FT-SPK	Synthetic Paraffinic Kerosene (SPK) derived from natural gas (Gas-to-Liquid; GtL) via FT process by Shell; mainly paraffins (normal and iso-).
Bio-SPK	Bio-Derived Synthetic Paraffinic Kerosene (Bio-SPK) composed of a combination of normal and iso-paraffins with a small percentage of cycloparaffins.
HVO	Hydrotreated Vegetable Oils (HVO) comprised of paraffinic hydrocarbons and free of sulphur and aromatics.
Cycloalkanes	Also known as naphthenes are types of alkanes that have one or more rings of carbon atoms in their molecular structure.
Aromatics	A hydrocarbon with alternating double and single bonds between carbon atoms forming rings; a key type of fuel species to swell elastomeric seals (8-25% v/v as required in current jet fuel specification).
ShellSol T	A synthetic isoparaffin (>98% isoparaffins, <2% naphthenes) hydrocarbon solvent.
Decalin	<p>Decahydronaphthalene, a cycloparaffinic compound.</p>  <p style="text-align: right;"><math>C_{10}H_{18}</math></p>
N-decane	<p>An alkane hydrocarbon with the chemical formula <math>C_{10}H_{22}</math>.</p> 

<sup>1</sup>ShellSol: a Shell Trademark.

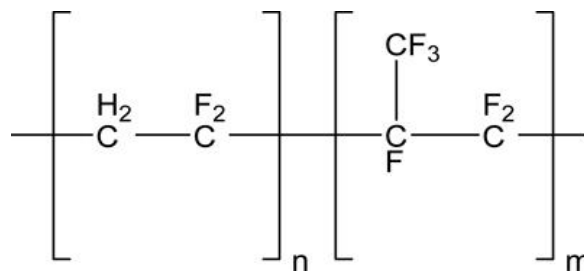
### 3.3 O-ring Materials

Three types of O-ring materials were chosen for testing: nitrile, fluorocarbon and fluorosilicone based polymers (Fig. 36). They were chosen not only because they

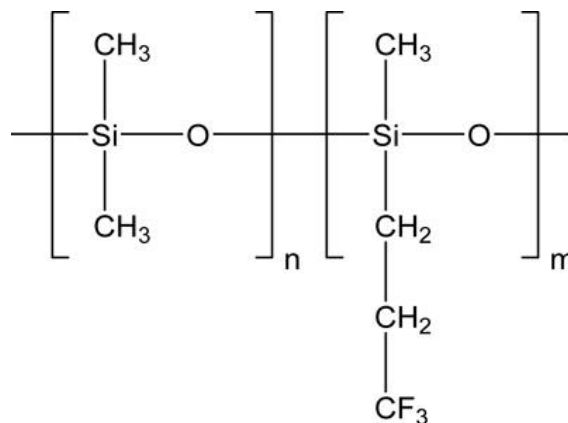
represent the types of O-rings used in the current market, but also the trend of changing standard of O-ring materials employed in the aviation industry. The fluorosilicone (FVMQ) O-rings were supplied by Parker Hannifin Corporation and both nitrile (NBR) and fluorocarbon (FKM) O-rings were provided by Trelleborg. All O-rings have the standard AS568 113 size [102], and each type of O-rings was from the same batch to ensure the similar specification and quality. Specifications of each material are provided in Table 10.



(a)



(b)



(c)

**Figure 36** Typical molecular structure of: (a) nitrile polymer; (b) fluorocarbon polymer; and (c) fluorosilicone polymer [103].

**Table 10** Specifications and physical properties of the sample O-rings.

<b>Specification or Physical Property</b>	<b>Fluorosilicone</b>	<b>Nitrile</b>	<b>Fluorocarbon</b>
Part No.	L1218 2-113	100-113-1109	100-113-2326
Colour	Blue	Black	Black
ID (mm)	13.94±0.18		
CS (mm)	2.62±0.08		
Density (kg/m <sup>3</sup> )	1650	1000	1850
Elongation (%)	250	300	350
Tensile strength (MPa)	9	18	12
Young's modulus (MPa)	5.6	4	7.8
Hardness (Shore)	55	70	80
Thermal conductivity (W/mK)	0.3	0.25	0.5
Glass temperature (°C)	-56	-40	-25

## **4 Results – Stress Relaxation Tests**

Solid results from extensive stress relaxation tests were obtained. To better demonstrate the considerable amount of outcomes, the following result section will be presented by each of the O-ring materials, i.e. in the order of nitrile, fluorosilicone and fluorocarbon O-rings. Results from all fuels or solvents will be compared and analysed accordingly.

When the raw data was obtained from the stress relaxation tests,  $F_t / F_0$  was generated first to evaluate how fast each compression force relaxed with time. Here,  $F_t$  (N) is the counterforce measured after the specified time (t) of the test;  $F_0$  (N) is the initial counterforce measured 30 min after completing the compression. The undulating shape of the relaxation curves were caused by ambient temperature fluctuation.

### **4.1 Nitrile O-Ring**

Previous research indicated nitrile O-ring is the most concerned material when adopting alternative fuels in an aircraft engine. However, due to the shortage of historical data on the material compatibility issue, no previous experience or reference could be used to compare the results. So the following section will be presented by the stress relaxation of nitrile O-ring (also for fluorosilicone and fluorocarbon O-rings) in different types of fuels respectively, with comparison to that in the baseline fuel Jet A-1. Jet A-1 is used as the baseline because it is currently employed as the standard aviation fuel worldwide and no elastomer compatibility issue was reported with it. The elastomer compatibility of any alternative fuel must be comparable to or even better than Jet A-1 in order to qualified as a 'drop-in' fuel.

#### **4.1.1 Relaxation Characteristics in Jet A-1: Baseline**

The stress relaxation characteristic of nitrile O-ring in Jet A-1 was shown in Figure 37. Generally, the relaxation process can be divided into three phases: quick

reduction, reversed increment, and further relaxation.

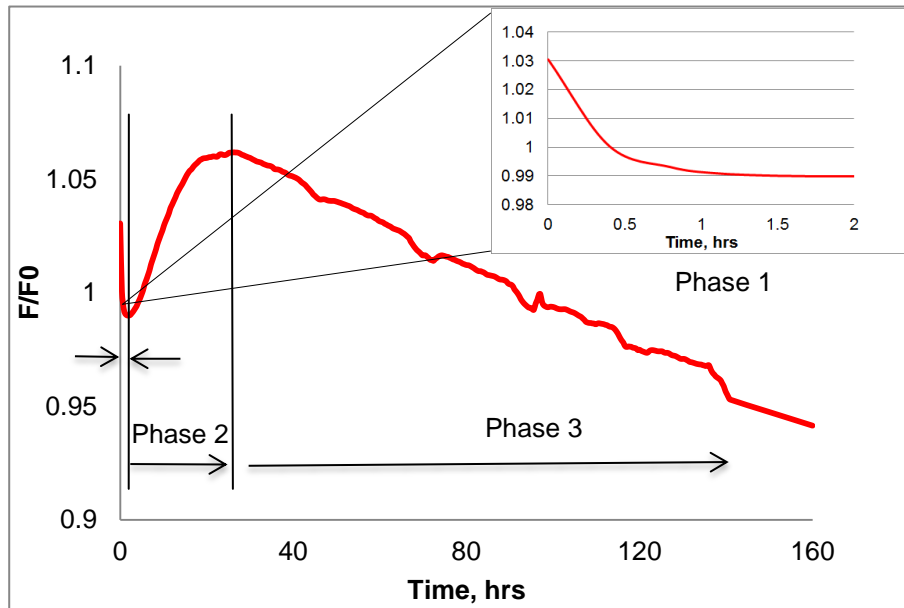


**Figure 37** The stress relaxation characteristic of nitrile O-ring in Jet A-1.

*Phase 1: Quick Reduction.* The counterforce decreases sharply especially within the initial 30 minutes (relaxes by 3.4%) during this phase as elastomeric material is viscoelastic, which means it has both the properties of viscous and elastic materials and, as such, exhibit time dependant strain [104]. From 30 minutes till 2 hours, the relaxation rate slows down gradually due to the effect of the fuel-polymer interaction.

*Phase 2: Swelling.* Rather than further relaxation, a reversed counterforce increment is observed during this phase as a result of the O-ring swelling. This is caused by particular fuel species, notably aromatic compounds diffusing into the polymer structure [38]. The space amongst the polymer molecules are occupied by the fuel molecules, resulting in an increase in volume. The fuel molecules also interact with the polymer molecules to form fuel-polymer bonds. The load cell of the relaxation rig senses the pressure imposed by the volume swell of the O-ring which results in the increase of compression force. This phase lasts for about 28 hours after the initial

quick reduction and the counterforce increases by 7% by the end of this phase.

*Phase 3: Further Relaxation.* When the volume swell and the compression reach equilibrium, the counterforce starts to decrease again gradually. The stress induced by the compression on the O-ring causes the polymer molecular movement, resulting in a conformational change of polymer structure. The molecular chains slip past one another, which causes a fast reputation. As a result, the stress required to maintain the strain decodes. The relaxation rate in this phase is relatively steady, approximately 0.09% per hour.

In order to compare the effects of various fuels on nitrile O-rings efficiently, a 160-hour test was conducted for each fuel sample as it was proved to be time-efficient and data-adequate. If the relaxation curve obtained in a fuel sample is above or similar to that in Jet A-1, it means the general relaxation rate of nitrile O-ring in this fuel is slower or similar to that in Jet A-1. In other words, the compatibility of nitrile O-ring with this fuel is better than or similar to Jet A-1. If a relaxation curve is below that in Jet A-1, it means the general relaxation rate of nitrile O-ring in this fuel is faster than the baseline.

#### **4.1.2 Relaxation Characteristics in Typical Alternative Fuels and Blends**

A range of alternative fuels which are regarded as the potential replacements for Jet A-1 (Jet A in the USA) were tested in this project. Detailed fuel compositions were listed in Table 11.

**Table 11** Compositions of alternative fuel samples tested.

<b>No.</b>	<b>Composition</b>	<b>Provider</b>
1	100% FSJF	Alfa-bird program <sup>1</sup>
2	100% FT-SPK	Shell
3	80% FT-SPK + 20% Aromatics <sup>2</sup>	Shell
4	80% FT-SPK + 20% Hexanol	Alfa-bird program
5	60% FT-SPK + 40% Naphthenes	Shell

6	50% FT-SPK + 50% Naphthenes	Alfa-bird program
7	50% FT-SPK + 30% Naphthenes + 20% Aromatics	Shell
8	75% HVO + 25% Jet A-1	SWAFEA program <sup>3</sup>
9	50% HVO + 50% Naphthenes	SWAFEA program
10	50% Bio-SPK + 50% Jet A-1	SWAFEA program

<sup>1</sup>Alfa-bird program: Alternative Fuels and Biofuels for Aircraft Development, a project co-funded by the EU [16].

<sup>2</sup>All blends were prepared by volume.

<sup>3</sup>SWAFEA program: Sustainable Way for Alternative Fuel and Energy in Aviation, a European Commission funded research program [15].

#### 4.1.2.1 *FSJF (CtL) vs. FT-SPK (GtL)*

As two types of synthetic fuels produced from F-T process, FSJF and FT-SPK were compared together with the baseline fuel Jet A-1. Relaxation characteristics of nitrile O-rings in these neat synthetic fuels were presented in Figure 38.

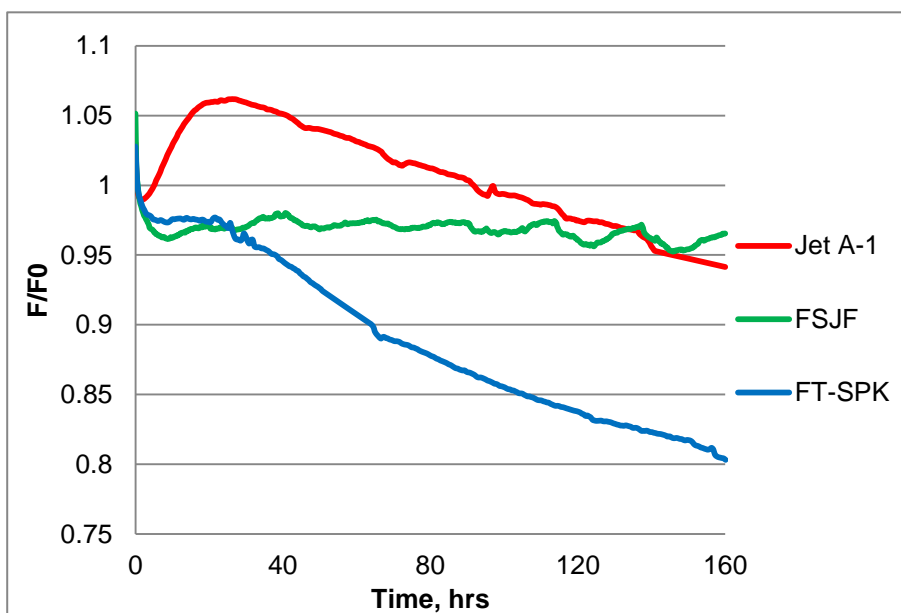


**Figure 38** The relaxation characteristics of nitrile O-rings in FSJF and FT-SPK.

Nitrile O-ring showed quite different behaviours in these two fuels. In FSJF, the counterforce maintained at a steady level around the  $F/F_0$  value of 0.97 after the initial quick reduction phase. Relaxation process started to continue slowly after 120

hours. By contrast, nitrile material relaxed quickly in FT-SPK despite of a short level-off phase (about 18 hours) after the initial quick reduction. The final normalized counterforce was 16% lower than that of FSJF, indicating a significant higher degree of relaxation.

When compared with the relaxation characteristic in Jet A-1, neither fuels were considered comparable to the baseline within the initial 120 hours of the tests, as O-rings in neither fuels presented obvious swelling behaviour. The counterforces in both fuels were far below the level in Jet A-1. After 120 hours, as O-ring in Jet A-1 further relaxed, the level of counterforce dropped to be close to that in FSJF. This indicated the compatibility of nitrile O-ring with FSJF might be comparable to Jet A-1 in a long-term service. As FSJF has already been approved to be used in current aircraft safely, it also indicates it is compatible with current sealing materials. The compatibility of nitrile material with FT-SPK is not comparable to Jet A-1.

The differences presented in the stress relaxation characteristics were a result of diversity of fuel compositions. FSJF has a significant amount of cycloparaffins (over 90% of its composition), while FT-SPK comprises of normal and iso-paraffins mainly. It is interesting to see how these components are actually influencing the stress relaxation process of sealing materials. Further investigation will be described in the 'triangle test' sections.

#### *4.1.2.2 FT-SPK based blends*

The overall stress relaxation characteristics of five FT-SPK based fuel blends were shown in Figure 39. There are two reasons for using FT-SPK as the base fuel rather than other alternative fuels; one is because FT-SPK is a promising alternative candidate in the aviation industry due to its excellent combustion properties and reduced emissions. The other reason is its elastomer compatibility is still a major concern due to its fuel composition and previous incident experienced in engine tests.

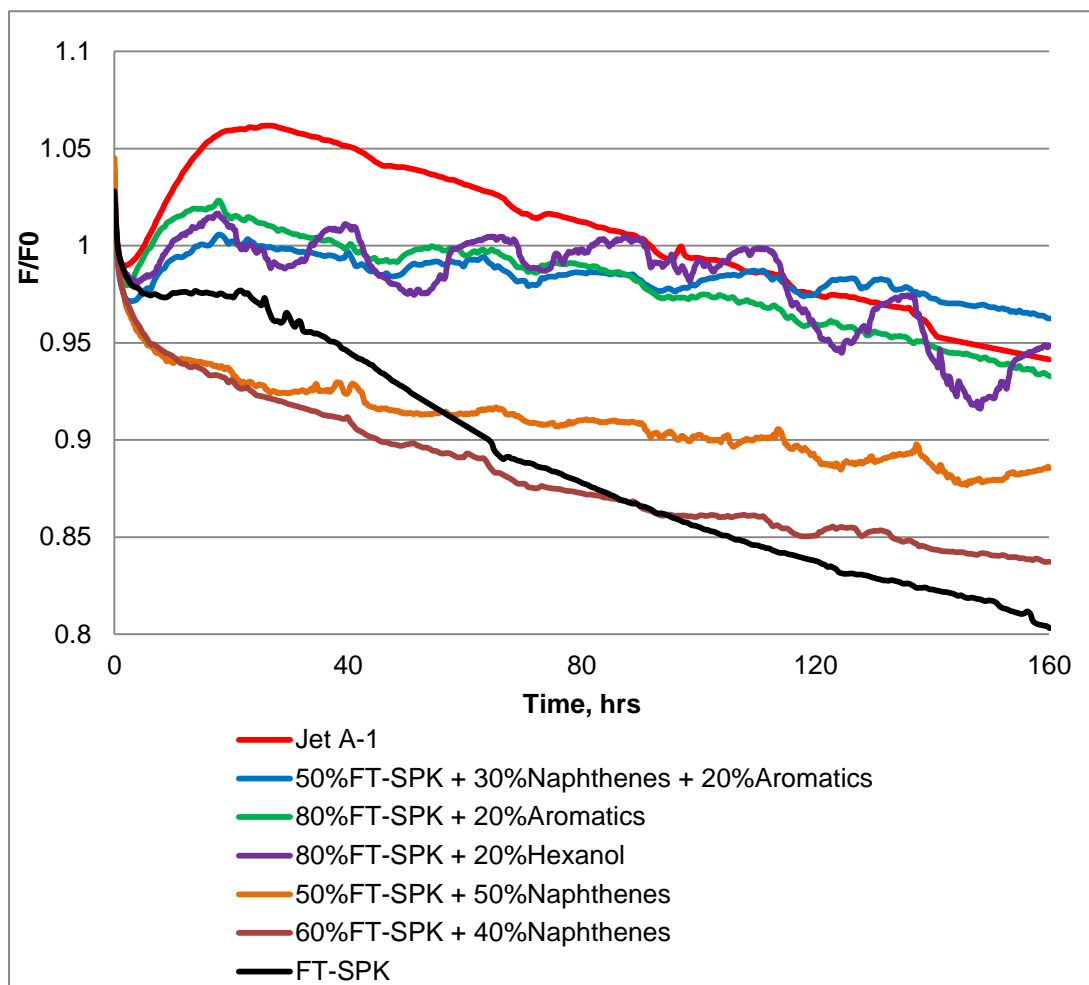


**Figure 39** Overall stress relaxation characteristics of nitrile O-rings in 5 FT-SPK based blends, with comparison to FT-SPK and Jet A-1.

Generally, all blends demonstrated better compatibility with nitrile O-rings than neat FT-SPK by the end of the 160-hour tests. Three blends, with either aromatics or hexanol, presented closer final relaxation counterforce value to Jet A-1. To better explain the results, these blends were compared in pairs.

#### FT-SPK + Naphthenes

With 10% more naphthenes (cycloparaffins) in the blends, the relaxation process of nitrile O-ring was slowed down in (50% FT-SPK + 50% Naphthenes) than (60% FT-SPK + 40% Naphthenes) (Fig. 40). Neither of them showed the 'level-off' phase within the initial 30 hours compared with neat FT-SPK, due to the reduction in FT-SPK concentration. However, the relaxation rates of nitrile O-rings in these two

blends were reduced notably. The addition of naphthenes slowed down the whole relaxation process; the more naphthenes in the blends, the slower the relaxation rate becomes.

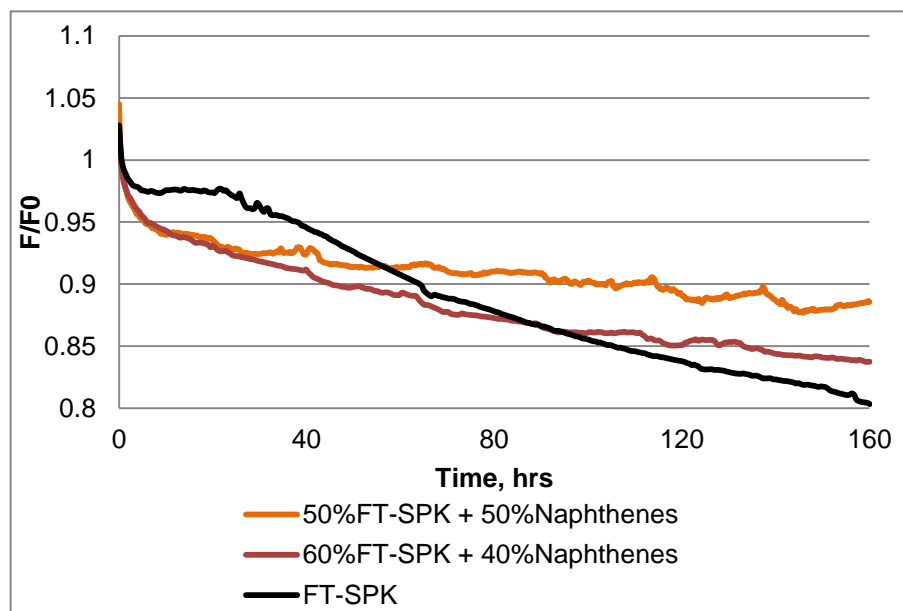


**Figure 40** Comparison between FT-SPK based blends with different proportions of naphthenes (nitrile).

#### FT-SPK + 20% Aromatics/Hexanol

Nitrile O-rings in FT-SPK blended with 20% aromatics presented similar relaxation characteristic to that in FT-SPK with 20% hexanol as shown in Figure 41. With the same proportion of FT-SPK, the relaxation characteristics actually reflected the effects of aromatics and hexanol on the material. O-rings in both blends experienced a certain amount of swelling, indicating both aromatics and hexanol molecules have the ability to penetrate into the polymer structure. After the swelling reaches equilibrium within the initial 40 hours, the counterforces could still maintain a relatively high level. And by the end of tests, both of them presented similar counterforces to Jet A-1. These results suggest hexanol or other compound with alcohol-like molecular structures may have similar O-ring swelling ability to aromatic compounds. However, further tests are needed to prove this indication.

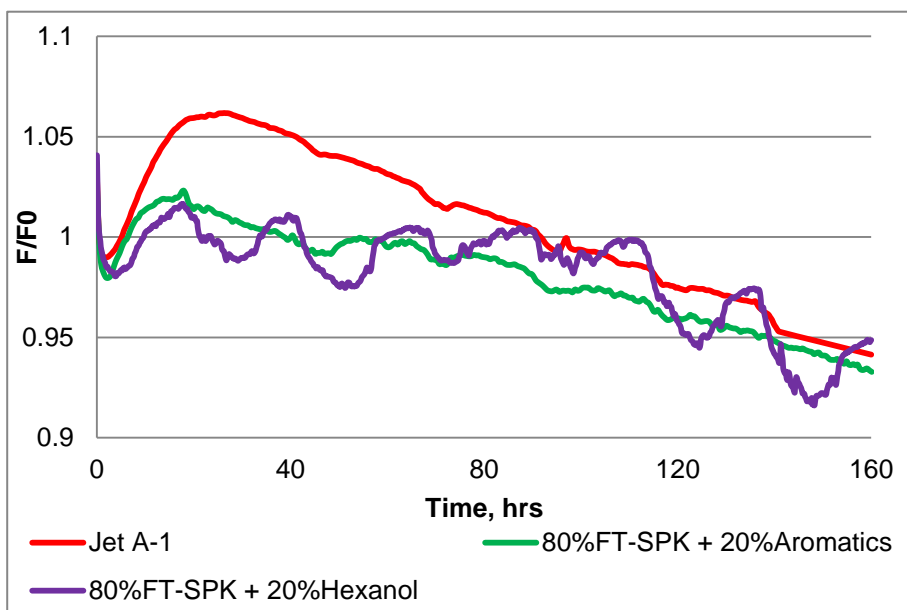


**Figure 41** Comparison between FT-SPK based blends with 20% aromatics/hexanol (nitrile).

#### FT-SPK + Naphthenes/Aromatics

Difference between the compositions of these two blends is the additional 20% aromatics/naphthenes (Fig. 42). As a result, when comparing the relaxation characteristics of nitrile O-rings in (50% FT-SPK + 30% Naphthenes + 20% Aromatics) and (50% FT-SPK + 50% Naphthenes), the different effects of aromatics and naphthenes were observed. Apparently, aromatics are more effective than naphthenes in term of nitrile O-ring swelling. The initial counterforce increase within the first 20 hours was caused by the presence of aromatics, which was also the reason for the different relaxation patterns. However, as the O-rings relaxed, the relaxation rates in both blends were relatively similar, which indicates the effect of aromatic compounds may be to swell the O-ring in the initial hours mainly due to their relatively small molecular size. Naphthenes, as discussed in previous comparison, may contribute in the relaxation rate slow-down process.

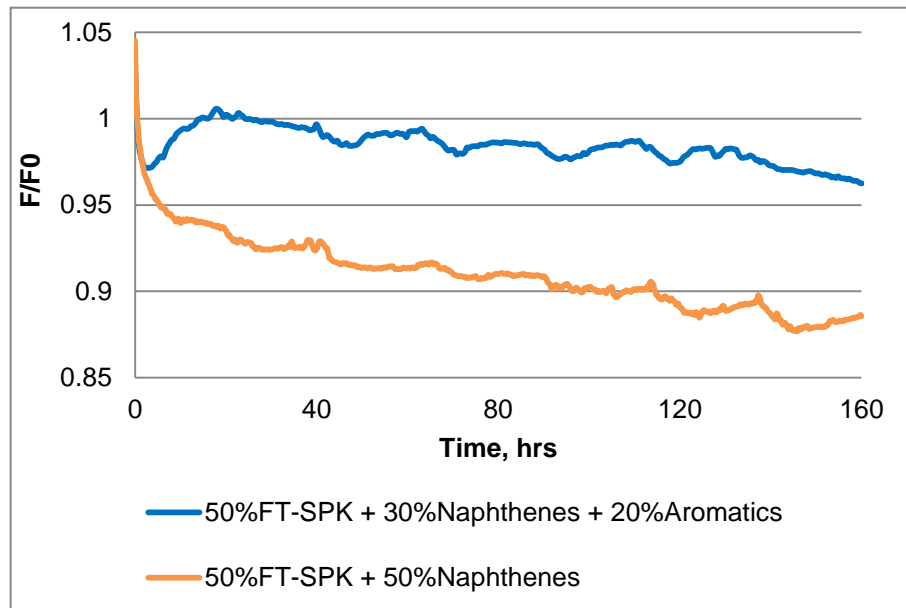


**Figure 42** Comparison between FT-SPK based blends with (naphthenes + aromatics) and naphthenes only (nitrile).

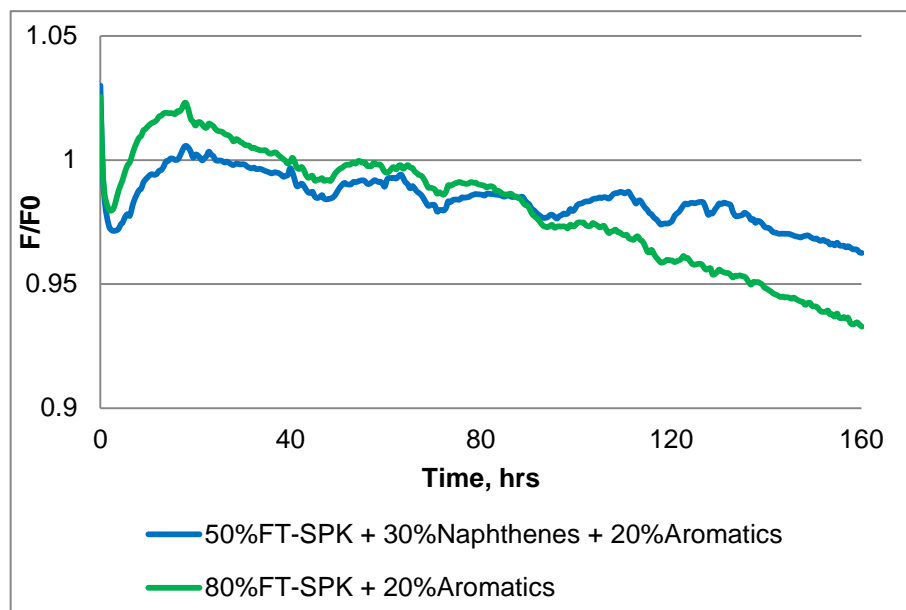


**Figure 43** Comparison between FT-SPK based blends with (naphthenes + aromatics) and aromatics only (nitrile).

This observation was supported when comparing the relaxation curves in (50% FT-SPK + 30% Naphthenes + 20% Aromatics) and (80% FT-SPK + 20% aromatics) (Fig. 43). As both blends have the same amount of aromatics, differences in the relaxation curves were caused by the additional 30% FT-SPK/naphthenes. The

additional 30% FT-SPK resulted in a larger amount of swelling in the initial 20 hours as the highest level of normalized counterforce reached 1.02 compared to 1.00 in the other blend. However, the relaxation rate after the initial swelling was faster in (80% FT-SPK + 20% aromatics), with 0.06% per hour compared to 0.03% per hour in (50% FT-SPK + 30% Naphthenes + 20% Aromatics). This result further proved the ability of naphthenes in slowing down the relaxation process of nitrile O-rings, and also indicated the role of FT-SPK played in the process; to participate in the initial O-ring swelling process and to accelerate the relaxation process afterwards. Further investigation into the effects of each fuel component in the FT-SPK have in this process will be presented in section 4.14. The mechanism of how naphthenes slow down the process need to be further understood.

In conclusion, the overall stress relaxation performance of the 5 FT-SPK blends in comparison with Jet A-1 and neat FT-SPK could be rated as follows:

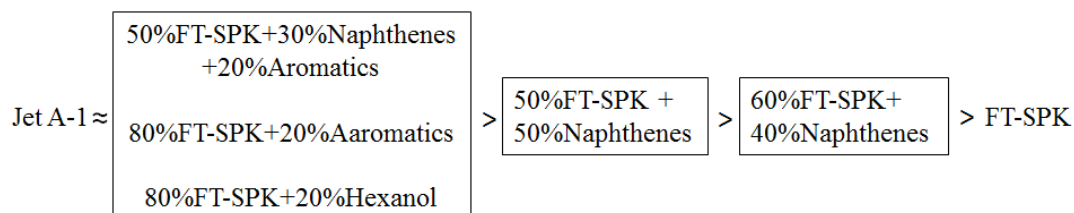


**Figure 44** Stress relaxation performance comparison of 5 FT-SPK blends (nitrile).

#### 4.1.2.3 *HVO and Bio-SPK blends*

Nitrile O-rings in HVO and Bio-SPK based blends did not show much difference in the stress relaxation characteristics (Fig. 45). Slight swelling behaviour was observed for the O-ring in (50% Bio-SPK + 50% Jet A-1) and all blends presented similar relaxation rate throughout the test. Although none of them showed comparable compatibility to Jet A-1, their final counterforces were all recorded around 0.9.

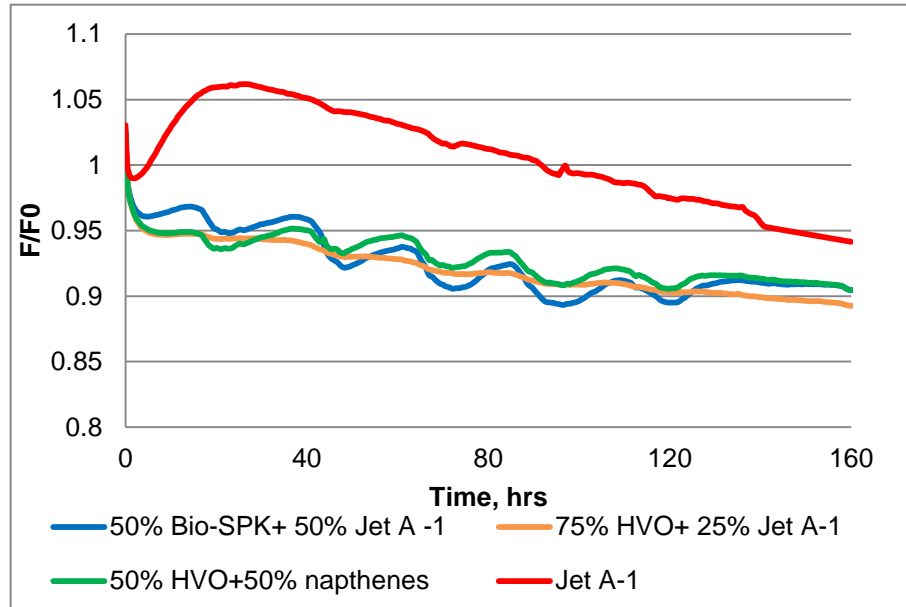


**Figure 45** Comparison between HVO and Bio-SPK based blends (nitrile).

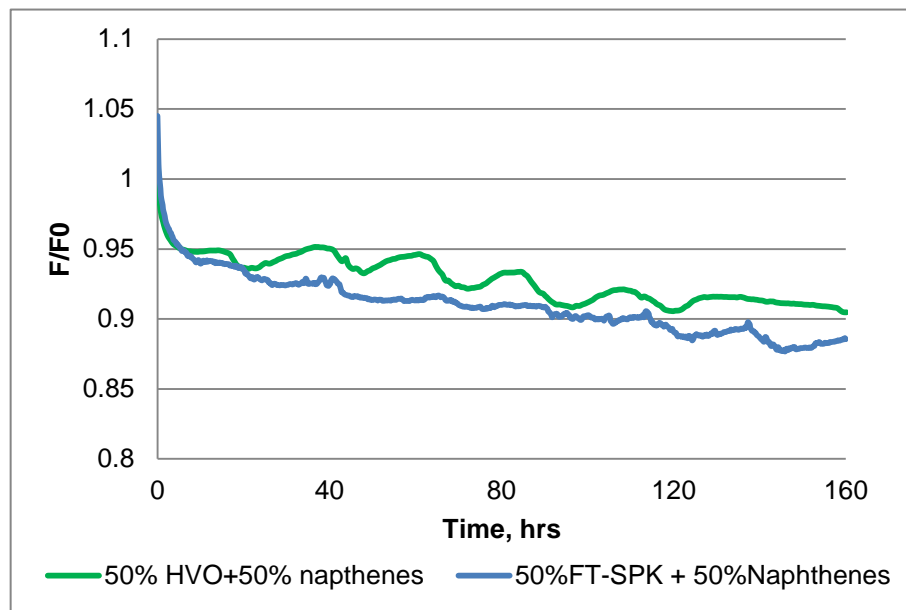


**Figure 46** Comparison between HVO and FT-SPK (nitrile).

If comparing (50% HVO + 50% naphthenes) with (50% FT-SPK + 50% naphthenes), the effects of HVO and FT-SPK on the relaxation process can be compared. Although both fuels comprise of paraffins, HVO demonstrated slightly better compatibility with nitrile O-rings than FT-SPK.

#### 4.1.2.4 Comparison with Jet A-1

As there is no standard criterion for testing elastomer compatibility with alternative fuels in the aviation industry, a comparative method was developed here to show the normalized final compression forces by the end of the 160h tests relative to the value in Jet A-1 (Fig. 47).

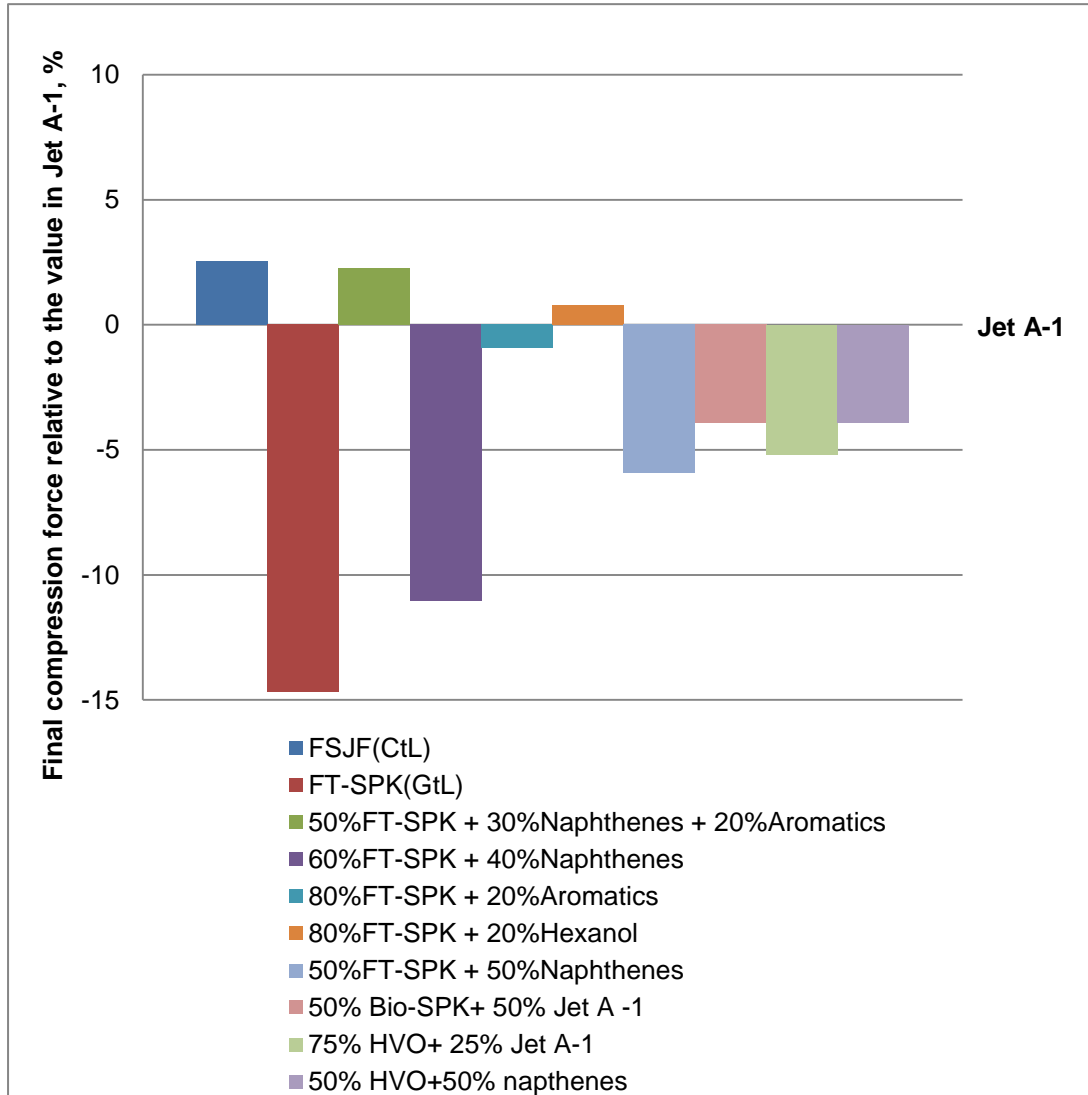


**Figure 47** Normalized final compression forces of nitrile O-rings in all alternative fuels or blends relative to the value in Jet A-1, %.

Figure 47 showed three fuels or blends lay above the line representing Jet A-1, which were (80% FT-SPK + 20% Hexanol), (50% FT-SPK + 30% Naphthenes + 20%

Aromatics), and FSJF, indicating the final compression forces or sealing forces of nitrile O-rings in these fuels were relatively higher than in Jet A-1. The rest of fuels or blends lay beneath Jet A-1; however, 4 of them lay relatively close (within -5% relative to Jet A-1), namely (75% HVO + 25% Jet A-1), (50% Bio-SPK + 50% Jet A-1), (50% HVO + 50% Naphthenes), and (80% FT-SPK + 20% Aromatics). (50% FT-SPK + 50% Naphthenes), (60% FT-SPK + 40% Naphthenes), and FT-SPK lay outside the  $\pm 5\%$  zone with the biggest difference appeared in FT-SPK (-14.68%).

Although these data are not sufficient to indicate if nitrile O-rings would perform enough sealing or would leak in these fuels, it provides an approach to demonstrate which fuel or blend is more similar to Jet A-1 in terms of elastomer compatibility. As previous experiences indicating neat FT-SPK (GtL) will cause fuel leakage (nitrile O-ring shrinkage), it may suggest the zone around -14.68% is not 'safe' for nitrile seals. Half-blended SPK with Jet A-1, also known as SSPK (semi-synthetic paraffinic kerosene) has been used safely in demonstrative flights; this may indirectly show its compatibility is acceptable (within -5% in the figure).

Based on the data obtained and information discussed, it may suggest that *nitrile seals are relatively safe to be used in an alternative fuel environment if the normalized compression/sealing force after 160-hour stress relaxation test is within  $\pm 5\%$  zone relative to that value in Jet A-1*. Further tests are needed to prove this 'safe zone' suggestion and to find the criterion below which nitrile seals are 'unsafe' to be used.

#### **4.1.3 Relaxation Characteristics in the 'Triangle' Blends**

To further investigate the effect of individual chemical species on elastomer compatibility, a "normal-iso-cycloparaffins" solvent triangle was designed. N-decane, ShellSol T (an isoparaffinic solvent), and decalin solvent were selected to represent each of the fuel species. As SPKs are composed of normal and iso-paraffins, this evaluation could explain the relaxation behaviour of nitrile O-rings in SPKs. Decalin,

as a representative of cycloparaffins (naphthenes), may also help to explain the effect of this species during stress relaxation. 25 blends with various combinations of these three solvents were developed within the triangle as shown in Figure 48. Each vertex of the triangle represented one single solvent. The big triangle was divided into six small triangles by the medians on each side. Then, the vertexes, intersection point of the medians, and the midpoints on each side of each small triangle were set as the sample points for blending. Detailed proportions of each solvent in these blends were listed in Table 12.

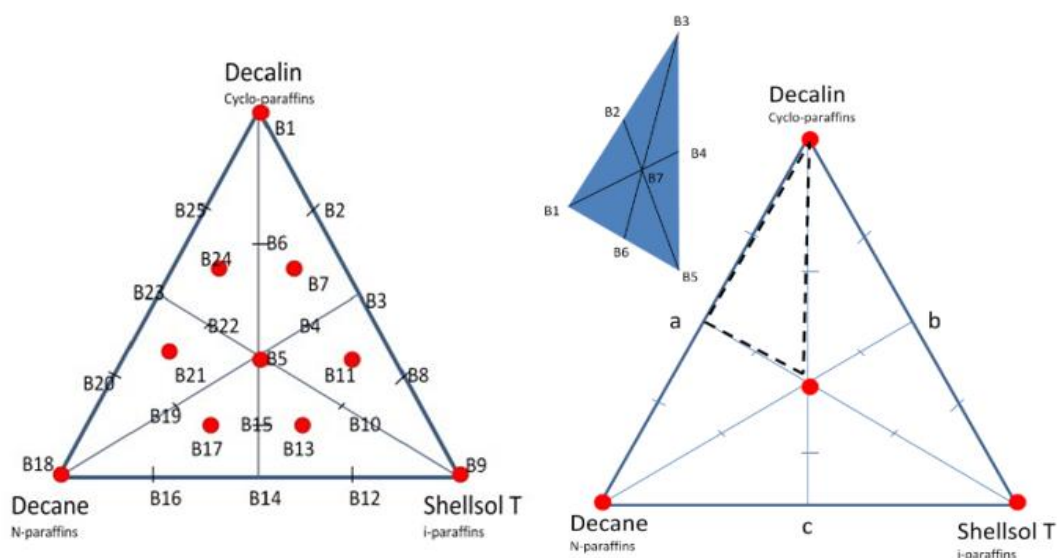


**Figure 48** “Normal-iso-cycloparaffins” solvent triangle.

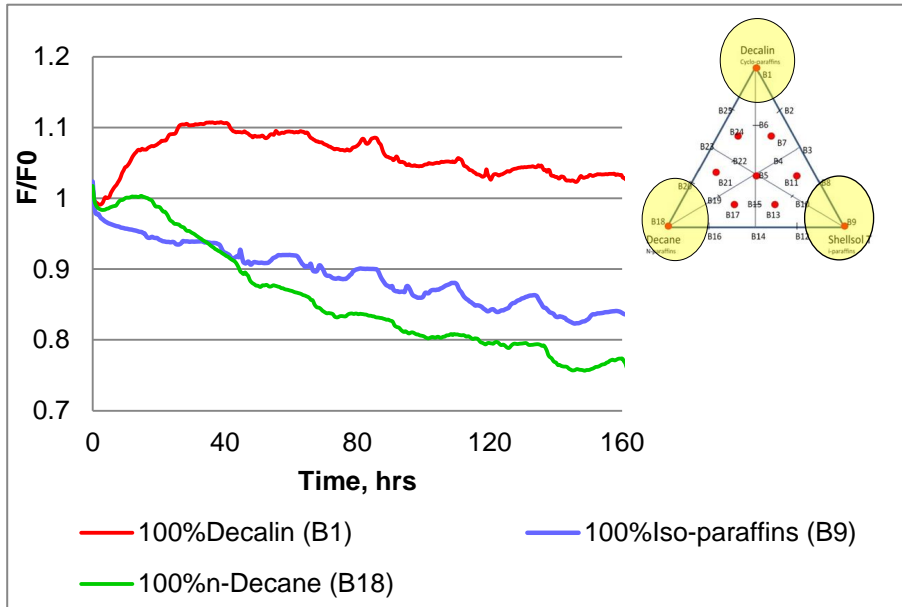
**Table 12** Solvent matrix for testing.

Blend No.	Composition (%)		
	Decalin (cyclo-)	ShellSol T(iso-)	N-decane (n-)
B1	100	0	0
B2	75	25	0
B3	50	50	0
B4	41.5	41.5	17
B5	33.3	33.3	33.3
B6	66	17	17

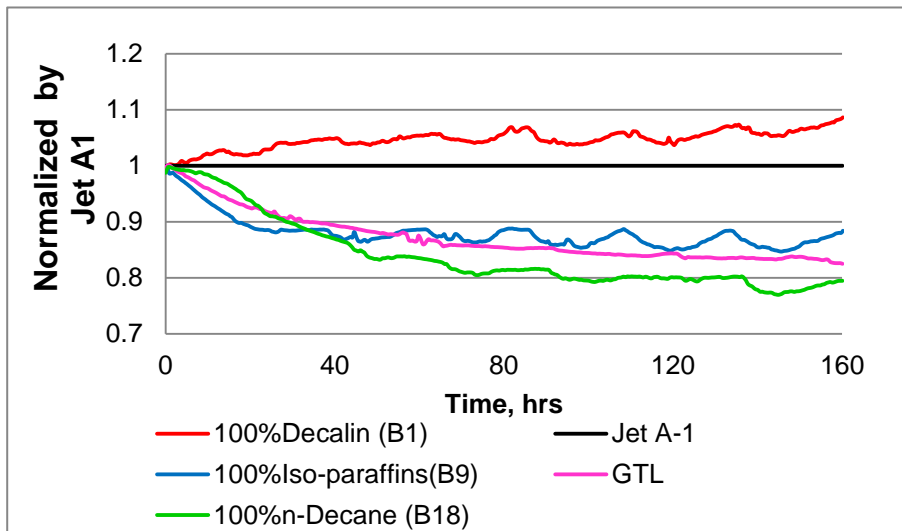
B7	61.1	27.8	11.1
B8	25	75	0
B9	0	100	0
B10	17	66	17
B11	27.8	61.1	11.1
B12	0	75	25
B13	11.1	61.1	27.8
B14	0	50	50
B15	17	41.5	41.5
B16	0	25	75
B17	11.1	27.8	61.1
B18	0	0	100
B19	17	17	66
B20	25	0	75
B21	27.8	11.1	61.1
B22	41.5	17	41.5
B23	50	0	50
B24	61.1	11.1	27.8
B25	75	0	25

#### *4.1.3.1 Vertexes of the Triangle*

Nitrile O-rings performed quite differently in these three solvents as shown in Figure 49 (a). In decalin and n-decane, the stress relaxation process could also be divided into three phases, ‘quick reduction’, ‘reversed increment’, and ‘further relaxation’, which was the same as in Jet A-1 (section 4.1.1).



(a)



(b)

**Figure 49** Relaxation process of nitrile O-ring: (a) in three single solvents respectively; (b) normalized by Jet A-1 with comparison to GTL kerosene (FT-SPK).

In phase 2, ‘reversed increment’, the observation proved that both decalin and n-decane have the ability to diffuse into the polymer structure of nitrile O-ring due to their relatively small molecular size. Decalin may also benefit from its ring-shape molecular geometry which is similar to naphthalene (diaromatics). Previous research suggested that alkanes are relatively ‘inactive’ to swell the O-ring and that is a main reason why a certain percentage of aromatics are needed in the composition of jet

fuel. Result here indicated alkanes are also capable to participate in the O-ring swelling process if their sizes are small enough. In phase 3, the relaxation rate of nitrile O-ring in n-decane was much faster than that in decalin suggested n-decane's ability to extract component out of this material is greater than decalin.

By contrast, nitrile O-ring in iso-paraffins did not present any swelling behaviour (Fig. 49 (a)). After the initial quick reduction in counterforce, O-ring relaxed gradually, with similar relaxation speed as that in decalin in its phase 3. This suggested iso-paraffin may not participate in the O-ring swelling process, which means this class of hydrocarbon compound is not a contributor with regard to fuel's O-ring swelling property.

When normalized by the stress relaxation behaviour in Jet A-1 fuel with comparison to FT-SPK (GTL kerosene) (Fig. 49 (b)), it can be seen that nitrile O-ring in decalin presented even better relaxation performance than that in Jet A-1. O-ring swelled to a larger amount of volume and relaxed slower afterwards, which suggested pure decalin solvent has good nitrile O-ring swelling property. Iso-paraffins, GTL kerosene, and n-decane solvents presented worse O-ring swelling ability than Jet A-1 fuel. GTL kerosene, as its main components are normal and iso-paraffins, presented a combined characteristic of both n-decane and iso-paraffins as its relaxation curve lied between those of the two solvents. Its ability to swell the nitrile O-ring was weaker but made the O-ring relaxed slower than pure n-decane solvent, due to the effect of iso-paraffins.

Regarding the ability to swell nitrile O-rings, these five types of fuels or solvents could be graded as follows:

**Table 13** O-ring swelling property (OSP)\* of five solvents.

Solvent	Jet A-1	GTL	Decalin	N-decane	ShellSol T
OSP	+	-	+	-	-

\*+: promote the O-ring swelling process

- : weaken the O-ring swelling process

#### 4.1.3.2 *Edges of the Triangle*

##### *Decalin ↔ N-decane*

Figure 50 showed the stress relaxation characteristics of nitrile O-rings in decalin blended with n-decane by 0%, 25%, 50%, 75% and 100% (v/v). It can be seen clearly that as the proportion of decalin (n-decane) increased (decreased) in the blends, nitrile O-ring relaxed slower, or its sealing performance was improved dramatically. Without considering the influence by the temperature fluctuation, its degree of relaxation was reduced roughly proportional to the percentage of decalin in the blends. It was proved again that the OSP of decalin is much better than that of n-decane. The relaxation behaviour of the blend could be comparable to that of Jet A-1 when the proportion of decalin reached 75%.

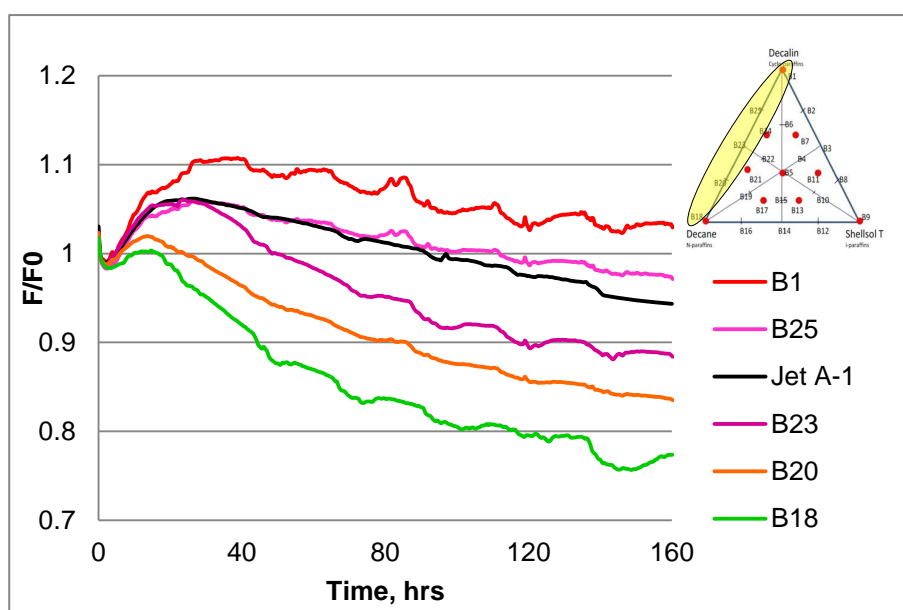


**Figure 50** Relaxation process of nitrile O-rings in the blends of decalin and n-decane solvents.

### *Decalin ↔ Iso-paraffins*

Figure 51 showed the stress relaxation behaviours of nitrile O-rings in decalin blended with ShellSol T solvent by 0%, 25%, 50%, 75% and 100% (v/v). It can be seen clearly that as the proportion of decalin (iso-paraffins) increased (decreased) in the blends, nitrile O-ring's sealing performance was improved dramatically. The degree of relaxation was also reduced roughly proportional to the percentage of decalin in the blends, when not taking the influence by the temperature fluctuation in consideration. It could be said that the OSP of decalin is also better than that of iso-paraffins. The relaxation behaviour of the blend could also be comparable to that of Jet A-1 when the proportion of decalin reached 75%.

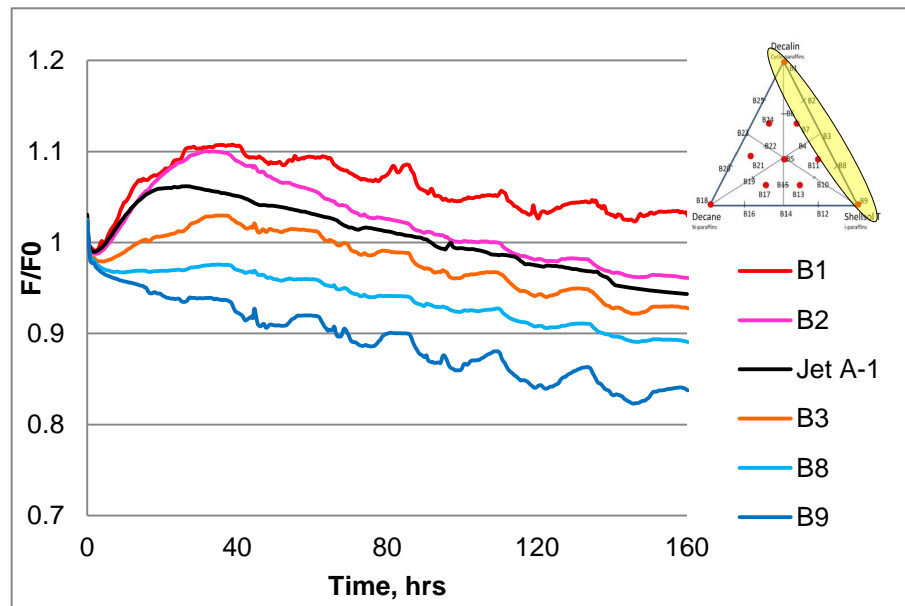


**Figure 51** Relaxation process of nitrile O-rings in the blends of decalin and isoparaffins.

### *Iso-paraffins ↔ N-decane*

Figure 52 showed the stress relaxation behaviours of nitrile O-rings in iso-paraffins blended with n-decane solvent by 0%, 25%, 50%, 75% and 100% (v/v). As the proportion of iso-paraffins (n-decane) increased (decreased), the relaxation curves raised slightly. Although iso-paraffins didn't participate in the O-ring swelling process, its ability of extracting material out of the O-ring was weaker than n-decane,

which makes it an “improver” when blended with the latter. So overall, its OSP is slightly better than that of n-decane. However, only mixing iso-paraffins and n-decane cannot provide enough O-ring swelling property to the blended solvents, no matter by what proportions; as O-ring relaxed much faster than that in Jet A-1.

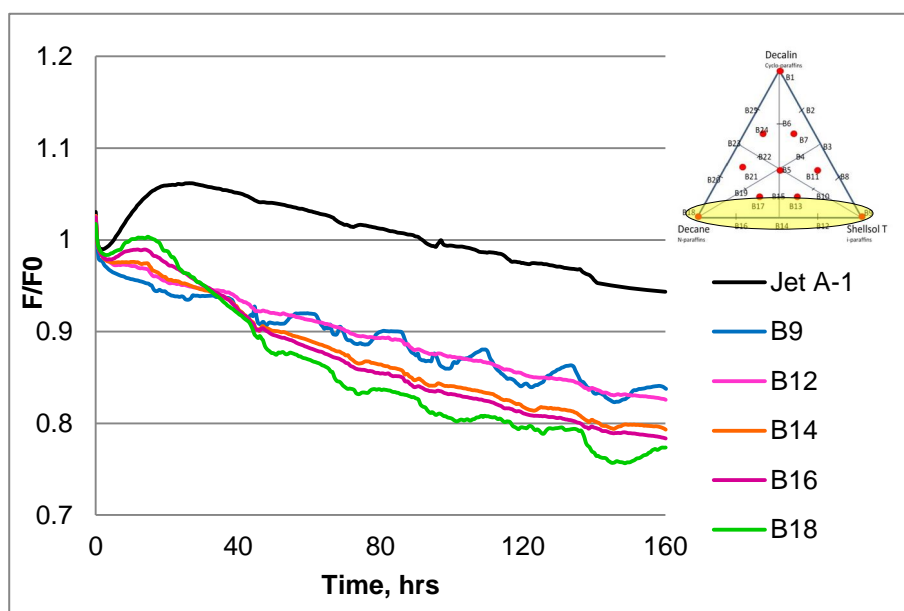


**Figure 52** Relaxation process of nitrile O-rings in the blends of iso-paraffins and n-decane solvents.

From the results obtained from the ‘edge of the triangle’, it can be clearly seen that when blending two of the three solvents together, only decalin can promote the OSP of the final blend. However, in order to be comparable to Jet A-1, the proportion of decalin in the blend need to be around 75%. The OSP of the three solvents in two component blends can be compared as:

Decalin > Iso-paraffins > N-decane

#### 4.1.3.3 Insides of the Triangle

In order to compare the respective effect of the three solvents in three-component blends, the insides of the triangle were divided into three regions, based on their relative position towards each vertex.

### *'Decalin Region'*

The 'decalin region' consisted of six blends, which were B4, B5, B6, B7, B22, and B24 (Fig. 53). The percentages of decalin in the blends ranged from 33.3% to 66%, while both iso-paraffins and n-decane were between 11.1% and 41.5%. O-rings in these blends all presented a certain degree of swelling; and as the proportion of decalin increased, the relaxation processes were improved. When the amount of decalin was certain, the more n-decane was in the blends, the worse the relaxation behaviour became. It seemed the blends need to have more than 66% of decalin in its composition in order to be comparable to Jet A-1.

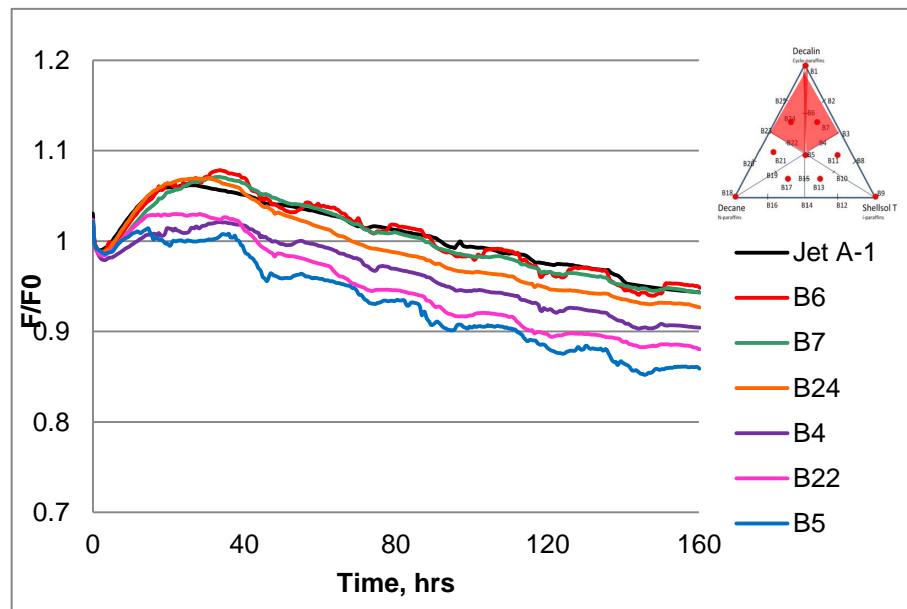


**Figure 53** Relaxation process of nitrile O-rings in the blends of 'decalin region' (in red).

### *'Iso-paraffin Region'*

The 'iso-paraffin region' consisted of six blends, which were B4, B5, B10, B11, B13, and B15 (Fig. 54). The percentages of iso-paraffins in the blends ranged from 33.3% to 66%, while both decalin and n-decane were between 11.1% and 41.5%. Compared with the 'decalin region', the whole spectrum of relaxation curves shifted downwards dramatically. Slight difference in the composition of the blends seemed not change the relaxation behaviour much (e.g. B10 and B13), though generally it

was still improved with the increase of decalin content.

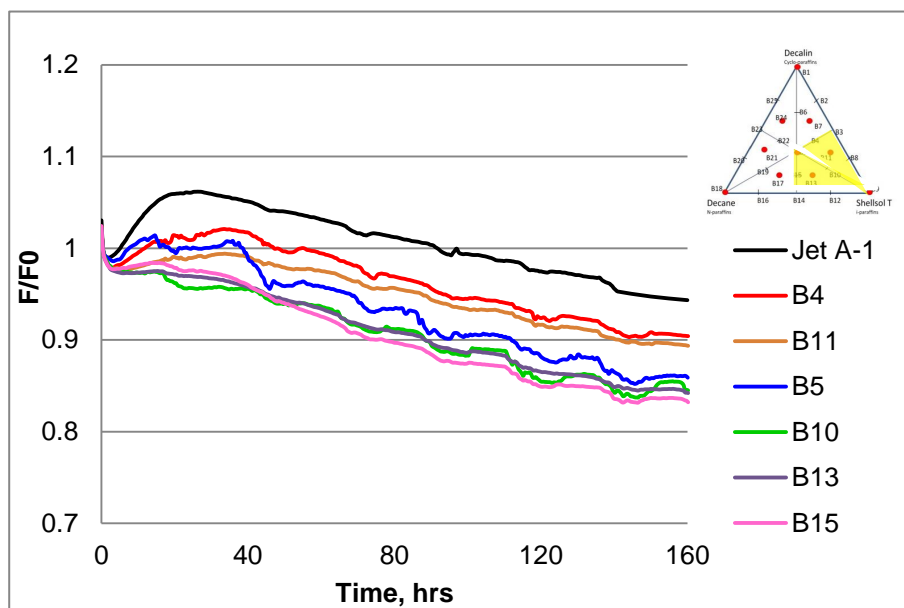


**Figure 54** Relaxation process of nitrile O-rings in the blends of ‘iso-paraffin region’ (in yellow).

#### ‘N-decane Region’

The ‘n-decane region’ also consisted of six blends, which were B5, B15, B17, B19, B21, and B22 (Fig. 55). The percentages of n-decane in the blends ranged from 33.3% to 66%, while both decalin and iso-paraffins were between 11.1% and 41.5%. Compared with the ‘iso-paraffin region’, the whole spectrum of relaxation curves shifted further downwards. Generally, the closer the blend was to the vertex of n-decane, the lower the relaxation curve would be; or in another word, the quicker O-ring relaxed in this blend. Although n-decane is able to swell the O-ring during the initial stage of relaxation, its main effect is ‘negative’ during the whole process.

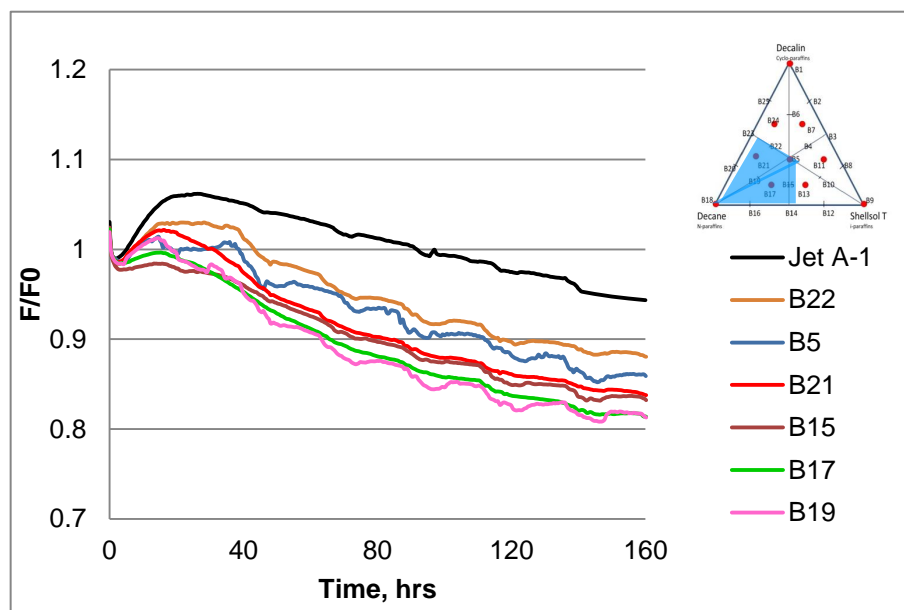


**Figure 55** Relaxation process of nitrile O-rings in the blends of ‘n-decane region’ (in blue).

Results obtained from the ‘insides of the triangle’ indicated the same conclusion as that of the ‘edges of the triangle’, which further approved decalin’s ability to promote the OSP of the final blend. The proportion of decalin in the blend needs to be more than 66%. The OSP of the three solvents in three component blends were still as:

$$\text{Decalin} > \text{Iso-paraffins} > \text{N-decane}$$

When all the stress relaxation curves were plotted in one graph (Fig. 56), the effects of the three solvents during the nitrile O-ring relaxation process could be seen more clearly. Generally, the relaxation curves shifted upwards with the increase of decalin in the blend, while moved downwards if the amount of n-decane became significant. Iso-paraffins played a similar role as n-decane in this process but its effect was slightly weaker. To make the blend be comparable to Jet A-1 fuel, more than 66% (v/v) of decalin was needed in the composition, while the proportions of other two solvents were not significant.

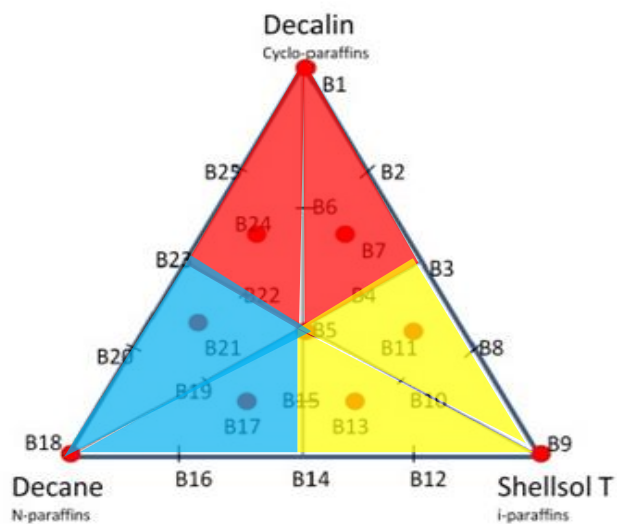
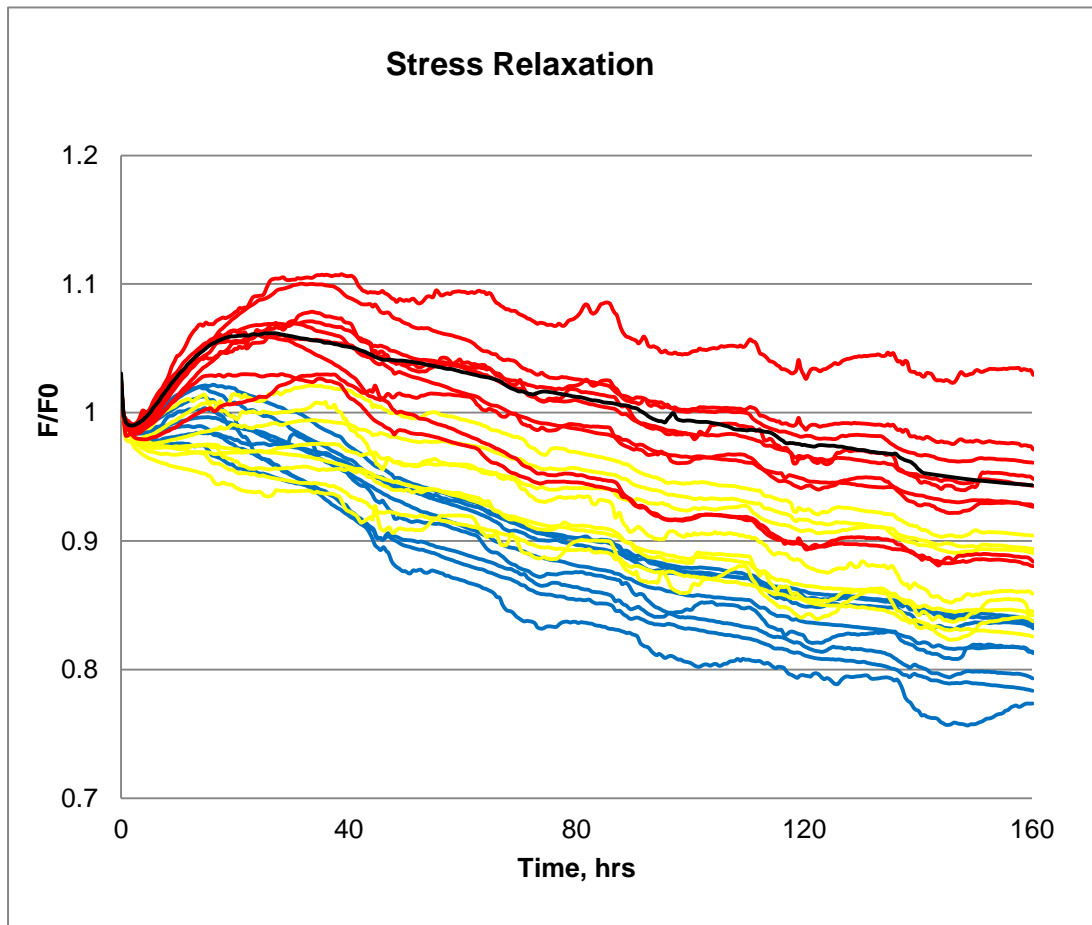


**Figure 56** Summary of the relaxation characteristics of nitrile O-rings in the solvent triangle.

#### **4.1.4 Summary**

Results from the stress relaxation tests conducted with various alternative fuels demonstrated the sensitivity of nitrile seals when exposed to different fuel compositions. In terms of chemical species, aromatic compounds present the strongest ability to penetrate into and swell the polymer material and more importantly, maintain a relatively high level of sealing force. Decalin (Decahydronaphthalene) also shows excellent seal swelling ability as presented in the ‘triangle test’; however, it cannot say all cycloparaffins (naphthenes) have the same property, as results from cycloparaffins only present ability to slow down the relaxation process. Iso-paraffins do not participate in the seal swelling process but only extracting materials out; but their extracting ability is weaker than n-decane, a normal paraffin which can initially penetrate into the polymer.

With regards to fuels, FSJF (CtL), mainly comprises of naphthenes, showed good compatibility with nitrile seals. Although no obvious swelling behaviour appears, the stress relaxation characteristic of nitrile seal maintained a relatively stable level. Bio-SPK and HVO demonstrate similar compatibility with nitrile O-rings which are slightly better than FT-SPK (GtL), although all the three alternative fuels consist of mainly paraffins. FT-SPK is the most concerned fuel when being sealed by nitrile seals. Further investigation into the effect of each fuel component indicates paraffins (both normal and iso-) are not a contributor in either polymer swelling or relaxation slow-down process. This results in a need of additives to be added into the fuel composition in order to promote its compatibility with nitrile seals.

#### **4.2 Fluorosilicone O-Ring**

The stress relaxation tests for fluorosilicone O-rings in each candidate fuel sample were carried out for 80 hours. The reason for a shorter test period is that preliminary tests indicated the stress relaxation characteristic of this material is fully presented during this period; and it is long enough to see the differences amongst various fuel samples. This also helps to arrange tests more efficiently during busy testing time.

#### 4.2.1 Relaxation Characteristics in Jet A-1: Baseline

The stress relaxation characteristic of fluorosilicone O-ring in Jet A-1 fuel was shown in Figure 57. No swelling behaviour was observed throughout the relaxation process. The whole process could be divided into two phases.

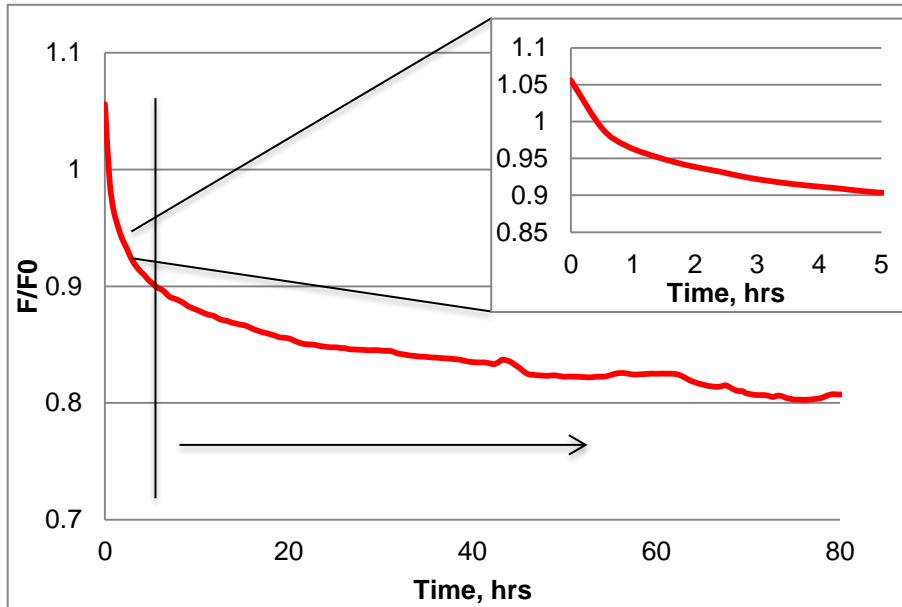


**Figure 57** The stress relaxation characteristic of fluorosilicone O-ring in Jet A-1.

*Phase 1: Quick Reduction.* Compression force reduced quickly during the initial 30 minutes, which was the same behaviour as presented in nitrile O-ring in Jet A-1. The relaxation rate in these 30 minutes was approximately 13.2% per hour. After the initial 30 minutes, the relaxation rate slowed down to averagely 2.0% per hour until 5 hours.

*Phase 2: Further relaxation.* After the quick reduction in the first 5 hours, the relaxation rate further slowed down and the relaxation curve became level off. The relaxation rate was averagely 0.1% per hour.

#### 4.2.2 Relaxation Characteristics in Typical Alternative Fuels and Blends

Alternative fuel samples tested were the same as listed in Table 11.

#### 4.2.2.1 *FSJF (CtL) vs. FT-SPK (GtL)*

Relaxation characteristics of fluorosilicone O-rings in FSJF and FT-SPK fuels were presented in Figure 58, with comparison the baseline fuel Jet A-1.

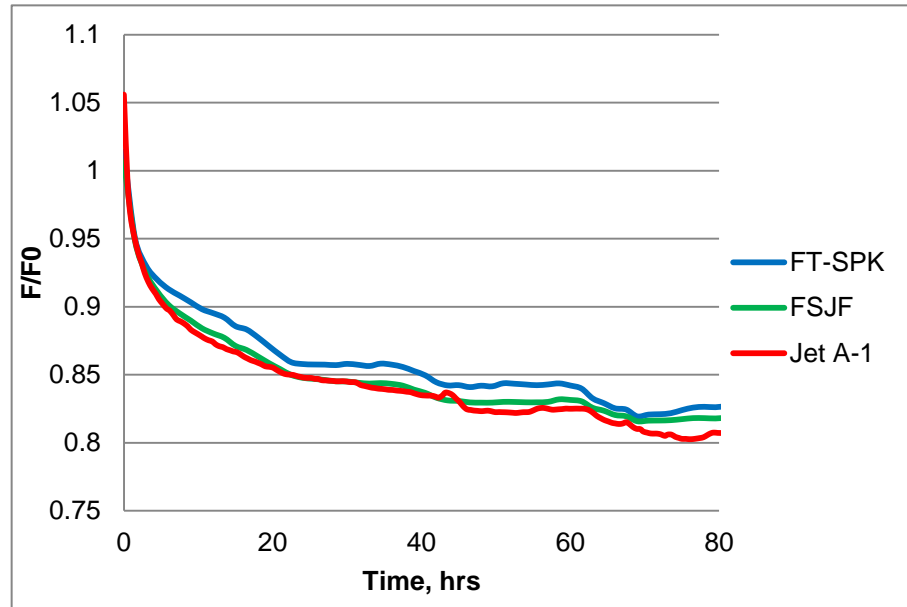


**Figure 58** Relaxation characteristics of fluorosilicone O-rings in FSJF and FT-SPK.

Fluorosilicone O-ring showed very similar stress relaxation characteristics in these three fuels. After the initial quick reduction, all counterforces relaxed gradually. This material presented slightly better compatibility in FSJF and FT-SPK than that in Jet A-1, as the final relative force values were 0.01 and 0.02 higher than in Jet A-1 respectively. The similarity presented in the relaxation processes indicated different fuel compositions have very limited impact on the sealing performance of fluorosilicone O-ring.

#### 4.2.2.2 *FT-SPK based blends*

The overall stress relaxation characteristics of five FT-SPK based fuel blends were shown in Figure 59.

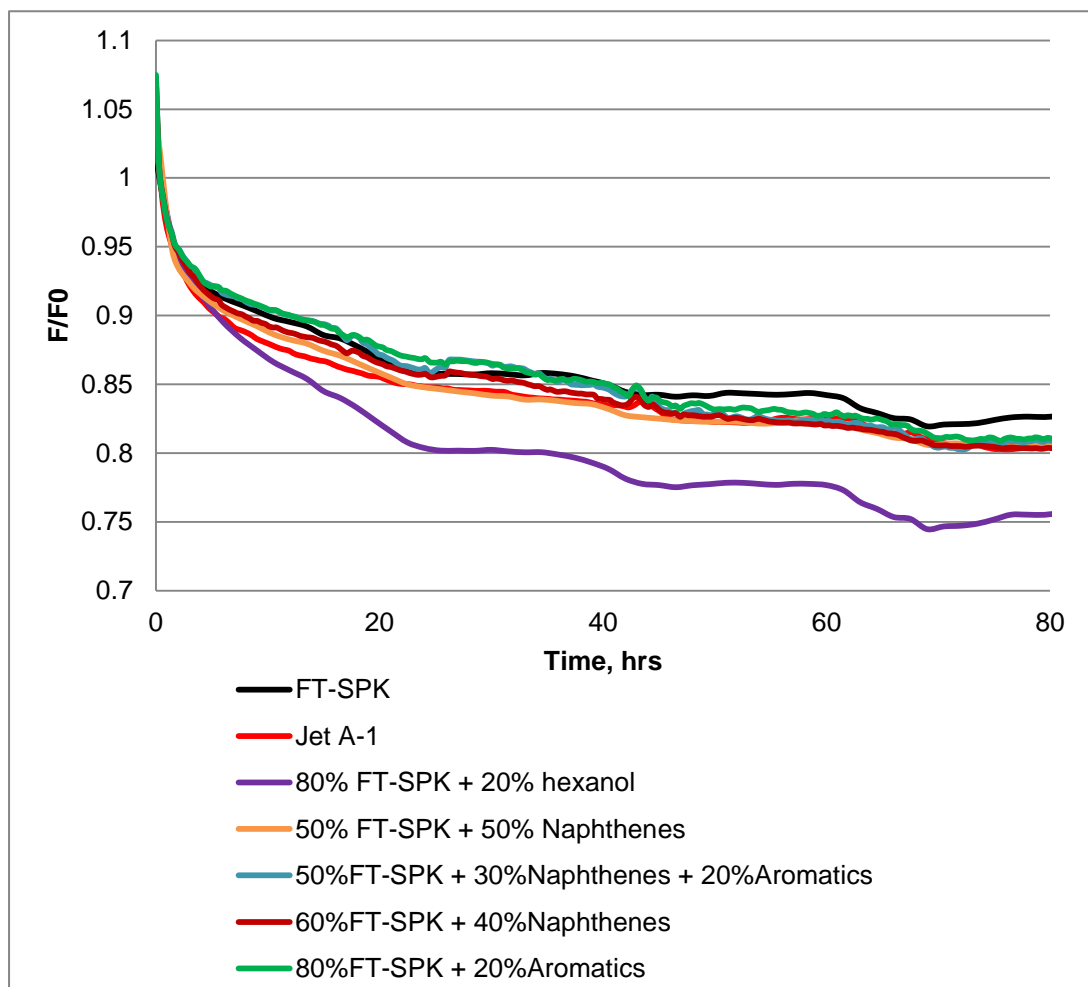


**Figure 59** Overall stress relaxation characteristics of fluorosilicone O-rings in 5 FT-SPK based blends, with comparison to FT-SPK and Jet A-1.

Generally, except for (80% FT-SPK + 20% hexanol), all the other blends demonstrated similar compatibility with fluorosilicone O-rings by the end of 80-hour tests. Fluorosilicone material seems not compatible with hexanol (representing alcohols), presenting a notable further relaxation compared with those in other solvents.

#### FT-SPK + Naphthenes

With 10% more naphthenes (cycloparaffins) in the blends, the relaxation process of fluorosilicone O-rings showed little difference in (50% FT-SPK + 50% Naphthenes) compared with (60% FT-SPK + 40% Naphthenes) (Fig. 60). Both relaxation curves

lay slightly below that in FT-SPK, indicating the compatibility of fluorosilicone O-rings is slightly better in neat FT-SPK than FT-SPK blended with naphthenes.

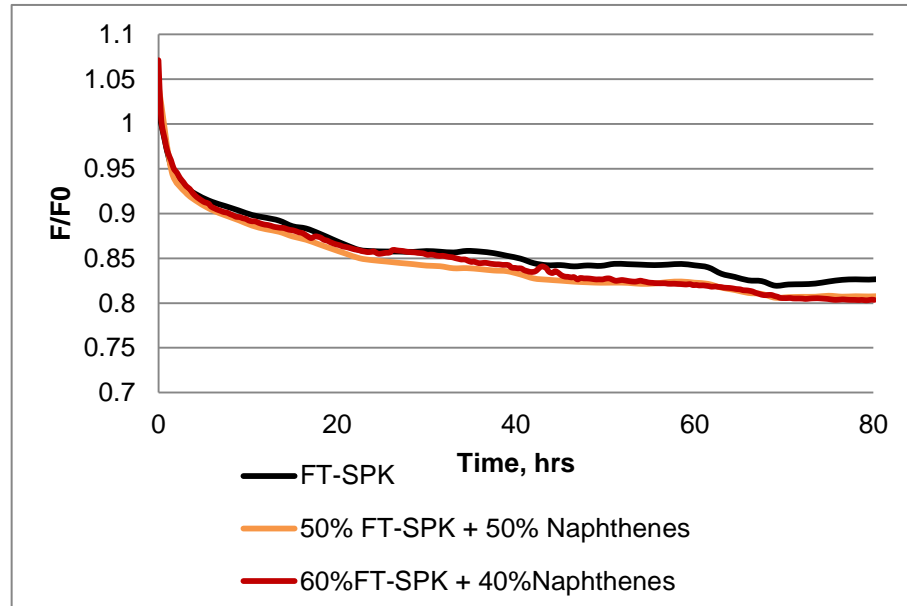


**Figure 60** Comparison between FT-SPK based blends with different proportions of naphthenes (fluorosilicone).

#### FT-SPK + 20% Aromatics/Hexanol

Fluorosilicone O-rings in FT-SPK blended with 20% aromatics presented similar relaxation characteristic to that in FT-SPK as shown in Figure 61. After the first 40 hours, the relaxation curve in (FT-SPK + 20% Aromatics) shifted slightly below that in neat FT-SPK. This observation demonstrates aromatic compound is not a particularly ‘favourite’ species for fluorosilicone material in terms of stress relaxation or compatibility.

With the same proportion of FT-SPK, the relaxation characteristics in the two blends actually reflected the effects of aromatics and hexanol on the material. It can be seen clearly that the presence of hexanol accelerated the relaxation of fluorosilicone O-ring. The relative final counterforce value was 0.75, approximately 0.06 lower than that in (FT-SPK + 20% Aromatics). This result suggests fluorosilicone material

might not be compatible with hexanol or other compound with alcohol-like molecular structures.

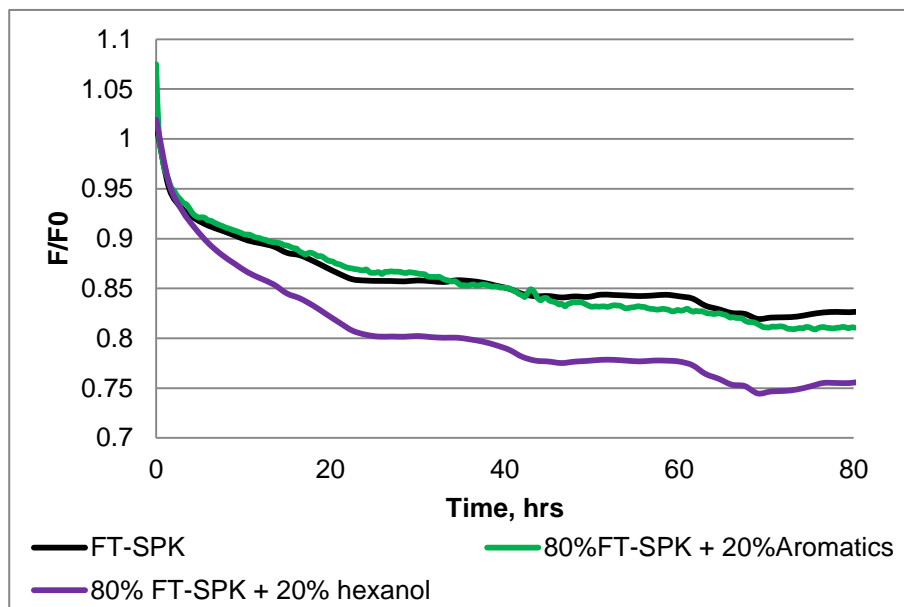


**Figure 61** Comparison between FT-SPK based blends with 20% aromatics/hexanol (fluorosilicone).

#### FT-SPK + Naphthenes/Aromatics

Difference between the compositions of these two blends is the additional 20% aromatics/naphthenes (Fig. 62). As a result, when comparing the relaxation characteristics of fluorosilicone O-rings in (50% FT-SPK + 30% Naphthenes + 20% Aromatics) and (50% FT-SPK + 50% Naphthenes), the different effects of aromatics and naphthenes were observed. The relaxation curve of (50% FT-SPK + 30% Naphthenes + 20% Aromatics) lay slightly above that of (50% FT-SPK + 50% Naphthenes) until around the 50<sup>th</sup> hour, indicating aromatics are slightly more effective than naphthenes in term of slowing down the relaxation process, or in another word, promoting the compatibility with fluorosilicone O-rings during this period. After 50 hours, two relaxation curves almost overlapped each other, presenting the same characteristics. Overall, fluorosilicone material seems to ‘prefer’ aromatics slightly over naphthenes in terms of compatibility; however, the difference

only exists during the initial relaxation process.

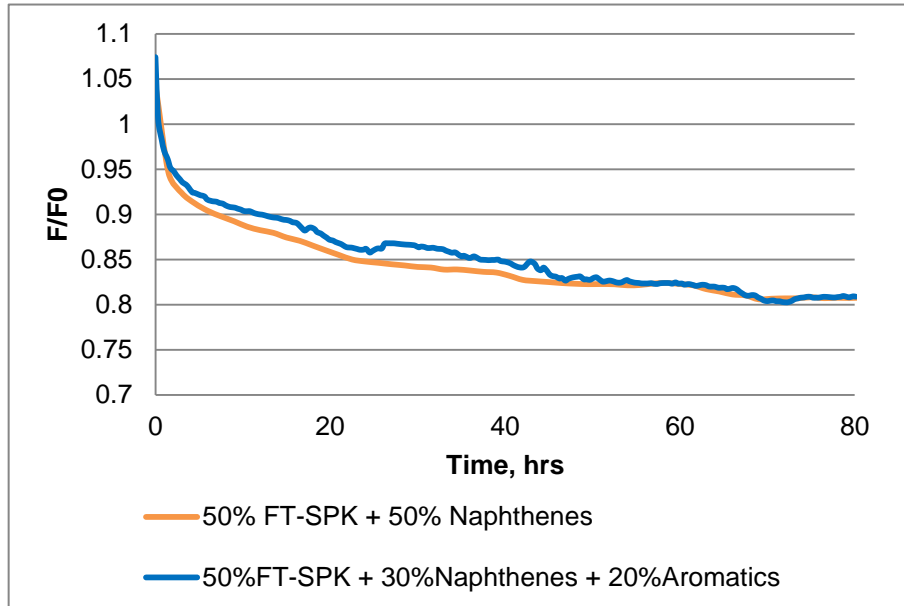


**Figure 62** Comparison between FT-SPK based blends with (naphthenes + aromatics) and naphthenes only (fluorosilicone).

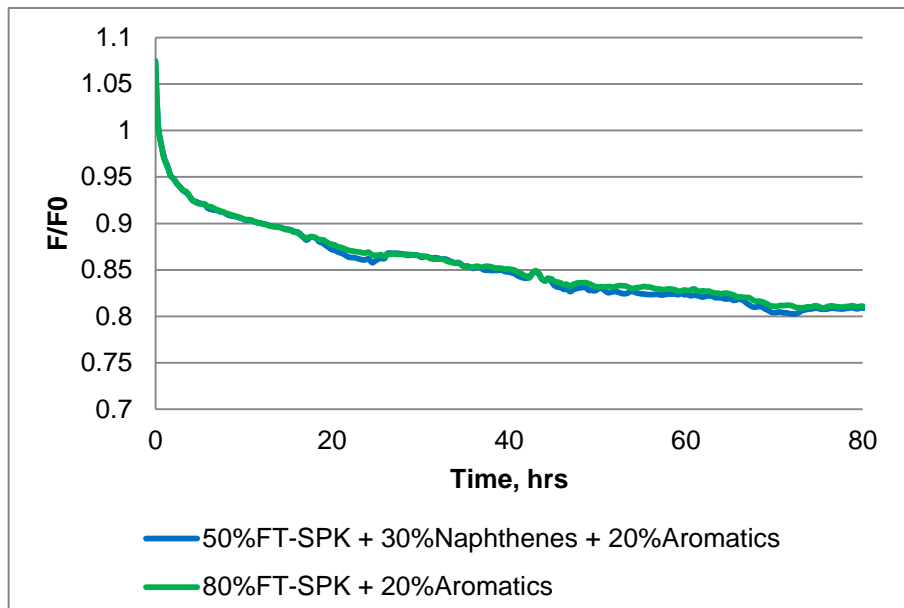


**Figure 63** Comparison between FT-SPK based blends with (naphthenes + aromatics) and aromatics only (fluorosilicone).

Figure 63 showed the relaxation curves of fluorosilicone O-rings in (50% FT-SPK + 30% Naphthenes + 20% Aromatics) and (80% FT-SPK + 20% aromatics). As both

blends have the same amount of aromatics, differences in the relaxation curves were caused by the additional 30% FT-SPK/naphthenes. Result showed no obvious difference between these two blends as two relaxation curves visually overlapped each other. This indicates fluorosilicone material has no preference between FT-SPK and naphthenes.

In conclusion, the overall stress relaxation performance of the 5 FT-SPK blends in comparison with Jet A-1 and neat FT-SPK could be rated as follows:

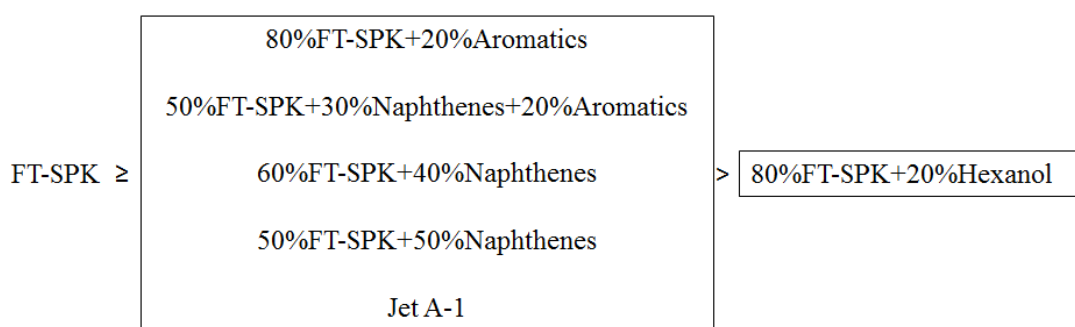


**Figure 64** Stress relaxation performance comparison of 5 FT-SPK blends (fluorosilicone).

#### 4.2.2.3 *HVO and Bio-SPK blends*

Fluorosilicone O-rings in HVO and Bio-SPK based blends did not show much difference in the stress relaxation characteristics (Fig. 65). Relaxation curve in (50% Bio-SPK + 50% Jet A-1) almost overlapped the one in Jet A-1, whilst two HVO based blends presented identical trends. Generally, HOV based blends showed slightly better relaxation characteristics, indicating fluorosilicone material may prefer slightly to this type of alternative fuels.

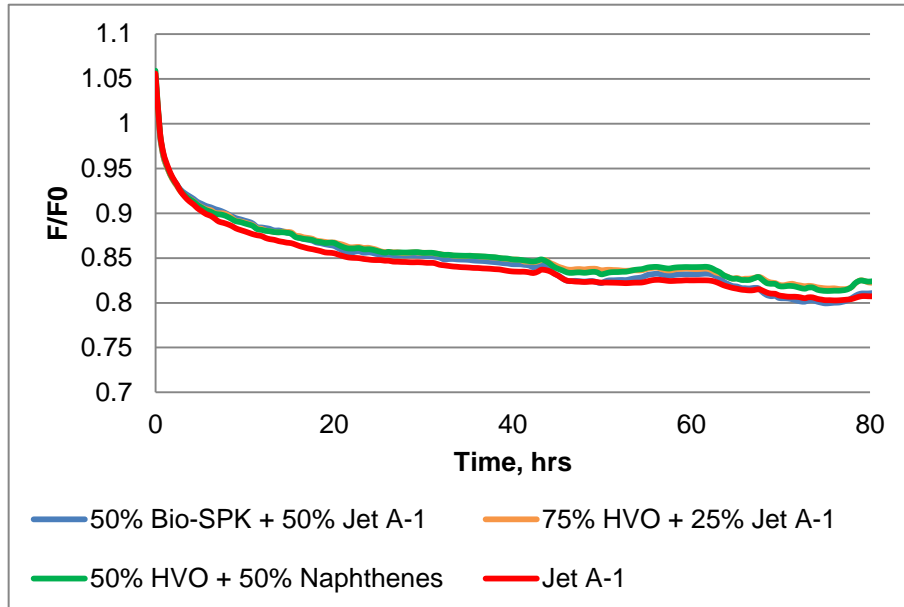


**Figure 65** Comparison between HVO and Bio-SPK based blends (fluorosilicone).

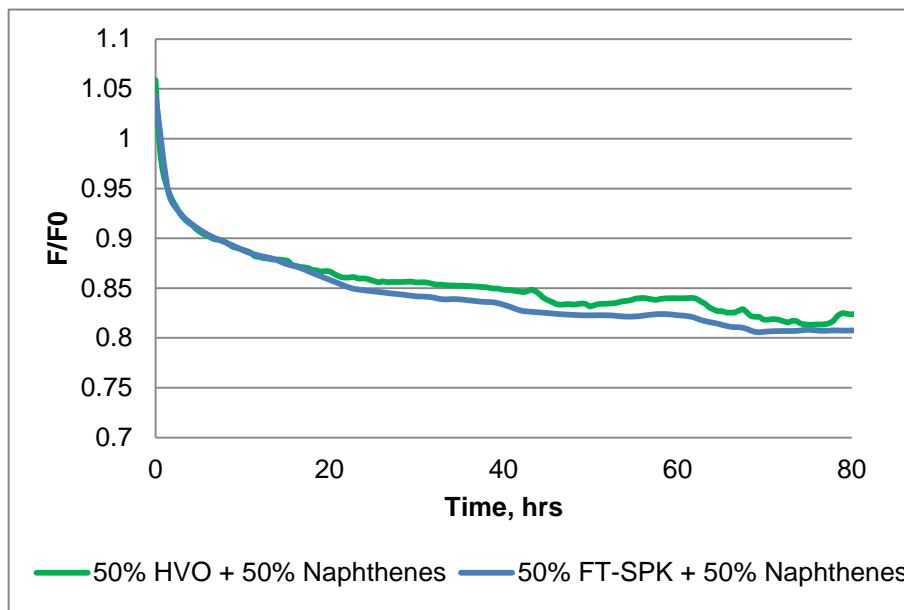


**Figure 66** Comparison between HVO and FT-SPK (fluorosilicone).

When comparing (50% HVO + 50% naphthenes) with (50%FT-SPK + 50% naphthenes) (Fig. 66), the effects of HVO and FT-SPK on the relaxation process can be compared. Although both fuels comprise of paraffins, HVO demonstrated slightly better compatibility with fluorosilicone O-ring than FT-SPK, which is the same observation for nitrile seals.

#### 4.2.2.4 Comparison with Jet A-1

The normalized final compression forces by the end of the 80h tests relative to the value in Jet A-1 were presented in Figure 67.

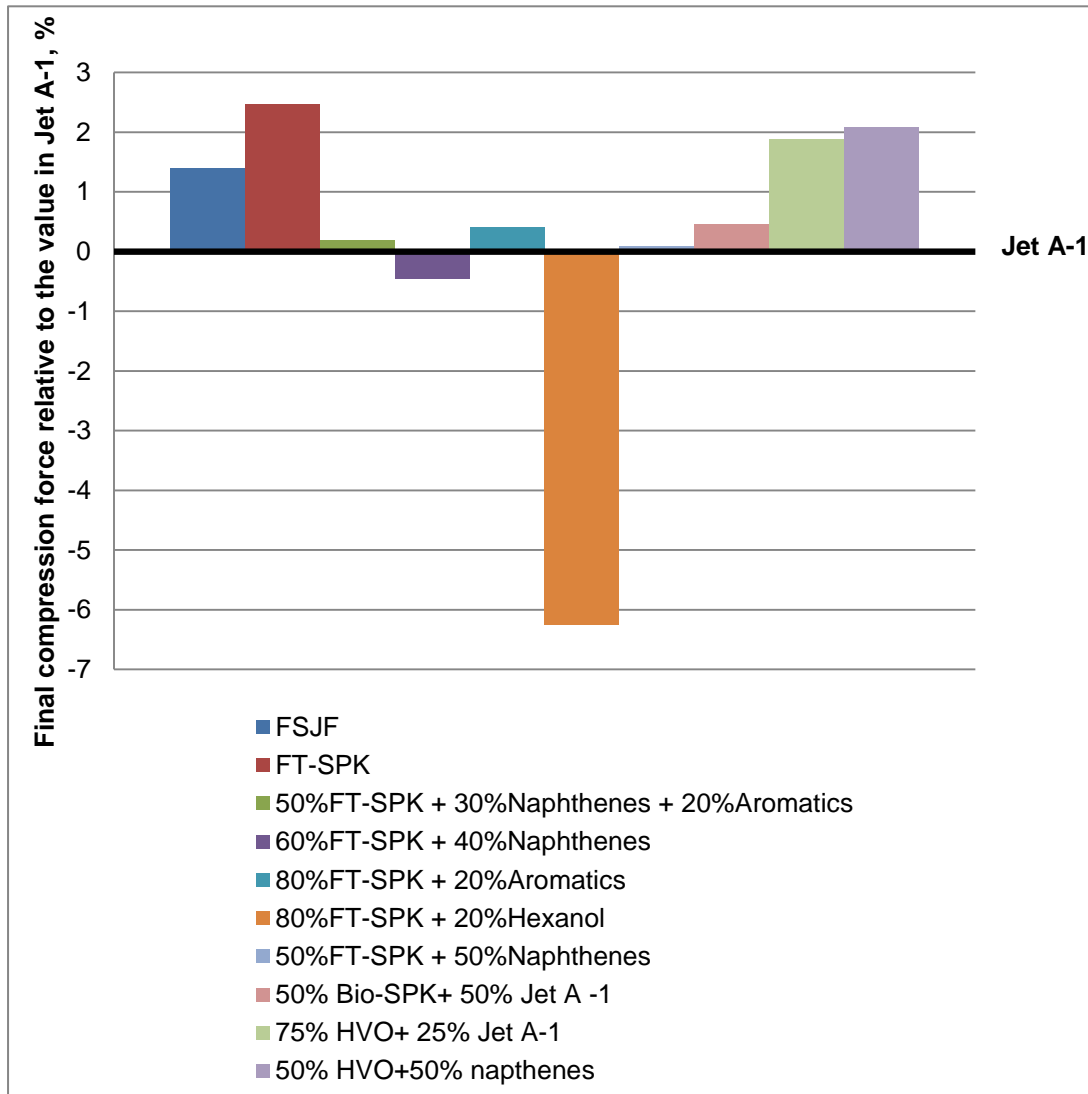


**Figure 67** Normalized final compression forces in all alternative fuels or blends relative to the value in Jet A-1, % (fluorosilicone).

Figure 67 showed most fuels or blends lay above or very close to the line representing Jet A-1, indicating the final compression forces or sealing forces of fluorosilicone O-rings in these fuels were very similar to that in Jet A-1. The only exception is (80%FT-SPK + 20%Hexanol), in which the final sealing force is 6.26%

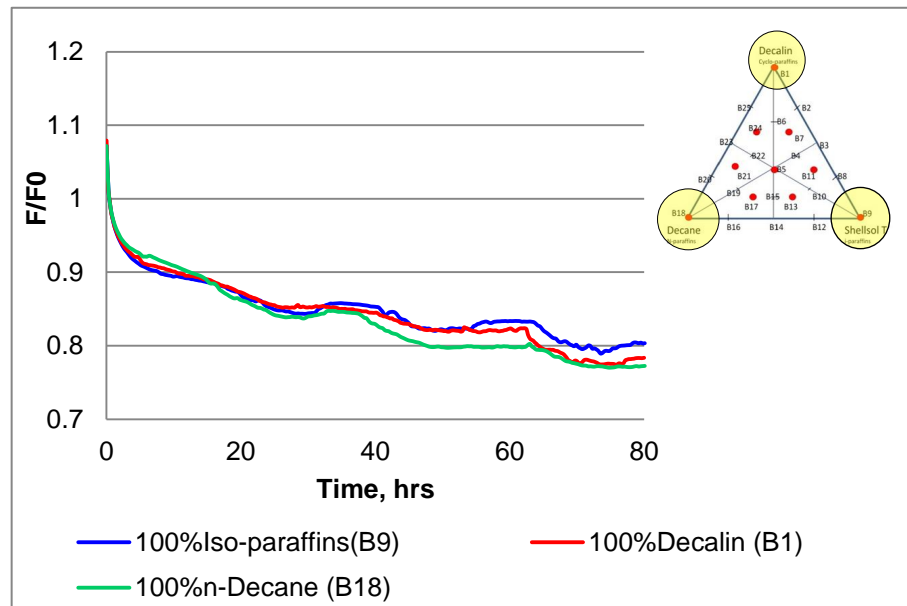
lower than that in Jet A-1. Although this observation is not sufficient to indicate if a fluorosilicone seal would fail in a hexanol (or alcohols) environment, it suggests extra attention is needed in this type of application.

Based on the data obtained and information discussed, it may suggest that *fluorosilicone seals are safe to be employed in an alternative fuel environment except for the presence of hexanol.*

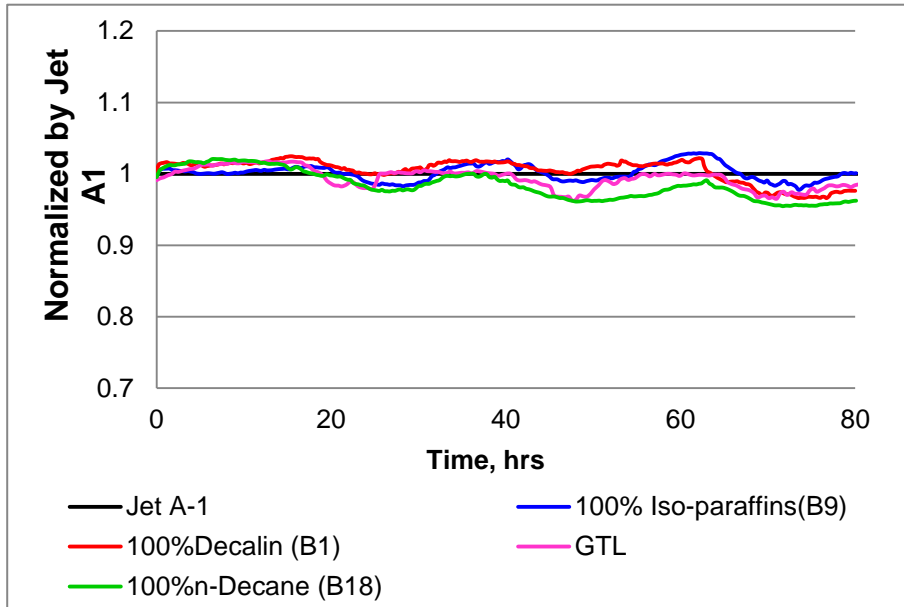
### 4.2.3 Relaxation Characteristics in the ‘Triangle’ Blends

#### 4.2.3.1 *Vertexes of the Triangle*

Fluorosilicone O-rings presented very similar relaxation characteristics in all three solvents (Fig. 68). No swelling process or obvious acceleration in the relaxation was observed. When compared with Jet A-1 and GTL kerosene, the relaxation curves almost overlapped each other, indicating excellent compatibility of this material with all solvents.



(a)



(b)

**Figure 68** Relaxation behaviour of fluorosilicone O-rings: (a) in three single solvents respectively; (b) normalized by Jet A-1, with comparison to GTL kerosene.

#### 4.2.3.2 *Edges of the Triangle*

Relaxation behaviours of the sample blends on all three edges of the triangle were plotted in Figure 69, with Jet A-1 as a reference. All relaxation curves lied closely to that of Jet A-1 which meant fluorosilicone O-ring exhibited quite similar relaxation characteristics in all these two-component solvents. It is relatively inert to the changes of fuel composition.

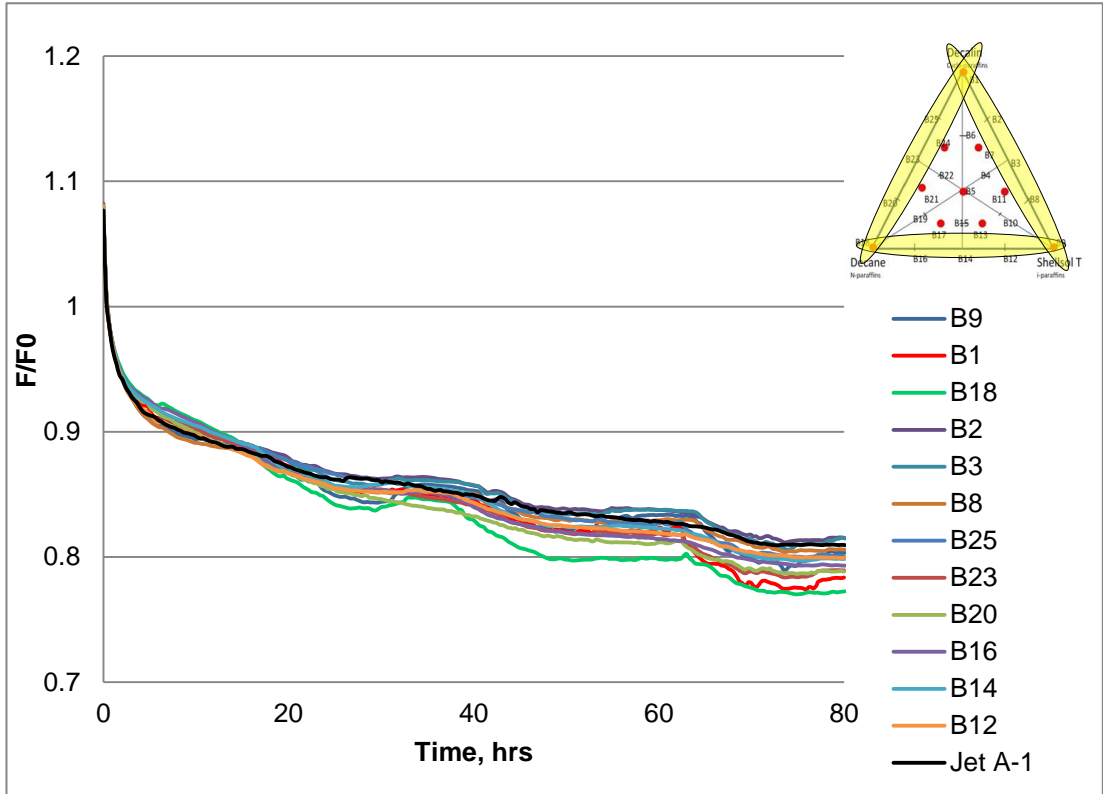


**Figure 69** Relaxation characteristics of fluorosilicone O-rings in the blends on the edges of the triangle.

#### 4.2.3.3 *Insides of the Triangle*

When three solvents were blended together, fluorosilicone O-ring presented even closer relaxation characteristics to that in Jet A-1 fuel (Fig. 70). No solvent preference was observed as the changes of blend composition did not affect O-ring's relaxation process.

Results from the triangle solvents indicated excellent compatibility of fluorosilicone O-rings with three solvents.

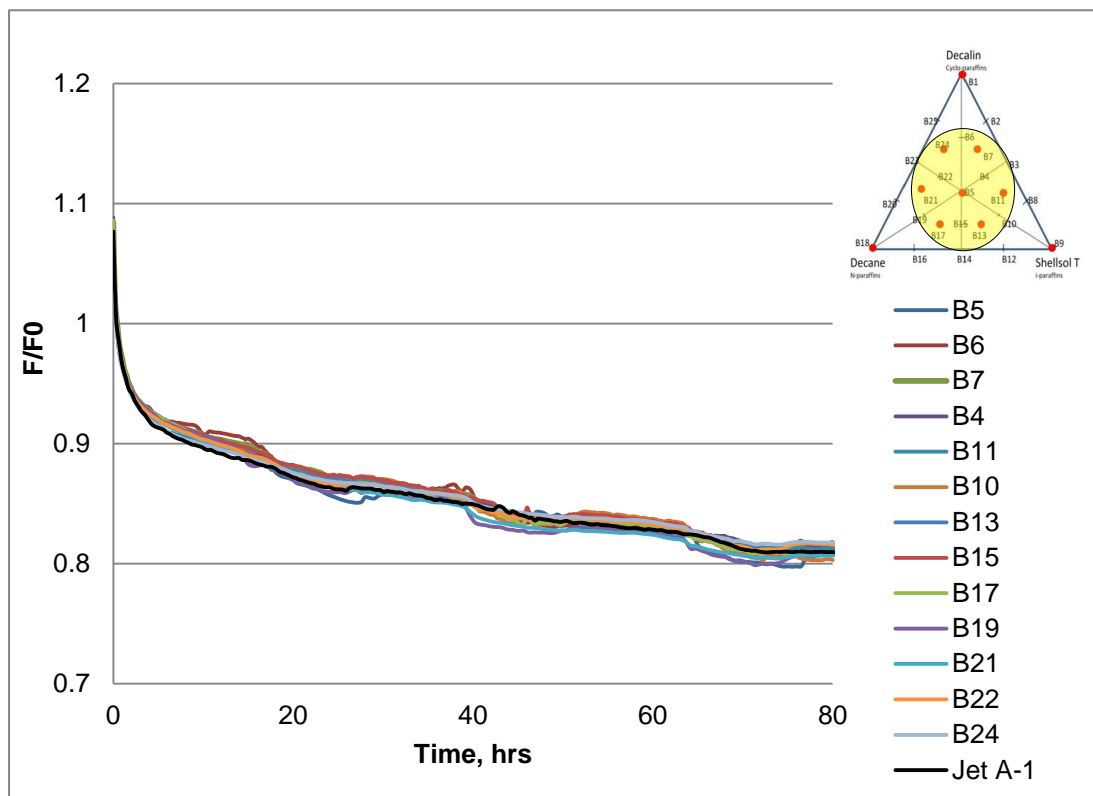


**Figure 70** Relaxation characteristics of fluorosilicone O-rings in the blends inside the triangle.

#### 4.2.4 Summary

Generally, fluorosilicone O-ring demonstrated excellent compatibility with alternative fuels as it presented very similar or even slightly better stress relaxation characteristics in these fuels than Jet A-1. The only exception observed was fuel blended with 20% hexanol, in which fluorosilicone O-ring relaxed notably faster than any other fuel tested. Impact of hexanol on fluorosilicone rubbers will be discussed in the following chapter. The ‘triangle’ test also proved this material is fully compatible with the three main components in GtL fuel. It indicates fluorosilicone O-ring can be safely employed in a GtL fuel environment under the test temperature condition.

### 4.3 Fluorocarbon O-Ring

#### 4.3.1 Relaxation Characteristics in Jet A-1: Baseline

The stress relaxation characteristic of fluorocarbon O-ring in Jet A-1 fuel was shown in Figure 71. No swelling behaviour was observed throughout the relaxation process.

The whole process could be divided into two phases.

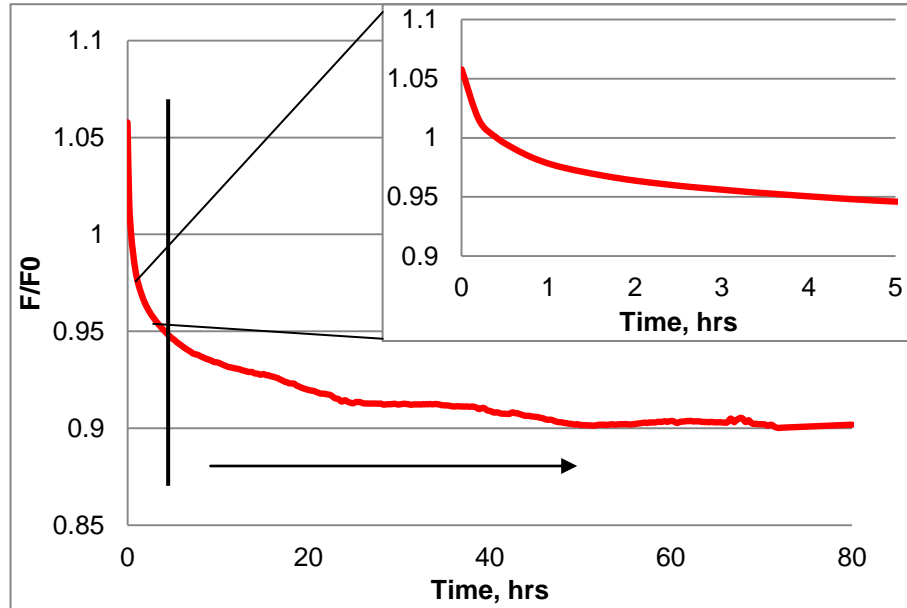


**Figure 71** The stress relaxation characteristic of fluorocarbon O-ring in Jet A-1.

*Phase 1: Quick reduction.* Compression force reduced quickly during the initial 30 minutes, which is the same behaviour as presented in fluorosilicone O-ring in Jet A-1. The relaxation rate in the 30 minutes was approximately 11.4% per hour. After the initial 30 minutes, the relaxation rate slowed down to averagely 1.1% per hour until 5 hours.

*Phase 2: Further relaxation.* After the quick reduction in the first 5 hours, the relaxation rate further slowed down and the relaxation curve became level off. The relaxation rate was averagely 0.07% per hour.

### 4.3.2 Relaxation Characteristics in Typical Alternative Fuels and Blends

Alternative fuel samples tested were the same as listed in Table 11.

#### 4.3.2.1 *FSJF (CtL) vs. FT-SPK (GtL)*

Relaxation characteristics of fluorocarbon O-rings in FSJF and FT-SPK fuels were presented in Figure 72, with comparison the baseline fuel Jet A-1.

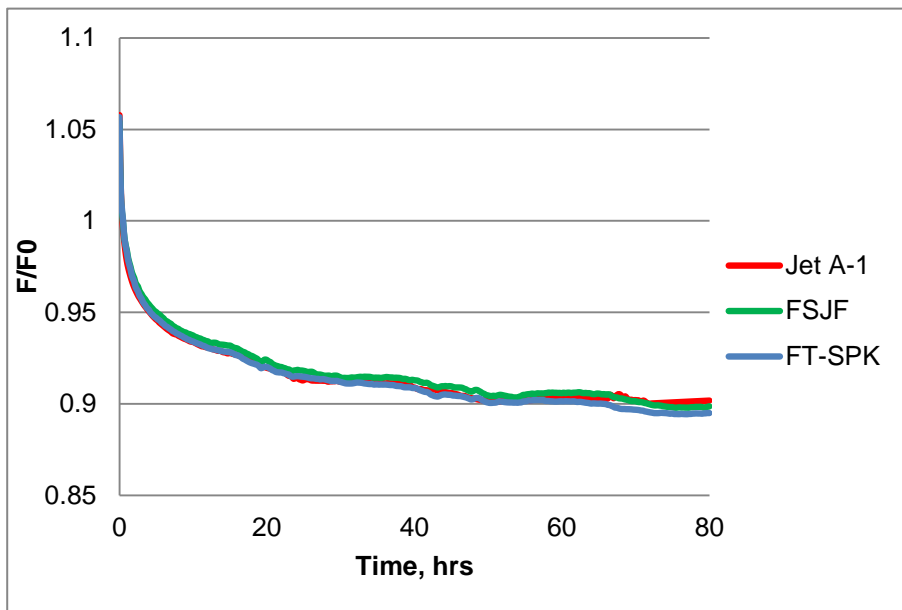


**Figure 72** Relaxation characteristics of fluorocarbon O-rings in FSJF and FT-SPK.

Fluorocarbon O-ring showed almost identical stress relaxation characteristics in these three fuels. After the initial quick reduction, all counterforces relaxed gradually. No obvious difference was observed during the test. The similarity presented in the relaxation processes indicated different fuel compositions have almost no impact on the sealing performance of fluorocarbon O-ring.

#### 4.3.2.2 *FT-SPK based blends*

The overall stress relaxation characteristics of fluorocarbon O-rings in five FT-SPK based fuel blends were shown in Figure 73.

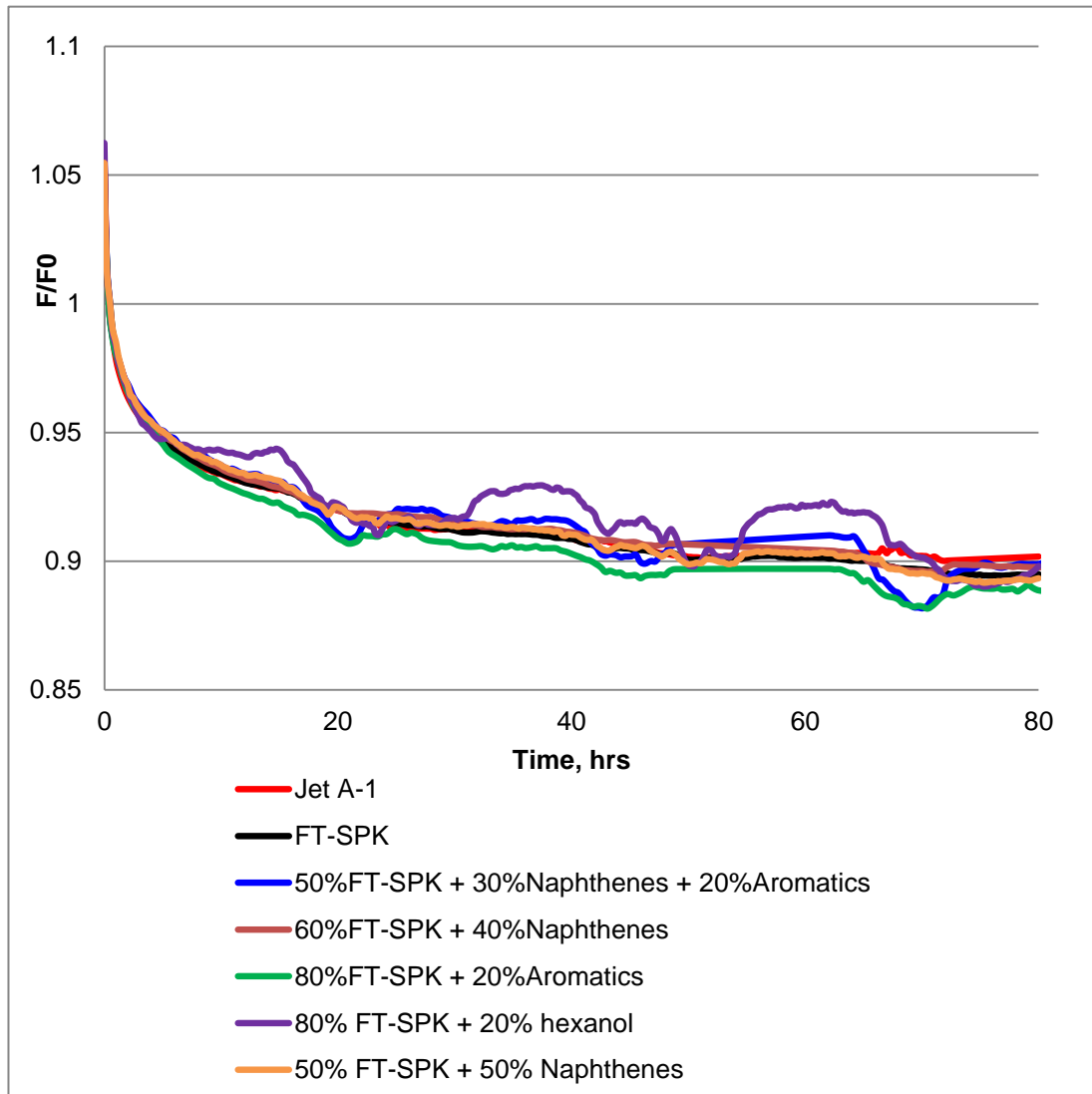


**Figure 73** Overall stress relaxation characteristics of fluorocarbon O-rings in 5 FT-SPK based blends, with comparison to FT-SPK and Jet A-1.

Generally, fluorocarbon O-rings demonstrated very similar stress relaxation characteristics in all fuels tested. No particular species was spotted to be incompatible with this material.

#### FT-SPK + Naphthenes

With 10% more naphthenes (cycloparaffins) in the blends, the relaxation process of fluorocarbon O-rings showed visually no difference in (50% FT-SPK + 50% Naphthenes) compared with (60% FT-SPK + 40% Naphthenes) (Fig. 74). Both

relaxation curves overlapped that in FT-SPK, indicating the compatibility of fluorocarbon O-rings is as good in neat FT-SPK as in FT-SPK blended with naphthenes.

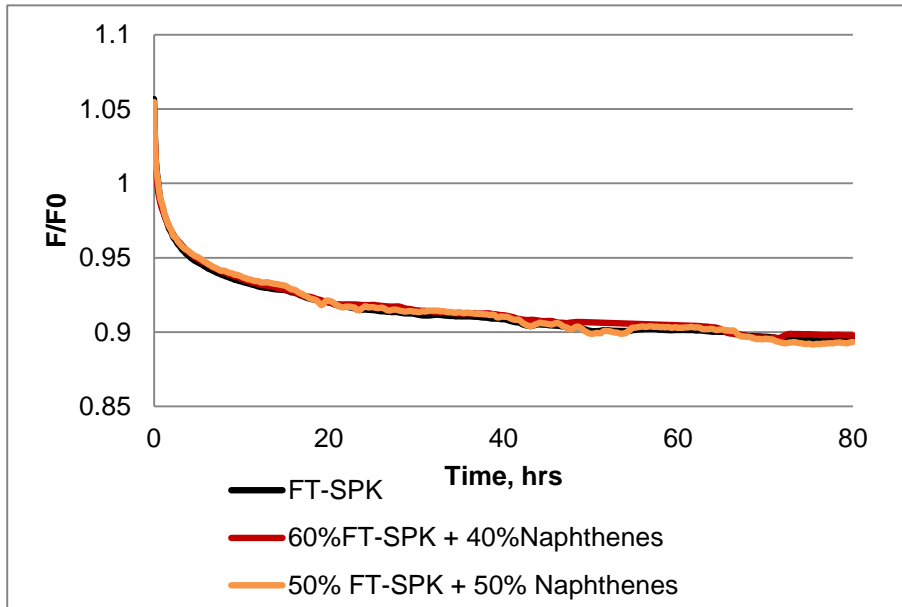


**Figure 74** Comparison between FT-SPK based blends with different proportions of naphthenes (fluorocarbon).

#### FT-SPK + 20% Aromatics/Hexanol

Fluorocarbon O-rings in FT-SPK blended with 20% aromatics presented similar relaxation characteristic to that in FT-SPK as shown in Figure 75. Compared with neat FT-SPK, the relaxation curve in (FT-SPK + 20% Aromatics) responded more actively to the ambient temperature influence as slight fluctuation was observed on an approximately 24h cycle; however, the fluctuation was fairly weak.

Unlike fluorosilicone material, the presence of hexanol did not accelerate the relaxation of fluorocarbon O-ring. Its relaxation characteristic was also similar to that in FT-SPK. However, a stronger fluctuation was observed compared with (FT-SPK + 20% Aromatics). Further test is needed to see if this fluctuation was somehow related to the presence of hexanol or purely temperature influence.

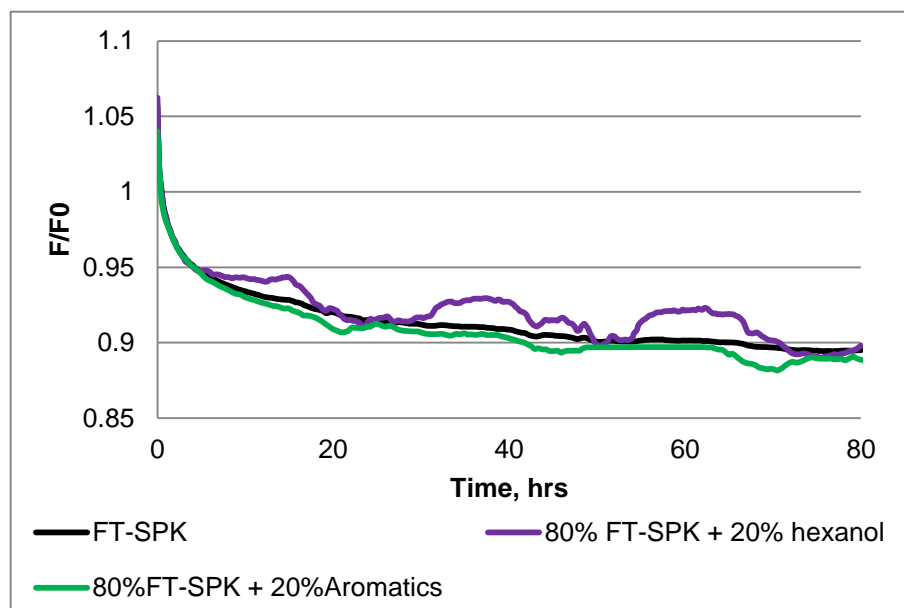


**Figure 75** Comparison between FT-SPK based blends with 20% aromatics/hexanol (fluorocarbon).

*FT-SPK + Naphthenes/Aromatics*

Fluorocarbon O-rings presented very similar relaxation characteristics in both (50% FT-SPK + 30% Naphthenes + 20% Aromatics) and (50% FT-SPK + 50% Naphthenes) (Fig. 76). The additional 20% of neither naphthenes nor aromatics could make any obvious impact on the relaxation process of this material. It can be said that fluorocarbon seals are compatible with both aromatic compound and naphthenes.

Figure 77 showed the relaxation curves of fluorocarbon O-rings in (50% FT-SPK + 30% Naphthenes + 20% Aromatics) and (80% FT-SPK + 20% aromatics). Slight difference was observed between the two relaxation curves due to temperature fluctuation. Generally, fluorocarbon material has no preference between FT-SPK and naphthenes.

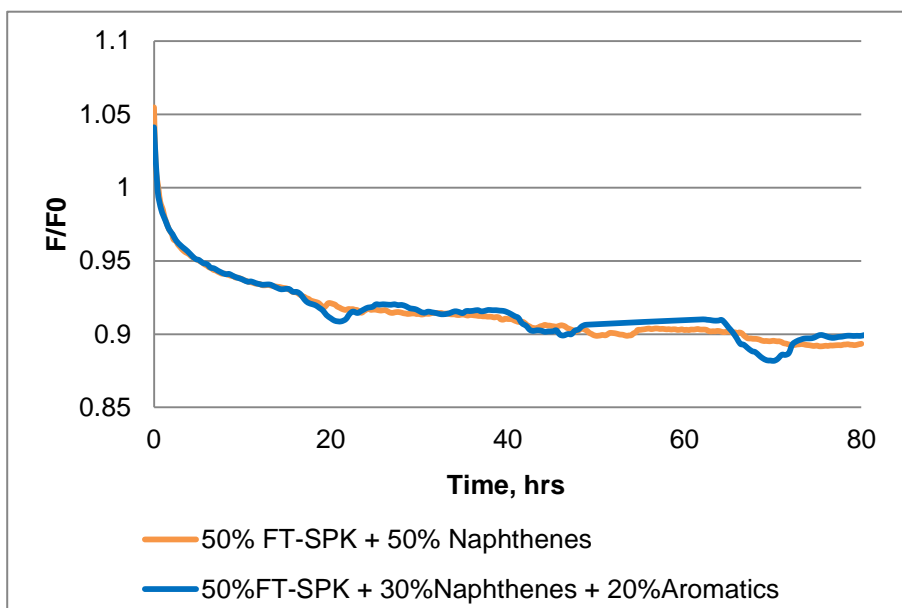


**Figure 76** Comparison between FT-SPK based blends with (naphthenes + aromatics) and naphthenes only (fluorocarbon).

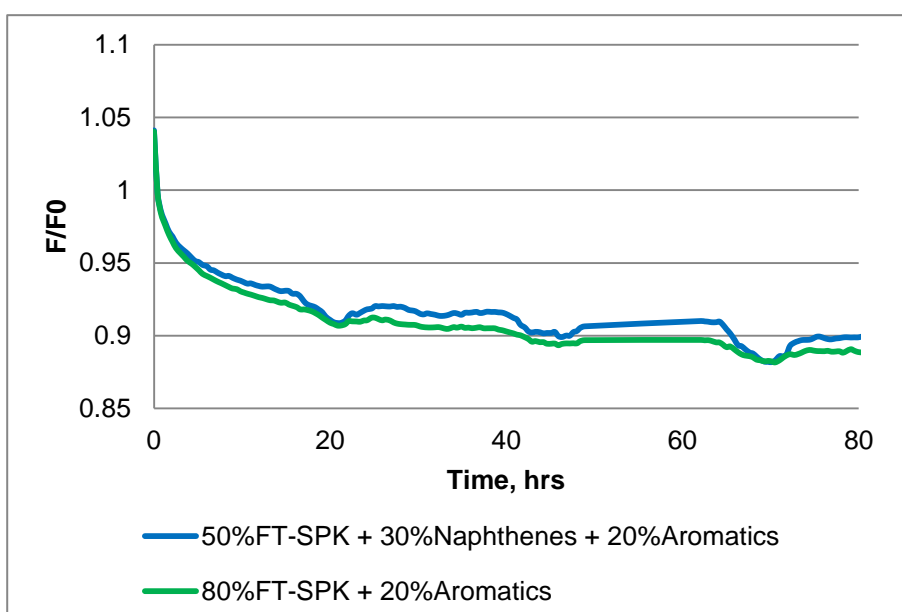


**Figure 77** Comparison between FT-SPK based blends with (naphthenes + aromatics) and aromatics only (fluorocarbon).

In conclusion, fluorocarbon O-rings showed no preference amongst various fuel compositions as the overall stress relaxation performances of the 5 FT-SPK blends were comparable to that in Jet A-1 and neat FT-SPK.

#### 4.3.2.3 HVO and Bio-SPK blends

Fluorocarbon O-rings in HVO and Bio-SPK based blends did not show much difference in the stress relaxation characteristics (Fig. 78). Without considering the temperature fluctuation influence, all three relaxation curves lay slightly below that in Jet A-1. Generally, no preference was observed between HOV and Bio-SPK based blends.

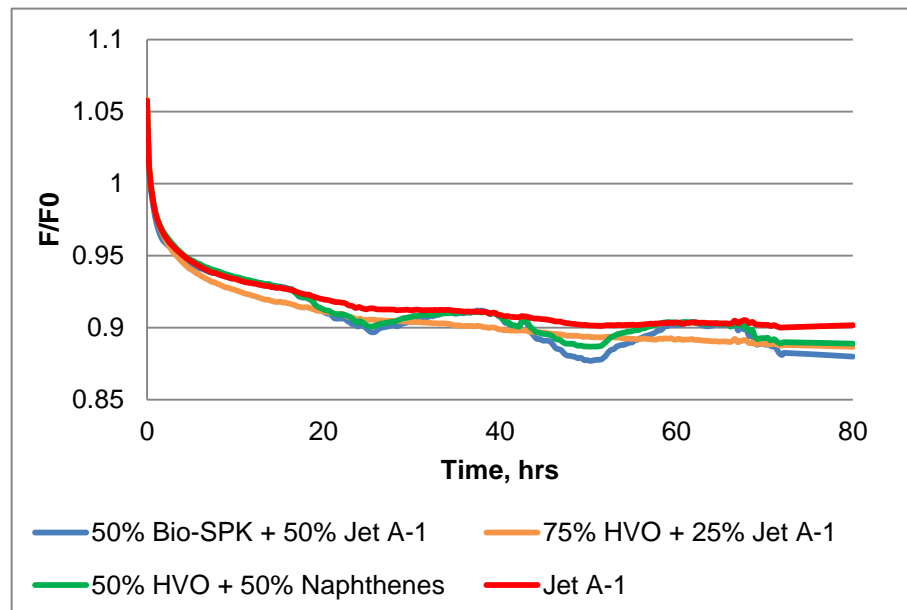


**Figure 78** Comparison between HVO and Bio-SPK based blends (fluorocarbon).

When comparing (50% HVO + 50% naphthenes) with (50%FT-SPK + 50% naphthenes) (Fig. 79), the relaxation curves in both blends almost overlapped each other, indicating similar compatibility with fluorocarbon material.

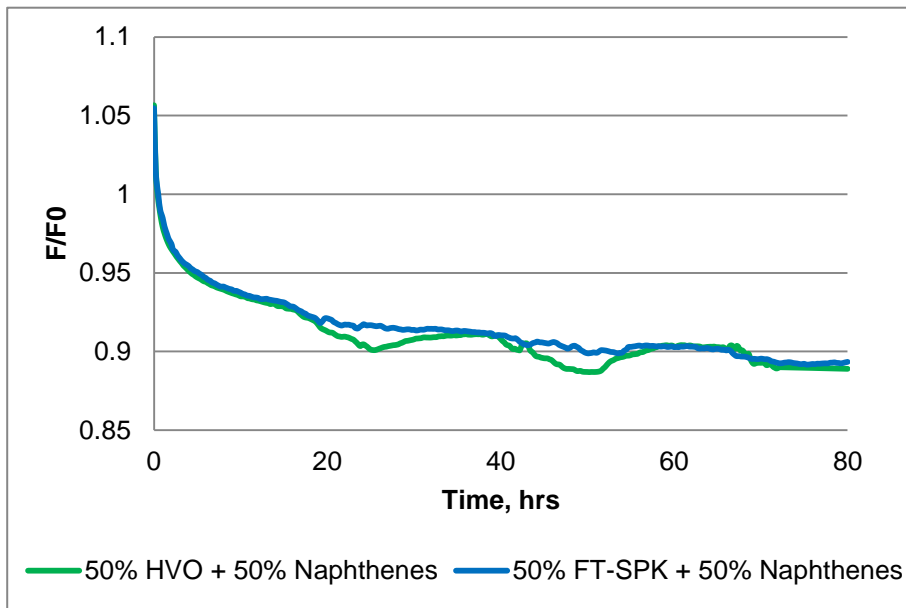


**Figure 79** Comparison between HVO and FT-SPK (fluorocarbon).

#### 4.3.2.4 Comparison with Jet A-1

The normalized final compression forces by the end of the 80h tests relative to the value in Jet A-1 were presented in Figure 80. Although none of the final compression force lay above that in Jet A-1 fuel, all of them were within 2% range of the reference, indicating excellent compatibility with all fuels tested.

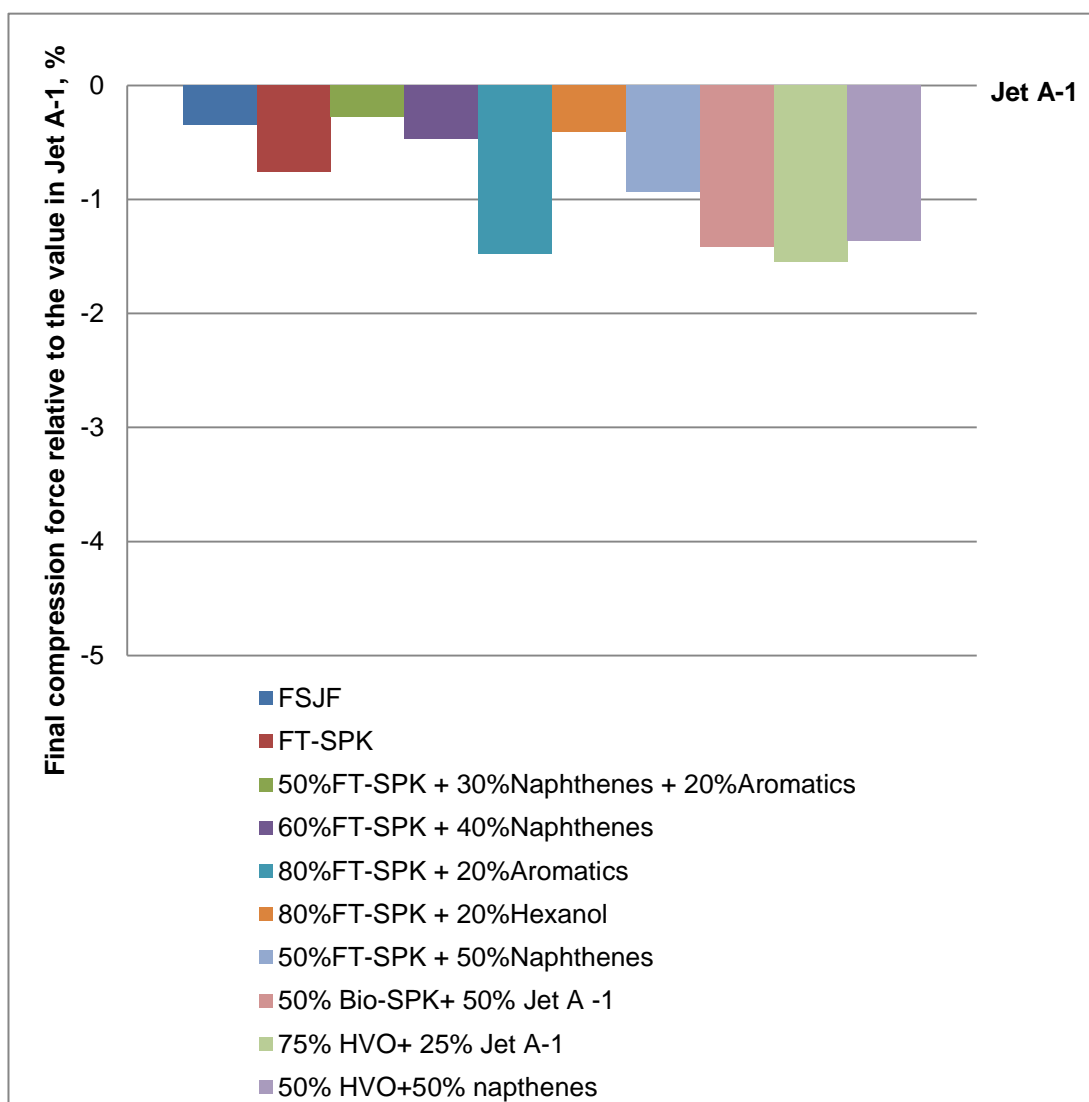


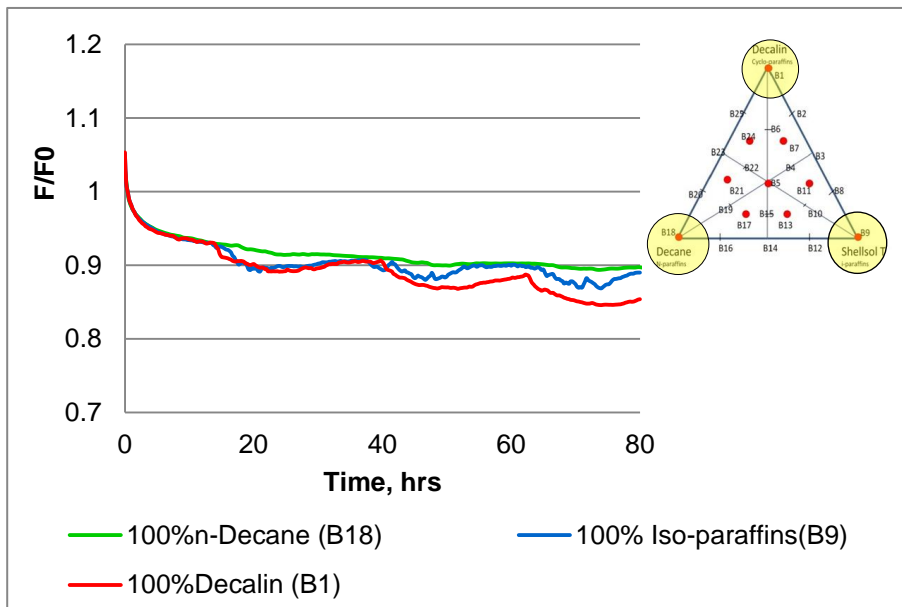
**Figure 80** Normalized final compression forces in all alternative fuels or blends relative to the value in Jet A-1, % (fluorocarbon).

### 4.3.3 Relaxation Characteristics in the “Triangle” Blends

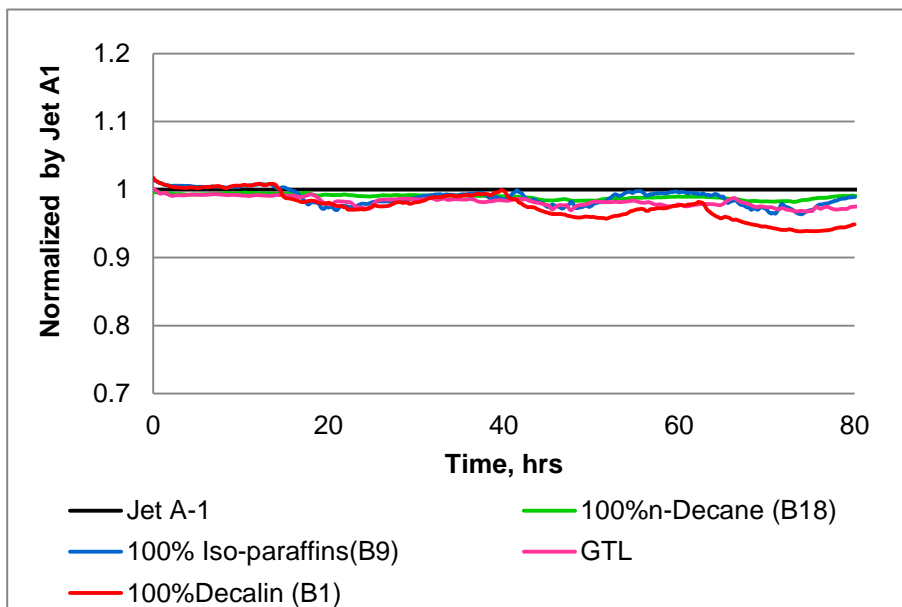
#### 4.3.3.1 *Vertexes of the Triangle*

Fluorocarbon O-ring also presented good compatibility with three solvents (Fig. 81). A slight difference was observed in decalin solvent as O-ring relaxed more than those in the other two solvents. By the end of the 80 hour-test, fluorocarbon O-ring relaxed less than fluorosilicone O-ring, with the  $F/F_0$  value ranged from 0.9-0.85 for the former and around 0.8 for the latter. When compared with Jet A-1, with comparison to GTL kerosene, all solvents showed excellent compatibility with

fluorocarbon O-ring. Although in decalin, the relaxation curve was below all the others; but the  $F/F_0$  value was still higher than 9.3.



(a)



(b)

**Figure 81** Relaxation characteristics of fluorocarbon O-rings: (a) in three single solvents respectively; (b) normalized by Jet A-1, with comparison to GTL kerosene.

#### 4.3.3.2 Edges of the Triangle

Relaxation behaviours of the sample blends on all three edges of the triangle were plotted in Figure 82, with Jet A-1 as a reference. All relaxation curves lied closely to that of Jet A-1 which meant fluorocarbon O-ring exhibited quite similar relaxation characteristics in all these two-component solvents.

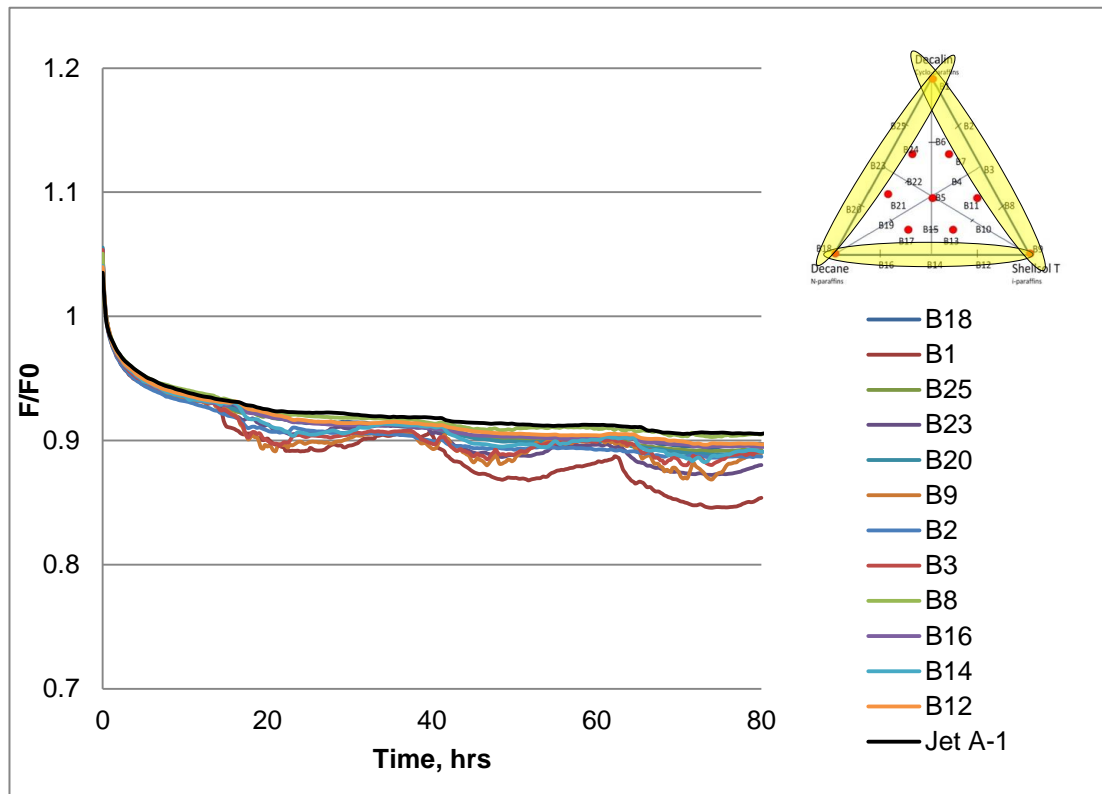


**Figure 82** Relaxation characteristics of fluorocarbon O-rings in the blends on the edges of the triangle.

#### 4.3.3.3 Insides of the Triangle

When three solvents were blended together, fluorocarbon O-ring presented quite similar relaxation characteristics to that in two-component blends (Fig. 83). No solvent preference was observed as the changes of blend composition did not affect O-ring's relaxation process.

Generally, fluorocarbon O-ring also has excellent compatibility with all the three solvents tested.

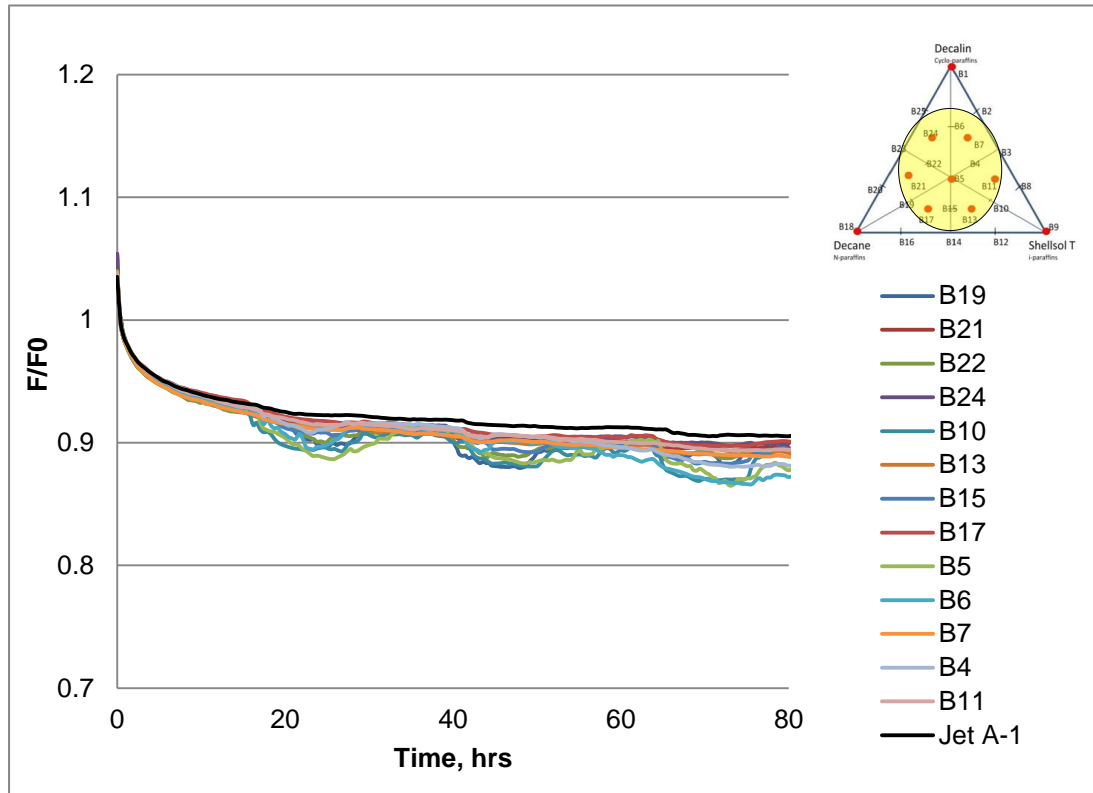


**Figure 83** Relaxation behaviour of fluorocarbon O-rings in the blends inside the triangle.

#### 4.3.4 Summary

Fluorocarbon O-rings showed excellent compatibility with all fuels tested in this project. Different fuel or solvent compositions have very limited impact on the performance of this seal material. The ‘triangle’ tests also proved this material is fully compatible with the three main components in GtL fuel. It indicates fluorocarbon O-ring can be safely employed in a GtL fuel environment under the test temperature condition.

## **5 Results – FTIR**

Data generated from the stress relaxation tests were then analyzed using various methods. For O-rings tested in various alternative fuels and blends, Fourier Transform Infrared (FTIR) Spectroscopy with Attenuated Total Reflection (ATR) was employed to analyse the molecular structure changes of O-rings after stress relaxation. The purpose of FTIR-ATR technique was to identify any possible molecular structure changes that occurred during the stress relaxation tests while the O-ring materials were exposed to the test fuels.

### **5.1 Nitrile O-ring**

The quality of spectra obtained for nitrile O-rings were not as good as those of fluorosilicone and fluorocarbon materials (Fig. 84). A possible explanation was the large carbon black content in the nitrile O-rings absorbs too much IR energy, resulting in a very low transmission rate, which in return prevented a detailed spectrum analysis [105]. To improve this, O-rings were sliced as thin as 10  $\mu\text{m}$ . However, even this approach did not improve the quality of spectra. A further attempt using an ATR with germanium (Ge) crystal was also tried as previous experiments indicated the shorter penetration distance of this crystal material might help improve the spectrum quality. However, this attempt was also unsuccessful. Further consideration need to be taken to obtain a more accurate spectrum.

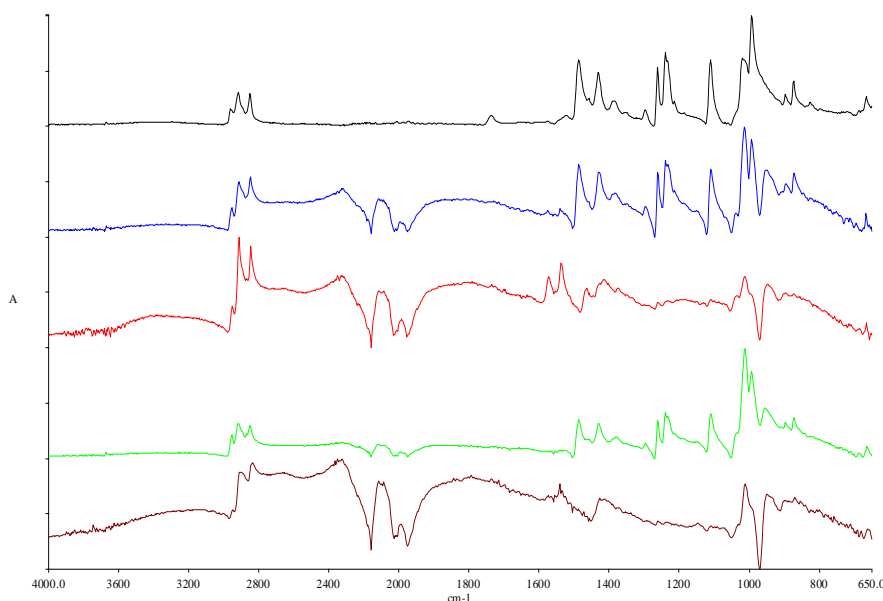


**Figure 84** Spectra examples of nitrile O-rings.

[Legend: untested O-ring -reference (black); FSJF (light blue); FT-SPK (red); FT-SPK + 20% hexanol (light green); FT-SPK + 50% naphthenes (brown)]

## 5.2 Fluorosilicone O-ring

The spectra of fluorosilicone O-rings were presented in Figure 85 and Figure 86. Figure 85 showed the strongest band at  $1006\text{ cm}^{-1}$ , which is caused by the vibration of C-F stretching. It could be seen that the intensity of the band near  $1060\text{ cm}^{-1}$ , which is corresponding to the (Si-O-Si) stretching, decreased sharply after the relaxation test. Similar observations can be made for the characteristic bands at  $1270\text{ cm}^{-1}$  cause by (Si-CH<sub>3</sub>) bending; and at  $1210\text{ cm}^{-1}$  because of C-F stretching [62]. By contrast, absorption at  $3680\text{ cm}^{-1}$ , as well as the region from  $3000\text{ to }2800\text{ cm}^{-1}$ , increased (Fig. 86). The characteristic band at  $3680\text{ cm}^{-1}$  is due to the O-H stretching, and C-H stretching is the mode for the bands from  $3000\text{ to }2800\text{ cm}^{-1}$ . Detailed assignment of possible molecular structures was listed in Table 14.

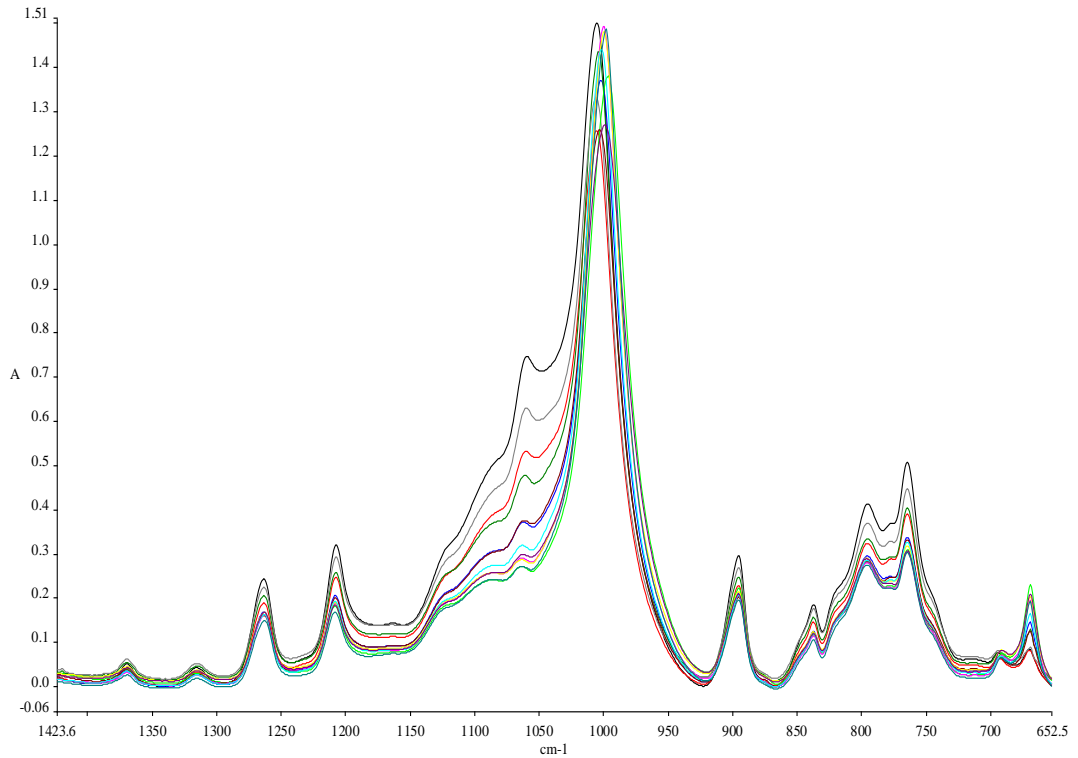


**Figure 85** Spectra of fluorosilicone O-rings (part 1).

[Legend: untested O-ring -reference (black); FSJF (light blue); FT-SPK (red); FT-SPK + 20% hexanol (light green); FT-SPK + 50% naphthenes (brown); 50% BSPK + 50% Jet A-1 (pink); 50% HVO + 50% naphthenes (yellow); 75% HVO + 25% Jet A-1 (light blue); Jet A-1 (purple); FT-SPK + 20% aromatics (dark green); FT-SPK + 60% naphthenes (grey); FT-SPK + 30% naphthenes + 20% aromatics (cyan)]

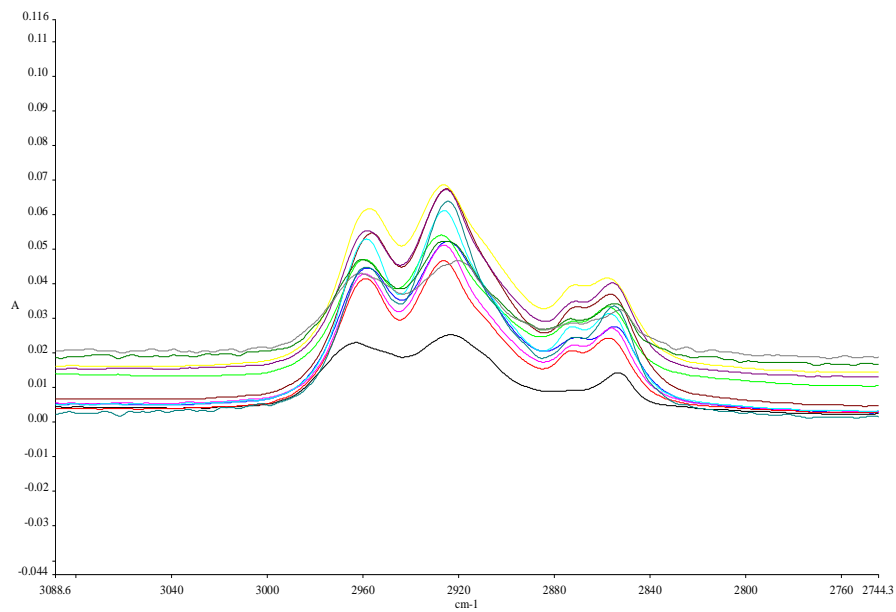


**Figure 86** Spectra of fluorosilicone O-rings (part 2).

[same legend as Figure 79]

**Table 14** Possible molecular structures corresponding to peaks in the spectra (fluorosilicone O-rings) [62] [106].

Peaks (cm <sup>-1</sup> )	Average Area Changes (%)	Possible Molecular Structure Assignments	
3677	81.99	Nonbonded hydroxy group, O-H stretch	O-H stretch
2963	112.88	Methyl (-CH <sub>3</sub> ) C-H stretch	C-H stretch
2932	118.75	Methylene (>CH <sub>2</sub> ) C-H stretch	
2853	218.03	Methylene (>CH <sub>2</sub> ) C-H stretch or Methyne (>CH-) C-H stretch	
1447	130.91	Methyl (-CH <sub>3</sub> ) C-H stretch	
1370	1.13	Methyl (-CH <sub>3</sub> ) C-H bend	C-H bend
1316	-17.13	Skeletal C-C vibrations	C-C vibrations
<b>1264</b>	<b>-28.08</b>		
1207	-38.78		
<b>1060</b>	<b>-44.02</b>	Organic siloxane (Si-O-Si)	Si-O-Si stretch
1006	-10.39	Aliphatic fluoro compounds, C-F stretch	C-F stretch
896	-20.65	Vinyl C-H out-of-plane bend	C-H bend
836	-32.42	Skeletal C-C vibrations	C-C vibrations
794	-23.77		
<b>764</b>	<b>-42.22</b>		
695	4.36	Alcohol, O-H out-of-plane bend	O-H bend
<b>669</b>	<b>97.33</b>		

From the observed phenomena, it is suggested that all the fuels tested might chemically influence the molecular structure of fluorosilicone O-rings. The reduction of intensity in certain regions of the spectra may indicate the breakdown of corresponding structures, while the increase of absorption may be the result of gaining certain chemical bonds. Although a fluorosilicone O-ring as a polymer

consists of macromolecules, its characteristic large size has little effect on its chemical properties. This means the functional groups in the molecule determine the kind of chemical reactions that would possibly occur [107]. Then, the key to understand the chemical reasons for fuel impact on fluorosilicone O-rings lies in investigating the potential chemical reactions which would occur amongst these functional groups.

As the strongest single bond in organic chemistry, C-F bond tend to be chemically inert and stable. The bond also strengthens as more fluorines are added to the same carbon on a chemical compound [108]. The highest peak caused by C-F stretching at  $1000\text{ cm}^{-1}$  in Figure 85 did not change much which also proved its stability. Conversely, the most notable break down occurred to the (Si-O-Si) bond, as the absorption at  $1060\text{ cm}^{-1}$  dropped dramatically. Results from the stress relaxation tests indicate a relatively incompatible performance of fluorosilicone O-ring in FT-SPK+20% hexanol. A possible explanation for this is that when the (Si-O-Si) bonds broke down, the -OH group in hexanol replaced the position of oxygen and formed a new (Si-OH) bond with silicone. This resulted in the reduction of absorption intensity of (Si-O-Si) bonds and the increase of O-H bonds in the final spectra.

### **5.3 Fluorocarbon O-ring**

The spectra obtained for fluorocarbon O-rings were not as good as fluorosilicone O-rings due to the certain black carbon content in the material. The middle range of the spectrum (from  $2500\text{ cm}^{-1}$  to  $1500\text{ cm}^{-1}$ ) could not be obtained clearly. The broadest and strongest absorption occurs between  $1200$  and  $1000\text{ cm}^{-1}$ , including C-F stretching. The intensity has been increased in this region whilst decreased generally from  $3000\text{ cm}^{-1}$  to  $2800\text{ cm}^{-1}$  corresponding to C-H stretching. Detailed assignment of possible molecular structures was listed in Table 15.

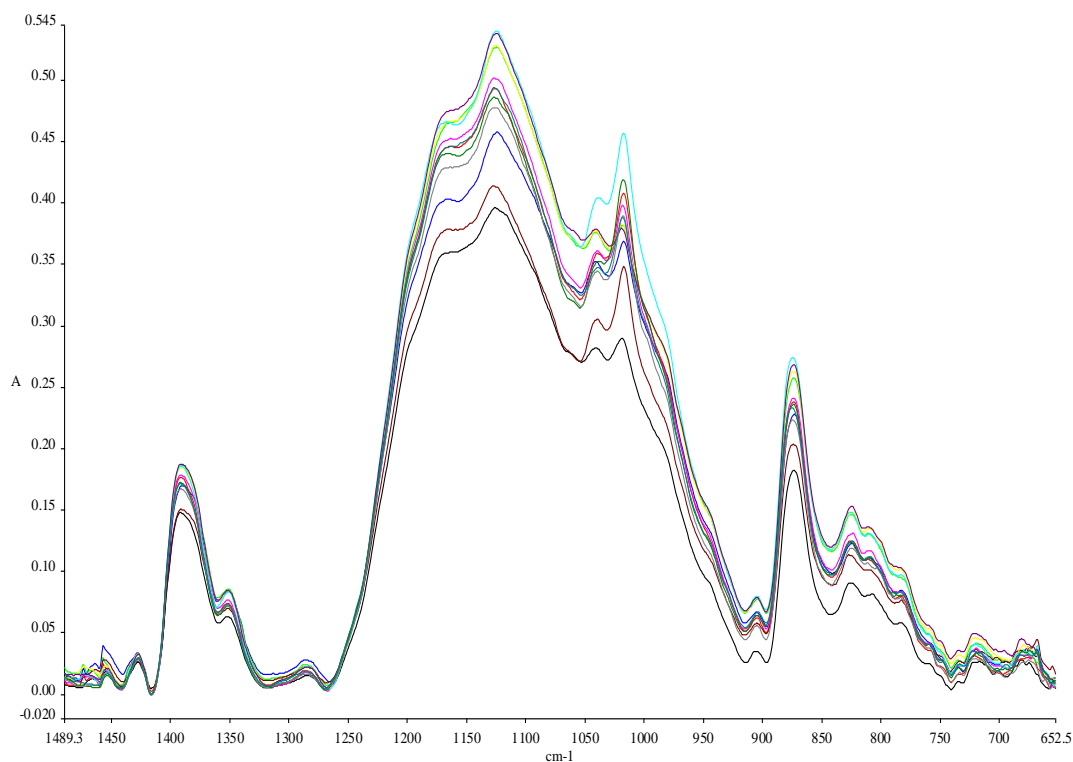


**Figure 87** Spectra of fluorocarbon O-rings (part 1).

[Legend: untested O-ring -reference (black); FSJF (light blue); FT-SPK (red); FT-SPK + 20% hexanol (light green); FT-SPK + 50% naphthenes (brown); 50% BSPK + 50% Jet A-1 (pink); 50% HVO + 50% naphthenes (yellow); 75% HVO + 25% Jet A-1 (light blue); Jet A-1 (purple); FT-SPK + 20% aromatics (dark green); FT-SPK + 60% naphthenes (grey); FT-SPK + 30% naphthenes + 20% aromatics (cyan)]

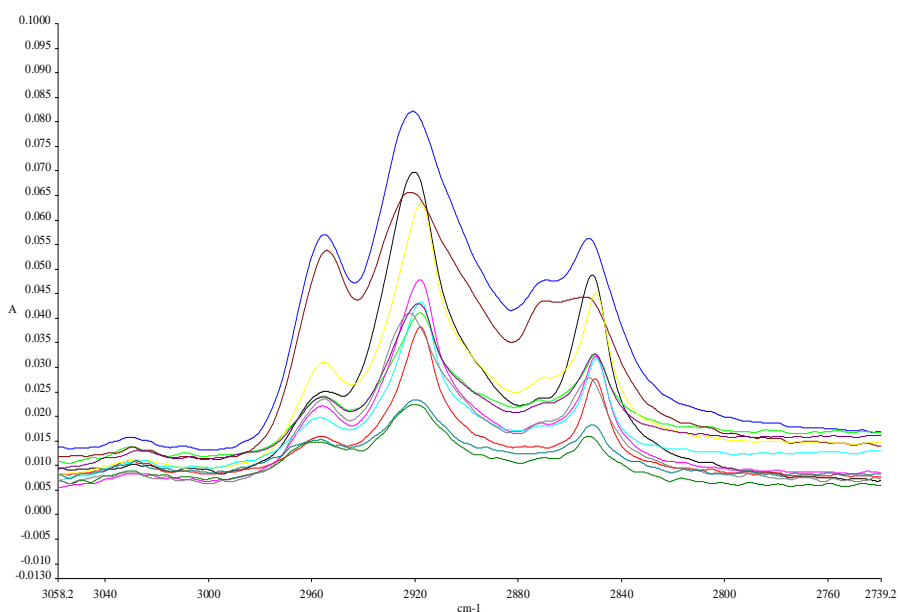


**Figure 88** Spectra of fluorocarbon O-rings (part 2);

[same legend as Figure 81]

**Table 15** Possible molecular structures corresponding to peaks in the spectra (fluorocarbon O-rings) [62] [106].

Peaks (cm <sup>-1</sup> )	Average Area Changes (%)	Possible Molecular Structure Assignments	
2954	26.44	Methyl (-CH <sub>3</sub> ) C-H stretch	C-H stretch
2920	-36.80	Methylene (>CH <sub>2</sub> ) C-H stretch	
2851	-2.02		
1454	35.07	Methylene (>CH <sub>2</sub> ) C-H bend	C-H bend
1427	16.02	Methyl (-CH <sub>3</sub> ) C-H bend	
1391	18.20	Trimethyl (-CH <sub>3</sub> ) <sub>3</sub>	(CH <sub>3</sub> ) <sub>3</sub>
<b>1352</b>	<b>35.94</b>	Skeletal C-C vibrations	C-C vibrations
<b>1283</b>	<b>53.66</b>		
1125	23.88	Aliphatic fluoro compounds, C-F stretch	C-F stretch
<b>1041</b>	<b>24.73</b>	Skeletal vibrations or C-F stretch	C-F or C-C stretch
1018	39.72		
905	114.58	Skeletal C-C vibrations	C-C vibrations
<b>873</b>	<b>47.19</b>		
825	58.46		

## **6 Results – Temperature Impact on Stress Relaxation**

The stress relaxation tests described in Chapter 4 were carried out under isothermal conditions, where test temperatures were all set at 30 °C. As an O-ring would experience various temperature conditions while serving a sealing, it is also important to understand how temperature factor would impact its stress relaxation process, especially when sealing fuels derived from alternative approaches.

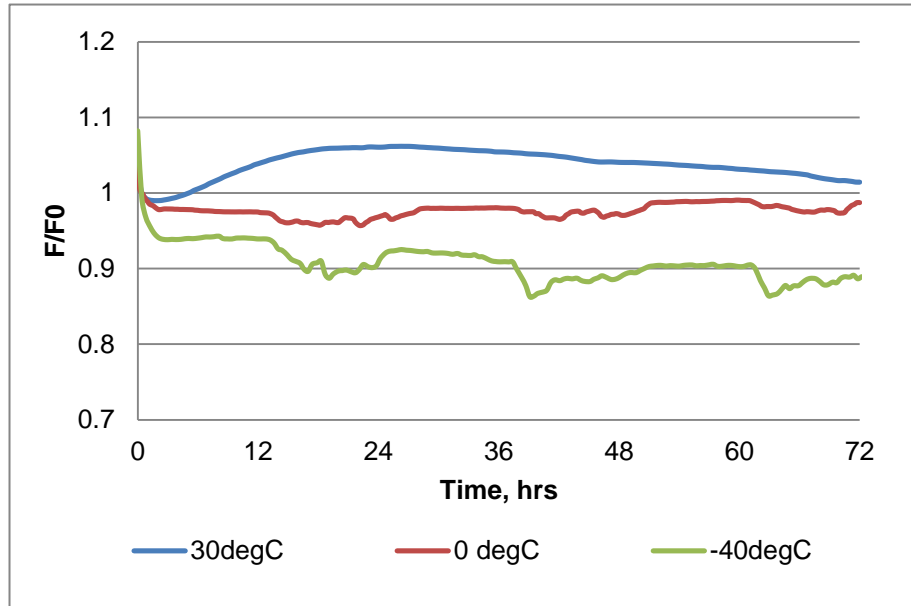
The objective of this set of tests is to investigate the impact of temperature conditions on O-ring's sealing performance in GtL kerosene (FT-SPK) and Jet A-1 using Elastocon EB 17 rig. Three tests were designed to achieve this purpose:

1. *Constant Temperature Testing*: O-ring materials undergo stress relaxation for 72h under 30, 0, and -40 °C, respectively;
2. *Temperature Switching Testing*: test temperature switches between 30 and -40 °C;
3. *24h-cycle Testing*: test temperature runs on a 24h cycle, ramping between 30 and -40 °C.

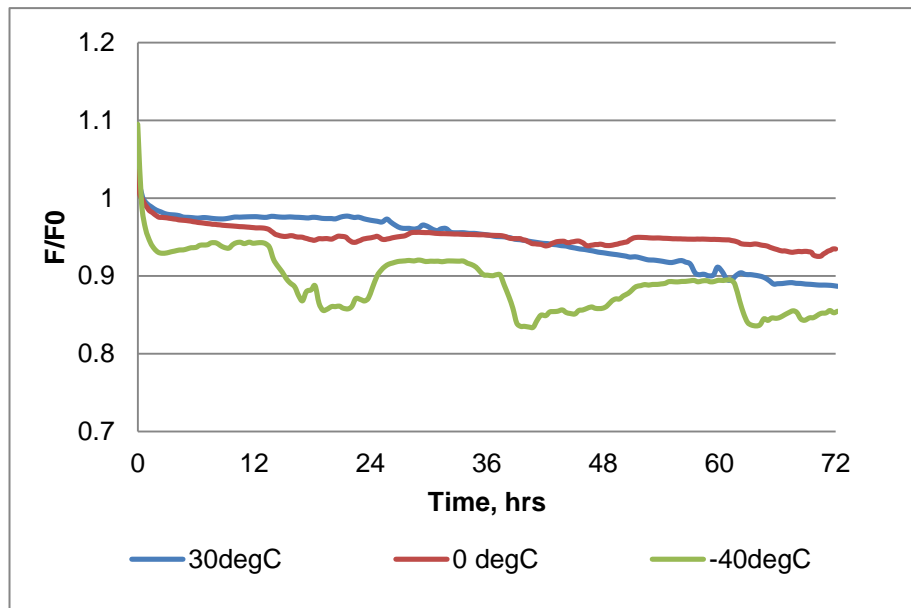
### **6.1 Constant Temperature Testing**

Stress relaxation results of three materials in both Jet A-1 and GtL fuels obtained under 0 °C and -40 °C were presented in Figure 89 – 91, with comparison to that under 30 °C.

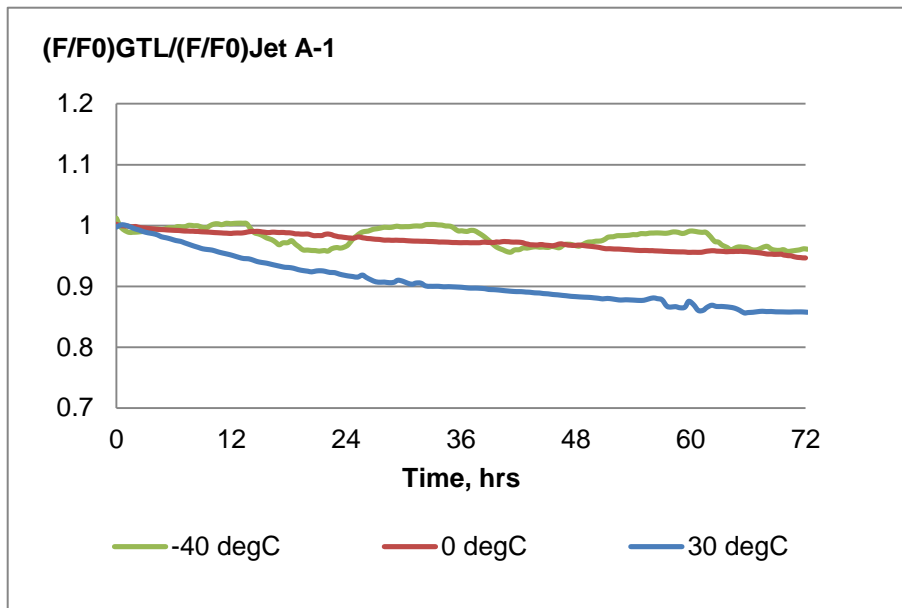
### 6.1.1 Nitrile O-rings



(a)



(b)



(c)

**Figure 89** Stress relaxation characteristics of nitrile O-ring under various constant temperatures in (a) Jet A-1 and (b) GtL fuels; and (c) comparison between the two fuels.

Figure 89 showed how nitrile seals behaved under three temperature conditions. In Jet A-1 (Fig. 89 (a)), nitrile O-ring swelled under 30 °C as discussed in the previous section (Chapter 4.1.1). However, when relaxation process occurred under 0 °C, no swelling behaviour was observed and the relaxation curve maintained at a relatively constant level. This could be explained as the interaction between fuel components and polymer material was not as active as under higher temperature condition (30 °C); however, it still occurred during the relaxation process and the weaker penetration of fuel species into polymer structures contributed to the maintenance of compression force. When temperature dropped down to -40 °C, compression force declined further compared with that under 0 °C as O-ring shrank and hardened at the extreme low temperature. Relaxation process seemed still occurring but at a fairly slow rate. The wavy shape caused by ambient temperature fluctuation was observed to be greater than those at other two temperature conditions due to the larger temperature difference at top and bottom ends of the relaxometer.

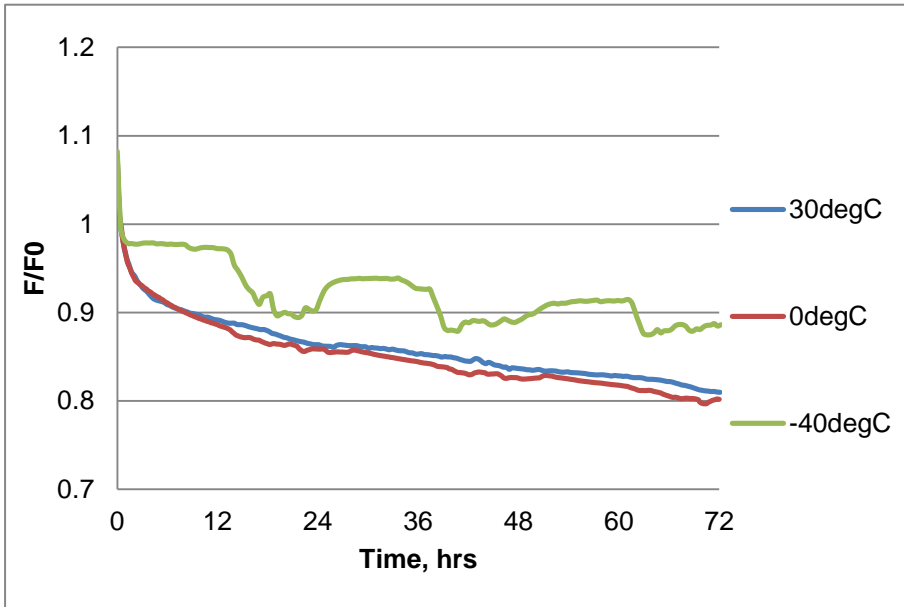
In GtL fuel (Fig. 89 (b)), nitrile seal relaxed quickly at 30 °C after the initial maintenance of compression force (as discussed in section 4.1.2.1) but its relaxation rate was dramatically slowed down at lower temperatures (both 0 °C and -40 °C). At 0 °C, no obvious fuel penetration phenomena were observed either within the initial 24 hours or later as seen in Jet A-1 fuel. Relaxation behaviour was very similar to that in Jet A-1 under -40 °C with also similar relaxation rate.

When the stress relaxation characteristics were normalized by those obtained in Jet A-1, different seal performance between GtL and Jet A-1 could be compared (Fig. 89 (c)). The closer the curve lay to value '1' line, the smaller the performance difference was between GtL and Jet A-1. At -40 °C, nitrile O-rings behaved very similarly in both fuels; however, as temperature increased from -40 to 30 °C, differences between GtL and Jet A-1 became greater. This indicates the higher the temperature becomes, the worse nitrile seals performed in GtL than in Jet A-1. At extremely low temperatures, nitrile seals become insensitive to fuel compositions and inert to relaxation.

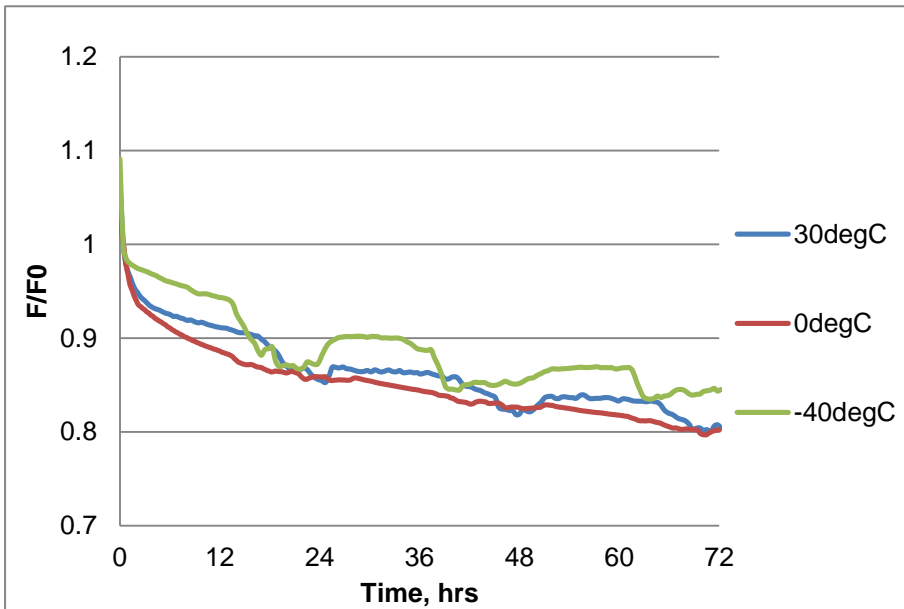
### **6.1.2 Fluorosilicone O-rings**

The stress relaxation characteristics of fluorosilicone O-rings were very similar under 30 and 0 °C in both Jet A-1 and GtL fuels, respectively (Fig. 90 (a) and (b)). Relaxation curve under 30 °C lay slightly above that under 0 °C, but the difference was tiny. However, when temperature dropped to -40 °C, the relaxation process was slowed down in both fuels. This may be explained by the hardening of polymer material resulting in a resistance to the relaxation process.

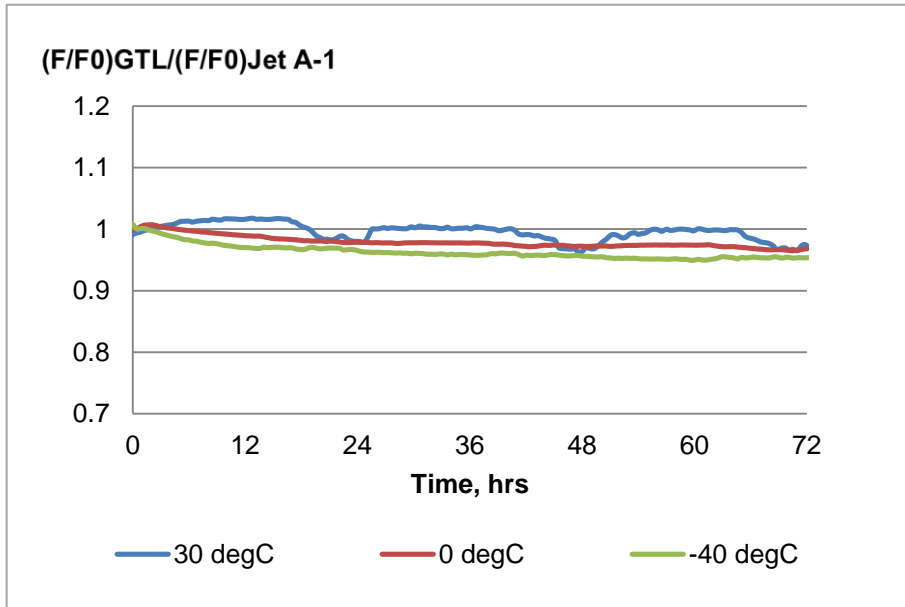
When normalized by Jet A-1 (Fig. 90 (c)), it can be seen that fluorosilicone material performed more similarly in both fuels as the temperature increased. However, the impact of temperature to cause the differences was very limited.



(a)



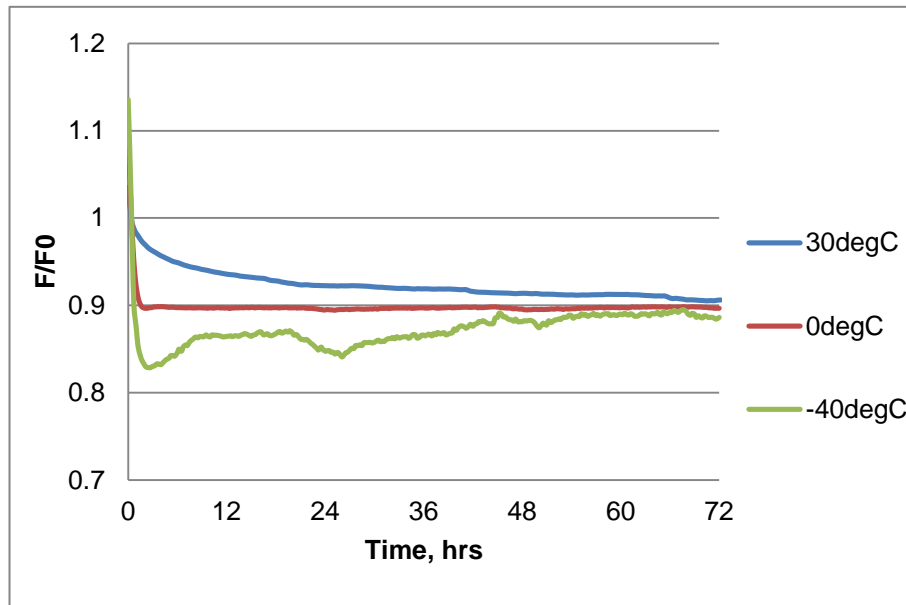
(b)



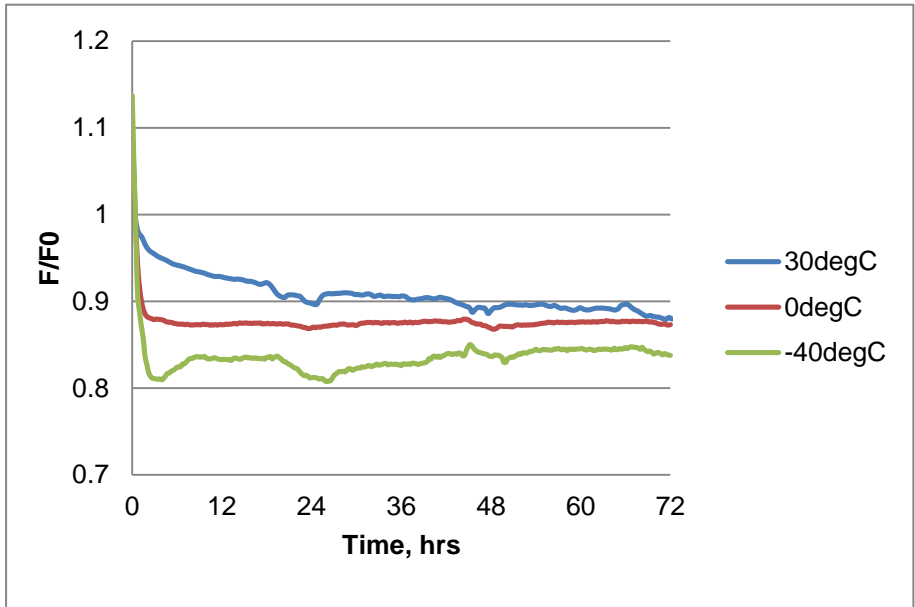
(c)

**Figure 90** Stress relaxation characteristics of fluorosilicone O-ring under various constant temperatures in (a) Jet A-1 and (b) GtL fuels; and (c) comparison between the two fuels.

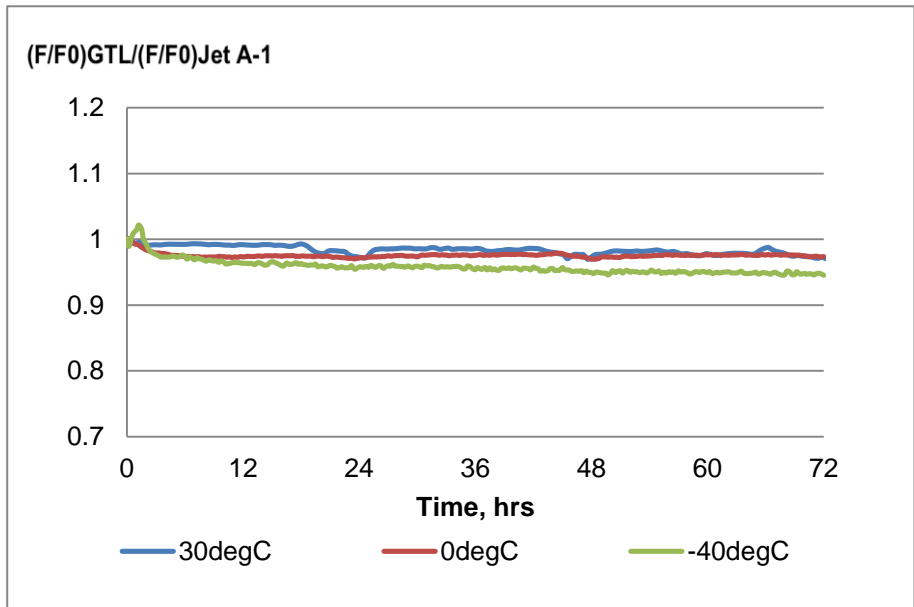
### 6.1.3 Fluorocarbon O-rings



(a)



(b)



(c)

**Figure 91** Stress relaxation characteristics of fluorocarbon O-ring under various constant temperatures in (a) Jet A-1; (b) GtL fuels; and (c) comparison between the two fuels.

Different relaxation characteristics were observed for fluorocarbon O-rings at 0 and -40 °C (Fig. 91). At 0 °C, the relaxation curves of this material were almost straight horizontal lines in both Jet A-1 and GtL fuels, indicating no relaxation occurred at this temperature. The most interesting observation was the relaxation characteristics

at -40 °C. After the initial quick relaxation, the compression force stopped declining but instead, slightly increased with time. The same behaviours were observed in both Jet A-1 and GtL fuels. Previous investigation on fluorocarbon O-ring's behaviour at low temperatures [109] [110] indicated that as the material reaches its 'glass-transition' temperature range, -25 to -6 °C as defined by different test methods, fluorocarbon O-ring would lose its elastic property as a rubber gradually and become stiffer, plastic-like. When O-ring became completely stiff, it would not be able to respond to the applied compression and no stress relaxation would occur. This could explain the cease of relaxation under -40 °C as O-rings became completely plastic; however, this could not introduce the increase in compression force. Further understanding on the stress relaxation behaviour at -40 °C is needed.

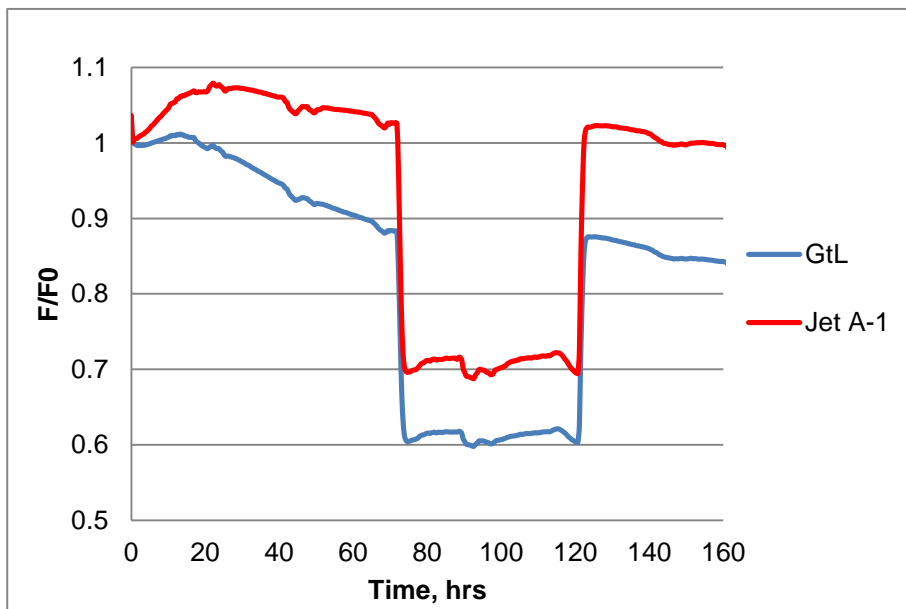
Generally, fluorocarbon O-rings showed little difference in GTL and Jet A-1 under various temperature conditions (Fig. 91 (c)). A reverse trend was observed when compared with nitrile O-rings; as temperature decreases, fluorocarbon O-rings relax slightly further in GtL than those in Jet A-1. It can be concluded that temperature has very little impact on the sealing performance of fluorocarbon O-rings when GTL fuel is used.

## **6.2 Temperature Switching Testing**

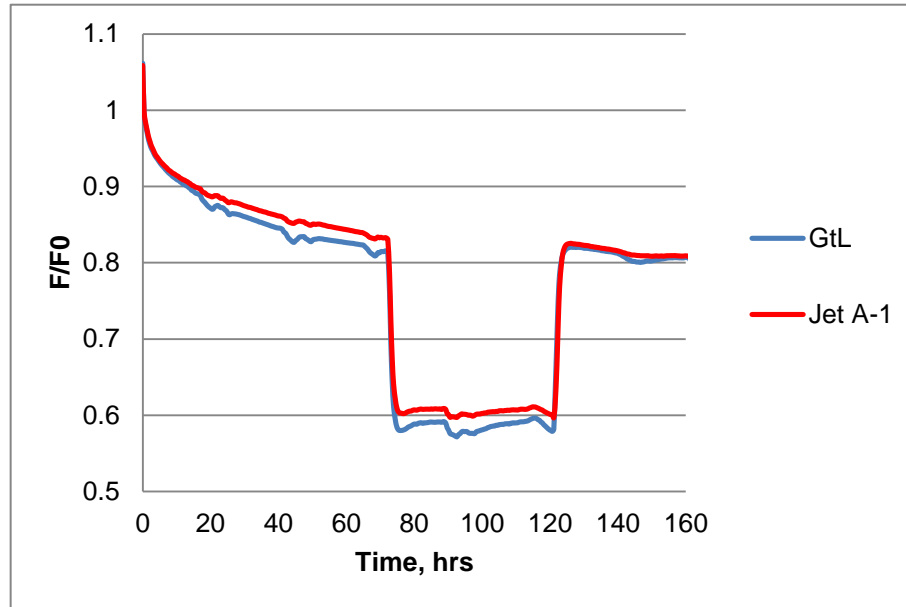
The test temperature was kept constant at 30 °C for about 72 hours before switched to -40 °C within two hours (0.58 °C /min) and kept constant for 48 hours, then back to 30 °C again. The practical purpose of this test is to look at how O-rings would react during fast temperature transition conditions, such as when an aircraft is taking-off or landing. Figure 92 showed the stress relaxation process of three O-ring materials in GtL and Jet A-1, respectively.

For nitrile O-ring (Fig. 92 (a)), the stress relaxation process occurred 'normally' during the first 72 hours, with the same pattern in Jet A-1 and GtL fuels respectively as discussed previously. When temperature dropped quickly from 30 to -40 °C, the

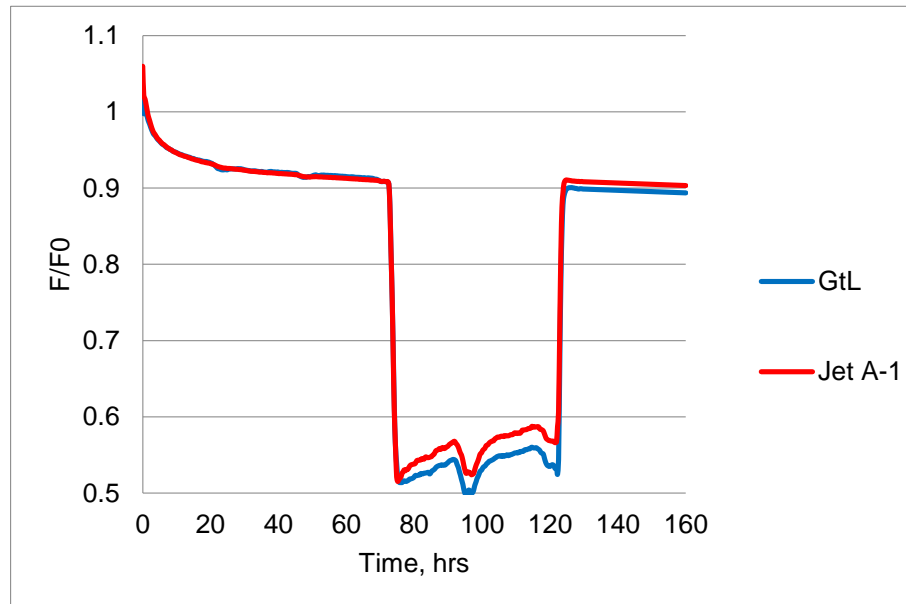
compression forces declined by 33% and 28% in Jet A-1 and GTL fuel respectively during the transition period. The physical reason behind this phenomenon is the thermal contraction of polymers as the temperature decreased quickly. This contraction in volume results in a reduced contact area with the compression platen, which is applying pressure on the seal, and therefore, causes the decrease in compression force. The faster the temperature drops, the quicker the compression force decreases. When temperature reached -40 °C, compression forces maintained at a relatively constant level in the following 48 hours in both fuels. This is the same behaviour as discussed in the ‘Constant Temperature Testing’, as O-rings become stiffer and inert to relaxation. When temperature switched back to 30 °C, compression force recovered to previous level and the relaxation process continued. It seems that stress relaxation process is closely related to temperature conditions; no relaxation would occur under fast temperature transition and extremely low temperature conditions.



(a)



(b)



(c)

**Figure 92** Relaxation process of (a) nitrile, (b) fluorosilicone and (c) fluorocarbon O-rings in GtL and Jet A-1 fuel respectively, with temperature switching between 30 to -40 °C.

Fluorosilicone O-rings showed little difference in both Jet A-1 and GtL fuel during the temperature cycling tests (Fig. 92 (b)). When temperature dropped from 30 to -40 °C, both compression forces dropped by about 24% and also kept constant as temperature remained at -40 °C. Compression forces also recovered to previous level

when temperature increased to 30 °C, and the relaxation process continued afterwards.

Fluorocarbon O-rings showed greater response to the temperature transition from 30 to -40 °C, as both compression forces dropped by approximately 45% (Fig. 92 (c)). A similar recovery behaviour which was observed at ‘constant temperature testing’ presented in both fuels when temperature was remained at -40 °C. Compression forces also recovered to previous level when temperature increased to 30 °C, and the relaxation process continued afterwards.

When normalized by Jet A-1, as shown in Figure 93, both fluorocarbon and fluorosilicone O-rings presented very similar performance in both GtL and Jet A-1 fuel; whilst nitrile in GtL performed not as well as that in Jet A-1. It relaxed by 17% further in GtL by the end of the 160h test.

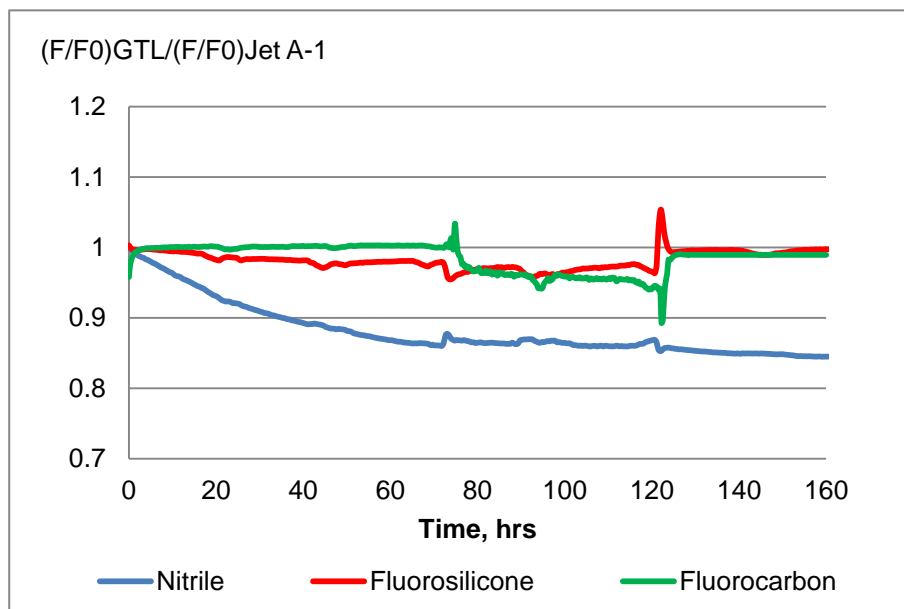
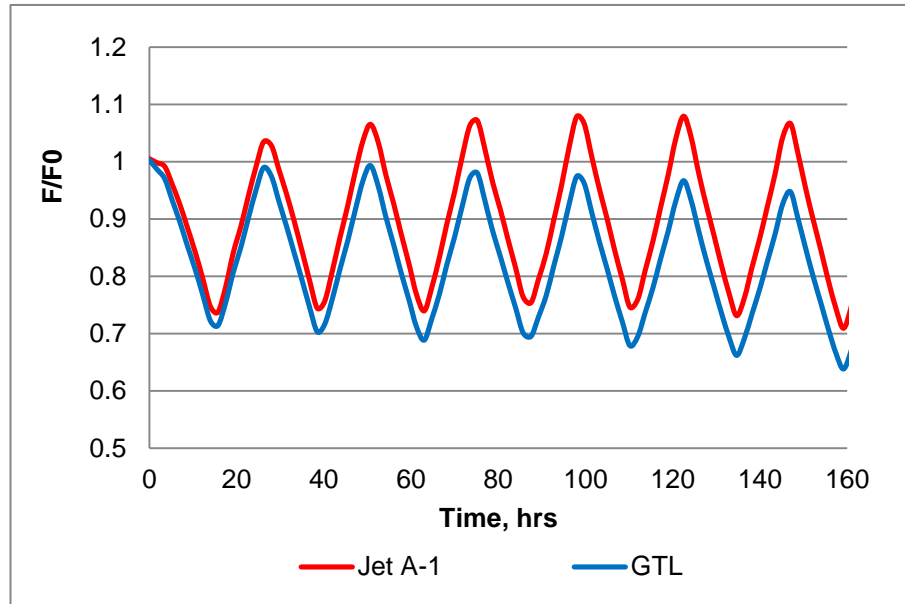


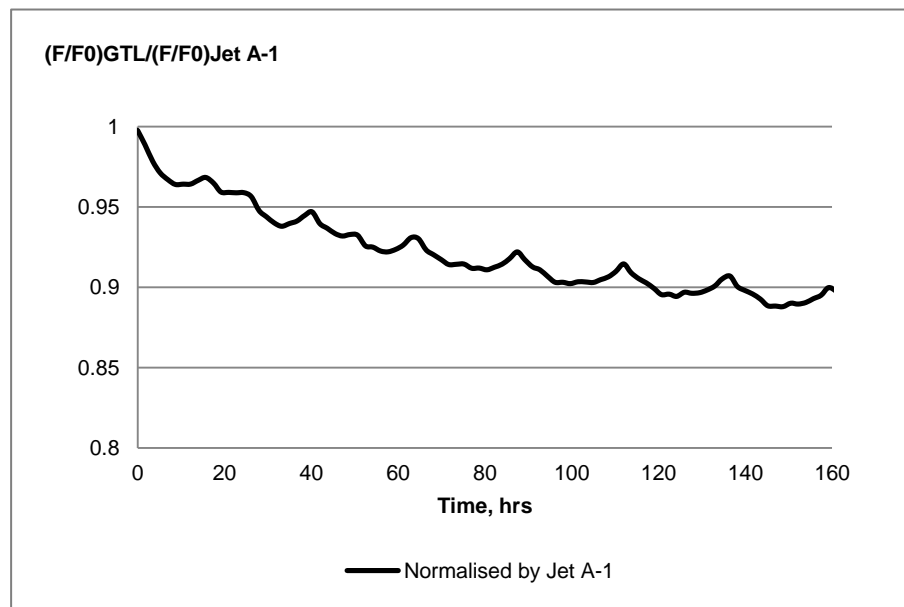
**Figure 93** Performance comparison of three O-ring materials in the temperature switching test.

### 6.3 24h-Cycle Testing

#### 6.3.1 Nitrile O-rings



(a)



(b)

**Figure 94** (a) Relaxation performance of nitrile O-ring in the 24h-cycle testing; (b) normalized by Jet A-1.

Generally, compression forces applied on nitrile O-rings decreased when the

temperature was dropped and increased when the temperature was raised back. That is where the sine wave shape of the relaxation process comes from (Fig. 94(a)). The overall relaxation patterns were very similar to that at 30 °C ‘constant temperature testing’ in both GtL and Jet A-1 fuels. Again, low temperatures seem to ‘freeze’ the relaxation process and the process continued when temperature was back to 30 °C. Details of the relation between temperature variation and compression force changes will be discussed in Chapter 7. When normalized by Jet A-1 (Fig. 94 (b)), nitrile O-ring also performed better in Jet A-1 than that in GtL fuel. It relaxed about 15% more in GtL by the end of 160 hours.

Comparing the results with the data obtained from the constant temperature testing (Fig. 95), it appears the 24h-cycle data lay between the data from 30 and -40 °C. The effect of low temperatures was to slow down the relaxation process.

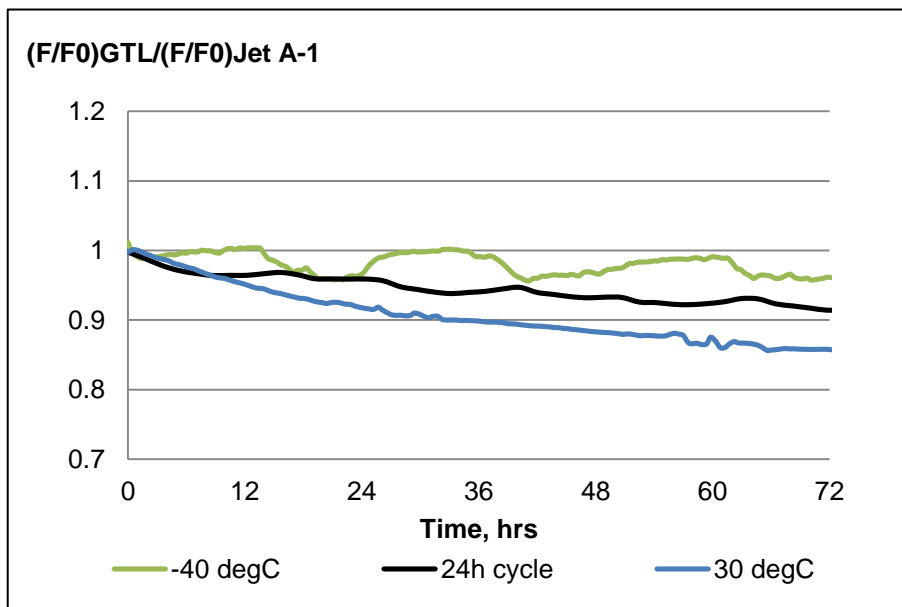
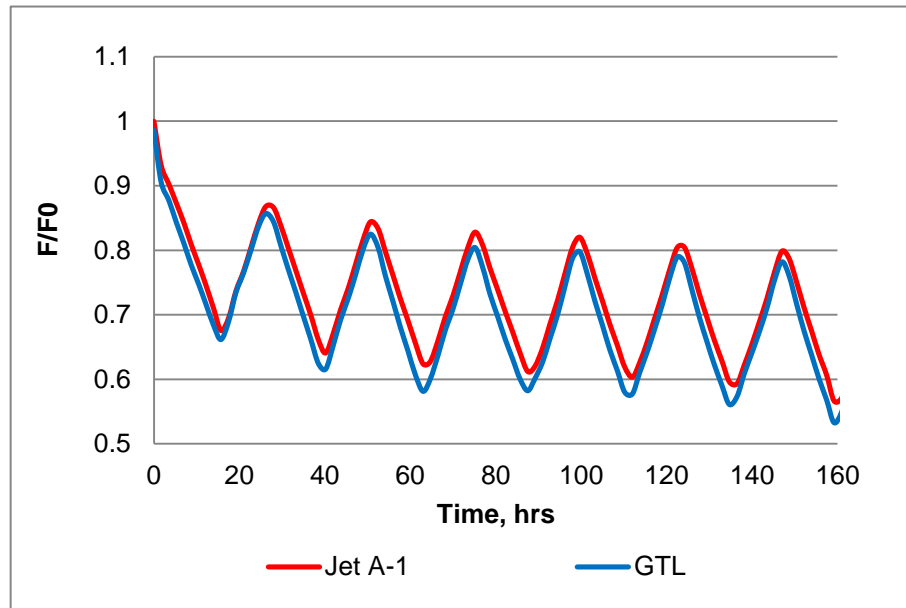
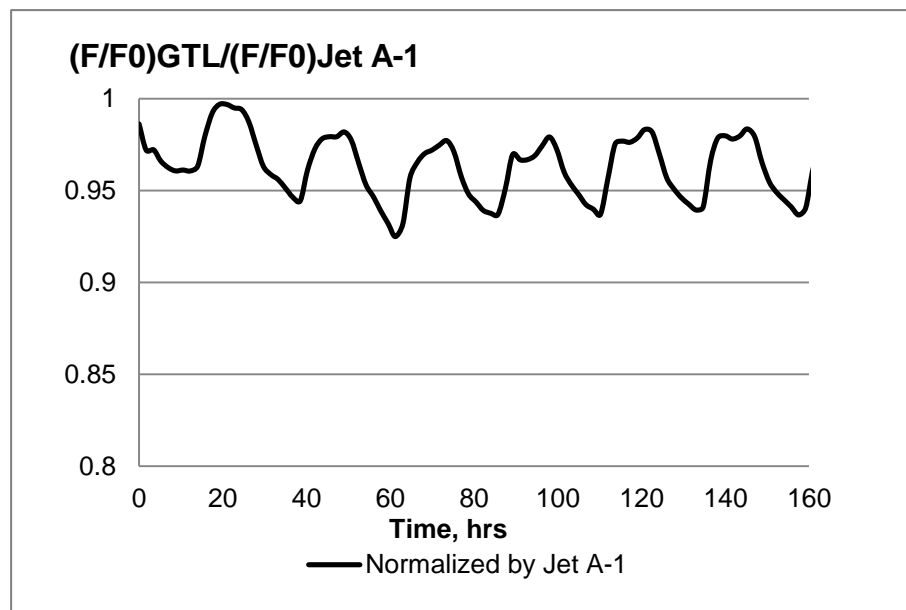


**Figure 95** Results from 24h-cycle testing compared with constant temperature testing (nitrile).

### 6.3.2 Fluorosilicone O-rings



(a)



(b)

**Figure 96** (a) Relaxation performance of fluorosilicone O-ring in the 24h-cycle testing; (b) normalized by Jet A-1.

Fluorosilicone O-rings performed similarly in both GtL and Jet A-1 fuel as can be seen in Figure 96 (a). They also followed the similar pattern as those at 30 °C

constant temperature testing. When normalized by Jet A-1, fluorosilicone O-ring in GtL performed slightly worse than that in Jet A-1; but generally this type of elastomeric material performed well in both fuels.

When compared with the results from constant temperature testing, fluorosilicone O-rings behaved excellently at all testing temperature conditions. Temperature has very limited impact on the performance of this type of O-ring materials.

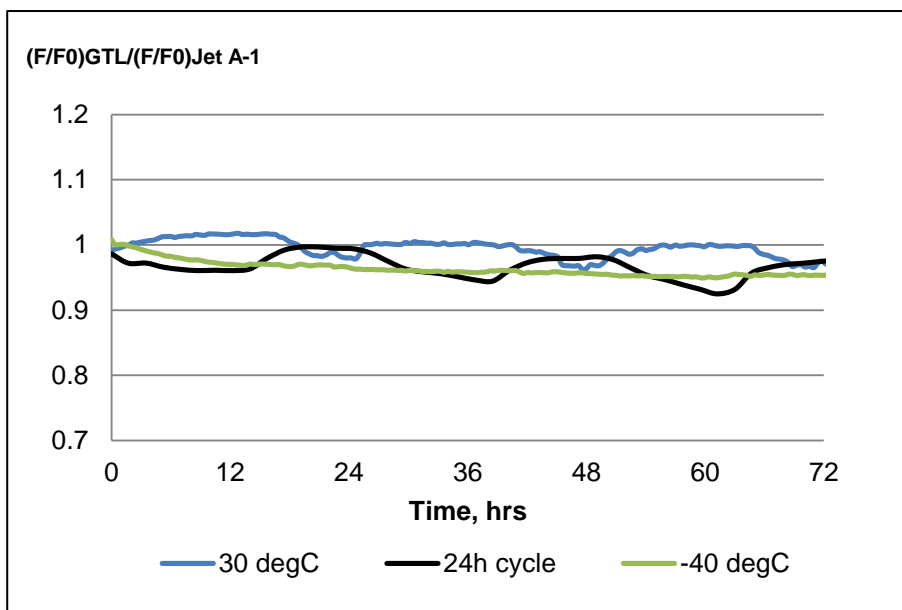
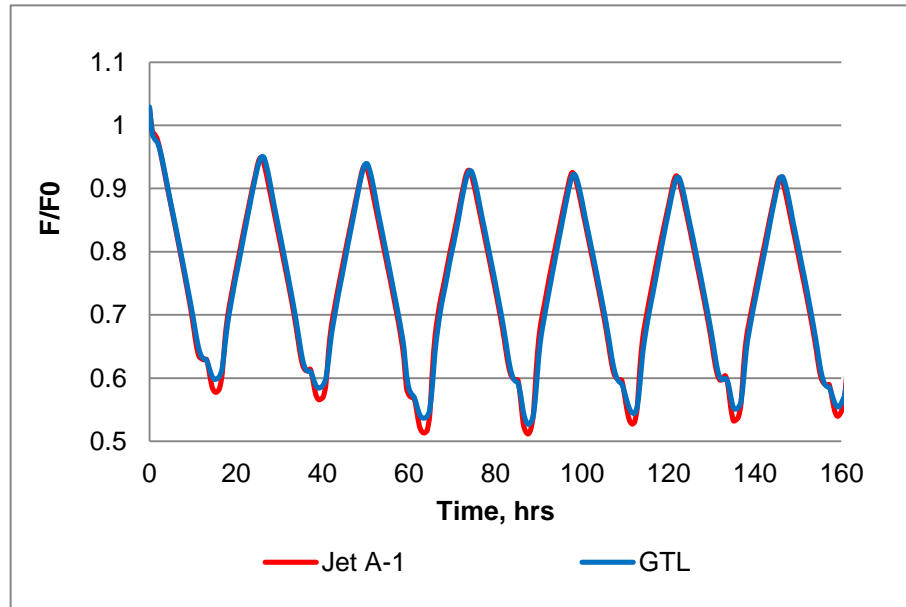


**Figure 97** Results from 24h-cycle testing compared with constant temperature testing (fluorosilicone).

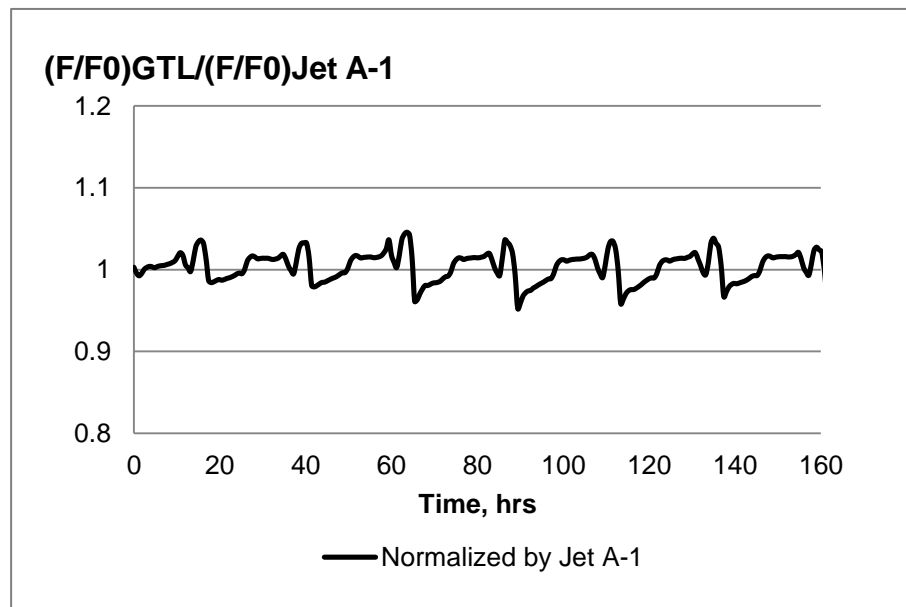
### 6.3.3 Fluorocarbon O-rings

The relaxation patterns of fluorocarbon O-rings in GtL overlapped that in Jet A-1, indicating these two fuels have the same effect on this polymer material in the 24h-cycle test (Fig. 98 (a)). They also followed the similar trends as those at 30 °C constant temperature testing. However, when compression forces dropped down to the bottom of each cycle (temperature dropped down to -40 °C), an irregular shape appeared and it repeated in each cycle. This is due to fluorocarbon O-ring became stiff when it reached its glass transition temperature range and its response to

compression was not long linear. Details of the discussion will be presented in the following chapter. The normalized curve also proved the excellent compatibility fluorocarbon O-ring in both fuels (Fig. 98 (b)).



(a)



(b)

**Figure 98** (a) Relaxation performance of fluorocarbon O-ring in the 24h-cycle testing; (b) normalized by Jet A-1.

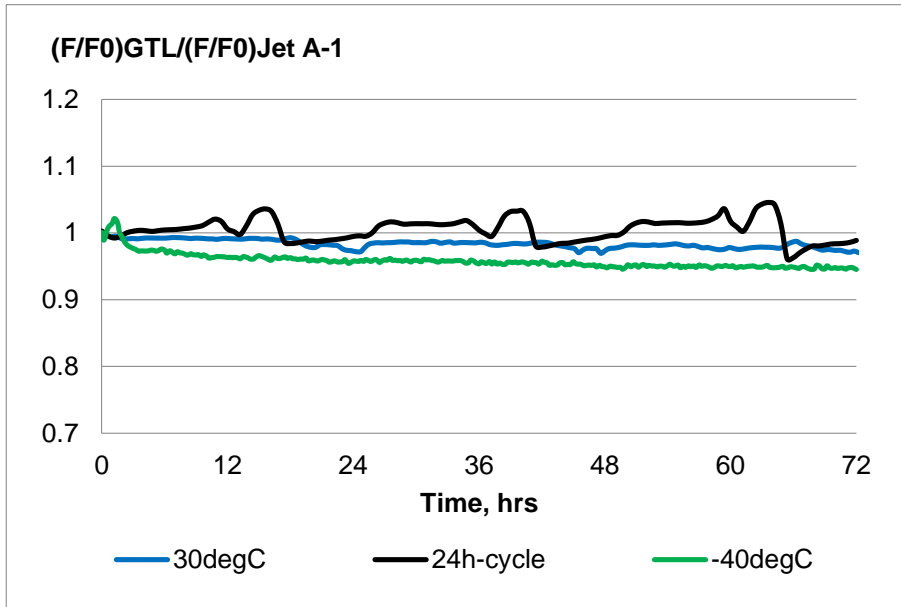


**Figure 99** Results from 24h-cycle testing compared with constant temperature testing (fluorocarbon).

Comparison amongst these three O-ring materials during the 24h-cycle test showed the same compatibility order as acknowledged from previous tests, which is:

fluorocarbon > fluorosilicone > nitrile

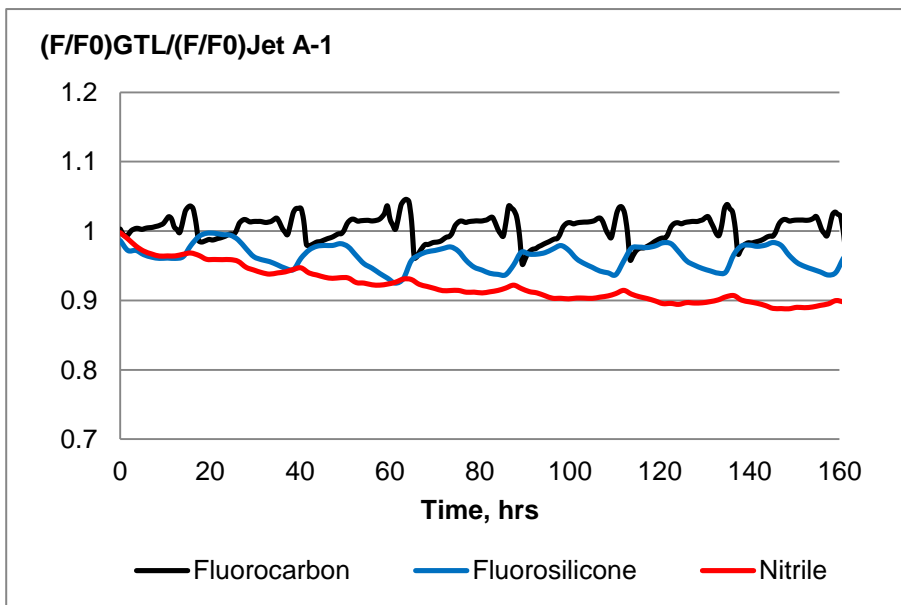


**Figure 100** Comparison of normalized relaxation performances of three O-ring materials in the 24h-cycle testing.

#### 6.4 Stress Relaxation of Elastomeric Seals in O-ring Grooves

Based on the understanding of the stress relaxation process acquired from a series of tests, a further step was taken to include O-ring grooves into consideration. The purpose of including an O-ring groove is to make the stress relaxation results more applicable to real sealing performance. According to the O-rings used in this project, a SAE ARP-1234 face seal O-ring groove was selected to be the target specification [111]. This specification allows external pressure to be applied on O-ring seals with a minimized mating face gap. Detailed specification is provided in Table 16.

**Table 16** SAE ARP-1234 face seal O-ring groove specifications.

Specification	Value (mm)
Internal Diameter ( $D_i$ )	14.00
Width (W)	4.44
External Diameter ( $D_e$ )	22.88
Height (H)	1.98
Desired Squeeze (Sq)	20%
Gap (G)	0.02

With the aim to evaluate the impact of aromatic content on O-ring materials, 4 types of fuels, with aromatic contents from 0 to 16% (v/v), were used in this set of tests. The various aromatic contents were achieved by blending a typical Jet A-1 fuel ( $\approx$ 16% aromatics) with a SPK fuel (0% aromatics) in different proportions. As the effect of aromatics on fresh nitrile O-rings have already been understood, it was decided to use preconditioned nitrile seals for this temperature cycling test. The preconditioning process was achieved by conducting standard stress relaxation test on nitrile O-rings in Jet A-1 fuel for over 150 hours. The purpose of this process was to ‘wash out’ the plasticizers and other removable additives out of the polymer material, making the resulting seals more representative in a practical manner. Fresh fluorosilicone and fluorocarbon O-rings were still employed as no need for preconditioning was noticed.

Temperature was cycling between 30 and -40 °C. Results were presented in Figure 101, 103 and 104, in the order of preconditioned nitrile, fluorosilicone, and fluorocarbon O-rings.

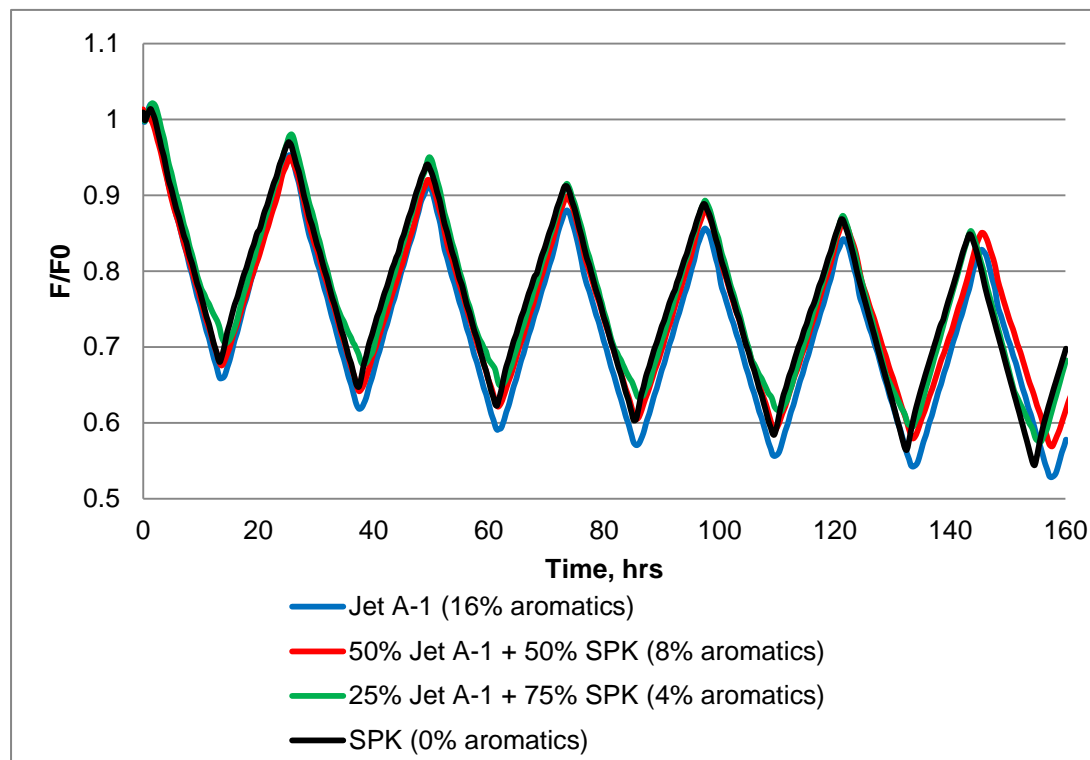


**Figure 101** 24h-cycle test results of preconditioned nitrile O-rings in grooves in fuels with various aromatic contents.

The variation of aromatic contents seemed to have little impact on preconditioned nitrile O-rings as the stress relaxation characteristics under cycling temperature conditions showed little difference amongst those four fuels as shown in Figure 101. This is quite a different observation compared with fresh nitrile seals because aromatics would swell them significantly in the initial contact period. However, when comparing the relaxation rates of fresh nitrile O-rings after the swelling period (initial 72 hours as shown in Fig. 102), differences between Jet A-1 and SPK fuel became very small, with 0.001/hour in the former and 0.0011/hour in the later. This indicated that the significantly different performances of fresh nitrile seals in Jet A-1 and SPK fuels were predominantly caused by the penetration of aromatic compounds

during the initial swelling period; sealing performances afterwards did not present much difference. The preconditioning process conducted in this test eliminated the effect of initial swelling period and thus the stress relaxation characteristics demonstrated more similar pattern. O-rings in fuels with lower aromatic contents presented even slightly better behaviour than in Jet A-1. Detailed analysis will be described in the next chapter.

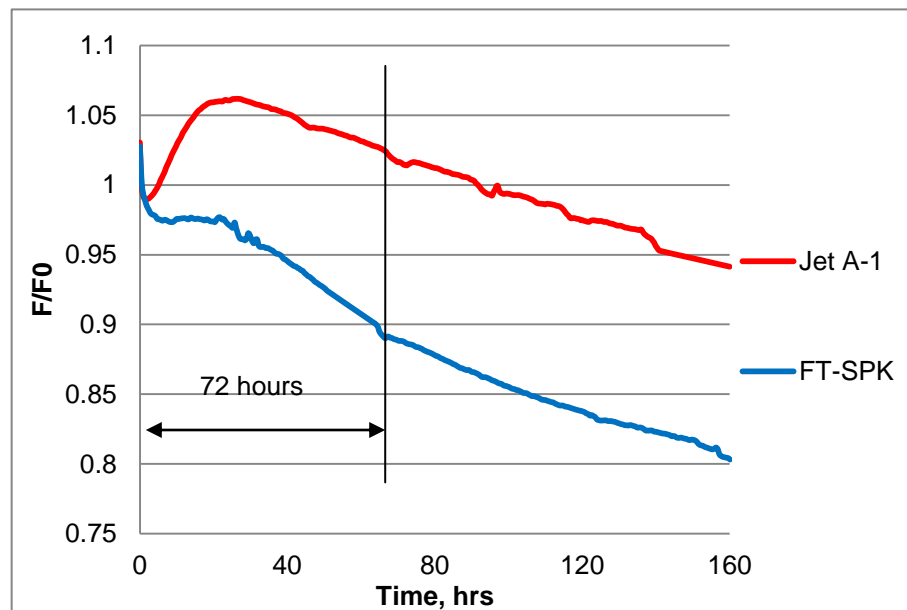


**Figure 102** Fresh nitrile O-ring relaxation rate comparison in Jet A-1 and SPK.

Fluorosilicone O-rings presented very similar stress relaxation characteristics in all fuels as expected due to its insensitivity to aromatic content (Fig. 103). As the cycle increased, its general relaxation trend levelled off indicating the material was reaching equilibrium during the temperature cycling process.

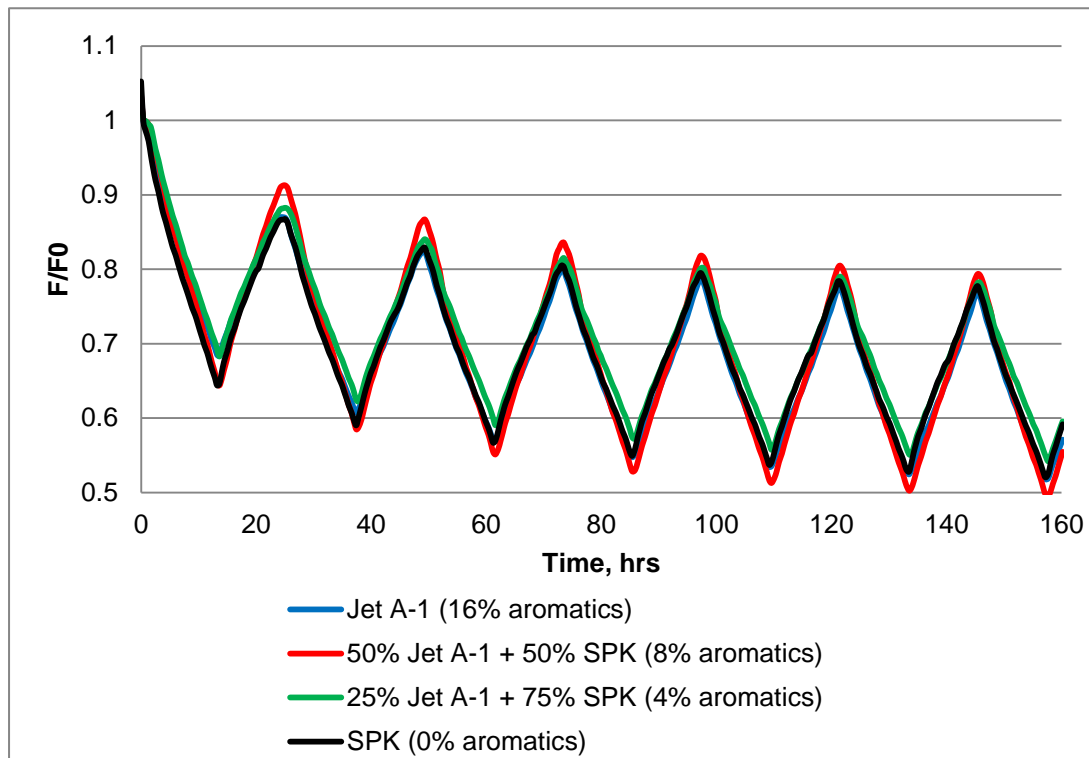


**Figure 103** 24h-cycle test results of fluorosilicone O-rings in grooves in fuels with various aromatic contents.

Fluorocarbon O-ring demonstrated even weaker relaxation trend during the test and aromatic content variation also had no impact on its performance (Fig.104). At extremely low temperatures, this material presented similar ‘irregular’ shape as those observed in ‘no groove’ tests which was caused by the material harden. Detailed comparison and analysis will be discussed in the following chapter.

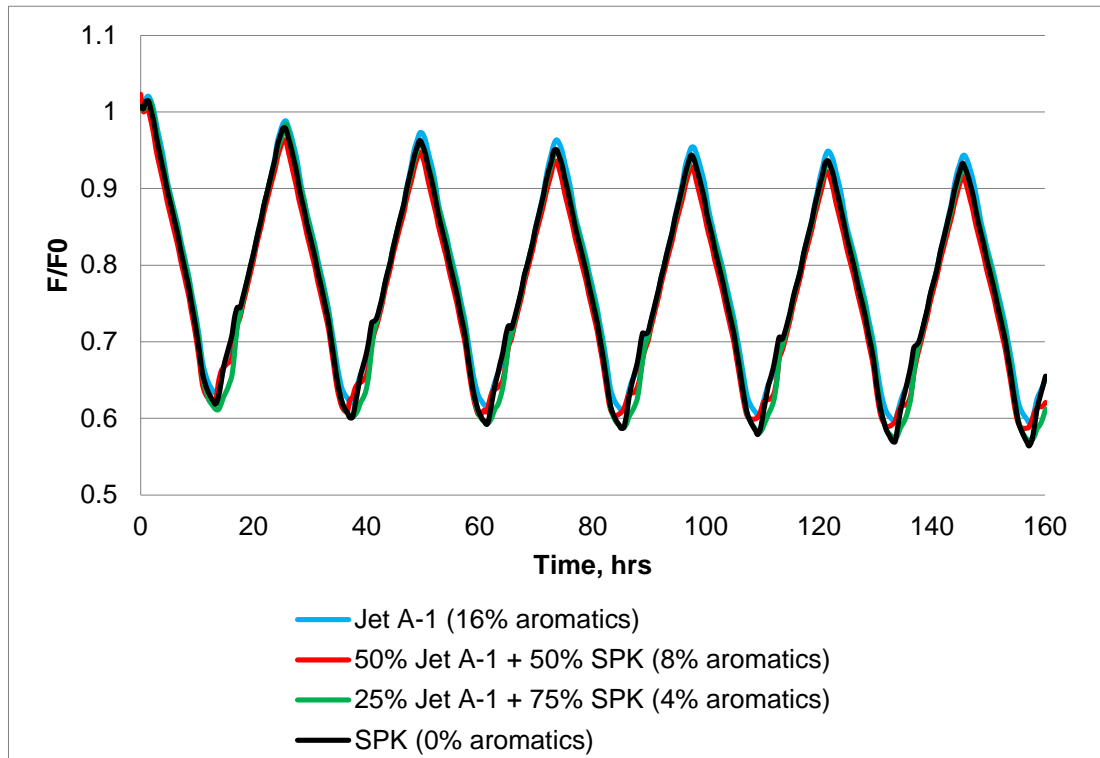


**Figure 104** 24h-cycle test results of fluorocarbon O-rings in grooves in fuels with various aromatic contents.

### 6.5 Summary

Various temperature testing conditions were set to see how the stress relaxation processes of three O-rings would be influenced. For nitrile O-rings, temperature is an influential factor for its sealing performance as temperature increases its sealing performance in GTL fuel becomes worse compared with that in Jet A-1. Fluorosilicone and fluorocarbon O-rings behaved similarly under all the testing temperature conditions in both fuels tested. Results from the temperature cycling test and 24h-cycle test indicated O-rings become very inert at extremely low temperatures. Fluorocarbon O-ring would become stiff as it goes through its glass transition temperatures and its response to compression force is no longer linear.

The addition of grooves expanded the understanding of O-ring's stress relaxation performance to a more practical extent. Generally, it introduces additional compression force on seals which results in an increase in relaxation rate but this

difference vary depending on materials. Impact on nitrile and fluorosilicone O-rings could be observed from the test results; however, its influence on fluorocarbon is limited.

## 7 Discussions

### 7.1 Hansen Solubility Parameters (HSPs) Analysis

HSPs were used to analyse the stress relaxation data generated from the ‘triangle’ test presented in section 4.1.3. As the composition variation did not have any obvious impact on fluorosilicone and fluorocarbon O-rings, analysis was focused on the relaxation data of nitrile seals in the normal, iso- and cycloparaffin triangle solvent matrix. The HSPs of the three solvents were listed in Table 17.

**Table 17** Hansen Solubility Parameters of the normal, iso- and cycloparaffin in the ‘triangle’ test.

Solvent/Polymer	Hansen Solubility Parameters (HSPs), MPa <sup>1/2</sup>			Molar Volume (cm <sup>3</sup> /mol)
	$\delta_D$	$\delta_P$	$\delta_H$	
n-Decane <sup>1</sup>	15.7	0	0	195.9
ShellSol T <sup>2</sup>	15.0	0	0	224.7
Decalin (Decahydronaphthalene)	18.4	0	0	156.9
Buna N Butadiene /Acrylonitrile (NBR)	17.8	3.2	3.4	-

<sup>1</sup>HSP data for n-decane, decalin and NBR are obtained from the HSP software database;

<sup>2</sup>HSP data for ShellSol T is obtained from the datasheet of ShellSol T solvent [112]. The solubility parameter given in the ShellSol T datasheet is the Hildebrand solubility parameter ( $\delta$ ) with a value of 7.35 (cal/cm<sup>3</sup>)<sup>1/2</sup>. To convert to SI unit (MPa<sup>1/2</sup>),  $\delta_D=2.0455 \delta=15.0$  MPa<sup>1/2</sup>.

As the actual HSP of the nitrile O-ring tested were not available, a set of theoretical values from the HSP software database was used ( $R_0=3.7$ ). As all three solvents present no polarity or hydrogen bonding, the blends consist of them will only have  $\delta_D$  value as well. The HSPs of the other 22 solvent blends could then be generated

according to the volume proportion of each solvent in the blends.

$$\delta_{D,B_n} = a\delta_{D,n-Decane} + b\delta_{D,ShellSolT} + c\delta_{D,Decalin} \quad (7.1)$$

where a, b, c are the percentage of each solvent in the blend. The HSPs of each blend were listed in Table 18. As previous studies indicated a correlation between elastomer swelling and HSP [87], an equilibrium value, achieved by the balance between volume swell and compression force (visually the maximum force achieved after the initial applied compression), was obtained from the stress relaxation data in each blend. Then a correlation was observed when the F/F0 at equilibrium was plotted against the RED number for nitrile O-ring calculated from the HSPs (Fig. 105).

**Table 18** Hansen Solubility Parameters and equilibrium values of the ‘triangle’ solvent blends.

<b>Blend</b>	$\delta_D$	$\delta_P$	$\delta_H$	<b>RED Number</b>	<b>Equilibrium Value</b>
B1	18.4	0	0	1.30	1.1052
B2	17.6	0	0	1.27	1.1002
B3	16.7	0	0	1.39	1.0296
B4	16.6	0	0	1.43	1.0210
B5	16.4	0	0	1.48	1.0138
B6	17.4	0	0	1.28	1.0784
B7	17.2	0	0	1.31	1.0709
B8	15.9	0	0	1.64	0.9759
B9	15.0	0	0	1.96	0.9606
B10	15.7	0	0	1.70	0.9748
B11	16.0	0	0	1.58	0.9942
B12	15.2	0	0	1.89	1.0197
B13	15.6	0	0	1.74	0.9752

B14	15.4	0	0	1.82	0.9760
B15	15.9	0	0	1.64	0.9841
B16	15.5	0	0	1.76	0.9894
B17	15.8	0	0	1.66	0.9964
B18	15.7	0	0	1.70	1.0034
B19	16.0	0	0	1.58	1.0124
B20	16.4	0	0	1.48	1.0197
B21	16.4	0	0	1.48	1.0216
B22	16.7	0	0	1.39	1.0297
B23	17.1	0	0	1.33	1.0603
B24	17.3	0	0	1.29	1.0696
B25	17.7	0	0	1.26	1.0604

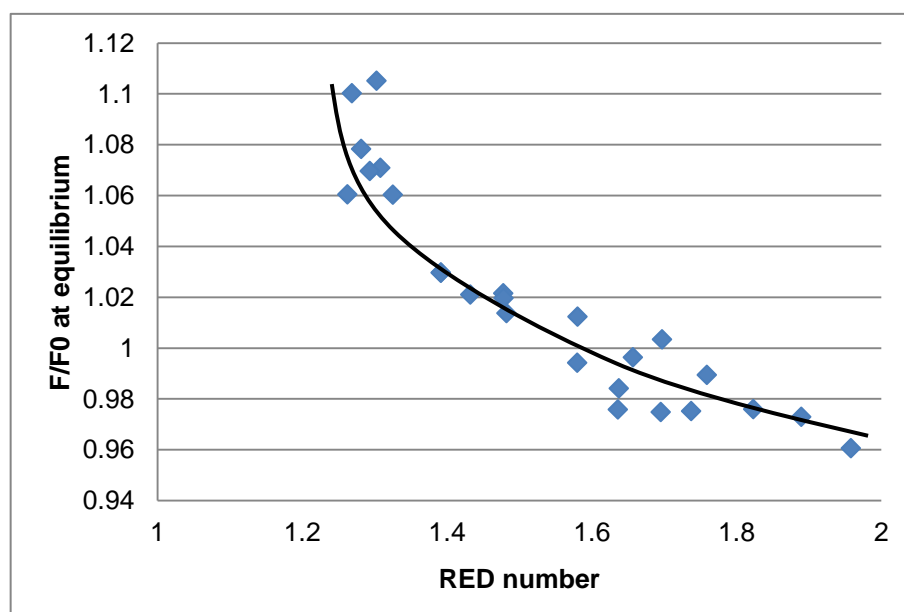


**Figure 105** Plot of  $F/F_0$  at equilibrium (experimental) versus RED number for nitrile O-ring (theoretical).

Figure 105 showed a good non-linear correlation between the equilibrium value and the RED number. The value of  $F/F_0$  at equilibrium reduces as the RED number

increases, indicating the further the solvent's HSP from the nitrile sphere, the weaker its ability to swell the O-ring. This result is in good consistency with previous study on relationship between elastomer swelling and HSP [87]. One thing needs to bear in mind is that the correlation is based mainly on the seal swell ability of the solvents. In this aspect, the HSP of decalin is the closest to the theoretical nitrile sphere while that of ShellSol T is the farthest. This means the more decalin (ShellSol T) in the blend, the better (worse) the seal swell ability the final blend has. It is not the same trend as shown in the stress relaxation data where n-decane played as the 'worst' solvent to relax the seal the quickest. This is because although n-decane has better seal swelling ability than ShellSol T solvent, its ability to extract material out of the polymer is also stronger than the latter. Further research is needed to look into the relations between the HSPs and the overall stress relaxation performance of nitrile seals.

## **7.2 Temperature Factor Analysis**

Temperature impacts on three O-ring materials were analysed based on the data generated from the 24h cycling tests. Original data were plotted as compression force against temperature range in both contraction (cooling) and recovery (heating) cycles. As temperature was changing at a fixed rate (2.92 °C/hour) throughout the tests, relationship between compression force changes and temperature gradient could be drawn. Analysis was conducted based on each O-ring material and further comparison between data in/without grooves was provided.

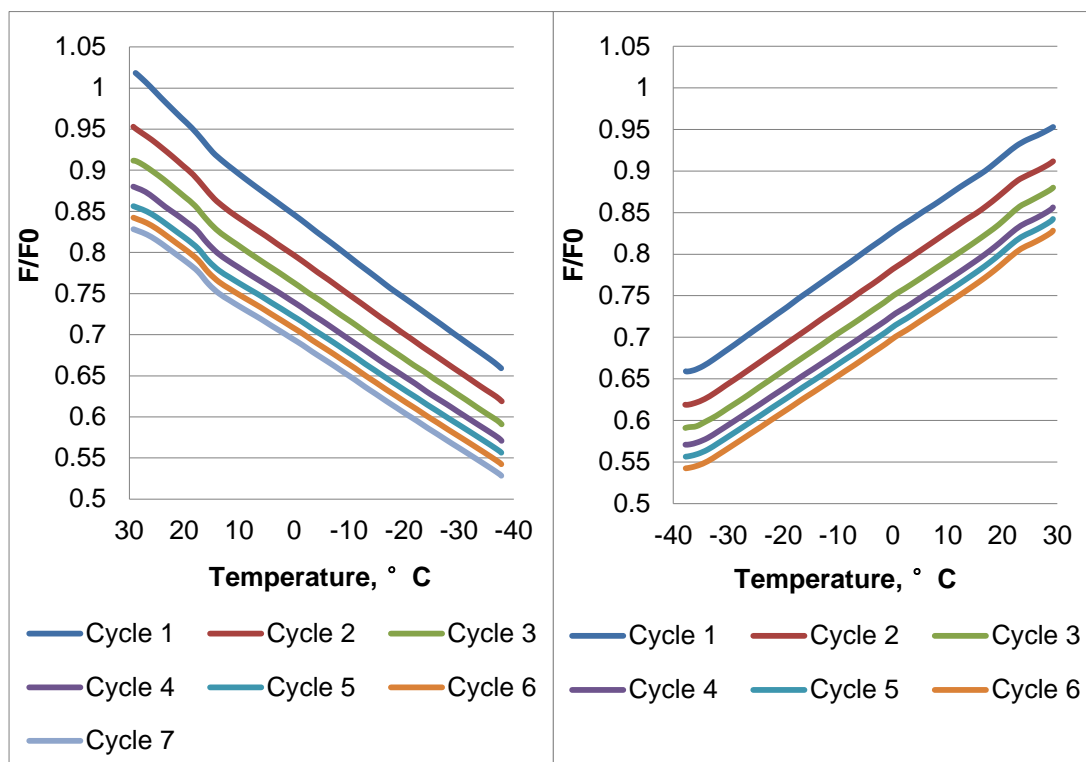
### **7.2.1 Nitrile O-rings**

#### ***7.2.1.1 In O-ring grooves***

Figure 106-109 presented the analysis for preconditioned nitrile O-rings tested in grooves in Jet A-1 (16% aromatics), 75% Jet A-1 + 25% SPK (8% aromatics), 50% Jet A-1 + 50% SPK (4% aromatics) and SPK (0% aromatics), respectively. Generally, the overall contraction and recovery behaviours of nitrile O-rings were similar in all

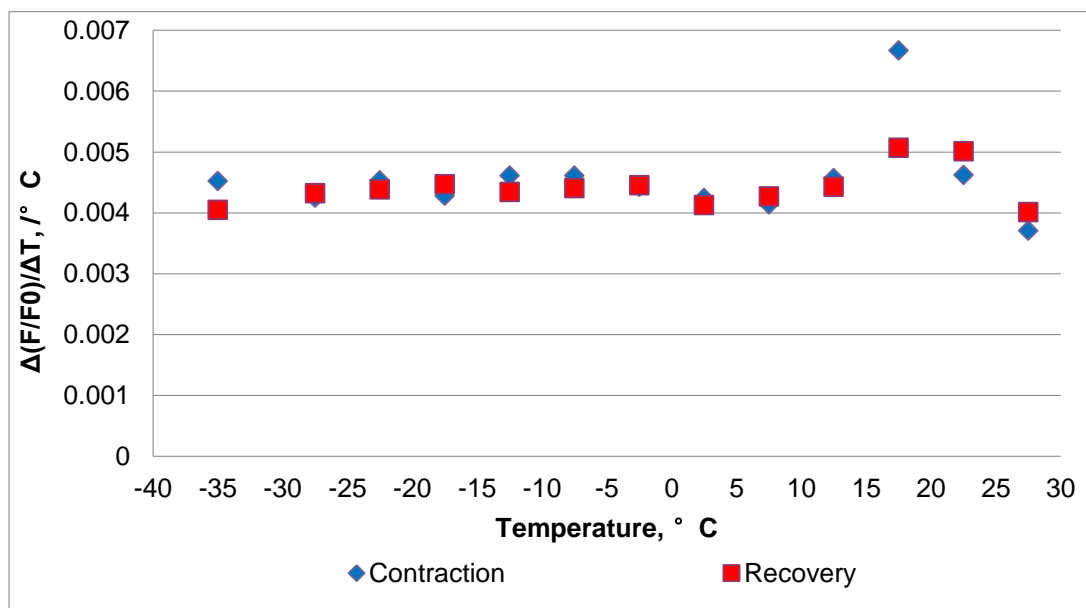
four fuels. During the contraction (recovery) cycles, the compression force reduces (increases) as temperature drops (rises). This could be explained by the difference in thermal expansion coefficients between the stainless steel compression platen and the elastomeric seal material. The O-ring contracts more when temperature decreases due to its much higher thermal expansion coefficient. The shrinkage of seal volume leads to a reduced contact area with the compression platen and therefore results in a compression force decline (e.g. Fig. 106 (a)). When temperature rises, the seal expands and increases the force applied on the platen, which leads to a recovery of compression force (e.g. Fig 106 (b)). Data also showed that as the cycle increases, the overall compression force decreases gradually in both contraction and recovery cycles due to the stress relaxation of the seal. Gap between two successive cycles was reducing, indicating the seal material was approaching equilibrium in each fuel. It should be noticed that the behaviour of the seal during the contraction and recovery cycles is the result of two physical processes occurring simultaneously; one is the thermal contraction and expansion of the elastomeric material during the cooling and heating processes, the other is the stress relaxation.

When investigating the relationship between temperature gradient and compression force, the whole temperature range was divided into a series of 5 °C temperature regions. The compression force change ( $\Delta (F/F_0)$ ) over each temperature gradient ( $\Delta T$ ) was plotted against the temperature range. In Jet A-1 (as shown in Fig. 106 (c)), values of  $\Delta (F/F_0)/\Delta T$  for both contraction and recovery cycles were almost identical and maintained at a steady ratio around 0.0045 / °C from -40 °C up to 15 °C. Both cycles presented a highest compression force change ratio over the temperature region between 15 to 20 °C and then a decrease as temperature continued increasing.



(a)

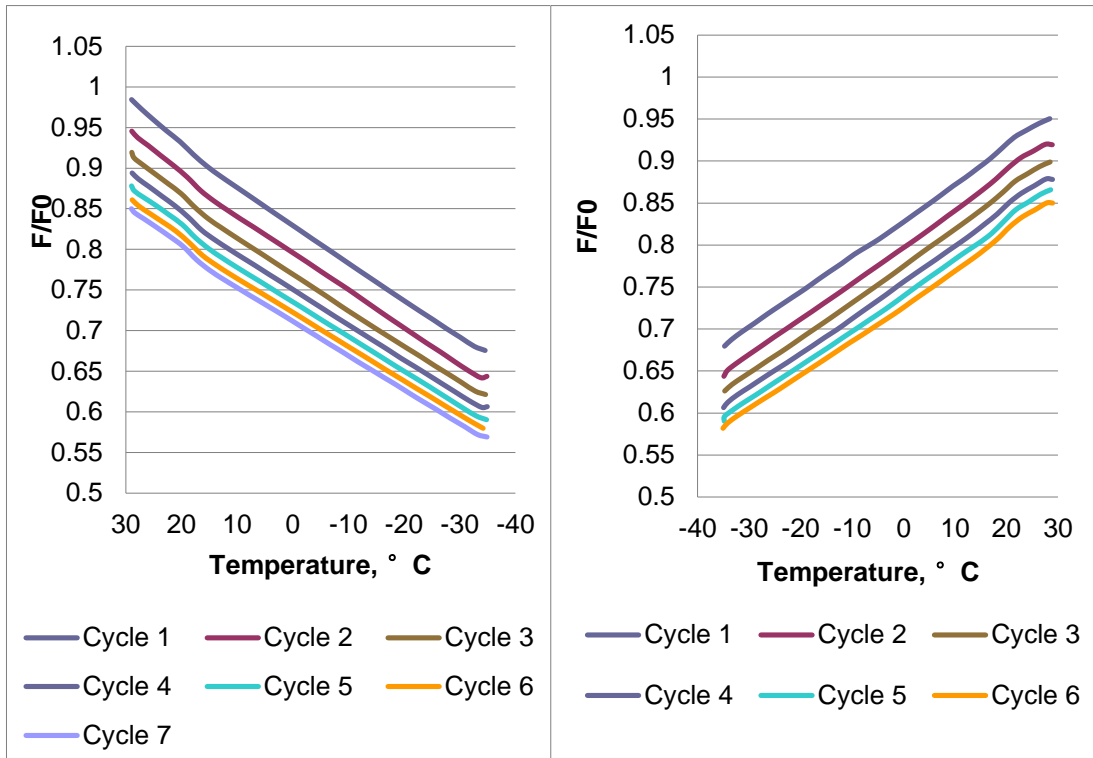
(b)



(c)

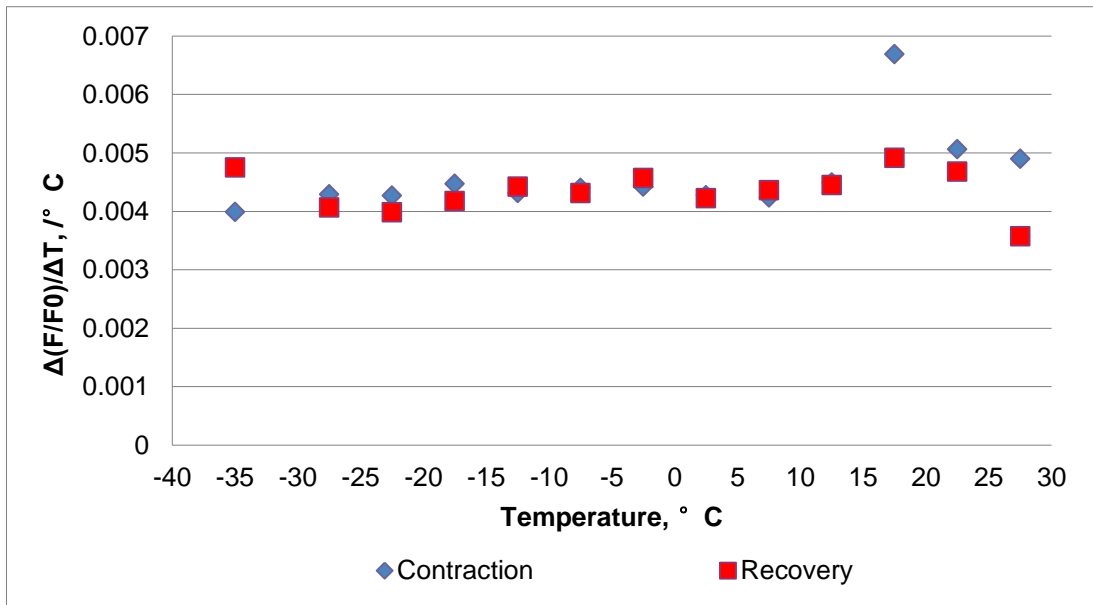
**Figure 106** Data analysis for the 24h-cycling test in groove in Jet A-1 (aged nitrile O-ring).

(a) compression force vs. temperatures, contraction cycles; (b) compression force vs. temperatures, recovery cycles; (c)  $\Delta(F/F_0)/\Delta T$  vs. temperatures.



(a)

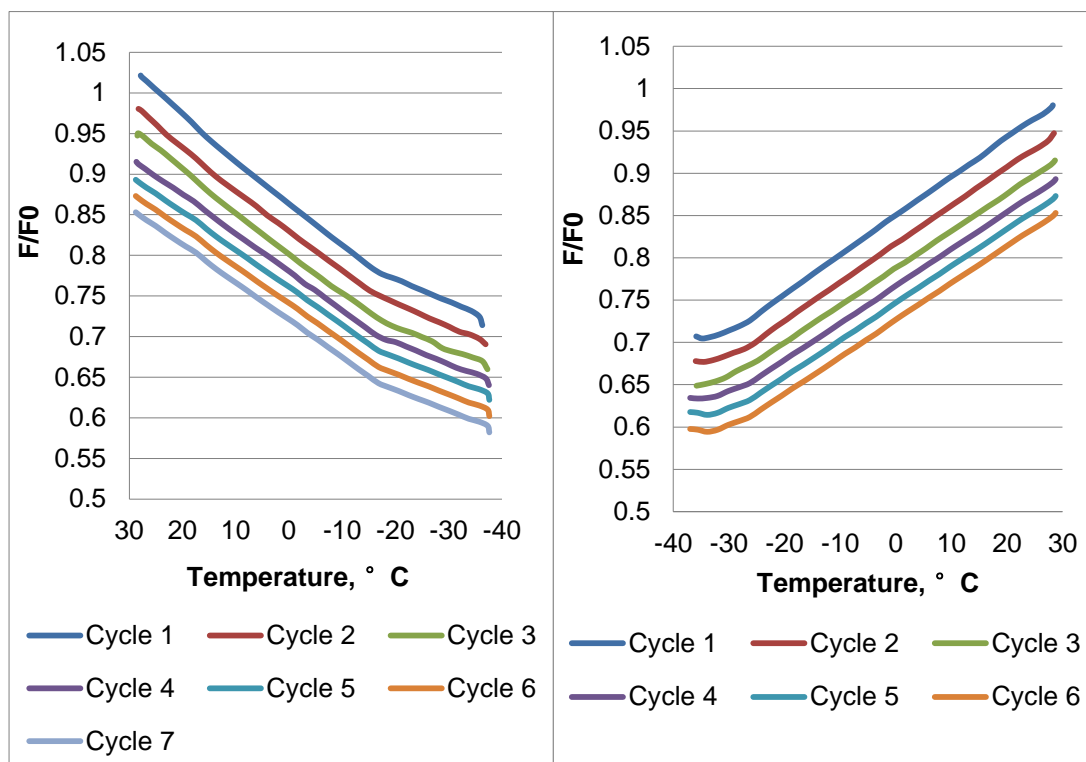
(b)



(c)

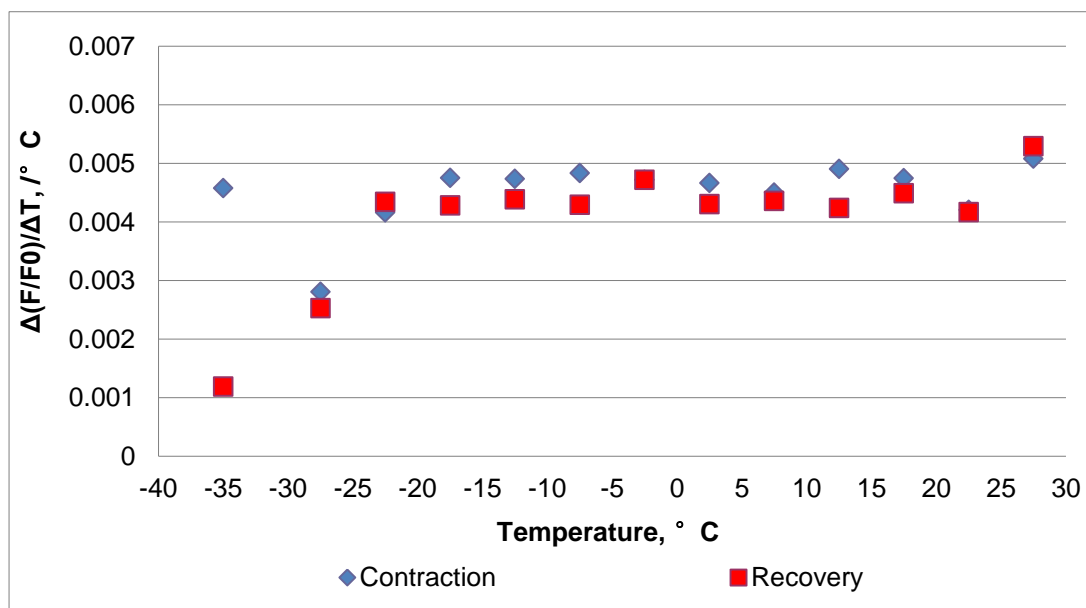
**Figure 107** Data analysis for the 24h-cycling test in groove in 8% aromatic fuel blend (aged nitrile O-ring).

(a) compression force vs. temperatures, contraction cycles; (b) compression force vs. temperatures, recovery cycles; (c)  $\Delta(F/F0)/\Delta T$  vs. temperatures.



(a)

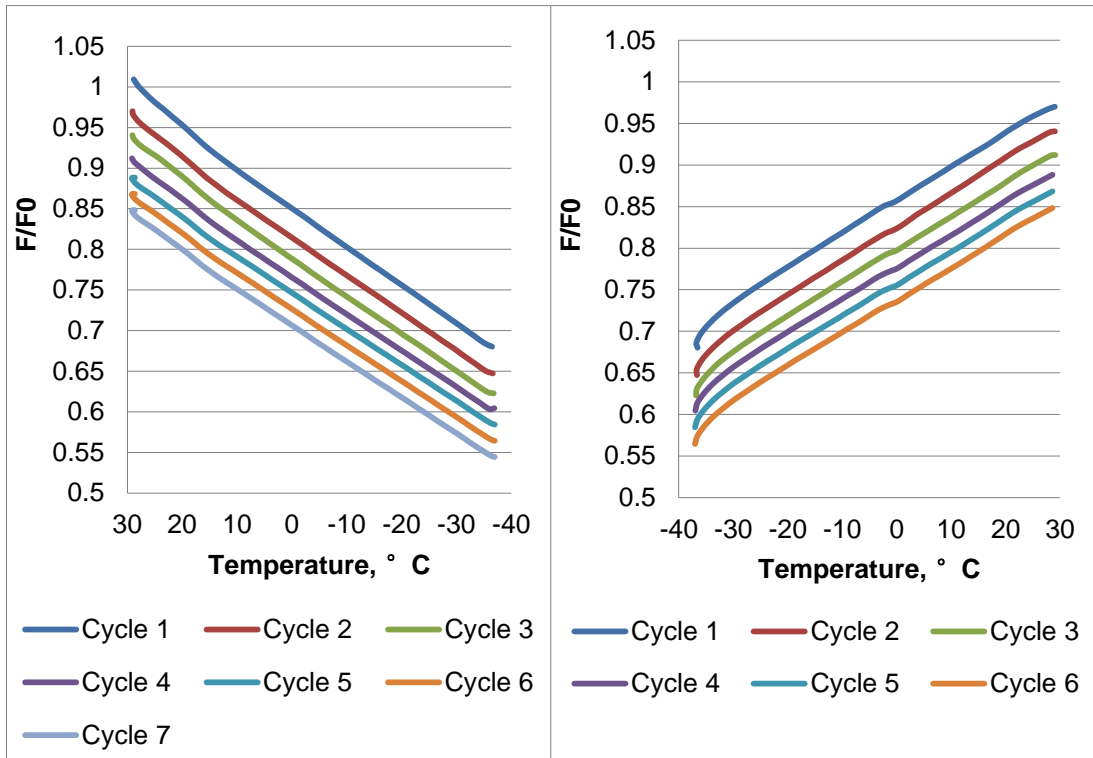
(b)



(c)

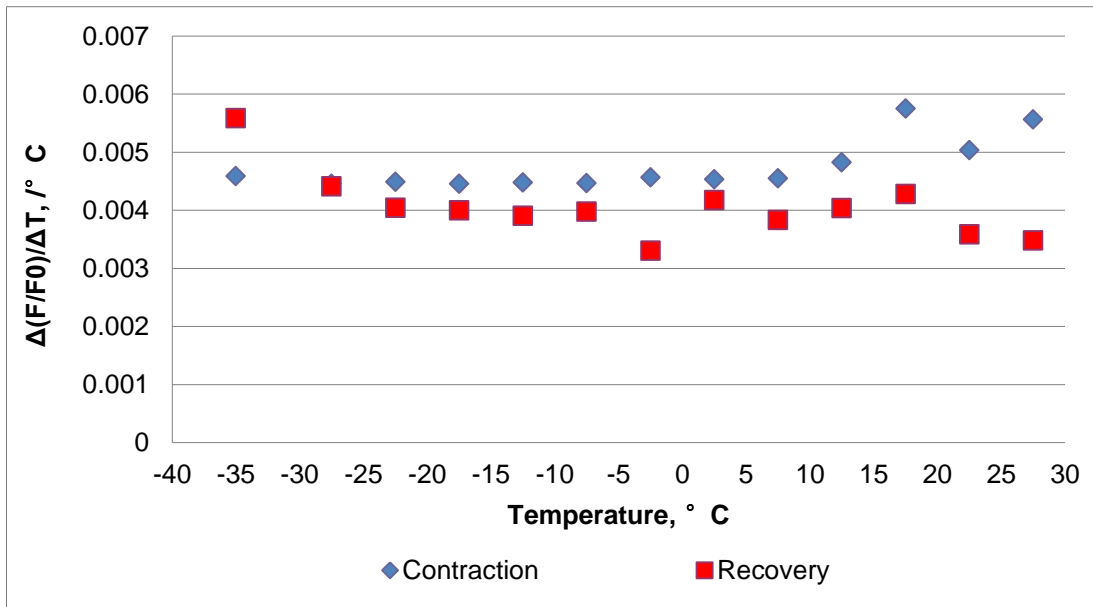
**Figure 108** Data analysis for the 24h-cycling test in groove in 4% aromatic fuel blend (aged nitrile O-ring).

(a) compression force vs. temperatures, contraction cycles; (b) compression force vs. temperatures, recovery cycles; (c)  $\Delta(F/F_0)/\Delta T$  vs. temperatures.



(a)

(b)



(c)

**Figure 109** Data analysis for the 24h-cycling test in groove in SPK (aged nitrile O-ring).

(a) compression force vs. temperatures, contraction cycles; (b) compression force vs. temperatures, recovery cycles; (c)  $\Delta(F/F_0)/\Delta T$  vs. temperatures.

Behaviour of preconditioned nitrile seals in 8% aromatic fuel blend was very similar to that in Jet A-1 (as shown in Fig. 107 (c)). Values of  $\Delta (F/F_0)/\Delta T$  for both contraction and recovery cycles were also maintained at a steady ratio around 0.0045 /°C from -40 °C up to 15 °C. Differences were spotted only at low and high temperature ends compared with Jet A-1, with a higher (lower) recovery (contraction) ratio at temperatures below -30 °C and a lower (higher) contraction (recovery) ratio at temperatures above 15 °C.

In 4% aromatic fuel blend (as shown in Fig. 108 (c)), preconditioned nitrile seals demonstrated a different behaviour at temperatures below -25 °C, as the recovery ratio was much lower than in higher aromatic content fuels. While at high temperature end, from 25 to 30 °C, recovery ratio accelerated rather than slowed down as in previous two fuels. It is difficult to say if this was caused by the different aromatic content at this stage as this behaviour was not observed in SPK.

In SPK (Fig. 109 (c)), the recovery ratio reached the highest at temperatures below -30 °C and maintained at a steady but lower level than contraction ratio. At temperatures above 25 °C, the recovery ratio reduced below average level.

To evaluate O-ring's ability to recover from thermal contraction, the average values of recovery ratio and contraction ratio throughout the whole temperature range were calculated and then the former was divided by the latter.

$$\text{Recovery Ability} = \frac{\text{Average recovery ratio over whole temperature range}}{\text{Average contraction ratio over whole temperature range}} \quad (7.5)$$

Figure 110 showed the relation between O-ring's recovery ability with aromatic content in the fuel. A linear relationship was found as preconditioned nitrile seal's ability to recover from thermal contraction depends on the aromatic content in the fuel; the higher concentration of aromatics, the better O-ring recovers from contraction.

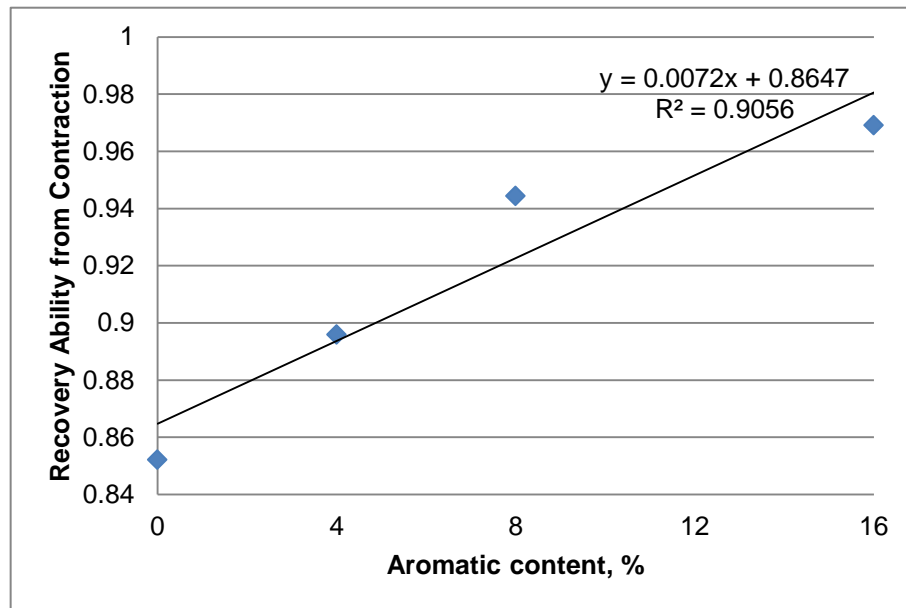
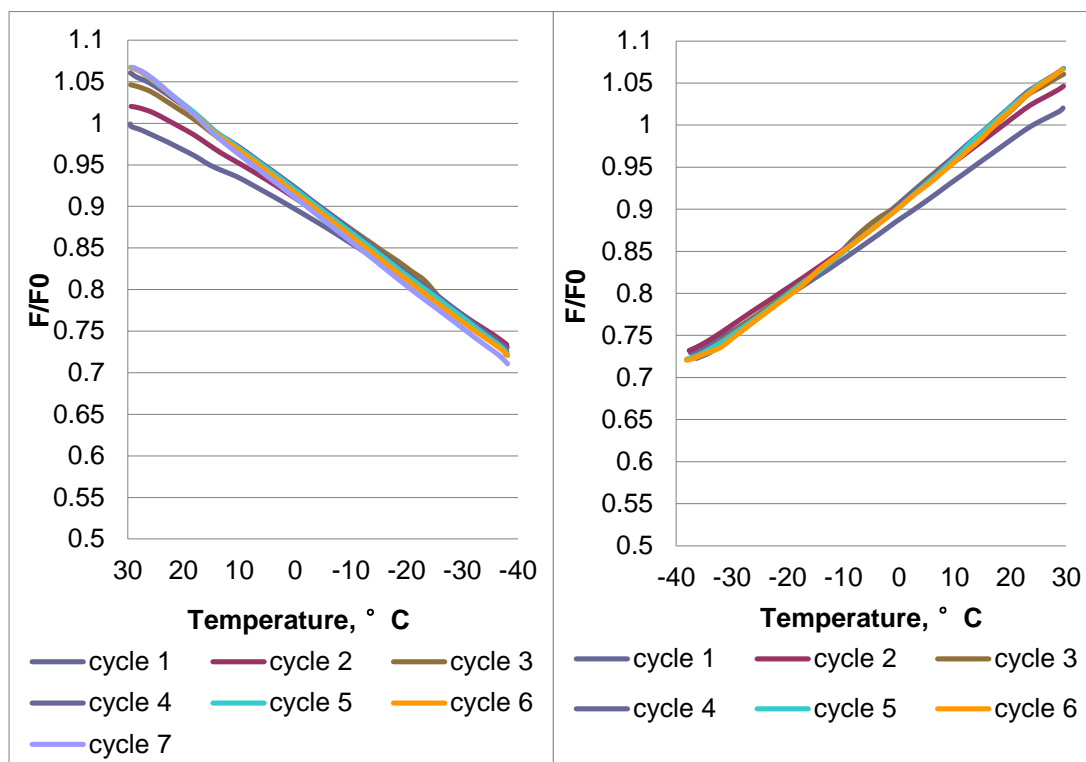


**Figure 110** Overall recovery ability of aged nitrile O-rings in fuels with various aromatic contents during the 24h-cycle testing.

To summarise, temperature impact on preconditioned nitrile O-rings seem to be more influential at low and high temperature ends of the cycling test. Generally, a relatively slow recovery ratio at higher temperatures (above 25 °C, with the exception of 4% aromatic fuel blend) was observed but the recovery ratio at low temperature end (below -30 °C) was difficult to predict. Averagely, preconditioned nitrile O-rings' ability to recover from thermal contraction was found to be linearly dependent on the aromatic content in the fuel.

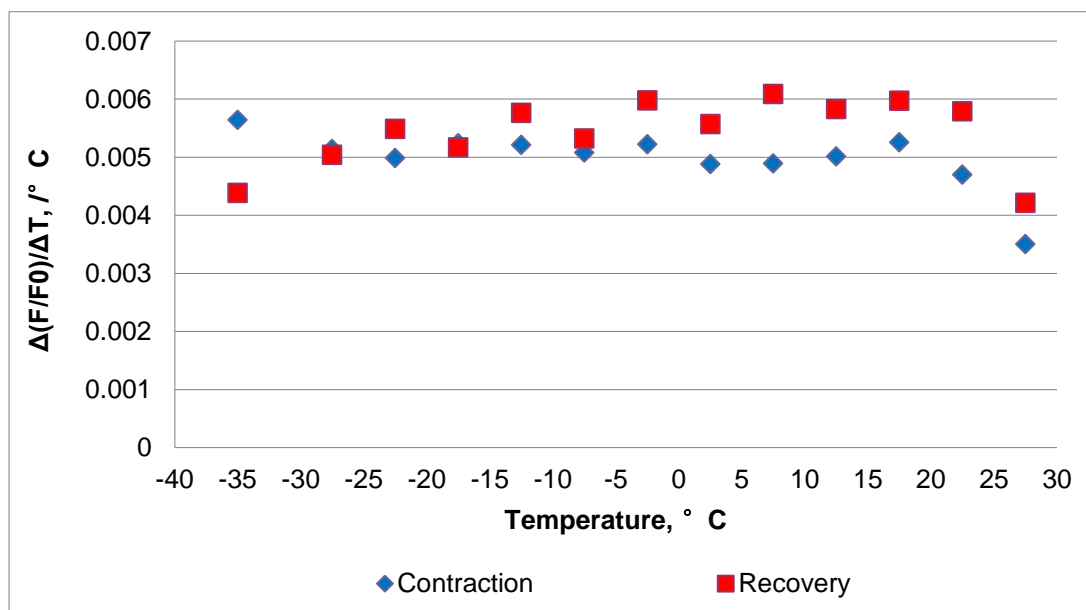
#### 7.2.1.2 Without O-ring grooves

Data from 24h-cycle tests without grooves presented different trends as fresh seals swelled especially in Jet A-1 (Fig. 111-112). Due to seal swelling, the recovery ratio was even higher than contraction ratio in Jet A-1. This observation further proved the need for preconditioning the seals to eliminate the influence of swelling during the temperature cycling test so the impact of temperature could be learned.



(a)

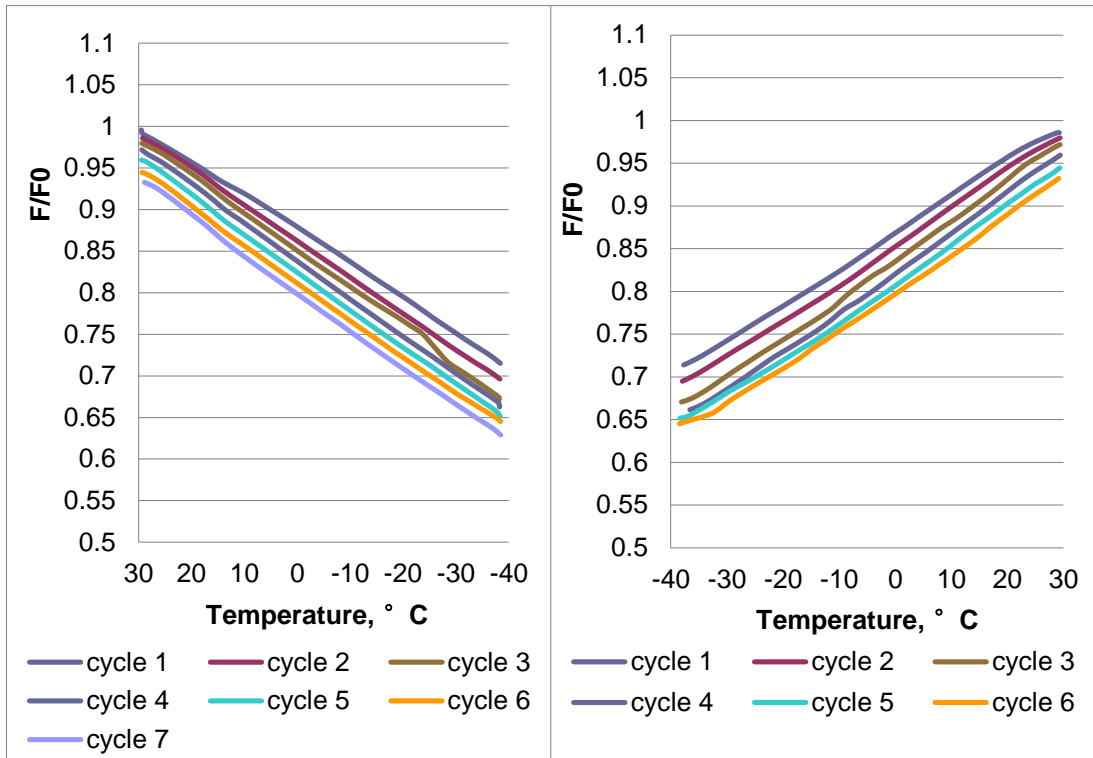
(b)



(c)

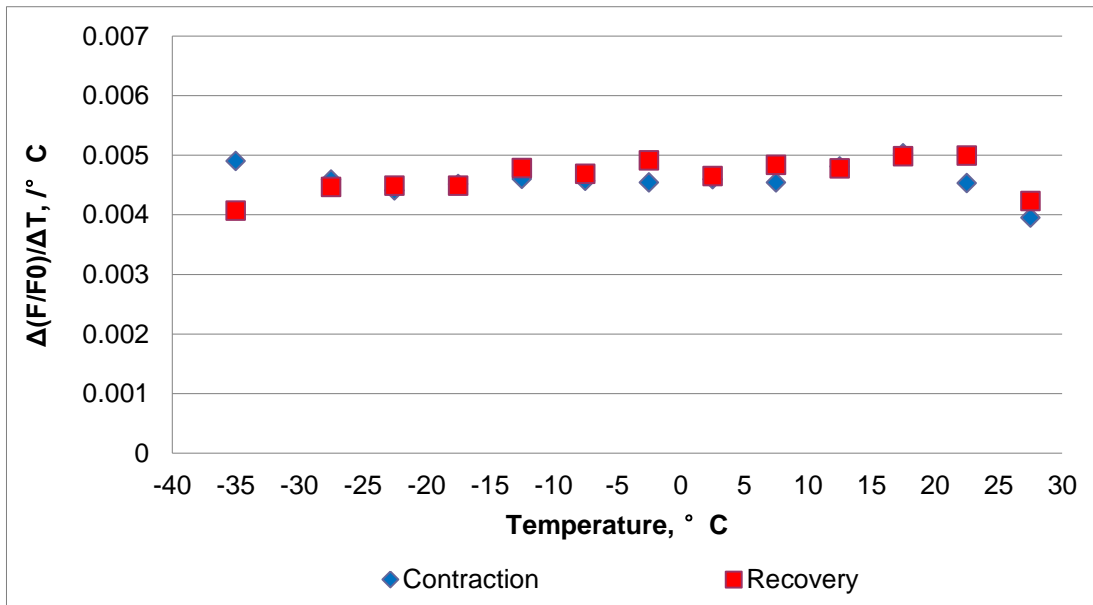
**Figure 111** Data analysis for the 24h-cycling test with no groove in Jet A-1 (fresh nitrile O-ring).

(a) compression force vs. temperatures, contraction cycles; (b) compression force vs. temperatures, recovery cycles; (c)  $\Delta(F/F0)/\Delta T$  vs. temperatures.



(a)

(b)



(c)

**Figure 112** Data analysis for the 24h-cycling test with no groove in SPK fuel (fresh nitrile O-ring).

(a) compression force vs. temperatures, contraction cycles; (b) compression force vs. temperatures, recovery cycles; (c)  $\Delta(F/F0)/\Delta T$  vs. temperatures.

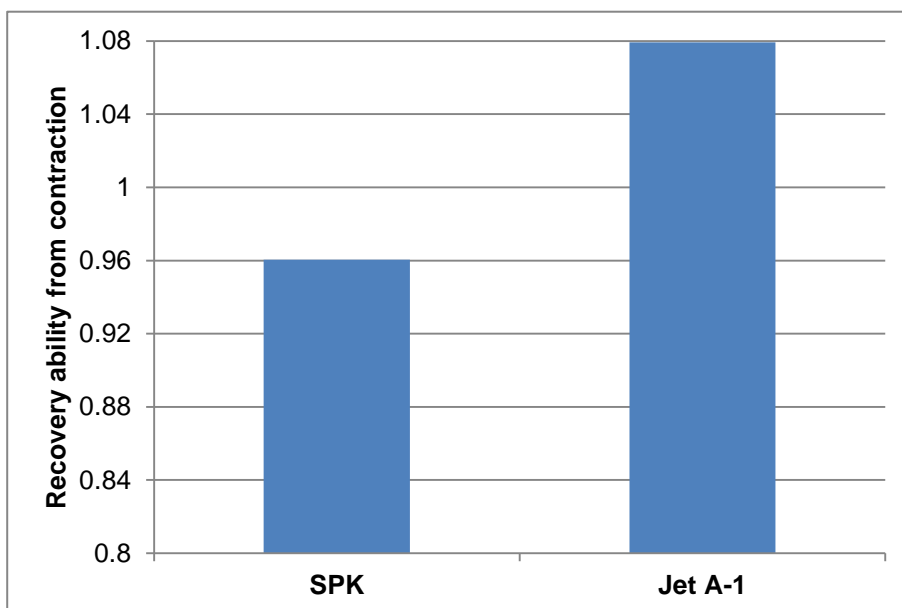


**Figure 113** Average recovery ability of fresh nitrile O-rings in Jet A-1 and SPK during the 24h-cycle testing without grooves.

The recovery ratio in both Jet A-1 and SPK increased as the temperature rise until 25 °C, after which a reduced ratio was observed. Figure 113 demonstrated that fresh nitrile seals' ability to recover from thermal contraction is better in Jet A-1 than SPK fuel. It is interesting to notice that the difference in recovery ability in Jet A-1 and SPK remains at a steady value (0.12 for both fresh and aged nitrile O-rings), despite of the impact by O-ring preconditioning and the groove. This may indicate that nitrile seals' ability to recover from thermal contraction is only dependent on the aromatic content in the fuel rather than removable polymer additives (plasticizers, etc.) and external pressure.

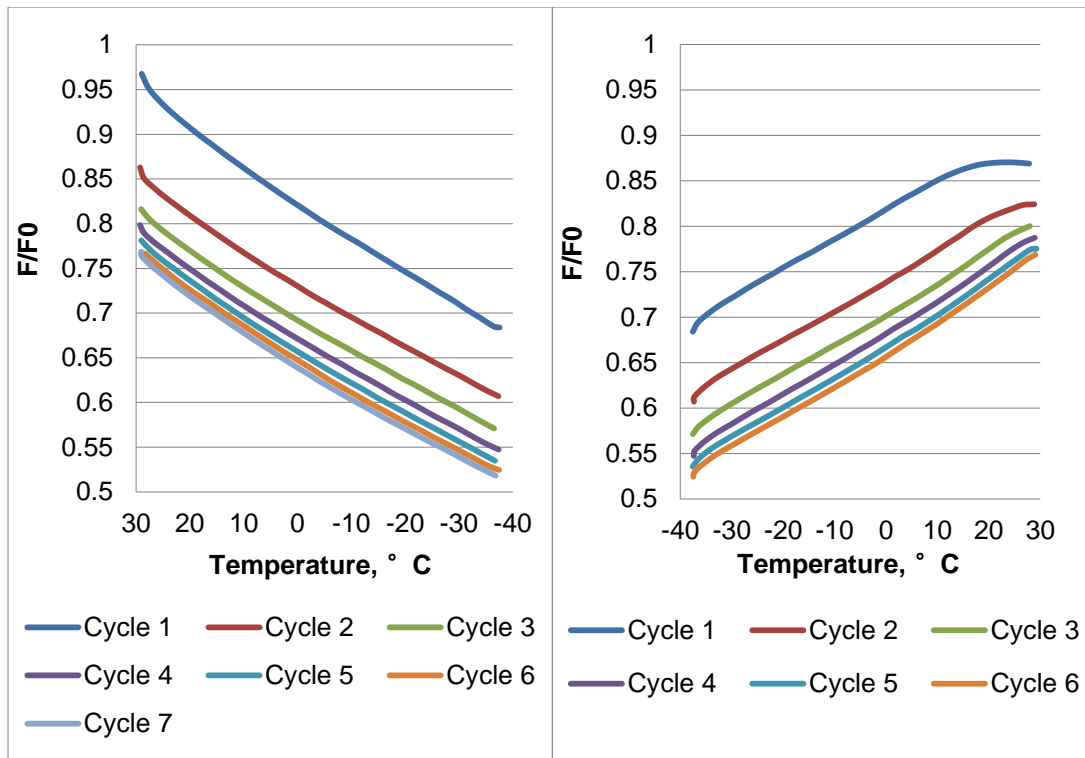
## 7.2.2 Fluorosilicone O-rings

### 7.2.2.1 *In O-ring grooves*

Figure 114-117 presented the analysis for fluorosilicone O-rings tested in grooves in Jet A-1 (16% aromatics), 75% Jet A-1 + 25% SPK (8% aromatics), 50% Jet A-1 + 50% SPK (4% aromatics) and SPK (0% aromatics), respectively. Generally, the overall

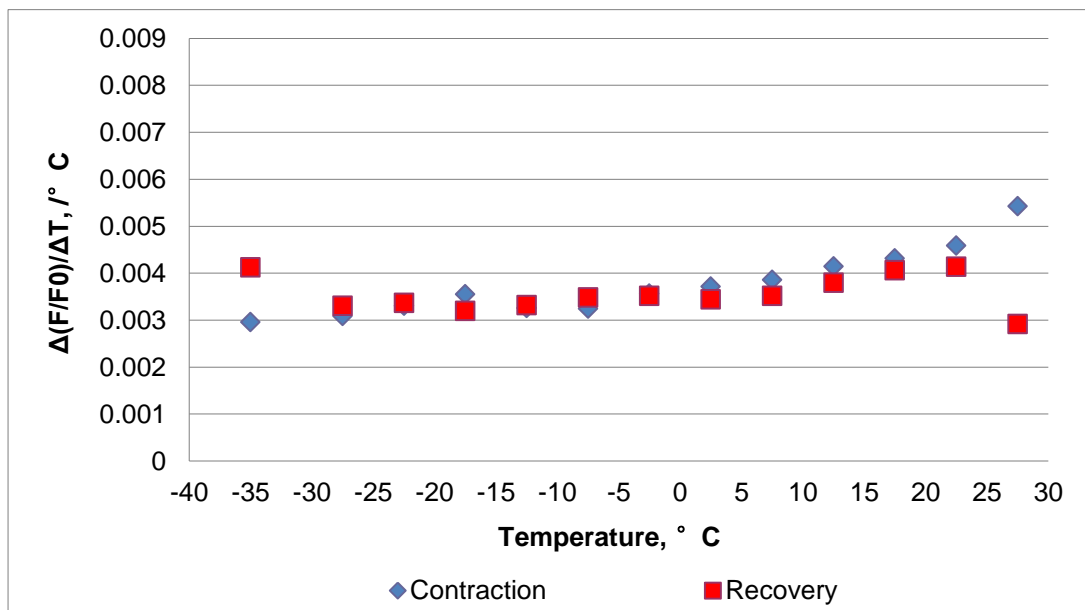
contraction and recovery behaviours of fluorosilicone seals were similar in all four fuels. As temperature dropped, the contraction ratio of this material in all fuels decreased gradually. When temperature rise, the recovery ratio increased slightly with the exception at both low and high temperature ends; the highest recovery ratio was observed at temperatures below  $-30\text{ }^{\circ}\text{C}$  whilst the lowest was at temperatures above  $25\text{ }^{\circ}\text{C}$ . This may indicate that fluorosilicone material's ability to recovery from thermal contraction is better at very low temperatures (below  $-30\text{ }^{\circ}\text{C}$ ) but worse when temperature reaches above  $25\text{ }^{\circ}\text{C}$ . Relatively high temperatures may cause this material to relax more than low temperatures, which lead to a higher contraction ratio and lower recovery ratio.

When calculating the average recovery ability from contraction, as shown in Figure 118, it appears the aromatic content in the fuel has no obvious impact on fluorosilicone O-ring. The recovery ratio in all four fuels stayed at a similar level (around 0.94) which proved there is no direct relationship between the recovery ability of fluorosilicone material and aromatic concentration in fuels.



(a)

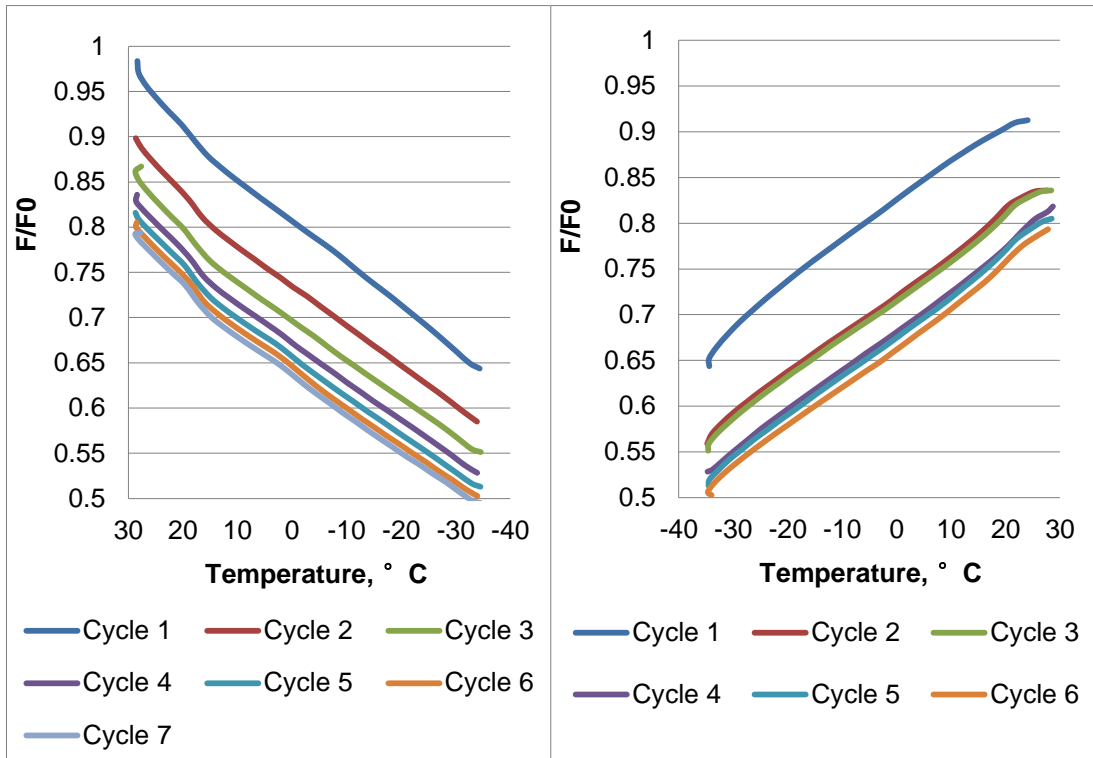
(b)



(c)

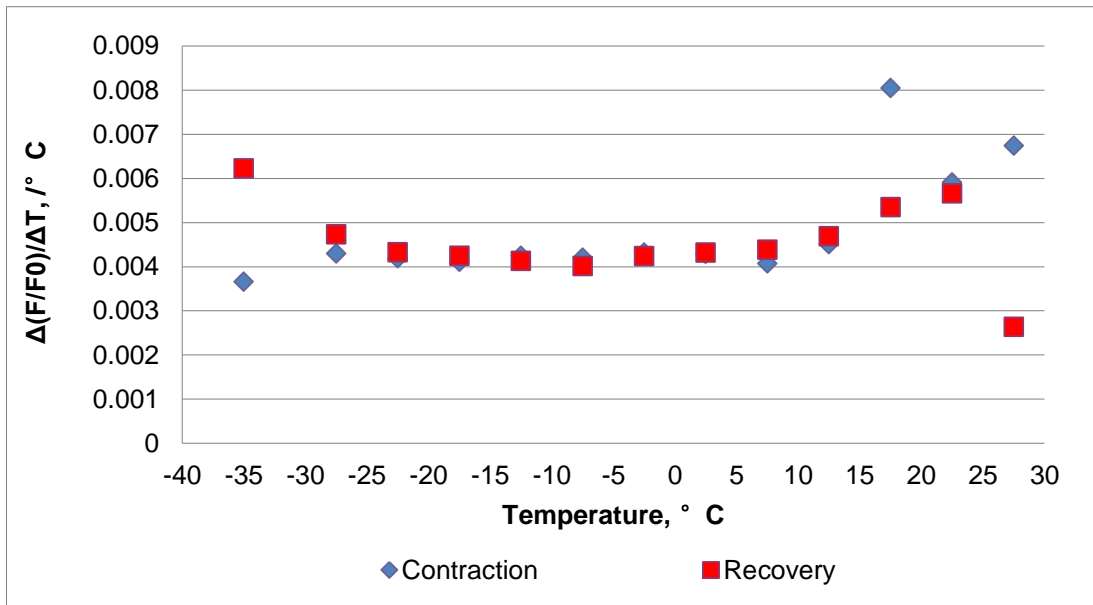
**Figure 114** Data analysis for the 24h-cycling test in groove in Jet A-1 (fluorosilicone O-ring).

(a) compression force vs. temperatures, contraction cycles; (b) compression force vs. temperatures, recovery cycles; (c)  $\Delta(F/F_0)/\Delta T$  vs. temperatures.



(a)

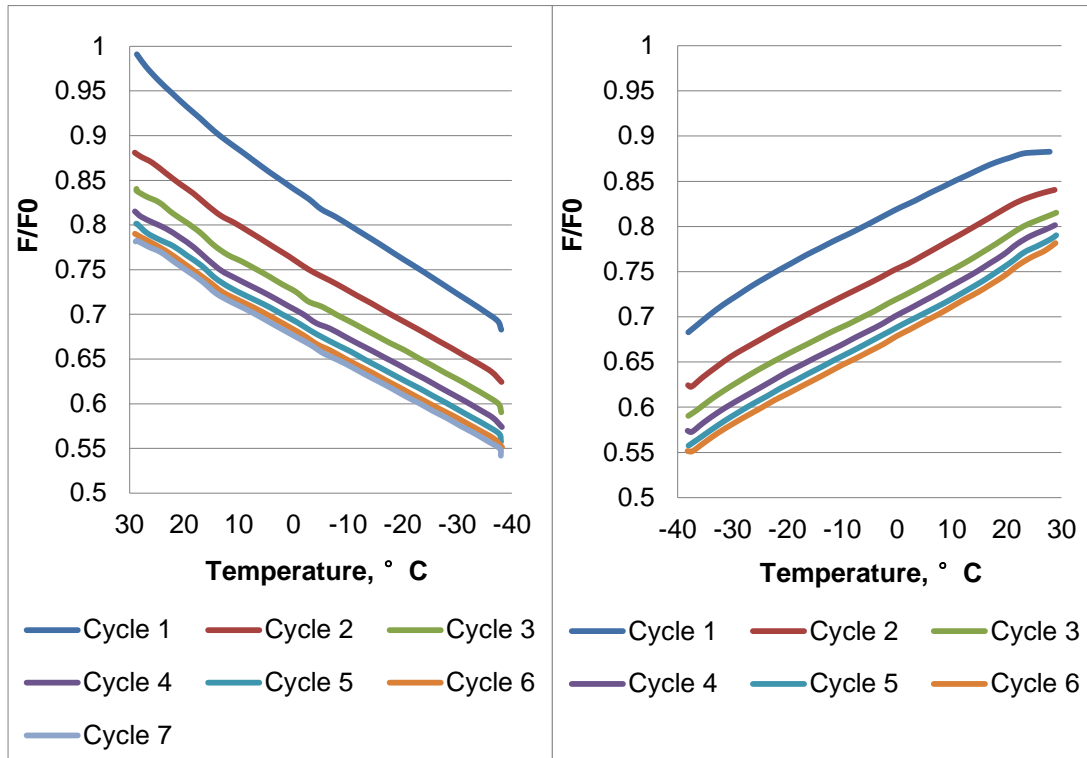
(b)



(c)

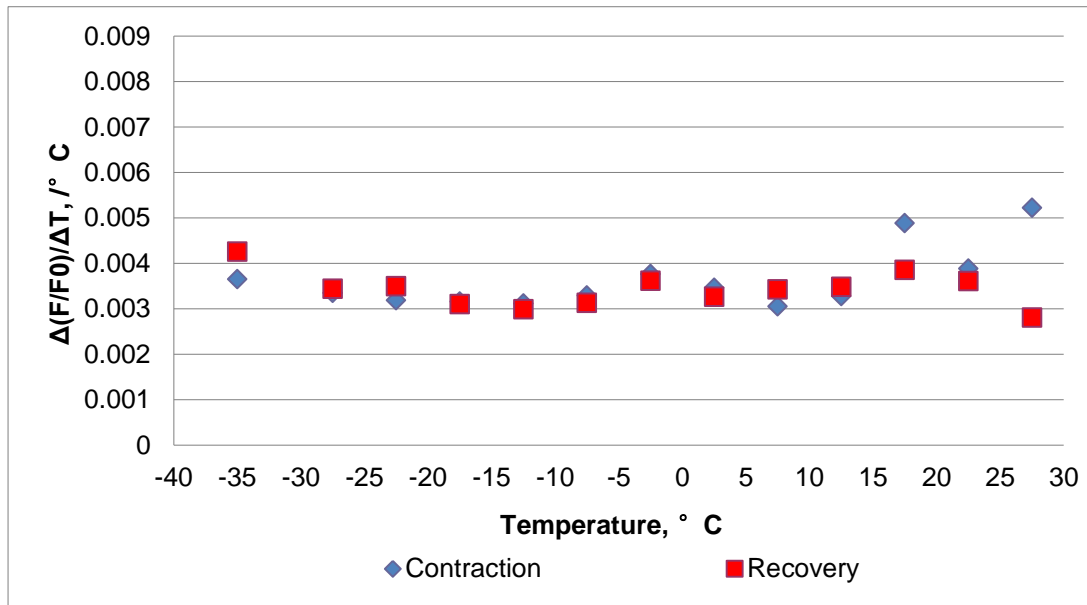
**Figure 115** Data analysis for the 24h-cycling test in groove in 8% aromatic fuel blend (fluorosilicone O-ring).

(a) compression force vs. temperatures, contraction cycles; (b) compression force vs. temperatures, recovery cycles; (c)  $\Delta(F/F_0)/\Delta T$  vs. temperatures.



(a)

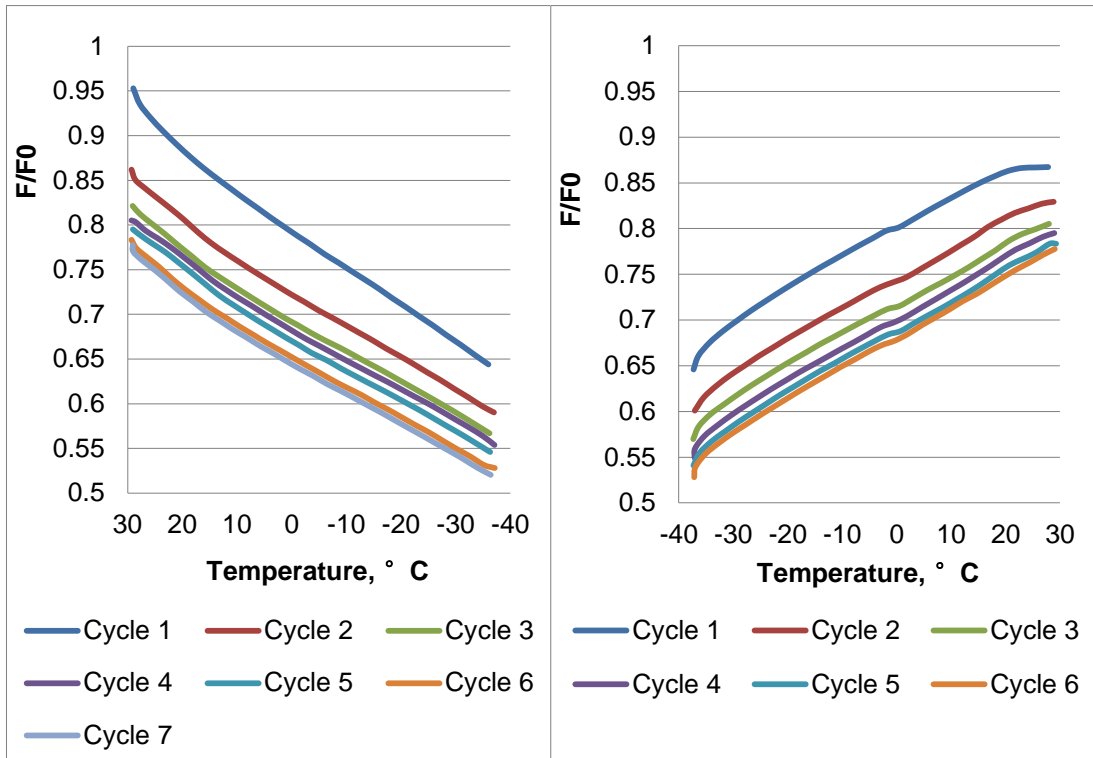
(b)



(c)

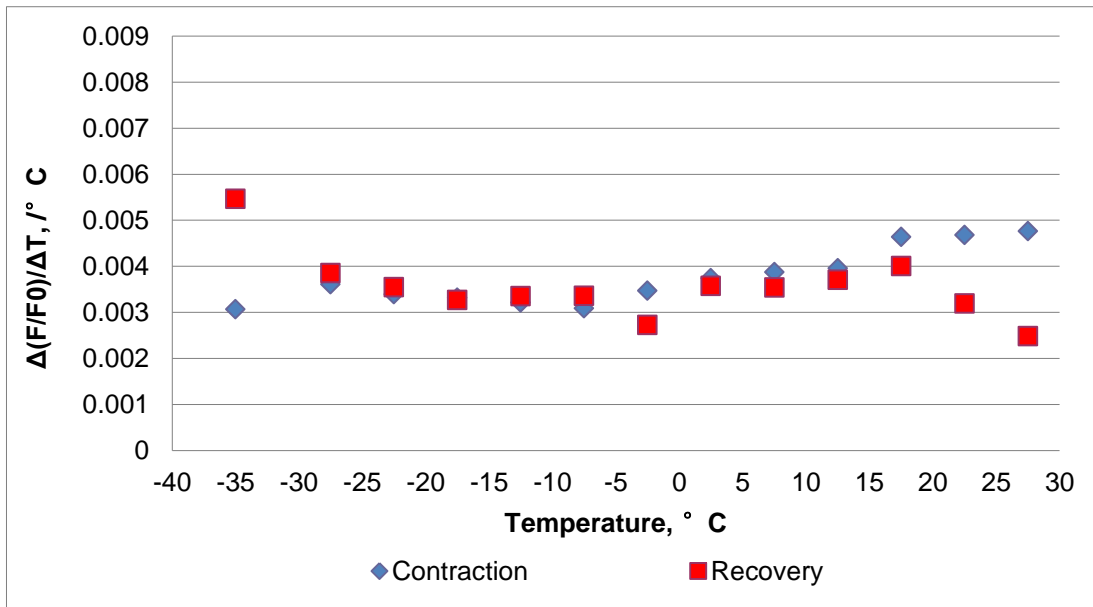
**Figure 116** Data analysis for the 24h-cycling test in groove in 4% aromatic fuel blend (fluorosilicone O-ring).

(a) compression force vs. temperatures, contraction cycles; (b) compression force vs. temperatures, recovery cycles; (c)  $\Delta(F/F_0)/\Delta T$  vs. temperatures.



(a)

(b)



(c)

**Figure 117** Data analysis for the 24h-cycling test in groove in SPK (fluorosilicone O-ring).

(a) compression force vs. temperatures, contraction cycles; (b) compression force vs. temperatures, recovery cycles; (c)  $\Delta(F/F_0)/\Delta T$  vs. temperatures.

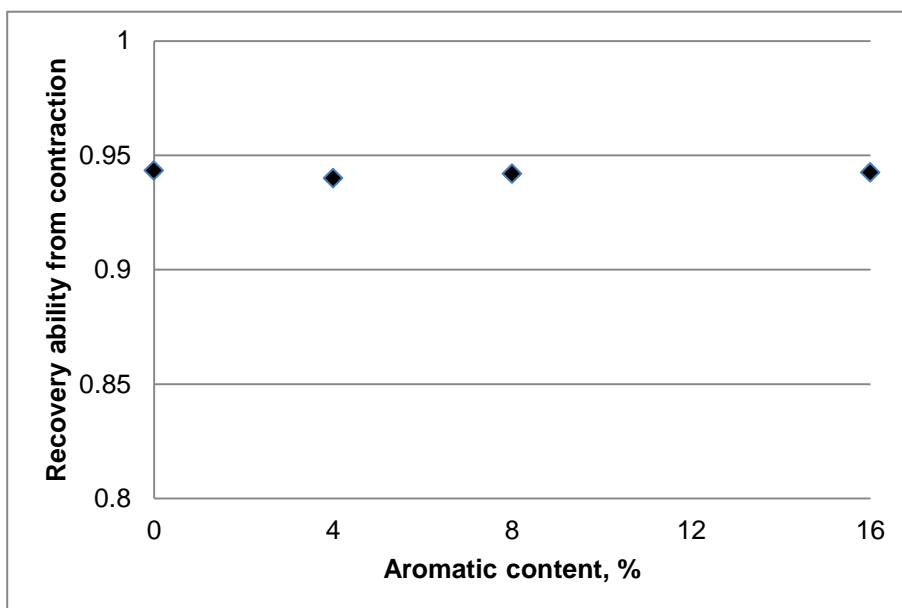
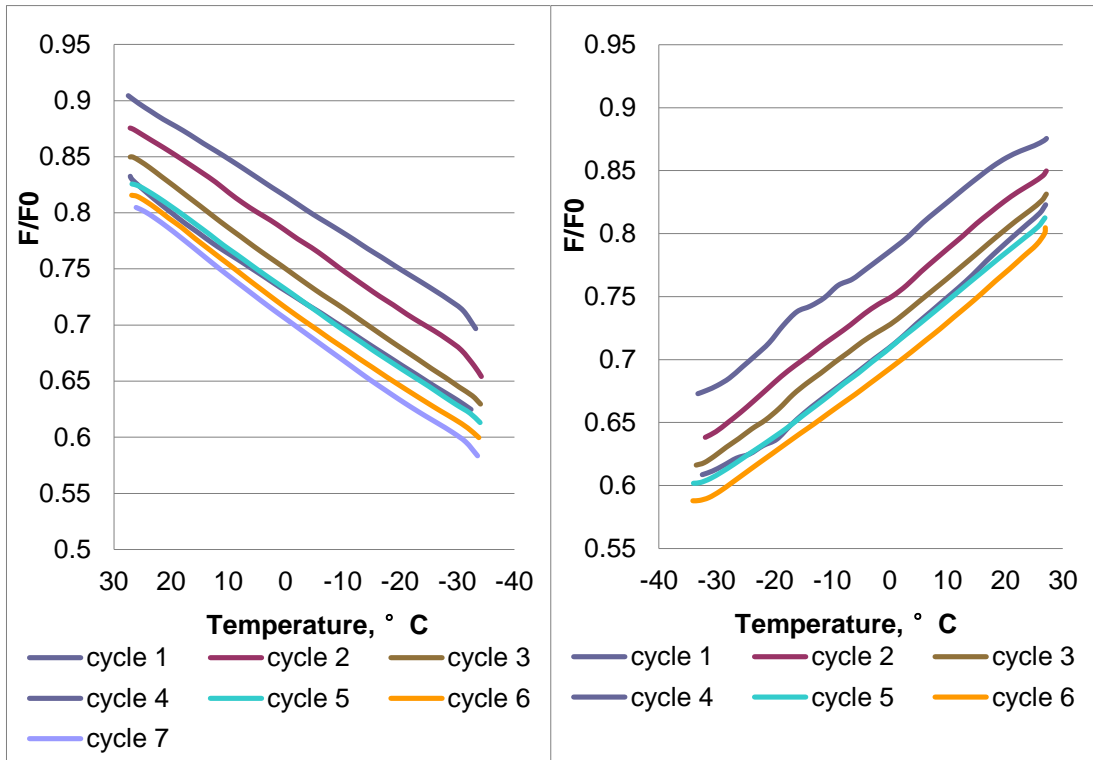


**Figure 118** Overall recovery ability of fluorosilicone O-rings in fuels with various aromatic contents during the 24h-cycle testing.

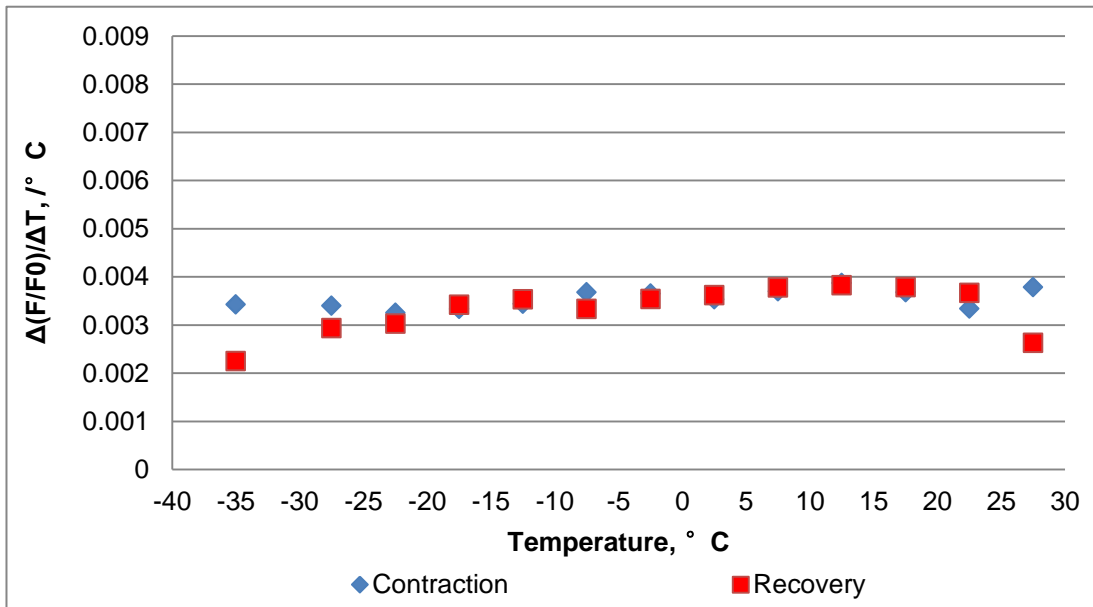
#### 7.2.2.2 Without O-ring grooves

Data from 24h-cycle tests without O-ring grooves demonstrated relatively steady contraction ratio in both Jet A-1 and SPK (Fig. 119-120). During the heating cycles, recovery ratio presented a slightly increase with temperature until it reached 25 °C. At temperatures above 25 °C, recovery ratio was reduced, which the same behaviour was observed during the tests in grooves. Different behaviour was spotted at temperatures below -30 °C; fluorosilicone O-ring presented a higher recovery ratio when tested in grooves but a lower one when tested without grooves. This may indicate the presence of O-ring grooves helps to overcome the hysteresis of this rubber material from thermal contraction. Comparison between the recovery ability in Jet A-1 and SPK indicated no obvious difference was observed between these two fuels (Fig. 121).



(a)

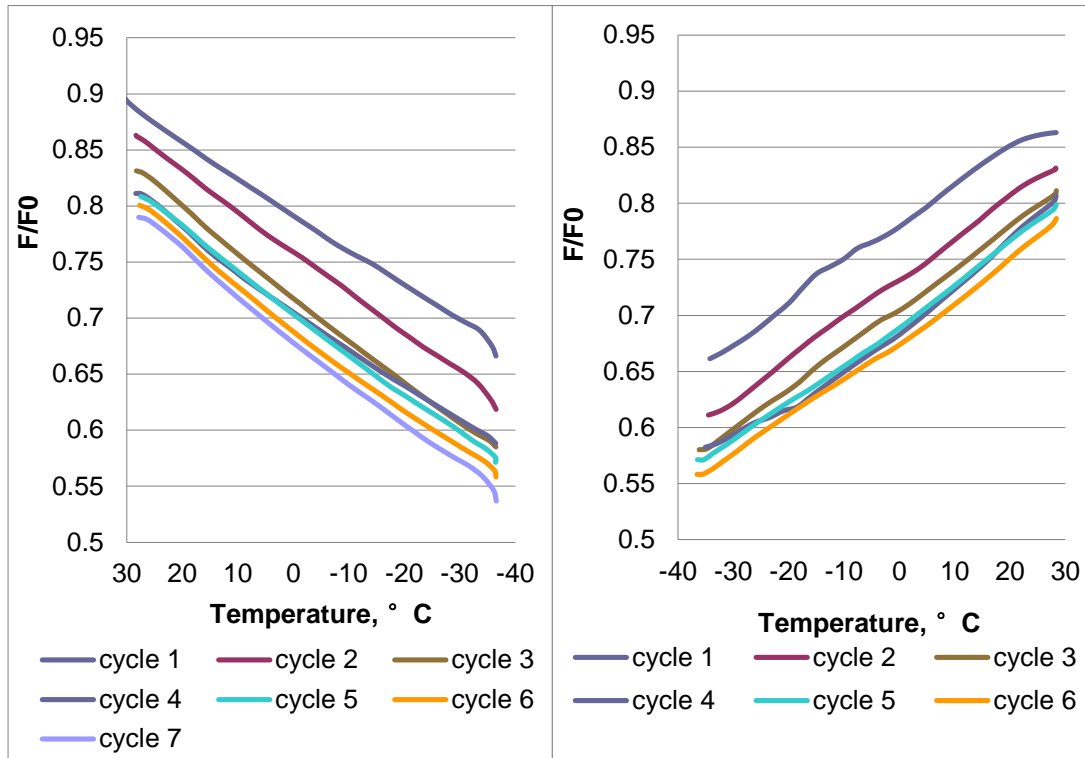
(b)



(c)

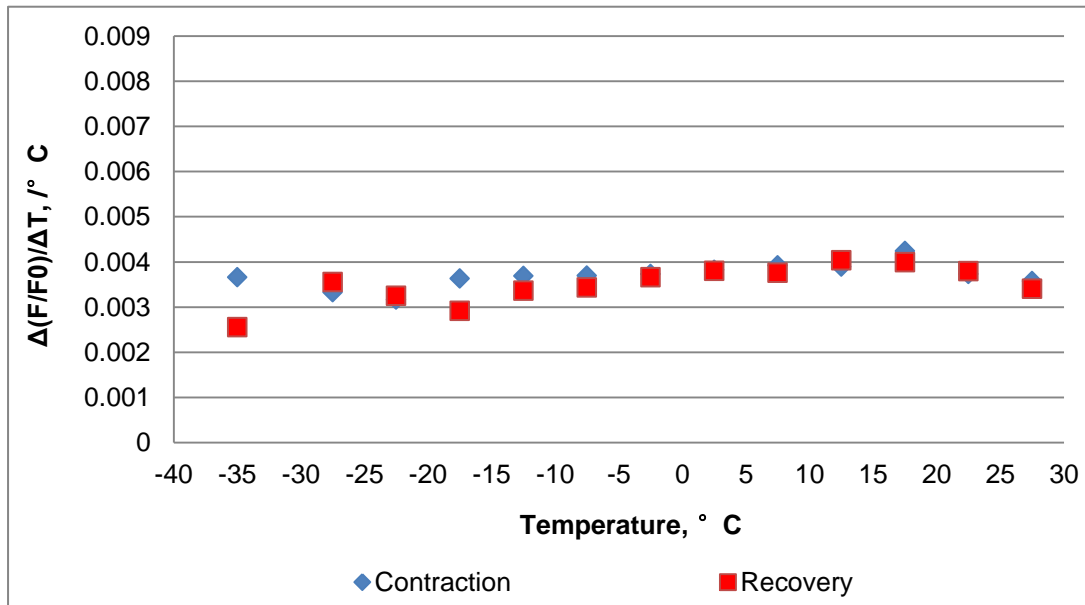
**Figure 119** Data analysis for the 24h-cycling test without groove in Jet A-1 (fluorosilicone O-ring).

(a) compression force vs. temperatures, contraction cycles; (b) compression force vs. temperatures, recovery cycles; (c)  $\Delta(F/F_0)/\Delta T$  vs. temperatures.



(a)

(b)



(c)

**Figure 120** Data analysis for the 24h-cycling test without groove in GtL fuel (fluorosilicone O-ring).

(a) compression force vs. temperatures, contraction cycles; (b) compression force vs. temperatures, recovery cycles; (c)  $\Delta(F/F_0)/\Delta T$  vs. temperatures.

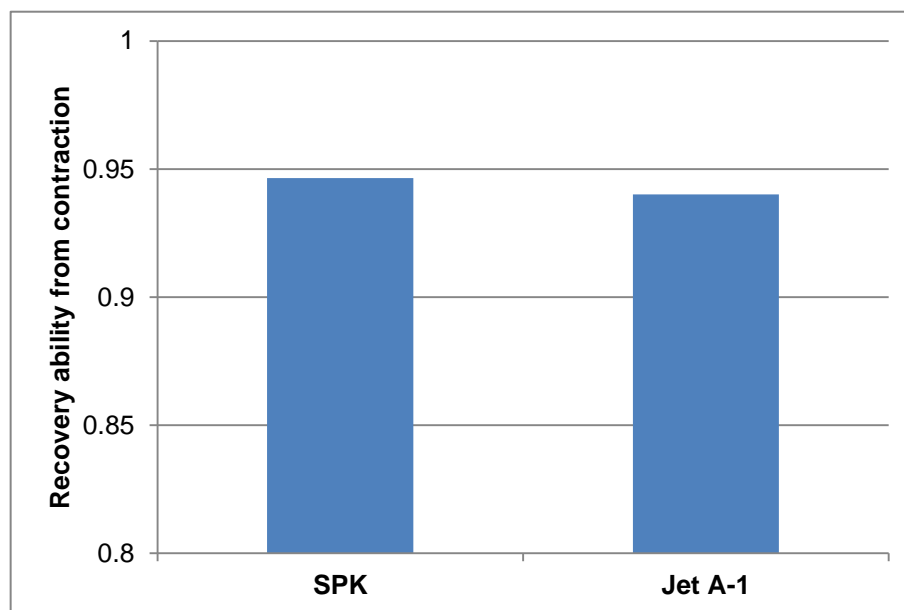


**Figure 121** Average recovery ability of fluorosilicone O-rings in Jet A-1 and SPK during the 24h-cycle testing without grooves.

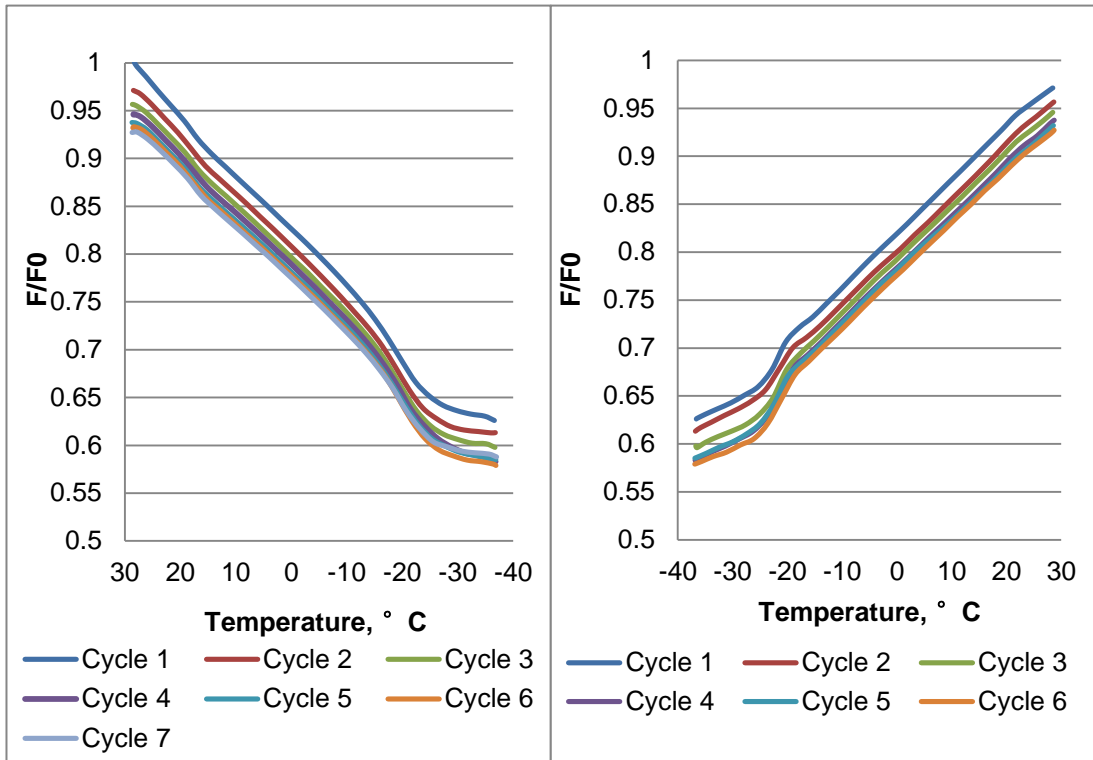
### 7.2.3 Fluorocarbon O-rings

#### 7.2.3.1 *In O-ring grooves*

A unique phenomenon observed from the 24h cycling test for fluorocarbon O-ring only was the ‘irregular’ shape at low temperatures, approximately around and below -20 °C. This is related to the glass transition of polymer as discussed in section 4.4.1.3. Figure 122-125 presented the analysis for fluorocarbon O-rings tested in grooves in Jet A-1 (16% aromatics), 75% Jet A-1 + 25% SPK (8% aromatics), 50% Jet A-1 + 50% SPK (4% aromatics) and SPK (0% aromatics), respectively. The contraction behaviour of fluorocarbon O-ring in all the fuels was very similar. Compression force decreased as temperature dropped until around -15 to -20 °C, where a sudden increase in contraction ratio was spotted. This was due to the increased loss of modulus during the glass transition [109]. Contraction ratio reduced dramatically when temperature dropped below -20 °C as seals became more stiff and plastic-like. Thermal expansion property of fluorocarbon polymer also changes as the temperature is varied through the glass transition. This observation could also be explained by the free-volume theory of glass transition. As the temperature drops

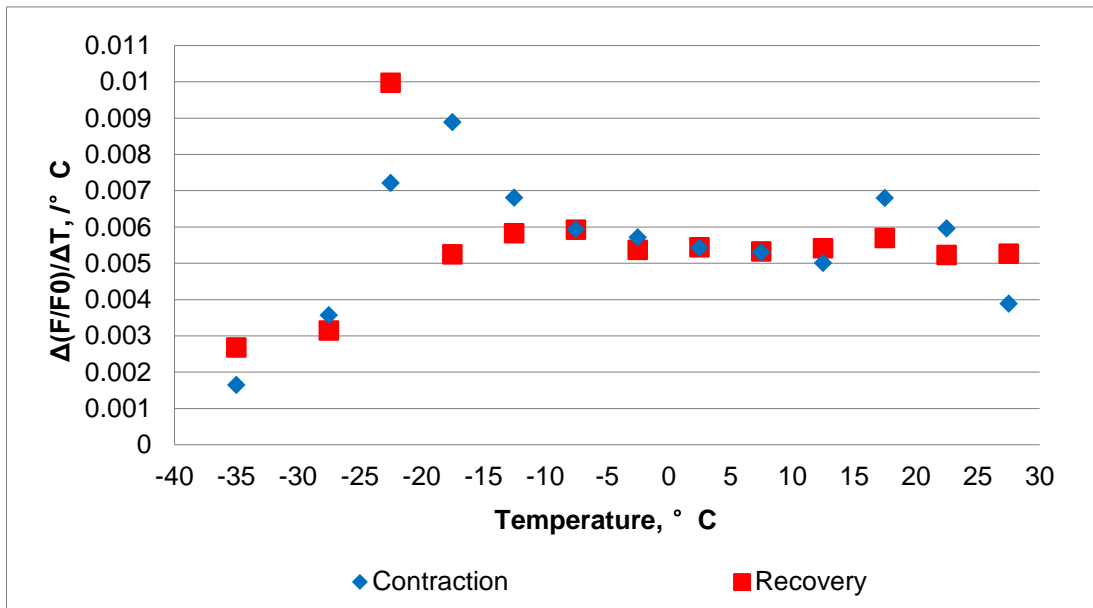
from a temperature well above glass transition temperature ( $T_g$ ), the free volume in the polymer reduces due to rearrangement of molecules, which results in the shrinkage of the total volume. When the temperature approaches  $T_g$ , the molecular motions became so slow that the volume of the material then contracts like that of a solid, with a coefficient of expansion that is generally about half that observed above  $T_g$  [109].

During the heating cycles, the recovery ratio initially increased slowly until temperature heated to around -25 to -20 °C where a sudden increase was observed. When temperature was above the glass transition temperature, recovery ratio stayed at a stable level. This is a reverse process to the cooling cycles, as fluorocarbon polymer recovers from the plastic-like status to the rubbery status. Two phenomena were observed during this recovery process. One was a different behaviour spotted in SPK fuel as the recovery ratio was much higher at temperatures below the glass transition temperature. The lowest recovery ratio appeared at temperatures between -20 to -15 °C. The only factor which may cause this difference is the fuel itself as all the other testing conditions were the same as for other fuels. However, there is no reasonable explanation at this stage. The other phenomenon observed was a shift in glass transition temperature between the cooling and heating cycles. The highest contraction ratios were all observed between -20 to -15 °C during the cooling cycles, while the highest recovery ratios were spotted between -25 to -20 °C during the heating cycles. To compare with the data obtained from 24h-cycle tests without O-ring grooves, it seems this shift was caused by the addition of groove (external pressure) as it did not appeared in those 'no groove' data.



(a)

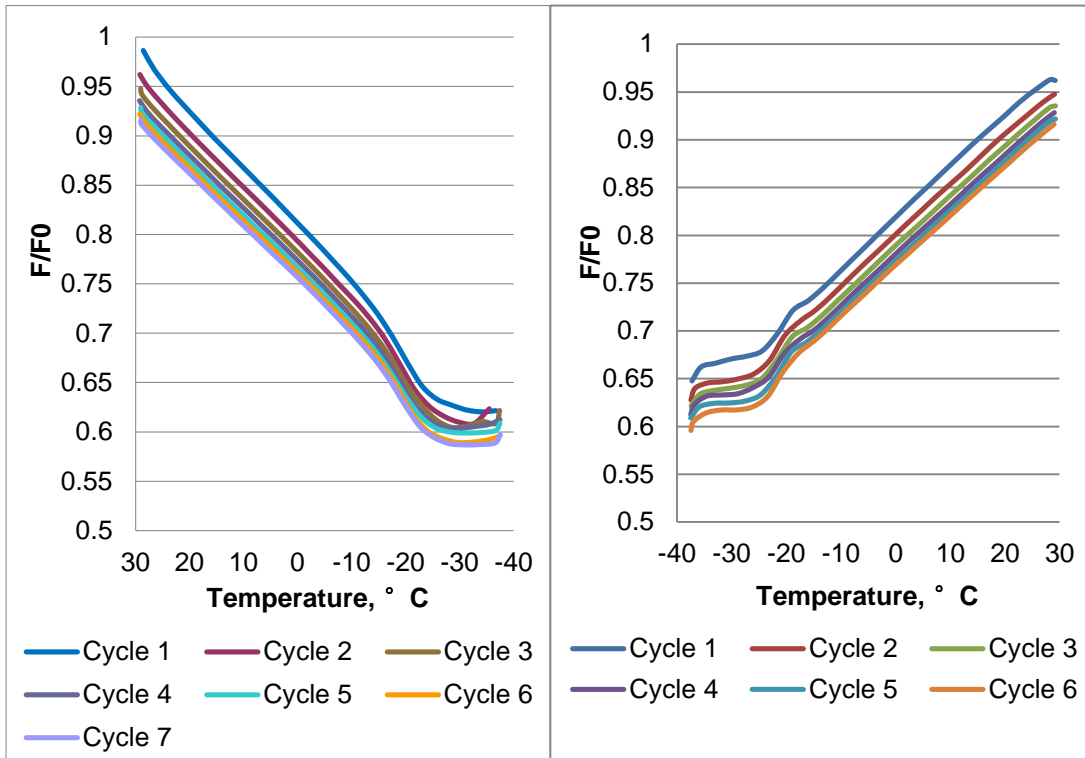
(b)



(c)

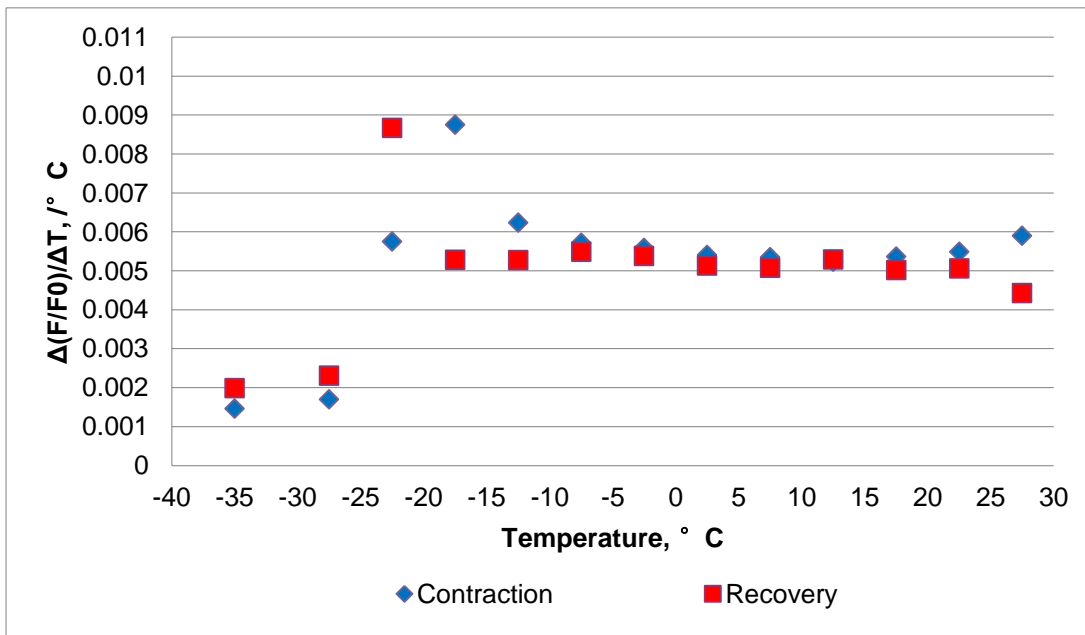
**Figure 122** Data analysis for the 24h-cycling test in groove in Jet A-1 (fluorocarbon O-ring).

(a) compression force vs. temperatures, contraction cycles; (b) compression force vs. temperatures, recovery cycles; (c)  $\Delta(F/F0)/\Delta T$  vs. temperatures.



(a)

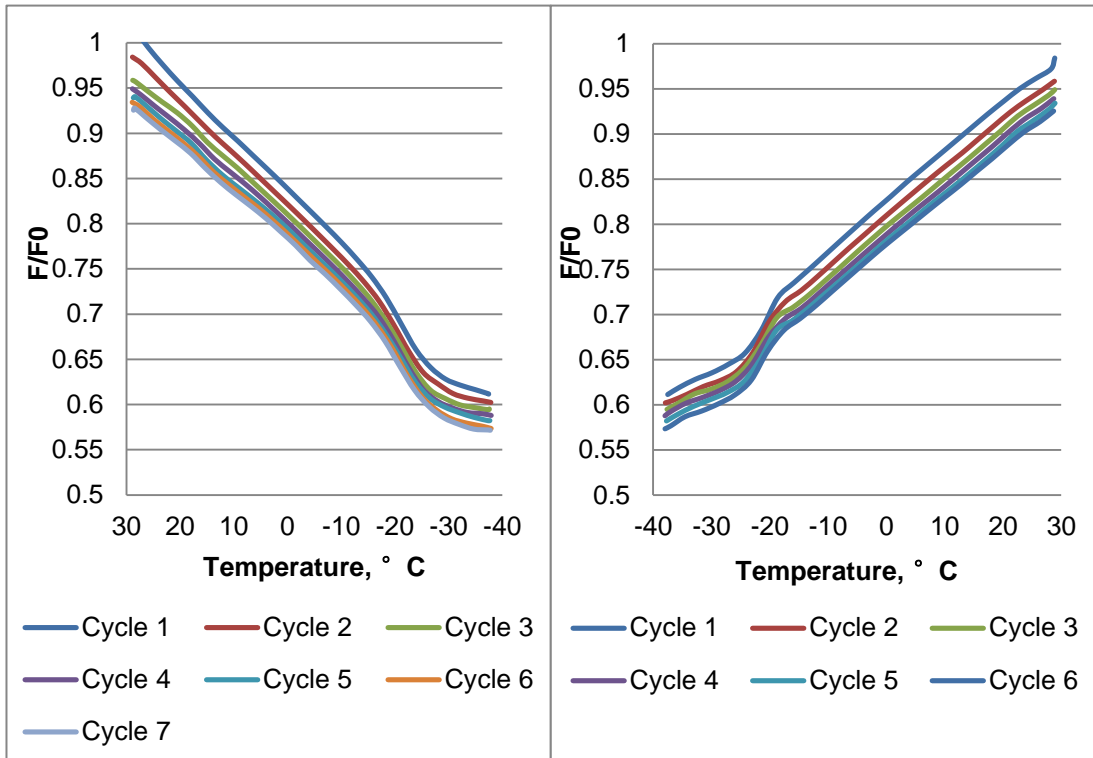
(b)



(c)

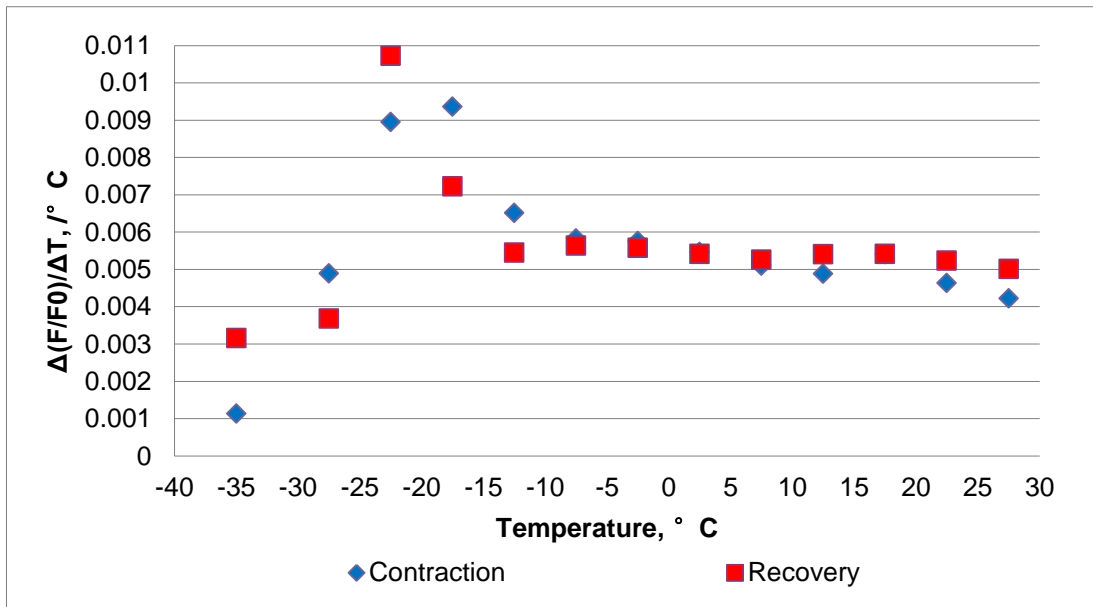
**Figure 123** Data analysis for the 24h-cycling test in groove in Jet A-1 (fluorocarbon O-ring).

(a) compression force vs. temperatures, contraction cycles; (b) compression force vs. temperatures, recovery cycles; (c)  $\Delta(F/F_0)/\Delta T$  vs. temperatures.



(a)

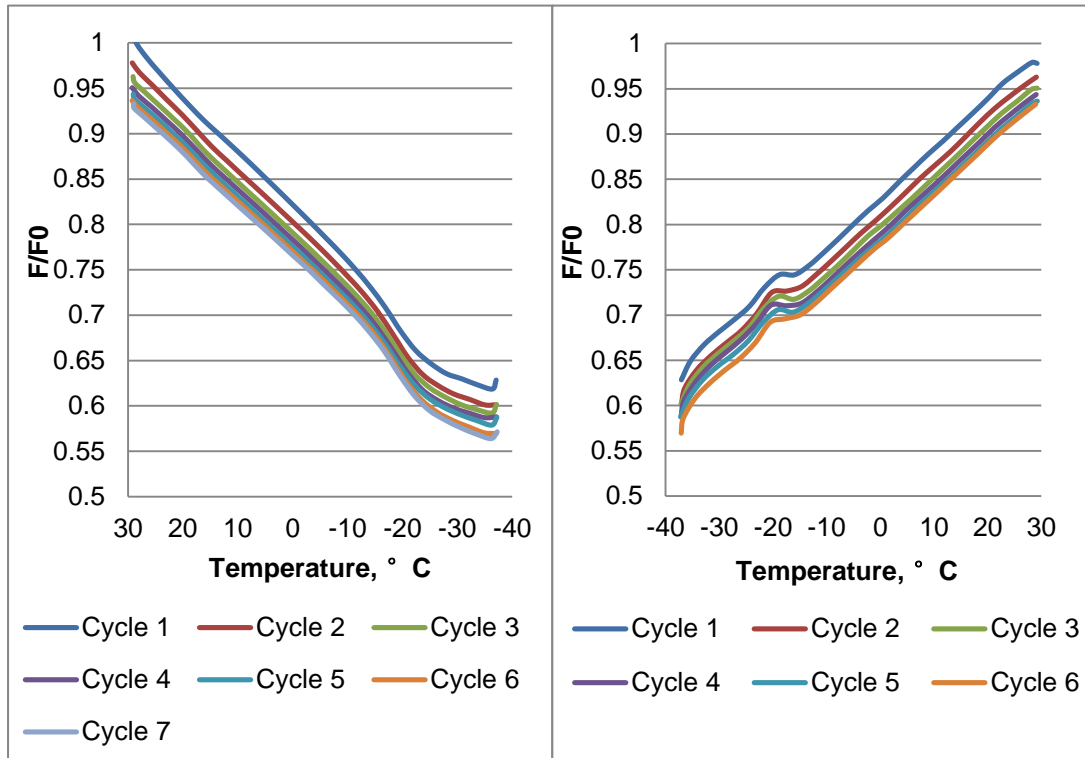
(b)



(c)

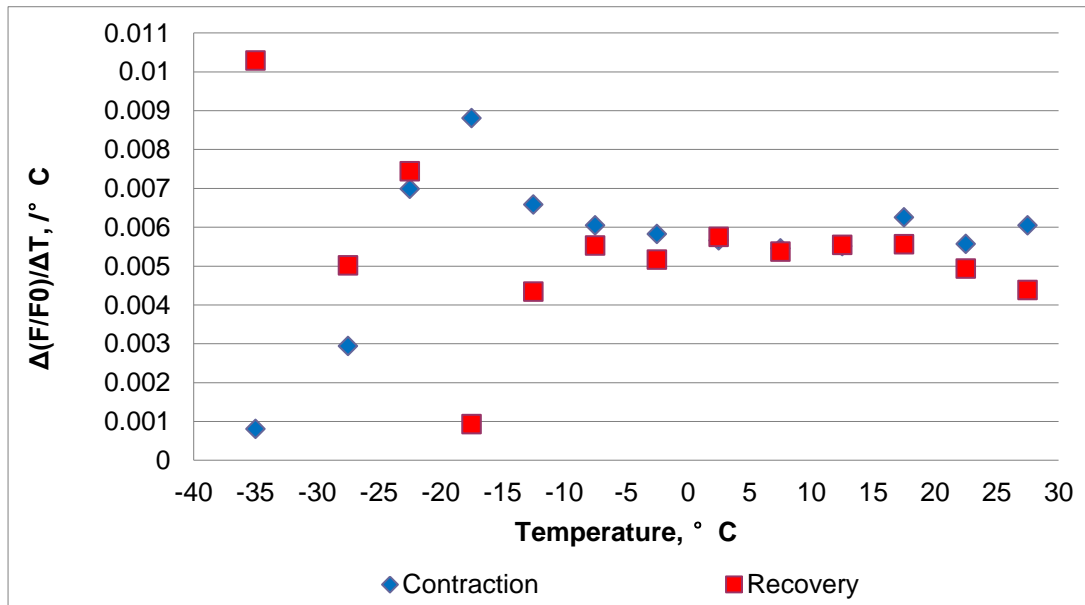
**Figure 124** Data analysis for the 24h-cycling test in groove in 4% aromatic fuel blend (fluorocarbon O-ring).

(a) compression force vs. temperatures, contraction cycles; (b) compression force vs. temperatures, recovery cycles; (c)  $\Delta(F/F_0)/\Delta T$  vs. temperatures.



(a)

(b)



(c)

**Figure 125** Data analysis for the 24h-cycling test in groove in SPK (fluorocarbon O-ring).

(a) compression force vs. temperatures, contraction cycles; (b) compression force vs. temperatures, recovery cycles; (c)  $\Delta(F/F_0)/\Delta T$  vs. temperatures.

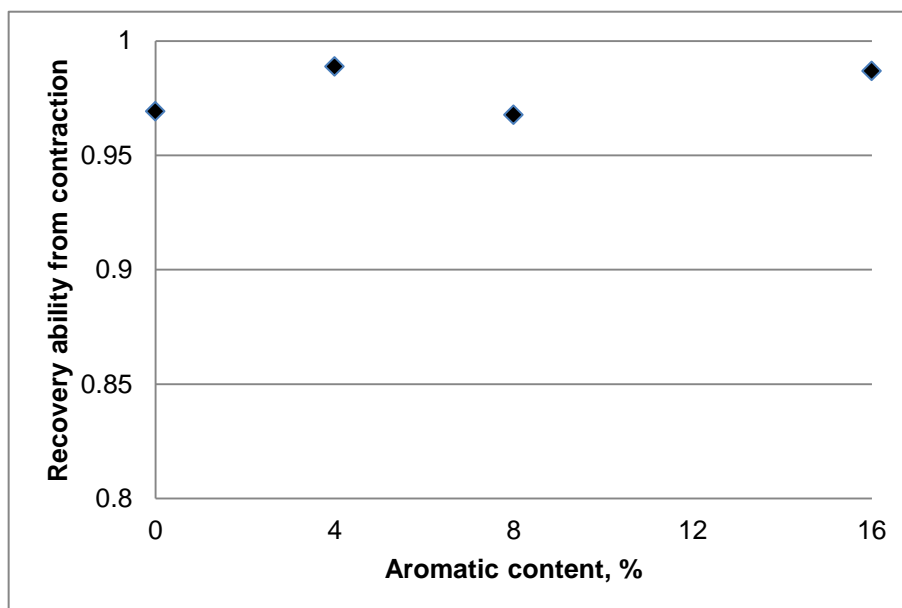
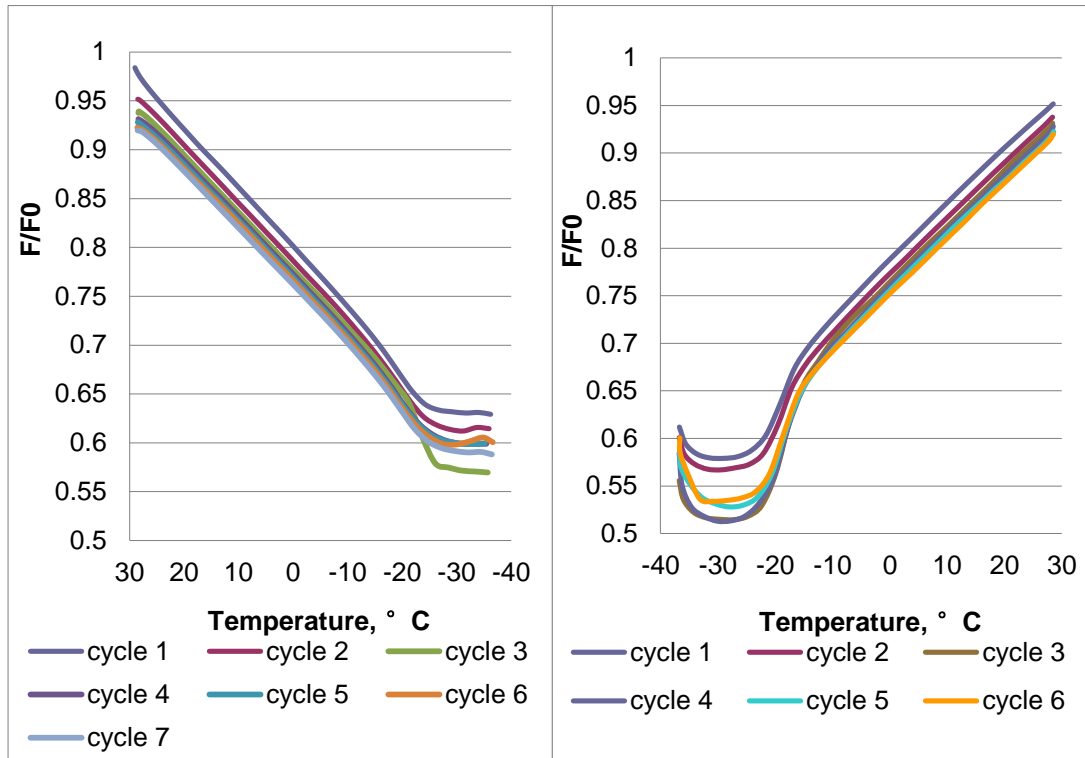


**Figure 126** Overall recovery ability of fluorocarbon O-rings in fuels with various aromatic contents during the 24h-cycle testing.

The recovery ability of fluorocarbon O-ring seems not depends on the aromatic content in the fuel as no linear relationship could be drawn between these two parameters (Fig.126).

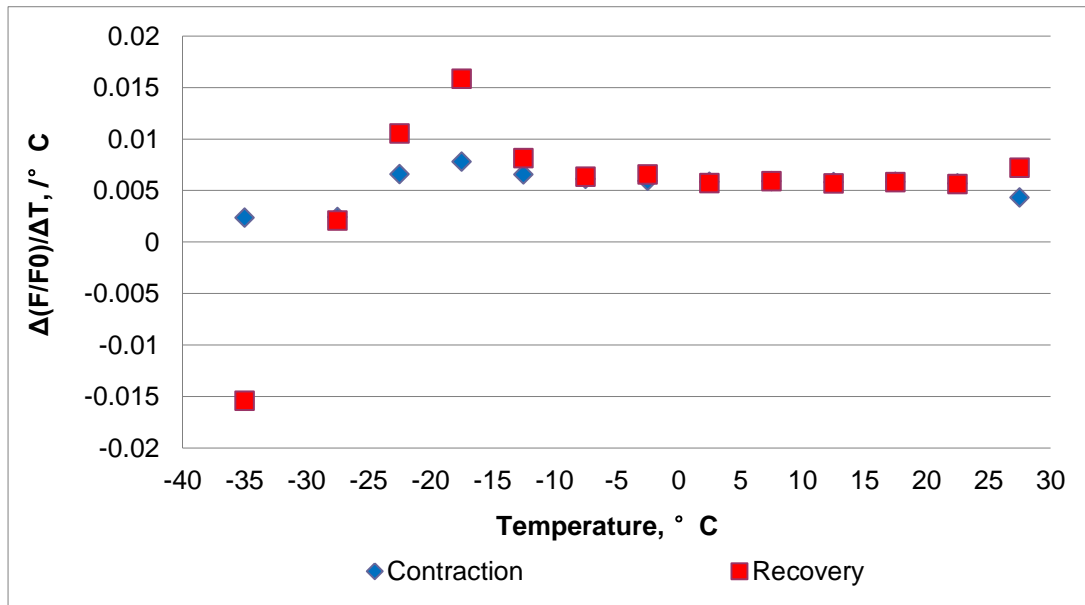
#### 7.2.3.2 *Without grooves*

Results from 24h-cycle tests without O-ring grooves demonstrated very similar characteristics in both Jet A-1 and SPK (Fig. 127-128). Compared with the data obtained with grooves, the contraction cycles in both fuels followed almost the same pattern, except for the relatively lower contraction ratio during the glass transition temperature. A major difference was observed at temperatures below -30 °C during the recovery cycles. When temperature started to rise, compression force declined and eventually reached a steady level around -30 °C and then started to increase. It seemed that as the temperature increased, the ‘frozen’ fluorocarbon polymer absorbed more energy and the mobility of molecules started to recover. Both stress



(a)

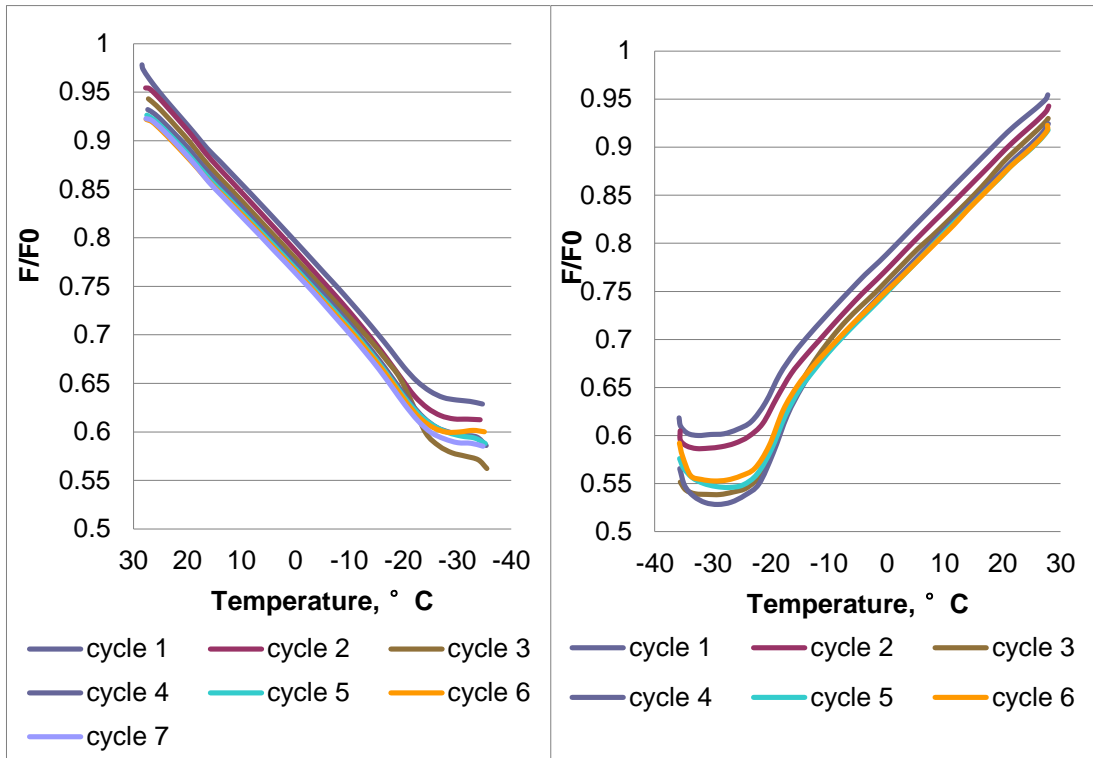
(b)



(c)

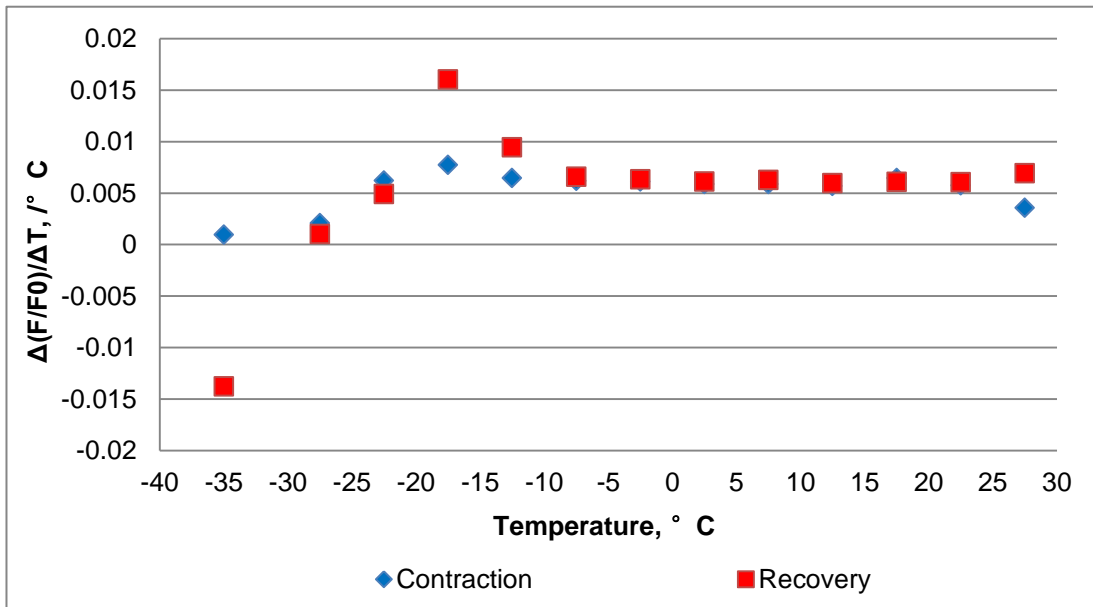
**Figure 127** Data analysis for the 24h-cycling test with no groove in Jet A-1 (fluorocarbon O-ring).

(a) compression force vs. temperatures, contraction cycles; (b) compression force vs. temperatures, recovery cycles; (c)  $\Delta(F/F_0)/\Delta T$  vs. temperatures.



(a)

(b)



(c)

**Figure 128** Data analysis for the 24h-cycling test with no groove in GtL fuel (fluorocarbon O-ring).

(a) compression force vs. temperatures, contraction cycles; (b) compression force vs. temperatures, recovery cycles; (c)  $\Delta(F/F0)/\Delta T$  vs. temperatures.

relaxation and thermal expansion occurred simultaneously and the change of compression force observed was an overall result of both physical processes. The stress relaxation process seemed to dominate the initial recovery phase until -30 °C where a temporary equilibrium was reached. After that, compression force started to increase following the similar pattern shown in data in grooves. The addition of O-ring groove seems to somehow offset the stress relaxation process during the initial recovery cycles. The recovery ability of fluorocarbon O-ring in both fuels was very similar (Fig. 129).

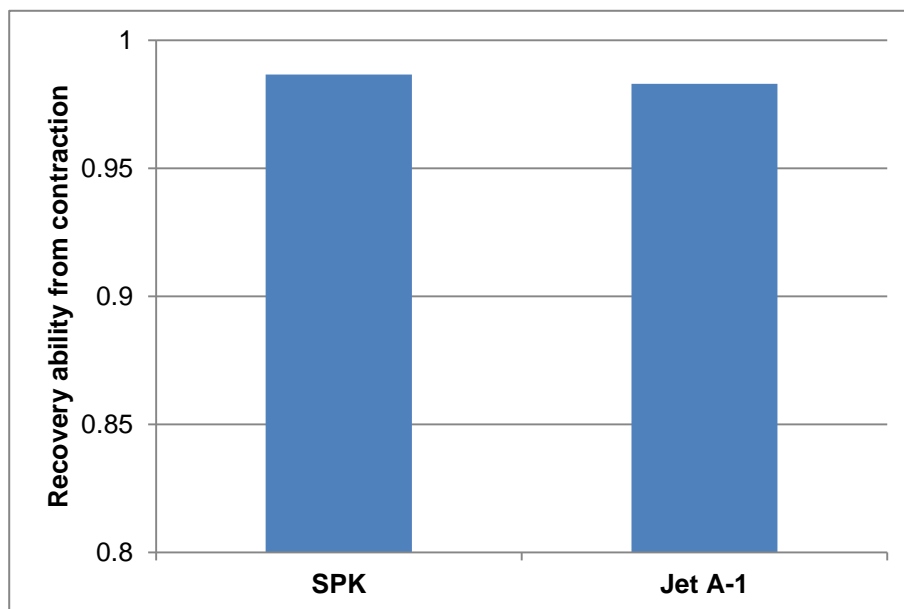


**Figure 129** Average recovery ability of fluorocarbon O-rings in Jet A-1 and SPK during the 24h-cycle testing without grooves.

## 8 Conclusions and Future Work

### 8.1 Conclusions

A wide range of valuable data regarding the elastomer compatibility with alternative fuels was collected and analyzed during this project. The work conducted here contributes to the understanding of the sealing performance of elastomeric materials in various fuel scenarios and temperature conditions. It also establishes a practical approach for testing elastomer's sealing performance and contributes to specification limitations for jet fuels and system design in the future. The key findings of this project are summarized as follows:

- The stress relaxation characteristics of nitrile, fluorosilicone and fluorocarbon O-rings in jet fuels produced via various sources and approaches were obtained. Comparison between alternative fuels and conventional jet fuel (Jet A-1) suggests that the introduction of Synthetic Paraffinic Kerosenes (SPKs) and Hydrotreated Vegetable Oils (HVOs) have no obvious impact on fluorosilicone and fluorocarbon O-rings but may significantly influence the performance of fresh nitrile seals due to the lack of aromatic compound. It is also noticed that preconditioned nitrile seals are much more compatible with alternative fuels than fresh ones as additives such as plasticizers were extracted from the polymer. Fully Synthetic Jet Fuel (FSJF) derived from coal demonstrated excellent seal compatibility due to its ability to maintain a stable sealing force.
- Individual fuel species have different impact on seals. Fluorocarbon O-ring demonstrated the best compatibility with all fuel species as its stress relaxation characteristics in all fuels and blends are fairly stable. Fluorosilicone O-ring also showed excellent compatibility with most fuel species except for hexanol (alcohol) due to its interaction with (Si-O-Si) bonds in the polymer structure as suggested by the FTIR analysis. Nitrile

O-ring behaves more 'actively' in various fuel species. Generally, aromatics presented the best elastomer swelling ability while hexanol (alcohol) also swelled the O-ring to a notable degree. Naphthenes (cycloparaffins) have the ability to slow down the stress relaxation process by maintaining the sealing force. The 'triangle' test also indicated decalin (cycloparaffin) has good seal swelling ability; however, only when the proportion of decalin reaches 60% can the blend to be considered similar to Jet A-1 in terms of seal compatibility. Iso-paraffins do not participate in the seal swelling process but only extracting materials out; but their extracting ability is weaker than n-decane, a normal paraffin which can initially penetrate into the polymer.

- Fourier Transform Infrared Spectroscopy (FTIR) proved to be a practical methodology to analyse the molecular structure change of elastomers. A correlation has been found between the stress relaxation force changes and the combination of a series of peak area changes in the spectra. This finding suggests that certain molecular bonds may break down or rearrange during the stress relaxation process, which in return, results in the relaxation. FTIR is also capable of identifying potential chemical reactions amongst molecular bonds.
- It proved the Hansen Solubility Parameters (HSPs) could be successfully utilized into the analysis of elastomer compatibility issue with aviation fuel. A good non-linear correlation between the equilibrium compression force and the RED number was generated from the 'triangle' test data. It suggests that if the HSP of a solvent is more similar to that of a polymer, it is more likely that this solvent will swell the polymer better, and eventually, benefit its sealing performance.
- Temperature could be an influential factor in terms of the sealing performance of an O-ring. Generally, the stress relaxation process slows

down (accelerates) as the temperature decreases (increases). At extremely low temperatures, seals become very inert and the relaxation process would stop. This also impact the sealing performance of nitrile seal in SPK and Jet A-1, as no obvious difference in these two fuels is observed under extremely low temperatures. Low temperatures have a significant influence on the property of fluorocarbon material due to its relatively high glass transition temperature. This would result in the hardening and plasticizing of the material and could eventually cause sealing issue.

- Temperature cycling tests indicated preconditioned nitrile O-rings' ability to recover from thermal contraction depends on the aromatic content in the fuel; the higher the aromatic content in the fuel, the better the seal recovers. The recovery ability of fluorosilicone and fluorocarbon O-rings did not show any dependence on aromatics. However, the recovery ratio of fluorosilicone O-ring tends to reduce at high temperature end indicating an accelerated stress relaxation process. Both the contraction and recovery ratios of fluorocarbon O-ring reached the peak values during the glass transition temperature. At temperatures below the glass transition temperature, O-rings become stiffer and both the contraction and recovery ratios reduced dramatically.
- The addition of O-ring grooves applied external pressure on the seals. For nitrile and fluorosilicone O-rings, this external pressure helped in the relatively quicker recovery at low temperature end but accelerated the stress relaxation process at high temperature end. For fluorocarbon O-ring, the groove somehow offset the stress relaxation process during the initial recovery cycles.

## 8.2 Future Work

Based on the knowledge gained from the research conducted in this project, a number of topics related to this area might be interesting to look into in the future.

- It is necessary and interesting to look at the effect of other cycloparaffinic compounds on the stress relaxation process of nitrile seals, because although decalin demonstrates good seal swelling ability, the bulk cycloparaffins tested in this project only show the ability to maintain the sealing force.
- Currently, all the efforts have been made to look at the impact of fuels on seals. As the fuel-polymer interaction is a two-way process, it would be valuable to analyse the fuels/solvents after the stress relaxation tests to determine possibly which compounds and how much of the elastomeric material was leached from the O-rings and to determine if any patterns would emerge that could be correlated back to the fuels/solvents.
- In addition to the temperature cycling test, it would be beneficial to include the fuel-switching process during the test. Fuel-switching process can be carried out between conventional jet fuel (Jet A-1) and synthetic fuels (with lower or no aromatics) to evaluate if seals could re-gain equilibrium after exposed to low aromatic environment for a period of time. Furthermore, a leakage test could be conducted during the test to see if there is any pressure drop inside the sealing. This could also contribute to establish a standard criterion on seal leakage evaluation.
- To extend the utilization of the HSP analysis, effort can be made to explore if a 'sweet-spot' exists in the Hansen space, which gives an optimized distance to the seal; it provides the desired degree of seal swelling without the danger of dissolving the polymer. The solvent possesses this specific HSP could be a blend of aromatic compounds or other fuel species or additives. The theoretical analysis could be supported by the stress relaxation experimental work. The outcome could be considered as a potential additive to synthetic fuels to promote its compatibility with elastomeric seals.

## References

- [1] C. A. Moses, "Comparative evaluation of Semi-Synthetic Jet Fuels," CRC, 2008.
- [2] A. Beyersdorf and B. Anderson, "An overview of the NASA Alternative Aviation Fuel Experiment (AAFEX)," Aachen and Maastricht, TAC-2 Proceedings, June 22-25 2009.
- [3] China Daily. (2011) China conducts its first jet biofuel trial. [Online]. [http://www.chinadaily.com.cn/bizchina/2011-10/29/content\\_14000985.htm](http://www.chinadaily.com.cn/bizchina/2011-10/29/content_14000985.htm)
- [4] Virgin Atlantic. (2008) Virgin Atlantic is the first airline to operate demonstration flight using a biofuel blend. [Online]. <http://www.virgin-atlantic.com/en/gb/allaboutus/environment/biofuel.jsp>
- [5] The New York Times. (2008) Air New Zealand flies on engine with Jatropa biofuel blend. [Online]. <http://green.blogs.nytimes.com/2008/12/30/air-new-zealand-flies-on-engine-with-jatropha-biofuel-blend/>
- [6] Houston Chronicle. (2009) Continental jet makes biofuel test flight. [Online]. <http://www.chron.com/business/energy/article/Continental-jet-makes-biofuel-test-flight-1739517.php>
- [7] Japan Airlines. (2009) JAL flight brings aviation one step closer to using biofuel. [Online]. <http://press.jal.co.jp/en/release/200901/001108.html>
- [8] Green Car Congress. (2009) Qatar Airways becomes first to operate commercial flight on GTL jet fuel blend. [Online]. <http://www.greencarcongress.com/2009/10/qatar-gtl-20091012.html>
- [9] Flightglobal. (2011) KLM used 50/50 blend for first scheduled biofuel flight. [Online]. <http://www.flightglobal.com/news/articles/klm-used-5050-blend-for-first-scheduled-biofuel-flight-358967/>
- [10] Clean Technica. (2012) Lufthansa declares biofuel trials successful. [Online]. <http://cleantechnica.com/2012/01/13/lufthansa-declares-biofuel-trials-successful-ceases-using-biofuel/>
- [11] AeroMexico. (2011) Aeromexico, ASA, and Boeing announce the first transcontinental flight in aviation history to use biofuel. [Online]. <http://www.aeromexico.com/us/ExperienceAeromexico/AeromexicoCorporate/PressRoom/Green-flight.html>
- [12] L. Q. Maurice, H. Lander, T. Edwards, and W. E. Harrison III, "Advanced aviation fuels: a look ahead via a historical perspective," *Fuel*, vol. 80, pp. 747-756, 2001.
- [13] Richard Striebich, Linda Shafer, Matthew J. DeWitt, and Zachary West, "Dependence of fuel properties during blending of iso-paraffinic kerosene and petroleum-derived jet fuel (interim report)," 2008.

- [14] Clifford A. Moses, "Development of the protocol for acceptance of synthetic fuels under commercial specification," 2007.
- [15] SWAFEA. (2013) Sustainable Way for Alternative Fuels and Energy for Aviation. [Online]. <http://www.swafea.eu>
- [16] Alfa-bird. (2013) Alternative fuels and biofuels for aircraft development. [Online]. [www.alfa-bird.eu-vri.eu](http://www.alfa-bird.eu-vri.eu)
- [17] Lucas Rye, Simon Blakey, and Christopher W. Wilson, "Sustainability of supply on the planet: a review of potential drop-in alternative aviation fuels," *Energy & Environmental Science*, vol. 3, pp. 17-27, 2010.
- [18] David L. Daggett, Robert C. Hendricks, Rainer Walther, and Edwin Corporan, "Alternative fuels for use in commercial aircraft," 2007.
- [19] IATA, "Report on alternative fuels," 2009.
- [20] James I. Hileman et al., "Near-term feasibility of alternative jet fuels," 2009.
- [21] Delanie Lamprecht, "Fischer-Tropsch fuel for use by the U.S. military as battlefield-use fuel of the future," *Energy & fuels*, vol. 21, pp. 1448-1453, 2007.
- [22] K. K. Gupta, A. Rehman, and R. M. Sarviya, "Bio-fuels for the gas turbine: A review," *Renewable and Sustainable Energy Reviews*, vol. 14, pp. 2946-2955, 2010.
- [23] James D. Kinder and Timothy Rahmes, "Evaluation of Bio-Derived Synthetic Paraffinic Kerosene (Bio-SPK)," 2009.
- [24] Christopher D. Klingshirn et al., "Hydroprocessed renewable jet fuel evaluation, performance, and emissions in a T63 turbine engine," in *ASME Turbo Expo 2011*, Vancouver, 2011.
- [25] CRC, *Handbook of aviation fuels.*: Society of Automotive Engineers, 2004.
- [26] Simon Blakey, Lucas Rye, and Christopher Willam Wilson, "Aviation gas turbine alternative fuels: A review," *Proceedings of the Combustion Institute*, vol. 33, pp. 2863-2885, 2011.
- [27] Airbus, "Alternative Fuels Programme-1st Phase GtL flight test final report," 2008.
- [28] Chris Wilson and Simon Blakey, "Preparing the way for gas turbines to run on alternative fuels," British Flame, Birmingham, 2007.
- [29] Eduardo Falabella Sousa-Aguiar, Lucia Gorestin Appel, and Claudio Mota, "Natural gas chemical transformations: The path to refining in the future," *Catalysis Today*, vol. 101, pp. 3-7, 2005.
- [30] PARTNER, "U.S. fuel trends analysis," in *the 4th meeting of the Group on International Aviation and Climate Change*, Montreal, 2009.
- [31] R. Altman, "Aviation alternative fuels, characterizing the options ," in *Aviation and Alternative Fuels (ICAO)*, Montreal, 2009.
- [32] Timothy Rahmes et al., "Sustainable Bio-derived Synthetic Paraffinic Kerosene (Bio-SPK) jet fuel flights and engine tests program results," in *9th*

- AIAA Aviation Technology, Integration, and Operations Conference (ATIO)*, Montreal, 2009.
- [33] Parker Hannifin Corporation, *Parker O-Ring Handbook*. Lexington, US: Parker Hannifin Corporation, 2007.
- [34] J. L. Graham, "Alternative fuels, final report," FAA OTA DTFAWA-10-C-0030, 2010.
- [35] George C Soney and Thomas Sabu, "Transport phenomena through polymeric systems," *Progress in Polymer Science*, vol. 26, pp. 985-1017, Aug. 2001.
- [36] N. Sombatsompop and K. J. Christodoulou, "Penetration of aromatic hydrocarbons into natural rubber," *Polymers & Polymer Composites*, vol. 5, no. 5, pp. 377-386, 1997.
- [37] M. Saleem, Abdul-Fattah A. Asfour, D De Kee, and Brian Harrison, "Diffusion of organic penetrants through low density polyethylene (LDPE) films: Effect of size and shape of the penetrant molecules," *Journal of Applied Polymer Science*, vol. 37, no. 3, pp. 617-625, Jan. 1989.
- [38] T. M. Aminabhavi and H. Phayde, "Molecular transport characteristics of santoprene thermoplastic rubber in the presence of aliphatic alkanes over the temperature interval of 25 to 70 degC," *Polymer*, vol. 36, no. 5, pp. 1023-1033, 1995.
- [39] Robert J. Gormley, Dirk D. Link, John P. Baltrus, and Paul H. Zandhuis, "Interactions of jet fuels with nitrile O-rings: Petroleum-derived versus synthetic fuels," *Energy & Fuels*, vol. 23, pp. 857-861, 2009.
- [40] Pat Muzzell, Leo Stavinoha, and Rebecca Chapin, "Synthetic Fischer-Tropsch (FT) JP-5/JP-8 aviation turbine fuel elastomer compatibility, final report," PE0603750D8Z, 2005.
- [41] Patsy A Muzzell, Leo L. Stavinoha, Eric Sattler, Angela Terry, and Luis Villahermosa, "Elastomer impact when switch-loading synthetic fuel blends and petroleum fuels," TARDEC 16028, 2006.
- [42] ASTM International, "Petroleum Products, Lubricants and Fossil Fuels," in *Annual Book of ASTM Standards.*, 2003, ch. 5.
- [43] X. Zabarnick, et al., "Evaluation and testing of the suitability of a coal-based jet fuel," Final report AFRL-RZ-WP-TR-2009-2063, 2008.
- [44] Matthew J. DeWitt, Edwin Corporan, John Graham, and Donald Minus, "Effects of aromatic type and concentration in Fischer-Tropsch fuel on emissions production and material compatibility," *Energy & Fuels*, vol. 22, pp. 2411-2418, 2008.
- [45] John L. Graham, Richard C. Striebich, Kevin J. Myers, Donald K. Minus, and William E. Harrison III, "Swelling of nitrile rubber by selected aromatics blended in a synthetic jet fuel," *Energy & Fuels*, vol. 20, pp. 759-765, 2006.
- [46] Dirk D. Link, Robert J. Gormley, John P. Baltrus, Richard R. Anderson, and Paul H. Zandhuis, "Potential additives to promote seal swell in synthetic fuels

- and their effect on thermal stability," *Energy & Fuels*, vol. 22, pp. 1115-1120, 2008.
- [47] Takahiro Yamada, John L. Graham, and Donald K. Minus, "Density functional theory investigation of the interaction between nitrile rubber and fuel species," *Energy & Fuels*, vol. 23, pp. 443-450, 2009.
- [48] J. C. Armah, A. W. Birley, K. P. Fernando, C. Hepburn, and M. Tahir, "Stress-relaxation measurements on rubbers in compression, equipment and methodology," *Rubber Chemistry and Technology*, vol. 59, pp. 765-778, Nov. 1986.
- [49] R. P. Brown, T. Butler, and S. W. Hawley, *Ageing of Rubber: Accelerated Heat Ageing Test Results.*: Rapra Technology Ltd., 2001.
- [50] Andrew Ciesielski, *An Introduction to Rubber Technology.*: Rapra Technology Ltd., 1999.
- [51] Alan N. Gent, *Engineering with Rubber: How to Design Rubber Components*, 2nd ed.: Hanser Verlag, 2001.
- [52] G. Spetz, "Stress relaxation tests," Elastocon AB, Technical report 1999.
- [53] James E. Mark and Burak Erman, *Science and Technology of Rubber*, 3rd ed. New York: Academic Press, 2011.
- [54] Susanta Mitra, Afshin Ghanbari-Siahkali, and Kristoffer Almdal, "A novel method for monitoring chemical degradation of crosslinked rubber by stress relaxation under tension," *Polymer Degradation and Stability*, vol. 91, pp. 2520-2526, 2006.
- [55] Susanta Mitra, et al., "Chemical degradation of crosslinked ethylene-propylene-diene rubber in acidic environment. Part I. Effect on accelerated sulphur crosslinks," *Polymer Degradation and Stability*, vol. 91, pp. 69-80, Jan. 2006.
- [56] Susanta Mitra, et al., "Chemical degradation of crosslinked ethylene-propylene-diene rubber in acidic environment. Part II. Effect of peroxide crosslinking in presence of a coagent," *Polymer Degradation and Stability*, vol. 91, pp. 81-93, Jan. 2006.
- [57] Kenneth T. Gillen, Mathew Celina, and Robert Bernstein, "Validation of improved methods of predicting long-term elastomeric seal lifetimes from compression stress-relaxation and oxygen consumption techniques," *Polymer Degradation and Stability*, vol. 82, pp. 25-35, 2003.
- [58] S. Ronan, T. Alshuth, S. Jerrams, and N. Murphy, "Long-term stress relaxation prediction for elastomers using the time-temperature superposition method," *Materials & Design*, vol. 28, pp. 1513-1523, 2007.
- [59] Mogon Patel, Mark Soames, Anthony R. Skinner, and Thomas S. Stephens, "Stress relaxation and thermogravimetric studies on room temperature vulcanised polysiloxane rubbers," *Polymer Degradation and Stability*, vol. 83, pp. 111-116, Jan. 2004.

- [60] Mogon Patel, Paul R. Morrell, and Julian J. Murphy, "Continuous and intermittent stress relaxation studies on foamed polysiloxane rubber," *Polymer Degradation and Stability*, vol. 87, pp. 201-206, Jan. 2005.
- [61] S. Ronan, M. Santoso, T. Alshuth, U. Giese, and R. H. Schuster, "The impact of chain oxidation on stress relaxation of NR-elastomers and life-time prediction," in *11th International Seminar on Elastomers (ISE)*, Freiburg, 2007.
- [62] B. Stuart, *Infrared Spectroscopy: Fundamentals and Applications*. Chichester: John Wiley & Sons, Ltd, 2004.
- [63] Donald L. Pavia, Gary M. Lampman, George S. Kriz, and James R. Vyvyan, *Introduction to Spectroscopy*, 4th ed. USA: Brooks/Cole, Cengage Learning, 2009.
- [64] J. M. Brown, *Molecular Spectroscopy*. Oxford, UK: Oxford University Press, 1998.
- [65] UC Davis by the University of California. (2010) Number of vibrational modes for a molecule. [Online]. [http://chemwiki.ucdavis.edu/Physical\\_Chemistry/Spectroscopy/Vibrational\\_Spectroscopy/Vibrational\\_Modes/Number\\_of\\_vibrational\\_modes\\_for\\_a\\_molecule](http://chemwiki.ucdavis.edu/Physical_Chemistry/Spectroscopy/Vibrational_Spectroscopy/Vibrational_Modes/Number_of_vibrational_modes_for_a_molecule)
- [66] Alfred A. Christy, Y. Ozaki, and Vasilis G. Grogoriou, *Modern Fourier-Transform Infrared Spectroscopy*. Amsterdam, The Netherlands: Elsevier, 2001.
- [67] Thermo Nicolet Corporation. (2001) Introduction to Fourier Transform Infrared Spectrometry. [Online]. <http://mmrc.caltech.edu/FTIR/FTIRintro.pdf>
- [68] Perkin Elmer. (2005) Technical note for ATR-FTIR. [Online]. [http://shop.perkinelmer.com/content/technicalinfo/tch\\_ftiratr.pdf](http://shop.perkinelmer.com/content/technicalinfo/tch_ftiratr.pdf)
- [69] Perkin Elmer. (2004) Technical note for ATR accessories: An overview. [Online]. [http://shop.perkinelmer.com/content/technicalinfo/tch\\_atraccessories.pdf](http://shop.perkinelmer.com/content/technicalinfo/tch_atraccessories.pdf)
- [70] T. N. Pliev, A. D. Chugai, V. N. Poletova, and L. E. Chechik, "Infrared absorption spectra of engineering rubber grades," *Journal of Applied Spectroscopy*, vol. 11, pp. 1068-1079, Dec. 1969.
- [71] S. Gunasekaran, R. K. Natarajan, and A. Kala, "FTIR spectra and mechanical strength analysis of some selected rubber derivatives," *Spectrochimica Acta Part A*, vol. 68, pp. 323-330, 2007.
- [72] S. Chakraborty, S. Bandyopadhyay, R. Ameta, R. Mukhopadhyay, and A. S. Deuri, "Application of FTIR in characterization of acrylonitrile-butadiene rubber (nitrile rubber)," *Polymer Testing*, vol. 26, pp. 38-41, 2007.
- [73] T. Kawashima and T. Ogawa, "Prediction of the lifetime of nitrile-butadiene rubber by FT-IR," *Analytical Sciences*, vol. 21, pp. 1475-1478, 2005.
- [74] M. W. Urban, *Fourier Transform Infrared and Fourier Transform Raman*

*Spectroscopy of polymers, Principles and applications.*: American Chemical Society, 1993.

- [75] A. Jansson, K. Moller, and T. Hjertberg, "Chemical degradation of a polypropylene material exposed to simulated recycling," *Polymer Degradation and Stability*, vol. 84, pp. 227-232, 2004.
- [76] J. M. Cervantes-Uc, J. V. Cauich-Rodriguez, H. Vazquez-Torres, and A. Licea-Claverie, "TGA/FTIR study on thermal degradation of polymethacrylates containing carboxylic groups," *Polymer Degradation and Stability*, vol. 91, pp. 3312-3321, 2006.
- [77] Rafael Torregrosa-Coque, Sonia Alvarez-Garcia, and Jose Miguel Martin-Martinez, "Migration of low molecular weight moiety at rubber-polyurethane interface: an ATR-IR spectroscopy study," *International Journal of Adhesion and Adhesives*, vol. 31, no. 6, pp. 389-397, Sep. 2011.
- [78] G. T. Fieldson and T. A. Barbari, "The use of FTIR-ATR spectroscopy to characterize penetrant diffusion in polymers," *Polymer*, vol. 34, pp. 1146-1153, 1993.
- [79] Kathleen Cogan Farinas, Lisa Doh, Subbu Venkatraman, and Russell O. Potts, "Characterization of solute diffusion in a polymer using ATR-FTIR spectroscopy and bulk transport techniques," *Macromolecules*, vol. 27, no. 18, pp. 5220-5222, 1994.
- [80] J. G. Alsten and S. R. Lustig, "Polymer mutual diffusion measurements using infrared ATR spectroscopy," *Macromolecules*, vol. 25, pp. 5069-5073, 1992.
- [81] C. Sammon, J. Yarwood, and N. Everall, "A FTIR-ATR study of liquid diffusion processes in PET films: comparison of water with simple alcohols," *Polymer*, vol. 41, pp. 2521-2534, 2000.
- [82] T. T. Do, M. Celina, and P. M. Fredericks, "Attenuated total reflectance infrared microspectroscopy of aged carbon-filled rubbers," *Polymer Degradation and Stability*, vol. 77, pp. 417-422, 2002.
- [83] J. Hilderbrand and R. L. Scott, *The Solubility of Nonelectrolytes*, 3rd ed. New York: Reinhold, 1950.
- [84] Charles M. Hansen, *The three dimensional solubility parameter and solvent diffusion coefficient: their importance in surface coating formulation*. Copenhagen: Danish Technical Press, 1967.
- [85] Charles M. Hansen, *Hansen Solubility Parameters: A user's handbook*, 2nd ed.: CRC Press, 2007.
- [86] Charles M. Hansen. Official website of Hansen Solubility Parameters. [Online]. <http://hansen-solubility.com/index.php?id=21>
- [87] T. B. Nielsen and Charles M. Hansen, "Elastomer swelling and Hansen solubility parameters," *Polymer Testing*, vol. 24, pp. 1054-1061, 2005.
- [88] Charles M. Hansen, "Polymer additives and solubility parameters," *Progress in Organic Coatings*, vol. 51, pp. 109-112, 2004.

- [89] D. L. Ho and C. J. Glinka, "New insights into Hansen's solubility parameters," *Journal of Polymer Science, Part B: Polymer Physics*, vol. 42, pp. 4337-4343, 2004.
- [90] E. Stefanis and C. Panayiotou, "Prediction of Hansen solubility parameters with a new group-contribution method," *International Journal of Thermophysics*, vol. 29, pp. 568-585, 2008.
- [91] ISO, "ISO 3384: Rubber, vulcanized or thermoplastic-Determination of stress relaxation in compression," in *ISO Standard.*: ISO, 2011.
- [92] Elastocon AB. Manual for Elastocon EB02 Relaxation Tester. [Online]. [www.polimate.com.br/poli/attachment.php?id\\_attachment=320](http://www.polimate.com.br/poli/attachment.php?id_attachment=320)
- [93] Elastocon AB. (2009) Manual for Cell Oven, EB01.
- [94] Eltex of Sweden AB. (2001) CombiLab 5 Handbook.
- [95] Elastocon AB. (2011) Manual for Cell Oven for stress relaxation EB17.
- [96] Julabo. (2012) Manual for LH85 PLUS Temperature Control System.
- [97] Perkin Elmer Corporation. (1998) Spectrum One FT-IR Spectrometer user's guide.
- [98] R. White, *Chromatography/Fourier transform infrared spectroscopy and its application*. New York: Marcel Dekker, 1990.
- [99] John Wiley & Sons, Ltd. (2004) The Internet Journal of Vibrational Spectroscopy. [Online]. <http://www.ijvs.com/volume5/edition5/section1.html>
- [100] UC Davis ChemWiki by University of California. (2010) FTIR: Hardware. [Online]. [http://chemwiki.ucdavis.edu/Wikitexts/UCD\\_Chem\\_115/Chemwiki\\_Module\\_Topics/How\\_an\\_FTIR\\_instrument\\_works/FTIR: Hardware](http://chemwiki.ucdavis.edu/Wikitexts/UCD_Chem_115/Chemwiki_Module_Topics/How_an_FTIR_instrument_works/FTIR:_Hardware)
- [101] Defence Standard. (2008) Def Stan 91-91: Turbine fuel, aviation kerosene type, Jet A-1. [Online]. [http://www.seta-analytics.com/documents/DEF\\_STAN\\_91-91\\_R6.pdf](http://www.seta-analytics.com/documents/DEF_STAN_91-91_R6.pdf)
- [102] SAE Standards, "Gland Design, O-ring and Other Elastomeric Seals, Static Applications," in *SAE Standards.*: SAE Standards, 2010, ch. AS5857.
- [103] C. E. Carraher, *Introduction to polymer chemistry.*: CRC Press, 2012.
- [104] M. A. Meyers and K. K. Chawla, *Mechanical Behaviour of Materials*. New York: Cambridge University Press, 2009.
- [105] M. Celina, J. Wise, D. K. Ottesen, K. T. Gillen, and R. L. Clough, "Oxidation profiles of thermally aged nitrile rubber," *Polymer Degradation and Stability*, vol. 60, pp. 493-504, 1998.
- [106] B. C. Smith, *Fundamentals of Fourier Transform Infrared Spectroscopy*, 2nd ed.: CRC Press, Taylor & Francis Group, 2011.
- [107] R. T. Morrison and R. N. Boyd, *Organic Chemistry*, International edition ed. London: Prentice-Hall, 1992.
- [108] K. J. Saunders, *Organic Polymer Chemistry*. London: Chapman and Hall,

1973.

- [109] M. Jaunich, K. Von der Ehe, D. Wolff, H. Voelzke, and W. Stark, "Understanding low temperature properties of elastomeric seals," *Packaging, Transport, Storage and Security of Radioactive Material*, vol. 22, no. 2, pp. 83-88, 2011.
- [110] H. P. Weise, H. Kowalewsky, and R. Wenz, "Behavior of elastomeric seals at low-temperature," *Vacuum*, vol. 43, no. 5-7, pp. 555-557, 1992.
- [111] SAE Standards, "Gland design, elastomeric O-ring seals, static axial, without back-up rings," in *E-25 General Standards for Aerospace and Propulsion Systems.*: SAE Standards, 2001, ch. ARP1234.
- [112] Shell. (2007) ShellSol T solvent datasheet. [Online]. <http://s03.static-shell.com/content/dam/shell/static/chemicals/downloads/products-services/datasheet-isoparaffinshellsoleurope.pdf>
- [113] L.R.G. Treloar, "The physics of rubber elasticity," Oxford University Press, New York, 1975.

## Appendix 1 List of Publications

1. Yue Liu, Simon Blakey, and Christopher W Wilson, "A novel method to evaluate the temperature impact on elastomeric seals using temperature cycling stress relaxation test", Proceedings of IASH 2013, the 13<sup>th</sup> International Conference on Stability, Handling and Use of Liquid Fuels, Rhodes, Greece, 6-10 October 2013.
2. Yue Liu, Christopher W Wilson, and Jeff Trewella, "Investigation into the impact of normal, iso- and cyclo-paraffins on elastomeric seals using stress relaxation test and Hansen Solubility Parameters", Proceedings of CRC Aviation Meetings 2013, Savannah, USA, 29 April-2 May, 2013.
3. Yue Liu, Christopher W Wilson, "Investigation into the impact of n-decane, decalin and iso-paraffinic solvent on elastomeric sealing materials", Gas Turbine Technology Special Issue, Journal of Advances in Mechanical Engineering, research article 127430, 2013.  
<http://www.hindawi.com/journals/ame/2012/127430/>
4. Yue Liu, Christopher W Wilson, "Investigation into the temperature impact on O-ring's sealing performance using advanced stress relaxation test", Journal of Applied Mechanics and Materials, 2012. Proceedings of AEROTECH IV conference, Kuala Lumpur, Malaysia, 21-22 November, 2012.  
<http://www.scientific.net/AMM.225.255>
5. Yue Liu, "Investigation into the impact of Gas-to-Liquid fuel components on elastomeric sealing materials in a gas turbine engine", Proceedings of Qatar Foundation Annual Research Forum, Doha, Qatar, 21-23 October, 2012.  
<http://www.qscience.com/doi/pdfplus/10.5339/qfarf.2012.EEP72>
6. Yue Liu, Christopher W Wilson, Simon G Blakey, Patrick Theato, "Investigation of elastomer compatibility with alternative fuels by mass change study, stress-relaxation test and FTIR spectroscopy", IASH 2011, the 12<sup>th</sup> International Conference on Stability, Handling and Use of Liquid Fuels, Sarasota, USA, 16-20 October, 2011.  
<http://toc.proceedings.com/14486webtoc.pdf>
7. Yue Liu, Christopher W Wilson, Simon Blakey, Tim Dolmansley, "Elastomer compatibility test of alternative fuels using stress relaxation test and FTIR spectroscopy", Proceedings of the ASME Turbo Expo 2011, GT2011-46100, Vancouver, Canada, 6-10 June, 2011.  
<http://proceedings.asmedigitalcollection.asme.org/proceeding.aspx?articleid=1631362>